UNCLASSIFIED

AD NUMBER

AD822349

NEW LIMITATION CHANGE

TO

Approved for public release, distribution unlimited

FROM

Distribution authorized to U.S. Gov't. agencies and their contractors; Critical Technology; SEP 1967. Other requests shall be referred to Army Missile Command, Attn: AMSMI-RR, Redstone Arsenal, AL, 35809.

AUTHORITY

usamc ltr, 4 jun 1973

THIS PAGE IS UNCLASSIFIED

AD822345



REPORT NO. RK-TR-67-7

SOLID PROPELLANT ROCKET MOTOR INTERNAL BALLISTICS COMPUTER PROGRAM (PROGRAM MANUAL)

Prepared By
The Boeing Company
Seattle, Washington

Under
Contract No. DA-01-021-AMC-15557(Z)

For
ARMY MISSILE COMMAND
REDSTONE ARSENAL, ALABAMA

September 1967

STATEMENT #2 UNCLASSIFIED

This document is subject to special export controls and each transmittal to foreign governments or foreign nationals may be made only with prior approval of AMSMI-RR.



U.S. ARMY MISSILE COMMAND
Redstone Arsenal, Alabama 35809

PREFACE

This document is volume one (D2-125286-1) of three volumes. It describes a FORTRAN IV digital computer program developed for analysis of solid rocket motor internal ballistics. Volume one, "Program Manual," explains the theory and describes the mathematical model, program capabilities and information necessary for program maintenance and revision. Volume two, "User's Guide," (D2-125286-2) describes program options, preparation of program input data and program output. Volume three, "Sample Case Results and Program Listings," (D2-125286-3) contains the sample case results and complete program listings of the computer program. The document is divided into three volumes for handling convenience. Section numbering is continuous through the three volumes. A complete table of contents appears in each volume.

CONTENTS

		PAGE
VOLUME 1 (D2-125286-1)		
	Preface	viii
	Abstract	xii
	Key Words	xiii
	Acknowledgements	xiv
	Definition of Terms	xv
	List of Illustrations	xvii
1.0	Introduction	1
1.1	General Information	1
1.2	History of Program Development	3
1.3	References	4
2.0	Program Capabilities and Limitations	5
2.1	Program Capabilities	5
2.1.1	Program Output	7
2.1.2	Program Assumptions	7
2.2	Limitations	8
3.0	Method of Solution	11
4.0	Gas Dynamic Equation Development	16
4.1	Gas Dynamics for Incremental Control Volumes	16
4.1.1	Steady Flow Gas Dynamics	19
4.1.2	Non-Steady Flow Gas Dynamics	23
4.1.3	Non-Steady Flow Gas Dynamics with Acceleration	33
4.2	Complete Motor Gas Dynamics	36
4.2.1	Fore-Head Pressure Convergence	36
4.2.2	Nozzle Gas Dynamics	39
4.3	Propellant Characteristics and Burning Rate Model	41
4.3.1	Propellant Gas Properties	41
4.3.2	Propellant Burning Rate Model	42
4.3.3	Anisotropic Propellant Burning	44
5.0	Geometrical Definition of Propellant Grain	56
5.1	Grain Cross Section Geometry	56

		PAGE
5.1.1	General Forked Wagon Wheel	56
5.1.2	Slotted-Cone	67
5.2	Grain Longitudinal Geometry	77
5.2.1	Head-End with Web, Fore-Head Section	77
5.2.2	Cylindrical Section	92
5.2.3	Straight-Through Grain, Motor End Sections	94
5.3	Moments of Inertia and CG Location	106
5.3.1	Roll Moment of Inertia	107
5.3.2	Pitch Moment of Inertia	108
5.3.3	CG of Sections	110
6.0	Detailed Programming Information	150
6.1	Subroutine Description	151
6.1.1	Subroutine Descriptions	151
6.1.2	Subroutine Linkage Table	161
6.2	Flow Charts	171
6.3	Storage Allocation and Computer System	188
6.4	Diagnostic Tools	206
6.5	Nomenclature	207
7.0	Results	234

VOLUME 2 (D2-125286-2)

	Preface	vi
	List of Illustrations	xvii
8.0	User's Guide	1
8.1	Description of Input Data	2
8.1.1	Grain Geometry	2
8.1.2	Propellant Properties	8
8.1.3	Nozzle Configuration	11
8.1.4	Internal Gas Dynamics	12
8.2	Preparation of Input Data	14
8.3	Output Description	47
8.3.1	Input Data Printout	47
8.3.2	Initial Geometry Printout	47

		PAGE
8.3.3	Geometry Table Printout	47
8.3.4	Inert Sliver Summary Printout	47
8.3.5	Internal Ballistic Solution Printout	48
8.3.6	Expanded Increment Dividing Plane Printout	51
8.3.7	Burnout Printout	52
8.4	Sample Cases	54
8.4.1	Base Case One and Variations Description	54
8.4.2	Base Case Two and Variations Description	55
8.5	Operating Information	57
VOLUME 3	(D2-125286-3)	
	Preface	xii
	List of Illustrations	xvi
9.0	Sample Case Results and Program Listings	1
9.1	Sample Case Results	1
9.2	Program Listings	313

ABSTRACT

This report describes a FORTRAN IV digital computer program developed to calculate internal ballistic performance of solid propellant rocket motors with high burning rates, short burning durations, and high vehicle accelerations. Forked wagon wheel, conventional wagon wheel, standard star, slotted-cone, and circular port monolithic and segmented grain designs may be considered. Accurate description of an inert sliver in the cylindrical section is allowed for all but the forked wagon wheel grain design. The effects of anisotropic burning of the propellant may be considered. The storage of mass and momentum (capacitance effects) and vehicle acceleration are included in the internal gas dynamic equations. Ignition transients may be calculated. Tabular input of the motor grain description is available for special grain configurations that cannot be described by the program geometry constants. Motor performance parameters such as delivered and vacuum thrust and total impulse, fore-head and aft-head total pressure, nozzle discharge flow, fore-head and aft-head total pressure integrals, pitch and roll moments of inertia, center of gravity locations, burn surface area, and weight of propellant remaining are printed for each time interval.

This report is divided into three volumes. Volume one is the Program Manual, volume two is the User's Guide, and volume three is the Sample Case Results and Program Listings.

KEY WORDS

The following Key Words identify the major program capabilities:

Internal Ballistics
Solid Propellant Rocket Motor
Monolithic Grain
Segmented Grain
One-Dimensional Gas Dynamics
Steady Flow Gas Dynamics
Non-Steady Flow Gas Dynamics
Isotropic Propellant Burning
Anisotropic Propellant Burning
Vehicle Acceleration
Ignition Transient Interval
Web-Time Interval
Tail-Off Interval
Fore-Head Section
Aft-Head Section
Cylindrical Section
Center of Gravity
Moment of Inertia
Grain Geometry
Nozzle

ACKNOWLEDGEMENTS

Acknowledgement is given to the Thiokol Chemical Corporation, Redstone Division, for the original SCAT machine language program from which this program was developed (References 1 and 2), and to the Thiokol Chemical Corporation, Wasatch Division, for the documentation of the grain geometry calculations from which the description of the mathematical model was developed (Reference 3).

DEFINITION OF TERMS

The following general definitions apply throughout this document:

Internal Ballistics: Analysis of the burning characteristics and progression of the propellant surface, dynamics of the gas flow, and the gas generation in the interior of solid propellant rocket motors.

Performance Characteristics: Parameters that specify motor performance, e.g., thrust vs time, maximum chamber pressure, specific impulse, and burn time.

Gas Dynamics: Study of the generation and flow of combustion products along the propellant grain and through the nozzle.

Steady Flow Gas Dynamics: Mass, energy, and momentum within a control volume are constant with time.

Non-Steady Flow Gas Dynamics: Mass, energy, and momentum within a control volume are not constant with time.

Grain Design: The cross sectional grain configuration of the propellant.

Monolithic Grain: The propellant grain is one single piece.

Segmented Grain: The propellant grain is divided up into a number of longitudinal segments.

Slots: The region between the segments which does not contain propellant.

Web: The minimum distance between the grain surface and the case wall.

Core: The region occupied by the combustion gases.

Reference Planes: The stations in the cylindrical section of a motor where the grain design is specified.

Increment Dividing Planes: The stations in the cylindrical section of the motor where the solution of the internal gas dynamic equations is obtained.

Mass Addition Region: The region between increment dividing planes.

Ignition Transient Interval: The time required to obtain motor operating pressure.

Web-Time Interval: The time required to burn through the web.

Tail-off Interval: The time interval after web burn through.

Isotropic Propellant Burning: Where the burning rate characteristics are independent of distance burned.

Anisotropic Propellant Burning: Where the burning rate characteristics are dependent on distance burned.

LIST OF ILLUSTRATIONS

FIGURE NUMBER	TITLE	PAGE
2.1	Grain Design Options	9
2.2	Typical Motor Configurations	10
3.1	Reference Plane and Increr c Dividing Plane Identification	14
3.2	Macroscopic Flow Chart	15
4.1	Mathematical Model of Mass Addition Region Control Volume	50
4.2	Mathematical Model of Slot Between Grain Segments	51
4.3	Reference Plane and Increment Dividing Plane Identification	52
4.4	Anisotropic Propellant Burning Configuration Near Case Wall Before Web Burnout	53
4.5	Anisotropic Propellant Burning Configuration Near Case Wall and Inert Sliver Before Web Burnout	54
4.6	Anisotropic Propellant Burning Configuration Near Case Wall After Web Burnout	55
5.1	Grain Design Options	112
5.2	One-Half Fork of General Modified Wagon Wheel Configuration	113
5.3	Part of Calculated Constants for One-Half Fork of General Modified Wagon Wheel Configuration by PLNCNS Subroutine	114
5.4	Part of Calculated Constants for One-Half Fork of General Modified Wagon Wheel Configuration Produced by PLNCNS Subroutine	115
5.5	Sector Definition	116
5.6	Slotted-Cone	117

FIGURE NUMBER	TITLE	PAGE
5.7	Slotted-Cone Addition to Standard Star Showing Location of Fixed Geometry Points	118
5.8	Complete Slotted-Cone Burning Surface for τ Less than R_2	119
5.9	Slotted-Cone Burning Surface Addition for τ Greater than R_2 and Less than T_{6max}	120
5.10	Slotted-Cone Burning Surface Addition for τ Greater than T_{6max} and Less than T_{7max}	121
5.11	Slotted-Cone Burning Surface Addition for τ Greater than T_{7max} and Less than T'_{V7} with T'_{V7} Less than T'_{V6}	122
5.12	Slotted-Cone Burning Surface for τ Greater than T'_{V7} with T'_{V7} Less than T'_{V6}	123
5.13	Slotted-Cone Burning Surface for τ Greater than T'_{V6} with T'_{V6} Less than T'_{V7}	124
5.14	Head-End with Web, Motor Fore-Head	125
5.15	Sectors for Block No. 1	126
5.16	Head-End with Web Plane Definition	127
5.17	Head-End with Web, Block 1 Plane Definition	128
5.18	Plane for Block 1 Analysis	129
5.19	γ_1 for Subroutine GAMSUB	130
5.20	γ_2 for Subroutine GAM2S	131
5.21	P_0 for Subroutine POSUB	132
5.22	P_3 for Subroutine P3SUB	133
5.23	Planes for Block 1 Analysis	134
5.24	Planes Produced In Sectors 3A and 3B or In Sectors 11A and 11B	135
5.25	Area for Block No. 2A and 2B	136
5.26	A_{lg} for Subroutine AIGSUB	137

FIGURE NUMBER	TITLE	PAGE
5.27	Sectors for Block 2B of Fore-Head Section	138
5.28	Sector for Block 2B	139
5.29	Distribution of Volume In Radial Burning Section	140
5.30	Motor Case Longitudinal Constants	141
5.31	Straight Through Grain Configuration	142
5.32	Sector Definition	143
5.33	Zone Definition	144
5.34	Sector Parameters, Zones B, C, and Web	145
5.35	Circular Arc Sector 3 Zone A	146
5.36	Element of Incremental Area for Zone B	147
5.37	Head-End Section, Volume Elements for MOI and CG Calculations	148
5.38	Cylindrical Section Volume Elements for MOI and CG Calculations	149
7.1	HIBEX Forehead Chamber Pressure Trace	255
7.2	Influence of Internal Flow and Burning Rate Model	256
8.1	Program Model	62
8.2	Typical Motor Configurations	63
8.3	Straight Through Grain Configuration	64
8.4	Straight Through Grain Configuration Inputs	65
8.5	Head-End Web	66
8.6	Grain Configuration Options	67
8.7	Reference Plane and Increment Dividing Plane Identification	68
8.8	General Forked Wagon Wheel Configuration Inputs	69

FIGURE NUMBER	TITLE	PAGE
8.9	Calculated Plane Constants	70
8.10	Calculated Plane Constants	71
8.11	LA Definition	72
8.12	Wagon Wheel Configuration Inputs	73
8.13	Star Grain Configuration Inputs	74
8.14	Slotted-Cone Grain Configuration Inputs	75
8.15	Circular Port Configuration Inputs	76
8.16	Nozzle Configuration Inputs	77
8.17	Motor Case Longitudinal Inputs and Constants	78
8.18	Base Case One	79
8.19	Base Case Two, Monolithic Grain	80
8.20	Base Case Two, Segmented Grain	81

LIST OF FLOW CHARTS - VOLUME 1

FLOW CHART NUMBER	TITLE	PAGE
1	MAIN Program	172
2	Subroutine MNCHN1	173
3	Subroutine MNCHN2	174
4	Compute Plane Constants	175
5	Subroutine AESUB	176
6	Subroutine MNCHN3	178
7	Subroutine SCI	179
8	Subroutine SCTOR1	180
9	Subroutine SCTOR2	181
10	Subroutine MNCHN4	182

FLOW CHART NUMBER	TITLE	PAGE
11	Subroutine SEGSUB	183
12	Subroutine SETPH	185
13	Subroutine TISUB	186
14	Check for Case Termination	187

[illegible]

1.0 INTRODUCTION

This report describes a FORTRAN IV digital computer program, developed by The Boeing Company for operation on an IBM 7094 computer with an IBSYS version 13 monitor system from an earlier Thiokol Chemical Corporation program, to perform dynamic analyses of solid propellant rocket motor internal ballistics. A complete description of the mathematical model, the engineering equation development, the method of solution, and detailed programming information is presented to explain program principles and theory and to facilitate program maintenance and revision.

This program was developed under contract from the Army Missile Command Propulsion Laboratory, Redstone Arsenal, Alabama, contract number DA-01-021-AMC-15557(Z) by the Engineering Digital Computing Organization 2-2640, with support from the Missile and Information Systems Division, Flight Technology Propulsion Organization 2-5711 of The Boeing Company.

1.1 General Information

The report is divided into three volumes. Volume I, the Program Manual, provides a technical explanation of the theory, mathematical model, program capabilities and information necessary for program maintenance and revision. Volume II, the User's Guide, describes program options, preparation of input data and program output. Volume III, the Sample Case Results and Program Listings, contains the complete program listings of the computer program. The following paragraphs describe briefly the sections of the report comprising each volume.

Volume I

The Program Capabilities and Limitations, Section 2.0, indicates the capability the program has to evaluate grain designs and internal ballistics and the program limitations that exist in these areas.

The Method of Solution, Section 3.0, describes the method the program uses to obtain the internal ballistic solutions and the organization of major program sections which divide the solution into logical blocks or core loads that reside in core at separate times.

The Gas Dynamic Equation Development, Section 4.0, presents the development of the equations for the non-steady flow gas dynamics for both segmented and monolithic motors, propellant description, and for an accelerating reference system. In general, this section describes modifications made to the original Thiokol Chemical Corporation program for conducting design studies of solid propellant configurations (Reference 1) to simulate the

1.1 (Continued)

Internal ballistics of high burning rate propellants with characteristically short burn durations. These modifications were made specifically to include the storage of mass and momentum in the gas dynamic equations, to consider the effects of very high vehicle acceleration on the internal ballistics, and to study anisotropic propellant burning. As a result of these modifications, ignition transients may be calculated.

The Geometry Equation Development, Section 5.0, explains in detail the setup and solution of the grain geometry equations which determine the perimeter length, cross sectional area, burn surface area, moments of inertia, and center of gravity location of the various grain options and longitudinal configurations. The equation development and figures presented in this section were obtained from References 1 and 3.

The Detailed Programming Information, Section 6.0, presents a brief description of all program subroutines, macroscopic program logic flow charts, a description of the computing system and program storage allocation, program diagnostic aids, and a list of the program nomenclature. Appropriate comments are placed throughout the program listings as a supplement to the subroutine flow charts to assist in program maintenance and revision.

The Results, Section 7.0, presents a comparison of a computer prediction with three full scale HIBEX motor firings. Dimensionless fore-head pressure traces are shown for the computer prediction and the motor firings.

Volume II

The User's Guide, Section 8.0, presents an explanation of the required program inputs, sample cases showing the available program options, a description of the output format, and the required control cards to permit effective program use and operation without knowledge of the program technical aspects. This section is arranged to be complete without reference to the program manual technical sections and may be used independent of the program manual.

Volume III

The Listings, Section 9.0, contains the sample case results and program listings of the computer program.

1.2 History of Program Development

In March 1960, work was initiated at the Thiokol Chemical Corporation, Redstone Division, under the auspices of Systems Analysis Laboratory, Army Rocket and Guided Missile Agency, Redstone Arsenal, Alabama, for the development of a solid propellant rocket motor design program (References 1 and 2). In 1962, The Boeing Company received a copy of this program, and in 1963 developed a segmented motor version. In 1964, the Saturn Branch of the Aerospace Division of Boeing at New Orleans converted the SCAT machine language program to FORTRAN II for operation on the IBM 7094 computer. In 1965, The Boeing Aerospace Division in Seattle, Washington, converted the FORTRAN II version to FORTRAN IV for operation on the SRU 1107 and made the modifications discussed in Section 1.1 for the HIBEX contract to add the transient capability. In May 1966, The Boeing Company proposed to the Army Missile Command to segment the existing SRU 1108 program, perform the necessary conversion for operation on the IBM 7094, and completely document the advanced program version. A contract was received in July 1966 from the Army Missile Command for a 6 month development effort to perform the required conversion.

1.3 References

1. Control No. U-A-61-28A, "Final Report Design Study of Solid Propellant Configurations," Thiokol Chemical Corporation, Redstone Division, July 1961.

2. Control No. U-A-62-18A, "Final Report, Design Study of Solid Propellant Configuration," Thiokol Chemical Corporation, Alpha Division, May 1962.

3. T263206, "Generalized Wagon Wheel Grain Design Study," Thiokol Chemical Corporation, Wasatch Division, June 1962.

4. D2-99598-1, "HIBEX Rocket Motor Performance, Design and Development Analysis (U)," Confidential, Aero-Space Division, The Boeing Company, March 1966.

5. D2-125060-2, "Small High Performance Interceptor Research (U)," Confidential, Aero-Space Division, The Boeing Company, December 1966.

6. Leipmann, H. W., and Roshko, A., Elements of Gas Dynamics, GALCIT Aeronautical Series, John Wiley and Sons, Inc., Third Printing, February 1960.

7. Shapiro, Ascher H., The Dynamics and Thermodynamics of Compressible Fluid Flow, Volume I, The Ronald Press Co., 1953.

8. Baumeister, Theodore, Mark's Mechanical Engineer's Handbook, Sixth Edition, McGraw-Hill Book Company, 1958.

9. Univac 1107 Fortran Programmers Guide, U-3540, August 1963.

2.0 PROGRAM CAPABILITIES AND LIMITATIONS

This computer program was developed to calculate solid propellant rocket motor internal ballistics. Because of its development from earlier grain design and ballistic performance programs, additional capabilities are present. Throughout the development effort, all prior program capabilities have been retained so that a general program exists with both grain design and internal ballistic evaluation capability.

2.1 Program Capabilities

The basic propellant grain design is the forked wagon wheel, however, the grain design equations are general so that the conventional wagon wheel, standard star and circular port as well as the slotted-cone may be described by variations in the input data. Figure 2.1 shows the five grain design options. Other more complicated grain designs may be evaluated by describing the perimeter length and burn area as a function of distance burned and input to the computer program as tabular data.

The propellant grain configuration may be either monolithic or segmented with up to 11 slots. The propellant case and port cavity may be either cylindrical or tapered. The fore-head section configuration may be a straight through grain or may contain a complete web. Figure 2.2 shows the various motor configuration options. The aft-head section configuration is a straight through grain.

The propellant characteristics are described by definitive properties of the combustion gases and a generalized burning rate equation. The propellant gas properties may be held constant or may be varied as a function of the static pressure in the port cavity. The burning rate model includes erosive burning and will allow either isotropic or anisotropic burning of the propellant surface.

Either steady or non-steady flow gas dynamics are available to obtain the internal ballistic solution. The steady flow gas dynamics solve the momentum and continuity equations without consideration of time dependent terms such that there is no storage of mass or momentum (no capacitance effects). The non-steady flow gas dynamics solve the momentum and continuity equations with respect to time so that the storage of mass and momentum is considered and the start transient and tail-off intervals may be determined.

The effects of vehicle acceleration on the internal ballistic solution may be considered. The acceleration term is included in the momentum equation.

The effect of a tapered inert sliver may be considered in the cylindrical section for all but the forked wagon wheel grain design.

2.1 Program Capabilities (Continued)

The following is a summary of the program capabilities:

1.0 Grain Design

A. Circular Port
B. Standard Star
C. Slotted-Cone
D. Conventional Wagon Wheel
E. Forked Wagon Wheel
F. Tables of Perimeter and Burn Area as a Function of Distance Burned can be Input

2.0 Motor Configuration

A. Cylindrical Section
   1) Monolithic grain
   2) Segmented grain
   3) Tapered inert sliver

B. Fore-head Section
   1) Straight through grain
   2) Complete web (head-end with web)

C. Aft-head Section
   1) Straight through grain
   2) Burning on aft face

3.0 Propellant Characteristics

A. Isotropic Propellant Burning
B. Anisotropic Propellant Burning
C. Erosive Burning
D. Variable Gas Properties (function of static pressure)

4.0 Internal Ballistics

A. Steady Gas Flow

B. Non-Steady Gas Flow
   1) Ignition transient interval
   2) Web-time interval
   3) Tail-off interval

C. Vehicle Acceleration

2.1.1 Program Output

The program provides the following output:

1.0 Motor

- A. Delivered Thrust
- B. Vacuum Thrust
- C. Fore-head Total Pressure
- D. Nozzle Total Pressure
- E. Fore-head Total Pressure Time Integral
- F. Nozzle Total Pressure Time Integral
- G. Delivered Total Impulse
- H. Vacuum Total Impulse
- I. Nozzle Discharge Flow Rate
- J. Polar and Rectangular Moment of Inertia
- K. Center of Gravity

2.0 Propellant Characteristics

- A. Weight of Propellant Remaining
- B. Forward Tangent Plane Propellant Burning Rate
- C. Aft Tangent Plane Propellant Burning Rate
- D. Total Weight of Propellant Expended

3.0 Grain Geometry

- A. Cylindrical Section Burn Area
- B. Fore-head Section Burn Area
- C. Aft-head Section Burn Area
- D. Grain Segment Face Burn Area
- E. Total Motor Burn Area

4.0 Nozzle Characteristics

- A. Throat Area
- B. Effective Expansion Ratio (flow separation accounted for)
- C. Pressure Ratio Across Nozzle
- D. Momentum Portion of Thrust Coefficient

2.1.2 Program Assumptions

The following assumptions were made to translate the physical system into the one-dimensional gas dynamic model:

1. Propellant burning during ignition and steady state operation occurs normal to the grain surface.

2. The burn rate in the fore-head and aft-head sections is assumed to be constant over the burning surface of the entire section.

2.1.2 Program Assumptions (Continued)

3. Mass addition occurs instantaneously with no velocity component along the motor's longitudinal axis ($dZ/dt = 0$).

4. The products of combustion obey the perfect gas law.

5. The gas flow is one-dimensional and adiabatic.

6. The combustion temperature is constant throughout the motor.

7. The heat capacity of the combustion gases is constant.

8. The friction forces of the combustion gases in the port cavity are negligible.

9. The moments of inertia about the pitch and yaw axis are equal.

2.2 Limitations

The program has the following limitations:

1. A maximum of 11 reference planes are allowed in the cylindrical section to describe the grain design.

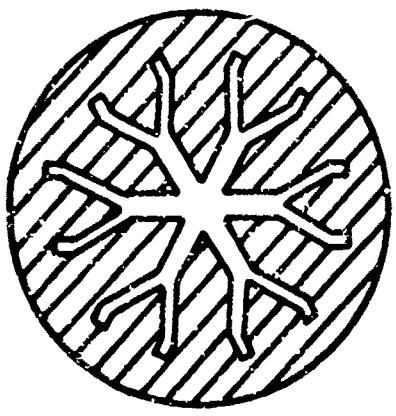
2. A maximum of 100 increment dividing planes are allowed in the cylindrical section to define the mass addition regions. If this restriction is exceeded by defining a ΔZ too small, the case execution will be terminated and an appropriate comment will be printed.

3. A maximum of 11 slots are allowed for segmented motors.

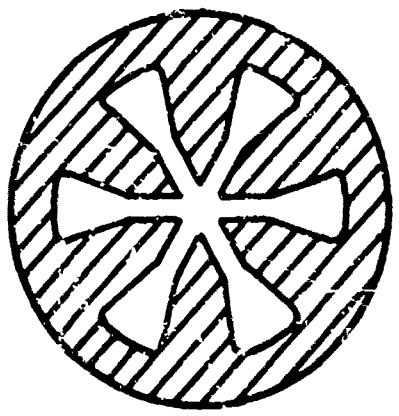
4. The slotted-cone grain design is applicable only to the cylindrical section. Burn area tables must be input for the forward and aft domes when this grain design is used.

5. The inert sliver option is restricted to the cylindrical section and does not apply to either end section.

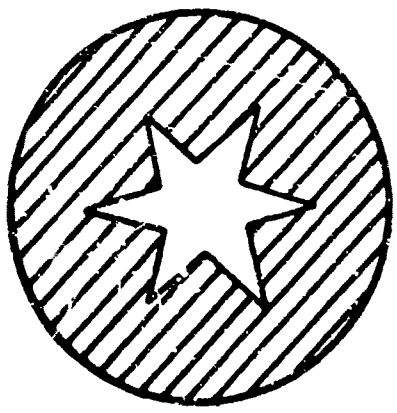
6. The effects of an accelerating reference system can be determined only for non-steady flow gas dynamics.



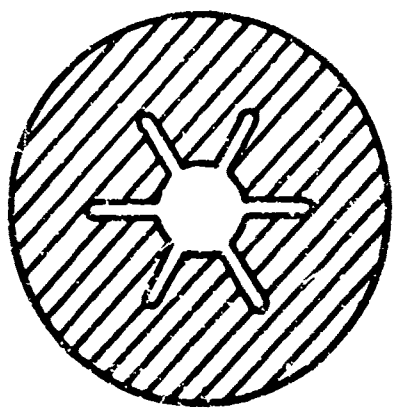
Forked Wagon Wheel



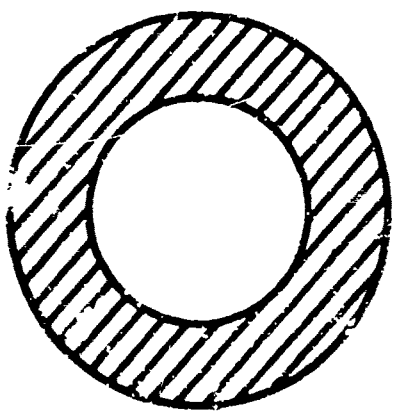
Conventional Wagon Wheel



Standard Star

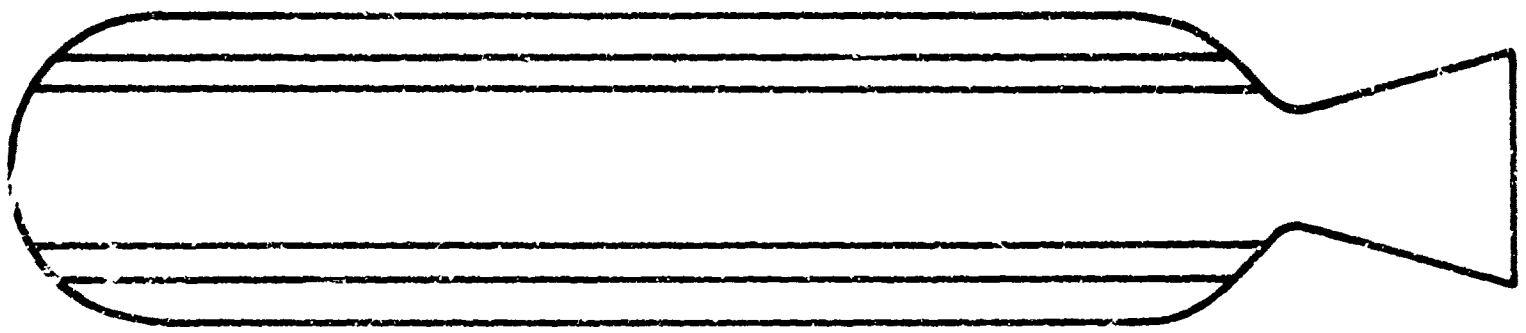


Slotted-Cone



Circular Port

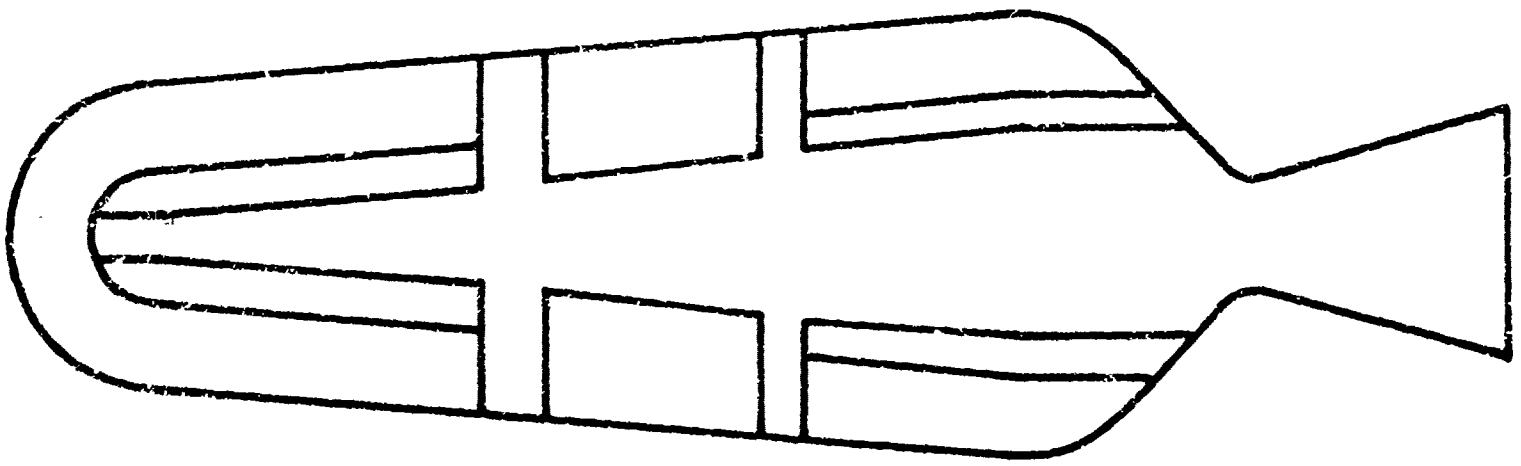
Figure 2.1. Grain Design Options



Monolithic Grain With Cylindrical Case



Monolithic Grain with Tapered Case
and Propellant Cutback in Aft-end



Segmented Grain with a Head-end with Web and Tapered Case

Figure 2.2. Typical Motor Configurations

3.0 METHOD OF SOLUTION

The program calculations are based on the geometrical model shown in Figure 3.1. The motor configuration is divided into three sections: the head-end section (forward dome), the cylindrical section, and the aft-head section (aft dome) or nozzle. The grain geometry is described by input reference planes within the cylindrical section. The cylindrical section, which may contain either a monolithic or a segmented grain, is further divided into a number of increments or mass addition regions by the location of increment dividing planes, at each reference plane and at specified intervals (ΔZ) from each reference plane until either a segment slot interface or the next reference plane is passed. During the computer solution of the gas dynamics, port perimeter, port cross sectional area and moments of inertia are determined at each increment dividing plane by linear interpolation between adjacent reference planes. Mass addition is assumed to occur as a step process between two increment dividing planes.

A

A

The program method of solution is divided into four separate computer core loads linked together by a main control program and a common data region. Each core load is unique, but dependent on preceding core loads for generated data. The flow chart shown in Figure 3.2 presents the macroscopic program order of solution with the separate core loads linked together.

The first computer core load contains the subroutines required to read the input data, initialize the data cells, compute the input reference plane constants, locate the increment dividing planes, check for input data errors, and print the program inputs and computed constants.

The second computer core load contains the geometry subroutines required to compute the initial propellant cross section area and perimeter length for the cylindrical section reference planes, the aft-head and straight through grain fore-head sections burn area and initial propellant volume as a function of distance burned. The moments of inertia and centers of gravity for the aft-head and straight through grain fore-head sections and the radius of gyration for the cylindrical section are also calculated. The computed values for each section are stored in tables for use during the solution of the internal ballistics in the fourth core load.

The third computer core load contains the geometry subroutines required to compute the initial propellant volume, burn area, moments of inertia, and CG location tables of the head-end with

web. The third core load is loaded only if a head-end with web is required after the cylindrical section and aft-head section geometry calculations have been completed in the second core load.

After the grain geometry calculations are performed in the first, second, and third core loads and the perimeter and area tables have been established, the internal ballistic solution is initiated in the fourth core load by determining the geometry values of each reference plane and each end section from a table look-up procedure in the geometry tables. For steady flow conditions, an initial estimate of the fore-head pressure is made, and the burning rate (which is assumed to be constant over the entire head-end section) is determined as described in Section 4.1.1. With this burn rate and the tabular value of the fore-head burn area, the instantaneous value of mass addition is determined for the fore-head section. The state and gas dynamic properties of the propellant at the forward tangent plane, the first increment dividing plane, are determined from the simultaneous solution of the momentum and continuity equations assuming perfect gas relationships.

The grain geometry at the first increment dividing plane is then determined and stored in temporary locations for future reference. The grain geometry of increment dividing plane two is determined. The increment section mass generation rate is determined from the perimeter lengths of increment dividing planes one and two, the increment length, and the burning rates at the upstream adjacent increment dividing planes. The propellant properties and mass flow at increment dividing plane two are then determined by a simultaneous solution of the momentum and continuity equations for either steady or non-steady flow conditions.

The above procedure is repeated for each cylindrical section mass addition region. Once the cylindrical section is complete, the same general calculations are performed for the aft-head section. The port cross sectional area and perimeter length and burning rate are assumed to be constant in the aft-head section and identical to the values at the aft tangent plane.

The nozzle throat area is compared to the maximum value that will maintain subsonic flow in the port. If this maximum value is exceeded, the program prints an error comment and terminates the case. If this maximum value is not exceeded, the flow rate of propellant discharge through the nozzle is computed on the basis of isentropic flow. This flow rate is compared to the flow rate of propellant discharged from the grain. If these two values do not agree within .1 percent, the fore-head pressure is adjusted and the program returns to the fore-head and repeats until

convergence is attained. Once equilibrium is reached, additional ballistic properties are computed and the performance data is printed.

Following the performance printout, the thickness burned in each increment dividing plane and slot interface is then determined from the previous web thickness. A check is then made to see if burnout has occurred at any of the increment dividing planes. If burnout occurs, a comment is printed that the increment dividing plane has burned out. The progression of the slot interfaces for segmented motors is indicated by a printout of the increment dividing plane longitudinal location.

The time is then incremented by the computed time interval and the program returns to the fore-head to compute new equilibrium conditions and determine new values of the perimeter length and port cross section area at each increment dividing plane and burn area for each end section. This process is then repeated until the termination option is exceeded.

The general program solution of the internal ballistics outlined above is modified for non-steady flow conditions. When the start transient interval is computed, the fore-head pressure is defined by tabular input of the fore-head pressure as a function of time, or the burn rate coefficient is defined by tabular input of the burn rate coefficient as a function of distance burned. When the fore-head pressure is input for the start transient, the burn rate coefficient is varied to obtain convergence; and when the burn rate coefficient is input for the start transient, the fore-head pressure is varied, as for steady flow conditions, to obtain convergence. When the fore-head pressure is input for the start transient, an initial estimate of the burn rate coefficient is made by computing a first guess of the burn rate coefficient from the motor configuration parameters and the fore-head pressure variation. With this burn rate coefficient, the instantaneous value of mass addition and mass discharge is determined for the head-end section. The propellant gas properties for the first increment dividing plane are then determined from a simultaneous solution of the non-steady gas flow equations as above. The remainder of the ballistic solution is unchanged.

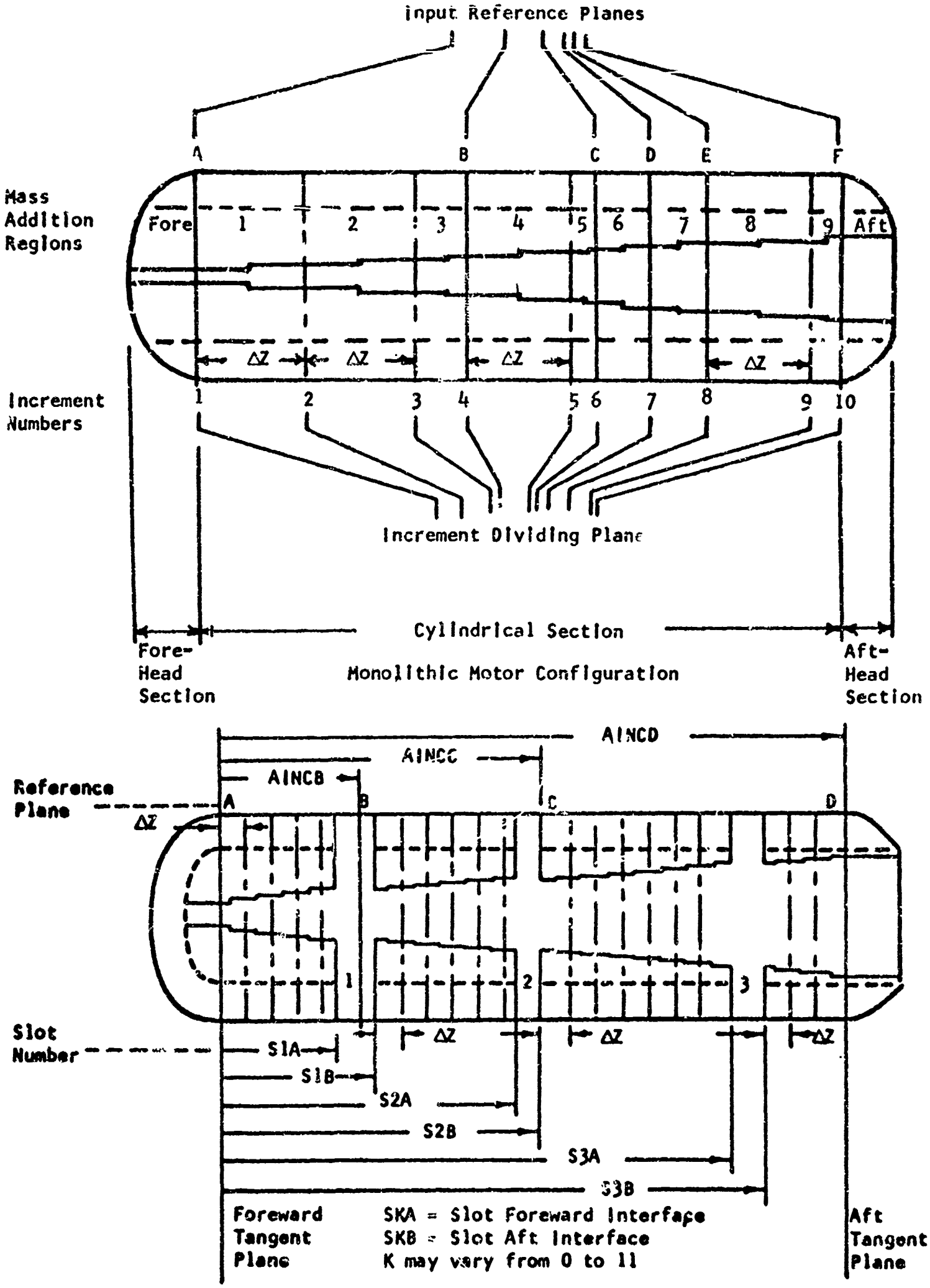


Figure 3.1 Reference Plane and Increment Dividing Plane Identification

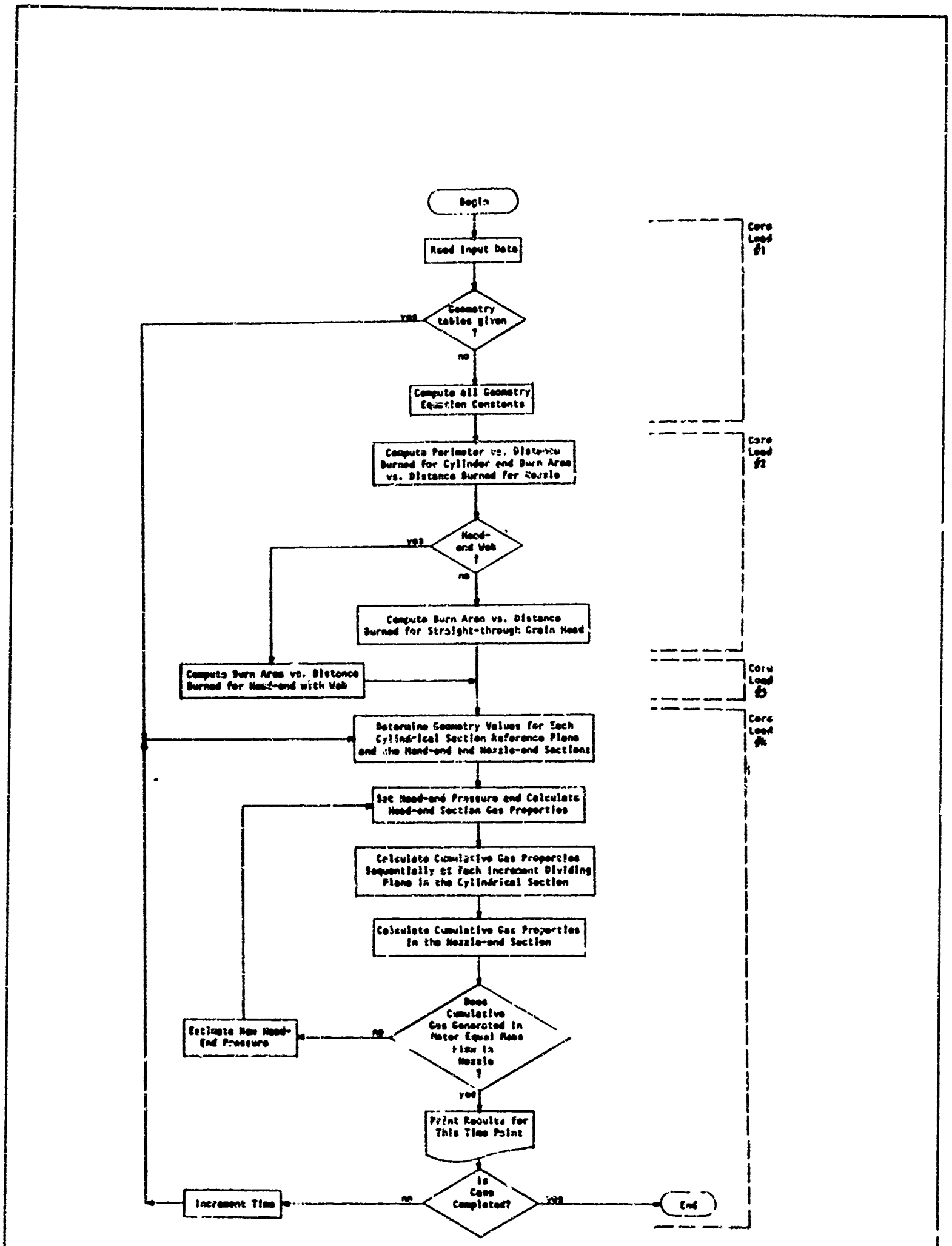


Figure 3.2 Macroscopic Flow Chart

4.0 GAS DYNAMIC EQUATION DEVELOPMENT

The static and total pressure, temperature, velocity, and flow rate of the gas along the length of the propellant grain and through the nozzle are required to determine the progression of the propellant burning surface and motor performance parameters such as chamber pressure, thrust, and total impulse. These parameters are obtained from an iterative solution of the perfect gas law and the equations of continuity, momentum, and energy for one-dimensional gas flow. The gas flow along the propellant grain is determined by dividing the grain into a number of increments which are termed mass addition regions. Two control volumes are shown in Figures 4.1 and 4.2 which define the mass addition regions for the monolithic and segmented motor configurations shown in Figure 4.3. The gas dynamic equations, which are solved for each mass addition region along the propellant grain, are described in the following sections. The isotropic and erosive burning rate equation, anisotropic mass generation model, and propellant gas properties required for the calculations are also described.

4.1 Gas Dynamics for Incremental Control Volumes

The solution of the continuity, momentum, and energy equations for the mass addition regions along the propellant grain and through the nozzle are described in this section. Steady flow, non-steady flow, or non-steady flow with acceleration may be selected.

The following assumptions are basic to the development of the gas dynamic equations:

1. Mass addition occurs as an instantaneous process with no velocity component parallel to the motor axis ($dZ/dt = 0$).

2. The products of combustion obey the perfect gas law.

3. The gas flow is one-dimensional and adiabatic.

4. The combustion temperature, specific heat ratio, and molecular weight are constant throughout the motor.

5. The friction forces of the combustion gases in the port cavity are negligible.

6. The static pressure is constant across the fore-head section, i.e., no static pressure loss resulting from mass addition or area change.

7. The port area and perimeter are constant across the aft-head section from the aft tangent plane to the grain exit, i.e., constant area duct.

4.1 Gas Dynamics for Incremental Control Volumes (Continued)

The control volume or mass addition region inlet is defined as station 1 and outlet is defined as station 2 as shown in Figures 4.1 and 4.2. The analysis of the mass addition regions along the grain segments is accomplished in subroutines AIBSUB and AIBST to obtain the solution for the discharge pressure, temperature, and flow rate from known inlet conditions at station 1 and a known value of the instantaneous mass generation rate. The instantaneous mass generation rate is determined from the port perimeters, upstream burning rates, and mass addition region incremental length as follows:

$$\dot{dW} = \frac{(L_{p1} R_{b1} + L_{p2} R_{b2})}{2} \Delta Z \rho_f$$

where

$\dot{dW}$ = mass generation rate, lb/sec

L_{p1} = port perimeter at station 1, in

L_{p2} = port perimeter at station 2, in

ΔZ = mass addition region length, in

ρ_f = solid propellant density, lb/in^3

R_{b1} = burning rate at station 1, in/sec (determined from conditions at adjacent upstream increment dividing plane)

R_{b2} = burning rate at station 2, in/sec (determined from conditions at adjacent upstream increment dividing plane)

A mass balance for the slots between the grain segments is obtained in subroutine SLOT. The instantaneous mass generation rate at each slot interface is determined as follows:

$$\dot{dW} = A_f \rho_f a P^n$$

where

A_f = burning area at slot interface, in^2

P = slot interface static pressure, lb/in^2

a = slot burn rate coefficient

n = slot burn rate coefficient pressure exponent

The general energy equation and the perfect gas law are applied at station 2 to obtain the state properties:

4.1 Gas Dynamics for Incremental Control Volumes (Continued)

$$U = \left[\frac{2 g_o R \gamma (T_o - T)}{\gamma - 1} \right]^{1/2} \qquad \text{(general energy)}$$

$$P = 12 \rho R T \qquad \text{(perfect gas)}$$

The continuity and momentum equations are iterated to obtain the discharge pressure, P_2, and flow rate, $\dot{W}_2$, for each mass addition region. For steady flow conditions, the basic equations are as follows:

$$12 \rho_1 A_1 U_1 + d\dot{W} = 12 \rho_2 A_2 U_2 \qquad \text{(continuity)}$$

$$P_1 A_1 + \frac{P_1 + P_2}{2} (A_2 - A_1) - P_2 A_2 = \frac{12 \rho_1 A_1 U_1}{g_o} (U_2 - U_1) + \frac{U_2 \, d\dot{W}}{g_o} \qquad \text{(momentum)}$$

For non-steady flow conditions, the basic equations are as follows:

$$\dot{W}_2 = \dot{W}_1 + d\dot{W} - \frac{dW}{dt} \qquad \text{(continuity)}$$

$$\frac{dW}{dt} = \frac{\partial}{\partial t} \left[\left(\frac{P_1 + P_2}{T_1 + T_2} \right) \frac{V}{12R} \right] \qquad \text{(perfect gas)}$$

$$\frac{\partial}{\partial t} \int_1^2 \frac{(\rho \, dA)}{g_o} dX + \frac{(\rho_2 U_2^2 A_2 - \rho_1 U_1^2 A_1)}{g_o} = P_1 A_1 - P_2 A_2 + \frac{P_1 + P_2}{2} (A_2 - A_1) \qquad \text{(momentum)}$$

where

P = static pressure, lb/in^2
U = velocity, ft/sec
$\dot{W}$ = flow rate, lb/sec

4.1 Gas Dynamics for Incremental Control Volumes (Continued)

T = static temperature, °R

A = port cross sectional area, in^2

V = port volume of mass addition region, in^3

ρ = density, lb/in^3

R = gas constant, °R/ft

4.1.1 Steady Flow Gas Dynamics

The original program developed by the Thiokol Chemical Corporation (references 1 and 2) based the internal gas dynamics on steady flow. Continuity and momentum equations were iterated to obtain mass addition region discharge pressure, temperature, and velocity. This capability is retained in subroutine AIBSUB. The steady flow solution for a segment slot is obtained in subroutine SLOT by neglecting the time dependent terms of the non-steady flow equations. Therefore the steady flow option can be exercised for both monolithic and segmented grain motor designs.

The solution of the steady flow gas dynamics is obtained from an iterative solution of the continuity and momentum equations with the general energy equation and perfect gas law applied at the discharge section to obtain the density and temperature of the combustion gases. The discharge flow rate is obtained from the sum of the mass generation rate and inlet mass flow. An initial value of the discharge velocity is then obtained from the momentum equation, assuming $P_2 = P_1$, and a starting value of the discharge density is obtained from the continuity equation. With the initial value of the discharge density, the following iterative procedure is employed to converge the steady flow equations.

Initially, a guess of the discharge velocity U_2 is obtained from the momentum equation by assuming no pressure loss, $P_2 = P_1$, as follows:

$$\frac{12\ \rho_1\ A_1\ U_1}{g_o}\ (U_2 - U_1) + \frac{U_2\ \dot{dW}}{g_o} = 0$$

or

$$\frac{\dot{W}_1\ U_2}{g_o} - \frac{\dot{W}_1\ U_1}{g_c} + \frac{U_2\ \dot{dW}}{g_o} = 0$$

4.1.1 Steady Flow Gas Dynamics (Continued)

and

$$\dot{W}_1 U_1 = \dot{W}_1 U_2 + U_2 d\dot{W} = \dot{W}_2 U_2$$

From the perfect gas law and continuity equation:

$$U_2 = \frac{\dot{W}_1 U_1}{\dot{W}_2} = \frac{\dot{W}_1 U_1}{\rho_2 A_2 U_2} = \frac{\dot{W}_1 U_1}{\frac{P_2 A_2 U_2}{12\ RT_2}}$$

or

$$U_2^2 = \dot{W}_1 U_1 \frac{12\ RT_2}{P_2 A_2}$$

Using the general energy equation:

$$\frac{2g_o R \gamma (T_o - T_2)}{\gamma - 1} = \dot{W}_1 U_1 \frac{12\ RT_2}{P_2 A_2}$$

Multiplying both sides of the above equation by $-2A_2$ and adding like terms to eliminate T_2 yields:

$$\frac{-2\ g_o R \gamma (T_o - T_2)}{\gamma - 1} 2A_2 + (A_1 + A_2) g_o R\ T_o - (A_1 + A_2) g_o R\ T_o$$

$$+ (A_1 + A_2) g_o R\ T_2 - (A_1 + A_2) g_o R T_2 = \frac{-2A_2\ \dot{W}_1 U_1 R T_2}{P_2\ A_2}$$

Rearranging and combining terms yields:

$$\left[\frac{-2g_o \gamma (T_o - T_2)}{\gamma - 1} 2A_2 + (A_1 + A_2) g_o R (T_o - T_2) \right] + \left[(A_1 + A_2) g_o R T_2 + \frac{2A_2\ \dot{W}_1 U_1 R T_2}{P_2 A_2} \right] - (A_1 + A_2) g_o R T_o =$$

Multiplying through by $\dot{W}_2$ and again rearranging terms yields:

4.1.1 Steady Flow Gas Dynamics (Continued)

$$\dot{W}_2 \frac{2g_o\gamma(T_o-T_2)}{\gamma-1}\left[-2A_2 + \frac{(\gamma-1)(A_1+A_2)}{2\gamma}\right] + \left[(A_1+A_2)g_oRT_2 + \frac{2A_2\dot{W}_1U_1RT_2}{P_2A_2}\right]\dot{W}_2 - (A_1+A_2)g_oRT_o\dot{W}_2 = 0$$

The terms in the second set of brackets may be rearranged with the perfect gas law, remembering that $P_2 = P_1$:

$$\dot{W}_2 \frac{2g_o\gamma(T_o-T_2)}{\gamma-1}\left[-2A_2 + \frac{(\gamma-1)(A_1+A_2)}{2\gamma}\right] + \left[(A_1+A_2)g_oP_1A_2 + 2A_2\dot{W}_1U_1\right]U_2 - (A_1+A_2)g_oRT_o\dot{W}_2 = 0$$

Thus, from the general energy equation:

$$-\dot{W}_2U_2^2\left[2A_2 - \left\{\frac{\gamma(A_1+A_2)}{2\gamma} - \frac{(A_1+A_2)}{2\gamma}\right\}\right] + \left[(A_1+A_2)g_oA_2P_1 + 2A_2\dot{W}_1U_1\right]U_2 - (A_1+A_2)T_oRg_o\dot{W}_2 = 0$$

The above equation is solved for U_2 using the quadratic formula as follows:

$$CAA = -\dot{W}_2\left[2A_2 - \left\{\frac{\gamma(A_1+A_2)}{2\gamma} - \frac{(A_1+A_2)}{2\gamma}\right\}\right]$$

$$CBB = (A_1+A_2)g_oA_2P_1 + 2A_2\dot{W}_1U_1$$

$$CC = -(A_1+A_2)T_oRg_o\dot{W}_2$$

$$RAD = CBB^2 - (4CC)CAA$$

$$Temp_6 = 1 - \frac{RAD^{1/2}}{CBB}$$

$$U_{Tmp} = \frac{CBB\ Temp_f}{2\ CAA}$$

4.1.1 Steady Flow Gas Dynamics (Continued)

where U_{Tmp} is based on the assumption of $P_2 = P_1$ and is used only once in calculating the initial value of ρ_{tmp}.

The continuity and momentum equations are iterated by converging on the discharge density as follows:

1. $\rho_{tmp} = \dfrac{\dot{W}_2}{12\ A_2\ U_{Tmp}}$ (continuity)

   where $\dot{W}_2 = \dot{W}_1 + d\dot{W}$

2. $U_{Tmp} = \dot{W}_2/12A_2\ \rho_{tmp}$

3. $T_{Tmp} = T_o - \dfrac{(\gamma-1)\ U_{Tmp}}{2g_o\ R\gamma}$ (general energy)

4. $P_{Tmp} = P_1 - \dfrac{2(\dot{W}_2\ U_{Tmp} - \dot{W}_1 U_1)}{g_o(A_1+A_2)}$ (momentum)

5. $\rho_2 = \dfrac{P_{Tmp}}{12\ R\ T_{Tmp}}$ (perfect gas)

6. $Temp = \rho_{tmp} - \rho_2$

7. If $\dfrac{|Temp|}{\rho_{Tmp}} \leq .0001$ go to 8, otherwise set $\rho_{tmp} = \rho_2$ and return to 2.

8. $P_2 = P_{Tmp}$
   $T_2 = T_{Tmp}$
   $U_2 = U_{Tmp}$

9. Determine discharge mach number,

4.1.1 Steady Flow Gas Dynamics (Continued)

$$M_2 = \left[\frac{2(T_o - T_{Tmp})}{(\gamma-1)T_{Tmp}} \right]^{1/2}$$

4.1.2 Non-Steady Flow Gas Dynamics

The non-steady flow gas dynamic equations were developed to predict ignition and tail-off transients. The non-steady gas flow equations account for mass, momentum, volume, and pressure within the control volume varying with time. The fundamental equations of momentum and continuity along with the perfect gas law are expressed in partial differential form and then integrated across the control volume describing an incremental mass addition region using the technique of finite differences.

The gas dynamic solution for the mass addition regions is obtained by iterating the continuity and momentum equations for the discharge pressure, temperature, and flow rate. When the solution of the above discharge parameters have converged, the discharge values of mach number, density, and total pressure are determined. The derivation of the time dependent momentum equation and discharge flow rate and pressure equations are presented in the following sections for a mass addition region, Figure 4.1, and a segment slot, Figure 4.2.

4.1.2.1 Mass Addition Region

This section develops gas dynamic equations and solutions for a mass addition region as shown in Figure 4.1. The equation development from fundamental engineering principles to obtain the discharge conditions is taken from reference 6 and is presented below. The discharge pressure,

$$P_2 = \left[\frac{\dot{W}_1 U_1}{g_o} - \frac{\dot{W}_2 U_2}{g_o} + P_1 A_1 + \frac{P_1+P_2}{2}(A_2-A_1) - \frac{(P_1+P_2)(U_1+U_2)(V-V')}{24 g_o R(T_1+T_2)\Delta t} - \frac{V(U_1+U_2)(P_1+P_2-P_1'-P_2')}{24 g_o R(T_1+T_2)\Delta t} \right] \Big/ A_2 + \left[\frac{(P_1+P_2)(A_1+A_2)a\,\Delta Z}{24 R(T_o+T_2)g_o} \right] \Big/ A_2$$

4.1.2.1 Mass Addition Region (Continued)

and discharge flow rate,

$$\dot{W}_2 = \dot{W}_1 + d\dot{W} - \frac{(P_1+P_2)}{12R(T_1+T_2)} \frac{V-V'}{\Delta t} - \frac{V(P_1+P_2-P_1'-P_2')}{12R(T_1+T_2)\Delta t}$$

where

V = current port volume, in^3

V' = one past time increment volume, in^3

P_1' = inlet past time increment pressure, lb/in^2

P_2' = discharge past time increment pressure, lb/in^2

Δt = time increment, sec

a = vehicle longitudinal acceleration, ft/sec^2

are iterated in subroutine AIBST to obtain the solution of the gas dynamic equations for a mass addition region. Total pressure, static temperature, mach number, and density are then calculated at the discharge station 2.

The derivation of the above equations and method of convergence follows:

Starting with the continuity equation:

1. $\frac{\partial}{\partial x}(\rho U A) + \frac{\partial}{\partial t}(\rho A) = 0$ (continuity equation)

Integrating with respect to x between station 1 and 2 gives:

2. $\rho_2 U_2 A_2 - \rho_1 U_1 A_1 + \frac{\partial}{\partial t} \int_1^2 \rho A \, dx = 0$

The first two terms are the discharge and inlet mass flow rates, $\dot{W}_1$ and $\dot{W}_2$, respectively. The integral is the rate of change of mass between the stations 1 and 2 and may be evaluated as follows:

3. $\frac{\partial}{\partial t} \int_1^2 \rho A \, dx = \frac{\partial}{\partial t} \rho_m V - d\dot{W}$

where

4.1.2.1 Mass Addition Region (Continued)

$$V = \int_1^2 A\,dx,\ in^3$$

ρ_m = average density, lbm/ft^3

$d\dot{W}$ = mass flow generated in the section, lb/sec

and upon differentiation:

$$4.\quad \frac{\partial}{\partial t}(\rho_m V) = \rho_m \frac{dV}{dt} + V \frac{d\rho_m}{dt}$$

Combining terms and using finite differences with the perfect gas law yields from the continuity equation the solution of the discharge mass flow in terms of the pressures and control volume:

$$5.\quad \dot{W}_2 = \dot{W}_1 + d\dot{W} - \frac{P_1+P_2}{12R(T_1+T_2)} \frac{V-V'}{\Delta t} - \frac{V}{12R(T_1+T_2)} \frac{P_1+P_2 - P_1'-P_2'}{\Delta t}$$

Euler's fluid acceleration equation for unit mass is:

$$6.\quad \frac{\partial U}{\partial t} + u \frac{\partial U}{\partial x} = -\frac{g_o}{\rho} \frac{\partial P}{\partial x}$$

Multiplying Euler's equation (6) by ρA and the continuity equation (1) by U gives:

$$7.\quad \rho A \frac{\partial U}{\partial t} + \rho U A \frac{\partial U}{\partial x} = -g_o A \frac{\partial P}{\partial x}$$

and

$$8.\quad U \frac{\partial}{\partial t}(\rho A) + U \frac{\partial}{\partial x}(\rho U A) = 0$$

Adding equations (7) and (8), and combining appropriate terms, yields the one-dimensional momentum equation:

$$9.\quad \frac{\partial}{\partial t} \frac{(\rho U A)}{g_o} + \frac{\partial}{\partial x} \frac{(\rho U^2 A)}{g_o} = -A \frac{\partial P}{\partial x} = -\frac{\partial}{\partial x}(PA) + P \frac{\partial A}{\partial x}$$

4.1.2.1 Mass Addition Region (Continued)

Then, integrating equation (9) with respect to x between station 1 and 2 gives:

$$10.\quad \frac{\partial}{\partial t}\int_1^2 \frac{(\rho UA)}{g_o}\,dx + \frac{(\rho_2 U_2^2 A_2 - \rho_1 U_1^2 A_1)}{g_o} = (P_1A_1 - P_2A_2) + \int_1^2 P\,dA$$

The last integral may be evaluated by defining a mean pressure, P_m, thus:

$$11.\quad \int_1^2 P\,dA = P_m(A_2 - A_1)$$

The first integral of equation (10) is the rate of change of momentum from nonstationary changes between stations 1 and 2 and may be evaluated by defining a mean density, ρ_m, and a mean velocity, U_m, and integrating with respect to x, thus:

$$12.\quad \frac{\partial}{\partial t}\int_1^2 \frac{(\rho UA)}{g_o}\,dx = \frac{\partial}{\partial t}\,\frac{(\rho_m U_m V)}{g_o}$$

and upon differentiation:

$$13.\quad \frac{\partial}{\partial t}\,\frac{(\rho_m U_m V)}{g_o} = \frac{\rho_m U_m}{g_o}\,\frac{dV}{dt} + \frac{\rho_m V}{g_o}\,\frac{d U_m}{dt} + \frac{U_m V}{g_o}\,\frac{d \rho_m}{dt}$$

Letting $\frac{d U_m}{dt} = 0$ and combining terms using finite differences with the perfect gas law yields from the momentum equation the solution of the discharge pressure in terms of the mass flows and pressures:

$$14.\quad P_2 = \left[\frac{\dot{W}_1 U_1}{g_o} - \frac{\dot{W}_2 U_2}{g_o} + P_1A_1 + \frac{P_1+P_2}{2}(A_2 - A_1) - \frac{(P_1+P_2)(U_1+U_2)(V-V')}{24\, g_o R(T_1+T_2)\,\Delta t} - \frac{V(U_1+U_2)(P_1+P_2-P_1'-P_2')}{24\, g_o R(T_1+T_2)\,\Delta t} \right] \Big/ A_2$$

The acceleration term to be added to equation 14 is derived in Section 4.1.3.

4.1.2.1 Mass Addition Region (Continued)

Equations (5) and (14) are iterated in subroutine AIBST to solve for discharge temperature, pressure, and flow rate at each mass addition region as follows:

1. Estimate a starting value of the discharge pressure and temperature using the influence coefficient equations for constant specific heat and molecular weight, reference 7.

$$DT = T_1(\gamma-1)\left[\frac{(1+\gamma M_1^2)\, M_1^2\, d\dot{W}}{(1-M_1^2)\,\dot{W}_1}\right]$$

a) $$T_{2guess} = T_1 - DT$$

$$DP = P_1\, d\dot{W}\, 2\gamma M_1^2 \left[\frac{1+\frac{(\gamma-1)\, M_1^2}{2}}{\dot{W}_1\,(1-M_1^2)}\right]$$

b) $$P_{2guess} = P_1 - DP$$

2. Determine the gas storage:

$$\frac{dW}{dt} \simeq \left[\frac{(P_1+P_{2guess})(2V-V')-V(P_1'+P_2')}{12\, R(T_1+T_{2guess})\,\Delta t}\right]$$

3. Determine the discharge flow rate:

$$\dot{W}_2 = \dot{W}_1 + d\dot{W} - \frac{dW}{dt}$$

4. Determine the discharge velocity:

$$U_2 = \frac{\dot{W}_2\, R\, T_{2guess}}{P_2\, A_2}$$

4.1.2.1 Mass Addition Region (Continued)

5. Determine the discharge pressure (equation 14 above):

$$P_2 = \left\{ \frac{\dot{W}_1 U_1}{g_o} - \frac{\dot{W}_2 U_2}{g_o} + P_1 A_1 + \frac{(P_1+P_{2guess})}{2} (A_2-A_1) - \left[V(U_1+U_2)(P_1+P_{2guess} - P_1' - P_2') + (P_1+P_{2guess})(U_1+U_2)(V-V') \right] \Big/ \left[24\, g_o\, R\, (T_1+T_{2guess})\Delta t \right] \right\} \Big/ A_2$$

6. If an accelerating reference system is considered (see Section 4.1.3 for derivation):

If $\frac{a}{g_o} > 0$, determine acceleration term:

$$Temp = \left[(P_1+P_{2guess})(A_1+A_2) \frac{a}{g_o} \Delta Z \right] \Big/ \left[24\, R (T_1+T_{2guess}) A_2 \right]$$

$$P_2 = P_2 + Temp$$

7. If $\left| \frac{P_2-P_{2guess}}{P_{2guess}} \right| \leq .001$, go to step 8, otherwise obtain new value of P_{2guess} using method of false position and return to step 1(b).

8. Determine U_2 based on converged P_2:

$$U_2 = \frac{\dot{W}_2 R T_{2guess}}{P_2 A_2}$$

9. Determine the discharge temperature using the general energy equation:

$$T_2 = T_o - \frac{(\gamma-1) U_2^2}{2 g_o \gamma R}$$

4.1.2.1 Mass Addition Region (Continued)

10. If $\left|\frac{T_{2guess} - T_2}{T_{2guess}}\right| \leq .001$, go to step 11, otherwise obtain new value of T_{2guess} using method of false position and return to step 1(a).

11. Solution is converged, determine discharge mach number, gas density, and total pressure:

$$M_2 = U_2 \Big/ \left[g_o \gamma R T_2 \right]^{1/2}$$

$$\rho_2 = \frac{\dot{W}_2}{12 A_2 U_2}$$

$$P_{02} = P_2 \left(\frac{T_o}{T_2} \right)^{\frac{\gamma}{\gamma-1}}$$

4.1.2.2 Segment Slot Mass Addition

The development of the gas dynamic equations for the region between grain segments of segmented motors (referred to as a slot) is similar to the non-steady gas flow equation development for a mass addition region, Section 4.1. The control volume for a slot is defined from the forward slot interface to the aft slot interface with mass addition occurring at each interface and not within the control volume. The control volume for a slot is shown in Figure 4.2.

The following assumptions are made in subroutine SLOT (including the assumptions of Section 4.1):

a. The static pressure and temperature at the slot interface is the same as the port static pressure, $P_1 = P_2$, $P_3 = P_4$, $T_1 = T_2$, and $T_3 = T_4$.

b. The mass flow generated at the slot interface is a function of the port static pressure only and is determined from the following burn rate equation:

$$d\dot{W} = A_f \rho_f a P^n$$

4.1.2.2 Segment Slot Mass Addition (Continued)

where:

$\dot{dW}$ = generated mass flow, lb/sec

A_f = burn area at slot interface, in^2

ρ_f = solid propellant density, lb/in^3

P = slot interface static pressure lb/in^2

a = burn rate coefficient

n = burn rate equation pressure coefficient.

c. Static pressure at station 3 is a function of the area change (dA/dx), and the capacitance effects (dP/dt and dV/dt) between stations 2 and 3, and acceleration of the vehicle.

The solution of the gas dynamics within a slot is obtained from the above assumptions and the equations developed in Section 4.0 as follows:

1. Determine the mass generation rate at the forward slot interface (station 2) from the static pressure at station 1 (port cavity discharge)

$$\dot{dW}_f = A_f \rho_f a P^n$$

2. Determine the inlet flow rate, velocity, and mach number:

$$\dot{W}_2 = \dot{W}_1 + \dot{dW}_f$$

$$U_2 = \frac{\dot{W}_2 R T_1}{P_1 A_2}$$

$$M_2 = \frac{U_2}{\left[g_o k R T_1\right]^{1/2}}$$

3. Determine the current slot volume and rate of change of volume:

$$V = \frac{A_2 + A_3}{2} (Z_3 - Z_2)$$

where

4.1.2.2 Segment Slot Mass Addition (Continued)

Z_3 = aft interface station location, in.

Z_2 = forward interface station location, in.

$$\frac{dV}{dt} = \frac{\pi}{2\Delta t}\left[\tau_f(R_{f2}^2 + R_{SLOTf}^2) + \tau_2(R_{f3}^2 + R_{SLOTa}^2)\right]$$

where

τ_f = current value of forward slot interface distance burned in.

τ_a = current value of aft slot interface distance burned in.

4. Guess the value of the slot aft interface static pressure and temperature using the influence coefficient equations for constant specific heat and molecular weight, reference 7.

$$dT = \frac{T_1(\gamma-1)(1+\gamma M_2^2) M_2^2 \dot{dW}_f}{(1-M_2^2)\dot{W}_2}$$

$$dP = \frac{P_1 \dot{dW}_f 4 g_o M_2^2 (1+\frac{\gamma-1}{2} M_2^2)}{\dot{W}_2(1-M_2^2)}$$

$$P_{3guess} = P_2 - dP$$

$$T_{3guess} = T_1 - dT$$

5. Determine the mass generation rate at the aft slot interface (station 3) from the guessed static pressure at station 3:

$$\dot{dW}_a = A_a a P_{3guess}^n$$

6. Determine the stored gas in the slot

$$\frac{dW}{dt} = \frac{(P_2+P_{3guess})}{12 R(T_1+T_{3guess})}\frac{dV}{dt} + \frac{V}{12 R(T_1+T_{3guess})}\frac{(P_2+P_{3guess}-P_2'-P_3')}{\Delta t}$$

4.1.2.2 Segment Slot Mass Addition (Continued)

where

$$\frac{dW}{dt} = \frac{\partial}{\partial t}\left(\frac{P\,V}{12\,RT}\right)$$

7. Determine the discharge flow rate and velocity:

$$\dot{W} = \dot{W}_2 + d\dot{W}_a - \frac{dW}{dt}$$

$$U_3 = \frac{\dot{W}_3\,R\,T_{3guess}}{P_{3guess}\,A_3}$$

8. Determine the aft slot interface static pressure (see Section 4.1.2.1, equation 14).

$$P_3 = \left[\frac{\dot{W}_2U_2}{g_o} - \frac{\dot{W}_3U_3}{g_o} + P_2A_2 + \frac{P_2+P_{3guess}}{2}(A_3 - A_2)\right.$$

$$- \frac{(P_2+P_{3guess})(U_2+U_3)}{24g_oR(T_{3guess}+T_1)}\,\frac{dV}{dt}$$

$$\left. - \frac{V(U_2+U_3)(P_2+P_{3guess} - P_2^i-P_3^i)}{24g_o\,R(T_{3guess}+T_1)\,\Delta t}\right] \Big/ A_3$$

$$+ \left[\frac{(P_2+P_{3guess})(A_2+A_3)a\,\Delta Z}{24g_o\,R(T_2+T_{3guess})}\right] \Big/ A_3$$

9. If $\left|\frac{P_3-P_{3guess}}{P_3}\right| \leq$ CRP, go to step 10, otherwise obtain new value of P_{3guess} using method of false position and return to step 5. If CRP is not input the program will set CRP equal to .001.

10. Determine the slot aft interface static temperature from the general energy equation:

4.1.2.2 Segment Slot Mass Addition (Continued)

$$T_3 = TO - \frac{(\gamma - 1)\, U_3^2}{2\, g_o\, \gamma\, R}$$

11. If $\left|\frac{T_3 - T_{3guess}}{T_3}\right| \leq$ CRT, go to step 12, otherwise obtain new value of T_{3guess} using method of false position and return to step 7. If CRT is not input the program will set CRT equal to .001. A A

12. Determine the slot discharge velocity, mach number, density, and total pressure:

$$U_4 = \frac{\dot{W}_3\, R\, T_3}{P_3\, A_4}$$

$$M_4 = \frac{U_4}{\left[g_o\, \gamma\, R T_3\right]^{1/2}}$$

$$\rho_4 = \frac{\dot{W}_3}{12\, A_4\, U_4}$$

$$PC = P_3 \left(\frac{T_0}{T_3}\right)^{\frac{\gamma}{\gamma-1}}$$

4.1.3 Non-Steady Flow Gas Dynamics with Acceleration

The effects of longitudinal acceleration of the vehicle on the internal ballistic solution is considered in this section. In conventional gas dynamic studies, the effects of gravitational forces are not considered because, for compressible fluids, gravitational forces are significantly less than surface forces. Recent development of missiles for low level ICBM intercept may require boost accelerations that are of significant magnitude to affect motor internal pressures and temperatures. In an accelerating reference system, the force field which results from the acceleration is equivalent to a gravitational force field in a nonaccelerating reference system.

4.1.3 Non-Steady Flow Gas Dynamics with Acceleration

The acceleration effects are considered only on the gas dynamic equations in the port cavity of the motor and not in the nozzle. Effect of acceleration on a nozzle is to move the sonic point upstream of the throat. The effect of acceleration on the motor internal ballistics is to reduce the pressure drop along the propellant grain as well as fore-head pressure.

The resulting acceleration term is added to the momentum equation as follows;

$$\frac{\partial}{\partial t}\int_1^2 \frac{(\rho U A)}{g_o}\,dx + \frac{(\rho_2 U_2^2 A_2 - \rho_1 U_1^2 A_1)}{g_o}$$

$$= (P_1 A_1 - P_2 A_2) + \int_1^2 P\,dA + \frac{(\rho_m A_m a\,\Delta Z)}{g_o}$$

where

a = vehicle longitudinal acceleration, ft/sec^2
ΔZ = length between increments, ft
ρ_m = average gas density in increment, lb/ft^3
A_m = average cross sectional area in increment, ft^2
g_o = conversion constant, 32.174 lbm/slug

The acceleration term is developed as follows:

1. From Newton's Second Law of motion:

$$F_{bf} = \frac{W}{g_o} a$$

where

F_{bf} = body force, lbf
W = weight, lbm
a = acceleration, ft/sec^2

4.1.3 Non-Steady Flow Gas Dynamics with Acceleration

2. The body force exerted on the gas within a mass addition region is:

$$F_{bf} = \frac{\rho_m A_m \Delta Z}{g_o} a$$

3. Assuming perfect gas relationships, the body force may be written as:

$$F_{bf} = \frac{(P_1+P_2)(A_1+A_2)\ \Delta Z\ a}{24\ g_o\ R(T_1+T_2)}$$

4. and from P = F/A:

$$\Delta P = \frac{(P_1+P_2)(A_1+A_2)\ \Delta Z}{24\ (T_1+T_2)A_2}\ \frac{a}{g_o}$$

where

ΔP = pressure change resulting from acceleration, lb/in^2

The pressure change resulting from vehicle acceleration is added to the discharge pressure of a mass addition region as shown in Section 4.1.2.1, step 6, for the iteration of the discharge pressure and flow rate.

4.2 Complete Motor Gas Dynamics

Solution of overall motor gas dynamics or internal ballistics from fore-head to nozzle exit is described in this section.

4.2.1 Fore-Head Pressure Convergence

Solution of motor internal ballistics for each time point is obtained by an iteration process which converges on fore-head pressure, PH, (Figure 3.1). An initial estimate is made for fore-head pressure either from the input value PHI at time = 0, or from the previous time solution of PH at time > 0. The fore-head section mass balance is obtained in subroutine MNCHN4 (flow chart No. 10) after geometry values have been determined. Then parameters necessary to solve cylindrical section mass addition regions in subroutine SEGSUB (flow chart number 11) are determined. When the cylindrical section is complete, the aft-head section mass balance is obtained in subroutine MNCHN4 and the fore-head pressure is checked for convergence in subroutine SETPH (flow chart number 12).

The fore-head pressure convergence check in subroutine SETPH is made as follows:

1. Determine the throat critical pressure ratio:

$$\frac{P_s}{P_0} = \left(\frac{2}{\gamma+1}\right)^{\frac{\gamma}{\gamma-1}}$$

2. Determine the nozzle total pressure:

$$P_{ON} = P\left(\frac{T_0}{T}\right)^{\frac{\gamma}{\gamma-1}}$$

where

P = aft-head section discharge static pressure, lbs/in^2

T = aft-head section discharge static temperature, °R

3. If $P_{ON}\left(\frac{P_s}{P_0}\right) \geq P_a$, the nozzle is choked. Determine the sonic nozzle flow rate:

4.2.1 Fore-Head Pressure Convergence (Continued)

$$DIS = \frac{g_o\ NN\ A_t\ P_{ON}}{C^*}$$

where

NN = number of nozzles

Go to 5.

4. If $P_{ON}\left(\frac{P_s}{P_0}\right) < P_a$, the nozzle is not choked. Determine the subsonic nozzle flow rate:

$$SDIS = NN\ P_{ON}\ A_{EE}\left(\frac{P_a}{P_{ON}}\right)^{\frac{1}{\gamma}}\left[\frac{2\gamma\ g_o}{T_o R(\gamma-1)}\left(1-\left\{\frac{P_a}{P_{ON}}\right\}^{\frac{\gamma-1}{\gamma}}\right)\right]^{1/2}$$

where

A_{EE} = nozzle exit plane area.

DIS = SDIS

5. If $\left|\frac{\dot{W} - DIS}{DIS}\right| > CRW$, estimate new fore-head pressure as follows ($\dot{W}$ = grain discharge flow rate). If CRW is not input the program will set CRW equal to .005. A A

a) $WD = \frac{\dot{W} - WDB}{P_H - P_{Hold}}$

where P_{Hold} = previous iterative value of P_H, psi

WDB = previous iterative value of WD, lb/sec

$\dot{W}$ = grain discharge flow rate, lb/sec

b) $DEED = \frac{DIS - DISB}{P_H - P_{Hold}}$

where DISB = previous iterative value of DIS

4.2.1 Fore-Head Pressure Convergence (Continued)

c) If DEED = WD or if DEED = 0:

$$\Delta P = P_H \left[\left(\frac{\dot{W}}{DIS} \right)^{1.4} - 1 \right]$$

d) If DEED ≠ WD:

$$\Delta P = \frac{\dot{W} - DIS}{DEED - WD}$$

e) WDB = $\dot{W}$

DISB = DIS

f) If $\dot{W} \leq DIS$, $P_{min} = P_H$

g) If $\dot{W} > DIS$, $P_{max} = P_H$

h) $P_{Hguess} = P_H + \Delta P$

i) If $P_{Hguess} \leq P_{min}$ and $P_{min} = 0$

$P_{Hguess} = 5.0$ lbs/in^2

j) If $P_{Hguess} \leq P_{min}$ and $P_{min} \neq 0$

$P_{Hguess} = 2.0\ P_H$

k) If $P_{min} < P_{Hguess} \geq P_{max}$:

$P_{Hguess} = .9(P_{max} - P_{min}) + P_{min}$

Return to fore-head section with = P_{Hguess}.

4.2.1 Fore-Head Pressure Convergence (Continued)

1) If $P_{min} < P_{Hguess} < P_{max}$, return to fore-head section with $P_H = P_{Hguess}$.

6. If $\left|\frac{\dot{W} - DIS}{DIS}\right| \leq CRW$, convergence has been attained. If CRW is not input the program will set CRW equal to .005. A A

4.2.2 Nozzle Gas Dynamics

After the fore-head pressure convergence criterion has been satisfied (step 5 and 6 of the previous section), the nozzle gas dynamics in subroutine SETPH are determined as follows:

1. Determine the nozzle exit area:

$$A_{EE} = \frac{\pi D_E^2}{4}$$

2. Determine the nozzle expansion ratio:

$$\epsilon_G = \frac{A_{EE}}{A_t}$$

3. Iterate the following equation for $\frac{P_E}{P_{ON}}$ using the method of false position:

$$\frac{P_E}{P_{ON}} = \left[\left(\frac{1}{\gamma+1}\right)^{1/\gamma} \left(\frac{2}{\gamma+1}\right)^{\frac{1}{\gamma-1}} / \epsilon_G\right] / \left[1 - \left(\frac{P_E}{P_{ON}}\right)^{\frac{\gamma-1}{\gamma}}\right]^{\frac{\gamma}{2}}$$

4. Determine the momentum portion of the thrust coefficient:

$$C_{fo} = \left[\frac{2\gamma^2}{\gamma-1} \left(\frac{2}{\gamma+1}\right)^{\frac{\gamma+1}{\gamma-1}} \left\{1 - \left(\frac{P_E}{P_{ON}}\right)^{\frac{\gamma-1}{\gamma}}\right\}\right]^{1/2}$$

4.2.2 Nozzle Gas Dynamics (Continued)

5. Determine the delivered vacuum thrust coefficient:

$$C_{foL} = (C_{fo}\,\lambda_n + \frac{P_E}{P_{ON}}\,\epsilon_G)\,C_m$$

6. Determine the delivered thrust at P_a for sonic flow:

$$F = (C_{foL}\,P_{ON}\,A_t - P_a\,\epsilon_G\,A_t)NN$$

7. Determine the delivered thrust for subsonic flow:

$$V_E = \left[\frac{2\gamma\,T_o\,R\,g_o}{\gamma-1}\left\{1-\left(\frac{P_a}{P_{ON}}\right)^{\frac{\gamma-1}{\gamma}}\right\}\right]^{1/2}$$

$$F = \frac{V_E\,\lambda_N\,\dot{W}\,C_m\,NN}{g_o}$$

8. Determine the fore-head pressure-time integral:

$$\int P_H dt = \int P_H dt + (P_{Hold} + P_H)\,\frac{\Delta t}{2}$$

9. Determine the nozzle total pressure-time integral:

$$\int P_{ON} dt = \int P_{ON} dt + (P_{ONold} + P_{ON})\,\frac{\Delta t}{2}$$

10. Determine the nozzle discharge flow-time integral:

$$\int \dot{W}_N dt = \int \dot{W}_N dt + (\dot{W}_{Nold} + \dot{W}_N)\,\frac{\Delta t}{2}$$

11. Determine the total impulse:

$$IT = IT + (F + F_{old})\,\frac{\Delta t}{2}$$

4.2.2 Nozzle Gas Dynamics (Continued)

The above iterative procedure is allowed to continue for no more than 11 iterations. If the fore-head pressure has not converged within 11 iterations, a summary of the last iteration is printed followed by a complete program data dump and the next case is set up. When convergence has been attained, the program output is printed and the next time increment solution is initiated by setting P_{Hguess} equal to the previous time increment solution of P_H. Program execution for each case continues until termination options are satisfied.

4.3 Propellant Characteristics and Burning Rate Model

The characteristics of the propellant are represented by a mathematical model of the burning rate and properties of the products of combustion. Basic assumptions of a perfect gas, constant combustion temperature and constant specific heat allow the propellant gas properties to be described by the characteristic velocity, C^*, the combustion temperature, T_o, the specific heat ratio, γ, and the gas constant, R.

The propellant burning rate model allows either isotropic or anisotropic burning of the propellant surface. Isotropic burning is defined as uniform combustion occurring normal to the propellant surface. In anisotropic burning, the burn rate varies with distance burned as well as with conditions at the gas-propellant interface. It results from non-homogeneous dispersion of propellant additives near the case wall and core during propellant casting.

4.3.1 Propellant Gas Properties

The propellant gas properties may be held constant or may be varied as a function of the static pressure in the port cavity. If the gas properties are to be held constant, the parameters T_o, C^*, γ, and R are input. If the gas properties are to be varied, tables of the combustion temperature (TCOMB), the molecular weight (AMWG), the specific heat ratio (GAMAG), and the characteristic velocity (CSTR), are input as a function of static pressure (PRESS).

When the gas tables are input, a spline interpolation procedure is used in subroutine CSTRSB to obtain the gas properties for the static pressure at the increment dividing plane. The spline interpolation procedure sets up a series of piecewise cubics between the table values to obtain an interpolated value corresponding to this static pressure.

4.3.2 Propellant Burning Rate Model

The propellant burning rate model may include the effects of erosive burning. Erosive burning is defined as the change in the local burning rate resulting from gas velocity parallel to the burning surface.

The propellant burning rate, R_B, at any increment dividing plane is determined from the following parameters at the adjacent upstream increment dividing plane:

1.	Static pressure	P
2.	Gas velocity	U
3.	Mass velocity per unit area	G
4.	Distance from stagnation point	h_{RB}
5.	Burning rate	R_{BIII}
6.	Solid propellant density	ρ_f

With the exception of ρ_f, these values are not input but are calculated within the program.

Fifty-one constants are available to define the burning rate equation. Only the constants that are required for the particular burning rate equation to be used are input. These constants are as follows:

KG1 through KG5
KU1 through KU5
KR1 through KR39
KSLOT1 through KSLOT2

Prior to calculating burning rate, critical values of velocity, UCR, and mass velocity per unit area, GCR, are obtained as follows:

$$UCR = KU1 + (KU2)\ P^{(KU3)} + (KU4)\ P^{(KU5)}$$

$$GCR = KG1 + (KG2)\ P^{(KG3)} + (KG4)\ P^{(KG5)}$$

Propellant burning rate is then calculated in one of two ways:

If G is greater than or equal to GCR, and U is greater than or equal to UCR, the following relation is used:

$$R_B = KR1 + (KR2)\ P^{(KR3)} + (KR4)\ P^{(KR5)} + (KR6)\ U^{(KR7)} + (KR8)\ U^{(KR9)} + (KR10)\ G^{(KR11)} + (KR12)\ G^{(KR13)}$$

4.3.2 Propellant Burning Rate Model

$$+ (KR14)\ P^{(KR15)}\ U^{(KR16)} + (KR17)\ P^{(KR18)}\ U^{(KR19)}$$

$$+ (KR20)\ P^{(KR21)}\ G^{(KR22)} + (KR23)\ P^{(KR24)}\ G^{(KR25)}$$

$$+ \frac{KR26}{(KR27)\ P^{(KR28)} + (KR29)\ P^{(KR30)}}$$

$$+ (KR31)\ \frac{G^{(KR32)}}{b_{RB}^{(KR33)}}\ e^{-\left[\frac{(KR34)\ R_{BHI}\ \rho_f}{G}\right]}$$

If the value of G is less than GCR or if the value of U is less than UCR, then the following relation is used:

$$R_B = KR35 + (KR36)\ P^{(KR37)} + (KR38)\ P^{(KR39)}$$

To prevent the values of GCR and UCR from being used simultaneously for choosing the burning rate model, one of these values must always be equal to zero. This is accomplished by setting the values of constants KG1, KG2, and KG4 or the values of constants KU1, KU2, and KU4 equal to zero. The program will automatically stop if any of the terms KG1, KG2, or KG4 are not equal to zero when any of the terms KU1, KU2, or KU4 are also not equal to zero. In such cases, the program will print-out a statement that the GCR or UCR coefficients are invalid. If KR26 is not zero, then neither KR27 nor KR29 can be negative or simultaneously equal to zero; if this restriction is exceeded, the program will stop and print-out a statement of invalid KR27 or KR29.

The burning rate at the segment slot face is calculated by

$$RBSLOT = (KSLOT1)\ P^{(KSLOT2)}$$

where P is the static pressure in the port at the segment interface.

4.3.3 Anisotropic Propellant Burning

Anisotropic propellant burning capability, where burn rate depends on distance burned, was added to the program because of Boeing's experience with the HIBEX motor. Anisotropic burning occurred during both ignition and tail-off. It appeared to be the result of two effects: 1) variation in the alignment of the staples between the bulk of the propellant at the case wall and the core interface, and 2) the burning distance required to develop "coning" about the staples. Anisotropic burning is most easily represented by variation of the constant "a" as a function of distance burned in the burn rate equation, $r = aP^n$. During ignition, mass generation is determined by multiplying the port perimeter by the anisotropic burning rate. During tail-off, regions exist where both isotropic and anisotropic burning occur. The port perimeter is subdivided accordingly. The total mass generation is then the sum of the individual mass generation rates.

The following assumptions have been made in developing the mathematical model:

1. The anisotropic region at both the core interface and the case wall is of uniform thickness along the motor length.

2. The thickness of the anisotropic region is the same at both the core interface and the case wall.

3. The burn rate variation through the anisotropic region is a function only of distance burned and local static pressure, $r = a(\tau)P^n$.

4. The anisotropic burn rate increases from the core interface toward the isotropic propellant and decreases from the isotropic propellant toward the case wall.

5. The fore-head and aft-head burning rate during motor tail-off is the same as the adjacent tangent plane isotropic burning rate.

The following limitations apply to the program:

1. Anisotropic burning cannot be considered for propellants with wagon wheel grain configurations during tail-off.

2. Anisotropic burning may be considered for non-steady flow options only during ignition and tail-off.

Program simulation of anisotropic burning is accomplished by altering normal program solution during the ignition transient interval to solve for the burn rate coefficient with a fixed

4.3.3 Anisotropic Propellant Burning (Continued)

value of the fore-head pressure at each time increment. The burn rate coefficient is stored in a table as a function of distance burned at a desired location within the cylindrical section (input NINCPL). A program option is available to input this anisotropic burn rate coefficient table and solve for fore-head pressure as discussed in Section 4.2.1. The burning rate within the fore-head and aft-head sections may be specified by inputs KRH and KRN or by the anisotropic burning rate table inputs. During the tail-off interval, when the burning surface is within the anisotropic propellant region, the burning rate at each increment dividing plane in sectors 6, 7, and 8 becomes a function of the distance from the case wall within the sector as shown in Figures 4.4, 4.5, and 4.6.

The program method of solution for anisotropic burning during the ignition transient interval, when the fore-head pressure trace is input, is altered to converge on the burn rate coefficient, KRST. At each time increment, an estimate of the burn rate coefficient is determined in subroutine RBSTSB from the fore-head pressure rise rate and the motor configuration as follows:

From the perfect gas law using finite differences:

$$1.\quad \frac{dP_H}{dt} = \frac{\partial}{\partial t}\left[\frac{12\, W_H\, R\, T}{V}\right] = \frac{12\, R\, T}{V}\,\frac{d\, W_H}{dt}$$

and,

$$2.\quad \frac{dW_H}{dt} = \dot{W}_{in} - \dot{W}_{out}$$

where

$\dot{W}_{in}$ = generated weight flow rate, lb/sec
$\dot{W}_{out}$ = nozzle discharge flow rate, lb/sec
V = free volume, in^3

The nozzle discharge flow rate is determined from the nozzle geometry:

$$3.\quad \dot{W}_{out} = \frac{g_o\, A_t\, P_{ON}}{c^*}$$

where

4.3.3 Anisotropic Propellant Burning (Continued)

g_o = gravitational constant, ft/sec^2
A_t = nozzle throat area, in^2
P_{ON} = nozzle total pressure, lb/in^2
C^* = characteristic velocity, ft/sec^2

and the generated weight flow rate is determined from the motor configuration:

4. $\dot{W}_{in} = R_b A_b \rho_f$

where

R_b = burn rate, in/sec
A_b = total burn area, in^2
ρ_f = propellant density, lb/in^3

5. $RT = \dfrac{\Gamma^2 C^{*2}}{g_o}$

where

$$\Gamma^2 = \gamma \left(\frac{2}{\gamma+1}\right)^{\frac{\gamma+1}{\gamma-1}}$$

Therefore:

6. $$\frac{dP_H}{dt} = \dot{P}_H = \frac{12\,\Gamma^2 C^{*2}}{V g_o}(R_b A_b \rho_f) - \frac{12\,\Gamma^2 C^*}{V}(P_{ON} A_t)$$

Combining and arranging terms with $P_{ON} = (TPR)P_H$, where TPR is an input estimate of the port pressure drop, we have:

7. $$R_b = \frac{\dot{P}_H + \dfrac{(12\,\Gamma^2 C^*)(A_t\ TPR\ P_H)}{V}}{\dfrac{12\,\Gamma^2 C^{*2} A_b \rho_f}{g_o V}}$$

and

4.3.3 Anisotropic Propellant Burning (Continued)

8. $KRST = \frac{R_b}{P_H^n}$

After the initial estimate of KRST is made, the ballistic solution is converged for the fixed fore-head pressure obtained from the input pressure trace using the convergence procedure outlined in Section 4.2.1. When the anisotropic burn rate coefficient table is input, the method of solution remains unchanged except that the burn rate coefficient which depends on distance burned at location NINCPL from the forward tangent plane is determined from the input table at each time increment.

The ignition transient interval is terminated when the value of time exceeds the last table value of the input fore-head pressure trace independent variable TIMEPH(NPH), or when the burn rate table is input, the termination option TST. The steady state interval will then continue with the last table value of the burn rate coefficient dependent variable AKRTAU(NAKRST) or the burn rate coefficient inputs KR(2) and KR(36) (depending on choice of inputs) in the general burning rate equation.

As the burning surface progresses toward the case wall, the anisotropic region is first exposed in the region of sector 8 as shown in Figure 4.4. This results in a non-uniform burning rate along the propellant burning surface during the tail-off interval.

Three burning rates are determined for the burning surface: R_{b8} which is determined from the anisotropic burning distance in sector 8, R_{b7} which is determined from an integration along the anisotropic perimeter of sector 7 between the isotropic and anisotropic burning distances using the anisotropic burn rate coefficient table, and the normal isotropic burn rate, R_b.

Two separate burn distances are defined: the isotropic burn distance in sectors 1 through 7, TAUZ(III), and the anisotropic burn distance in sectors 7 and 8, TAUZTO(III). The anisotropic burn rate becomes progressively less during motor tail-off, resulting in an anisotropic burn distance less than the isotropic burn distance and producing burning that is not normal to the grain surface.

Figures 4.4, 4.5, and 4.6 show the configurations of the anisotropic propellant region that can exist at the case wall for a standard star configuration with an inert sliver. The angles η_2, η_{22}, and "ANGLE" are used to determine the anisotropic pro-

4.3.3 Anisotropic Propellant Burning (Continued)

pellant perimeter lengths, AL_7 and AL_8, during motor tail-off. Angle η_2 is subtended from the R_5 radius vector and locates the intersection of the anisotropic propellant region with the isotropic propellant region. Angle η_{22} is subtended from the motor axis to the same intersection point for η_2. "ANGLE" is subtended from the motor axis and identifies the point of intersection of the isotropic burn distance vector, swung from R_5, with the case wall.

Subroutine LPTO contains the geometry calculations to determine the sector perimeter length of the anisotropic propellant for each reference plane during motor tail-off. The anisotropic propellant perimeter length in sector 8 is identified as AL8, and in sector 7 is identified as AL7. The perimeter length of sector 7 anisotropic propellant (AL7) is assumed to be a straight line between the points determined by the intersection of the isotropic propellant with the anisotropic propellant and the anisotropic burning distance with the case wall or with sector 8.

The distance burned of the anisotropic propellant in sectors 7 and 8 is computed from the burn rate of the anisotropic propellant in Sector 8 (RB8) in Subroutine SEGSUB. Once sector 8 has burned out, RB8 is determined from the first table value of the anisotropic burn rate coefficient (the minimum value). The progression of the intersection of the propellant with the case wall is assumed to proceed at the minimum burn rate.

The mass flow generated is determined in subroutine SEGSUB from the perimeter lengths of the anisotropic burning propellant (AL7 and AL8), and the isotropic burning propellant (ALP) and their corresponding burn rates as follows:

$$\dot{dW}_7 = NO\ \rho_f\ \Delta Z\ (AL_7\ R_{B7} + AL_{7HI}\ R_{B7HI})$$

$$\dot{dW}_8 = NO\ \rho_f\ \Delta Z\ (AL_8\ R_{B8} + AL_{8HI}\ R_{B8HI})$$

$$\dot{dW} = \left[\frac{\rho_f\ \Delta Z}{2}\ (ALP_{HI} - AL_{TOHI})\ RB_{HI} + (ALP - AL_{TO})\ R_B\right] + \dot{dW}_7 + \dot{dW}_8$$

where

$$AL_{TO} = (AL_7 + AL_8)2NO$$

4.3.3 Anisotropic Propellant Burning (Continued)

and subscripted "HI" values are at the inlet to the mass addition region. The non-subscripted ones represent the outlet to the mass addition region.

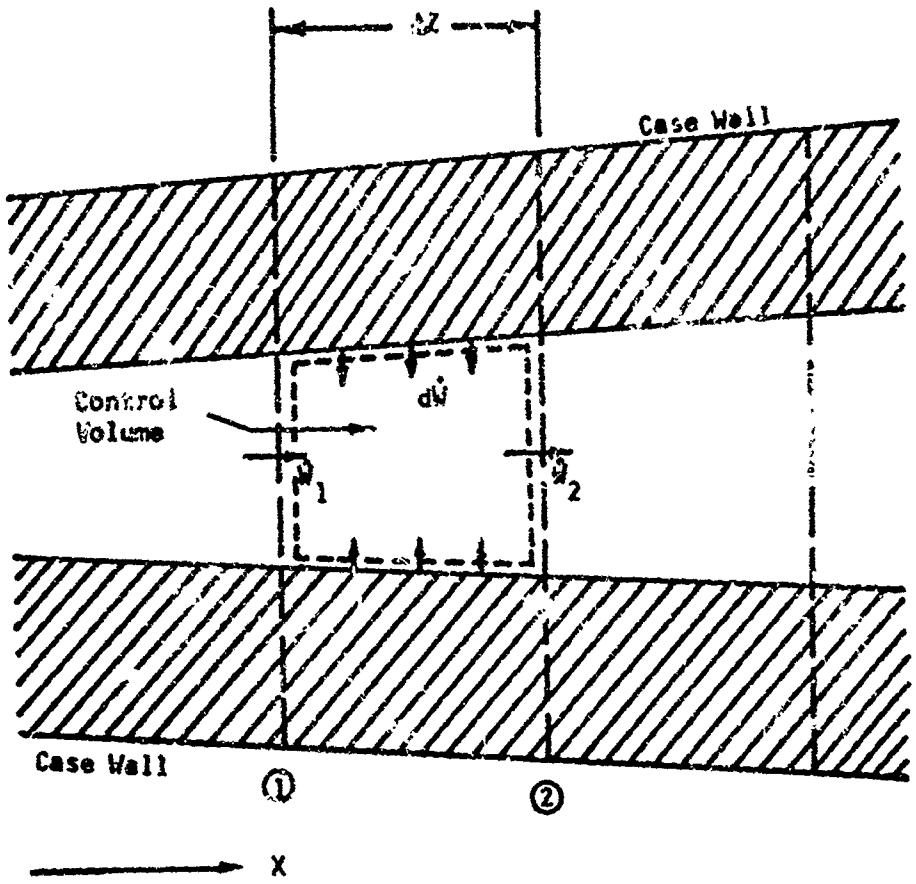
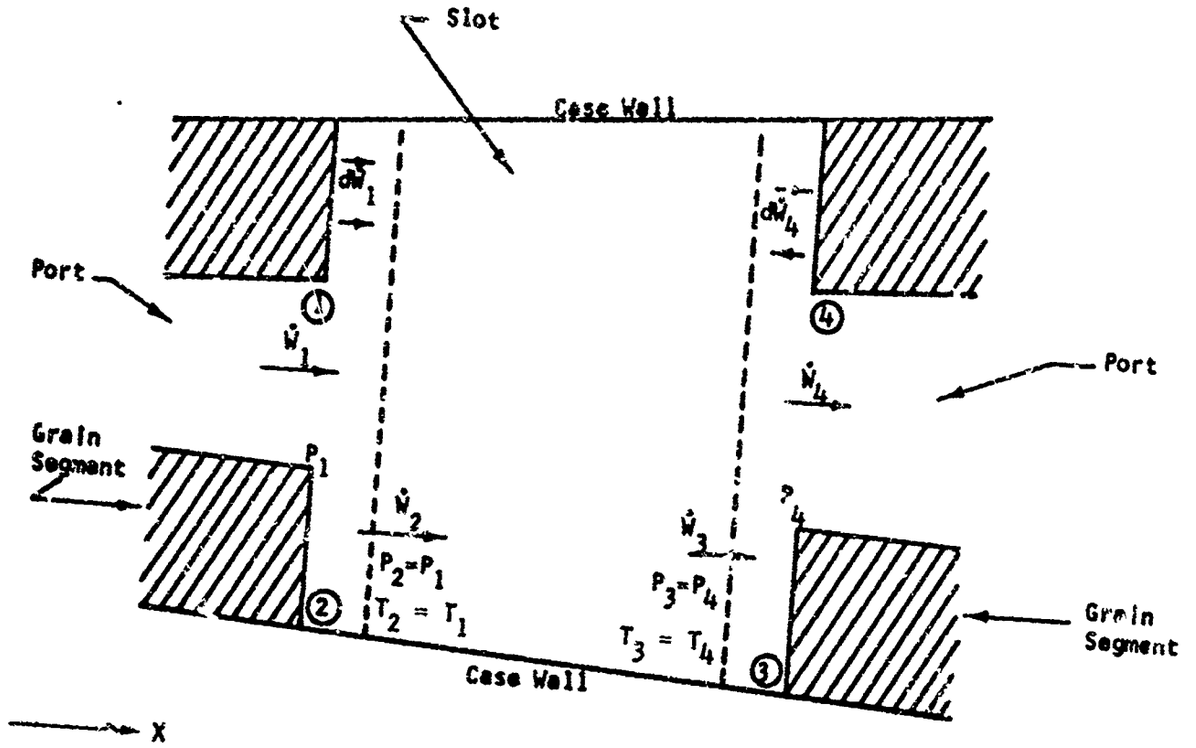


Figure 4.1. Mathematical Model of Mass Addition Region Control Volume



① Slot foreward interface

② Slot forward interface mass addition region

③ Slot aft interface mass addition region

④ Slot aft interface

Figure 4.2. Mathematical Model of Slot Between Grain Segments

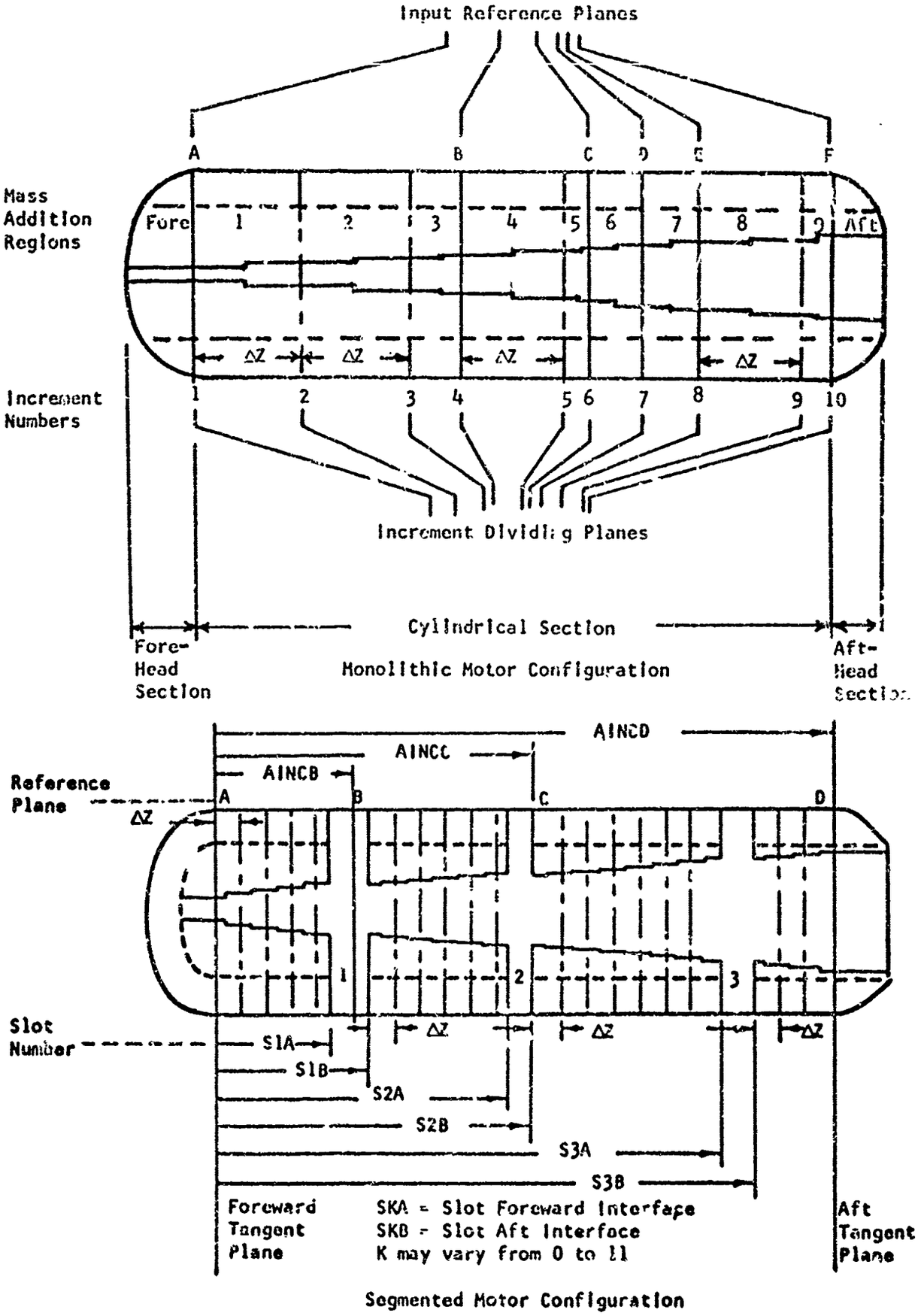


Figure 4.3 Reference Plane and Increment Dividing Plane Identification

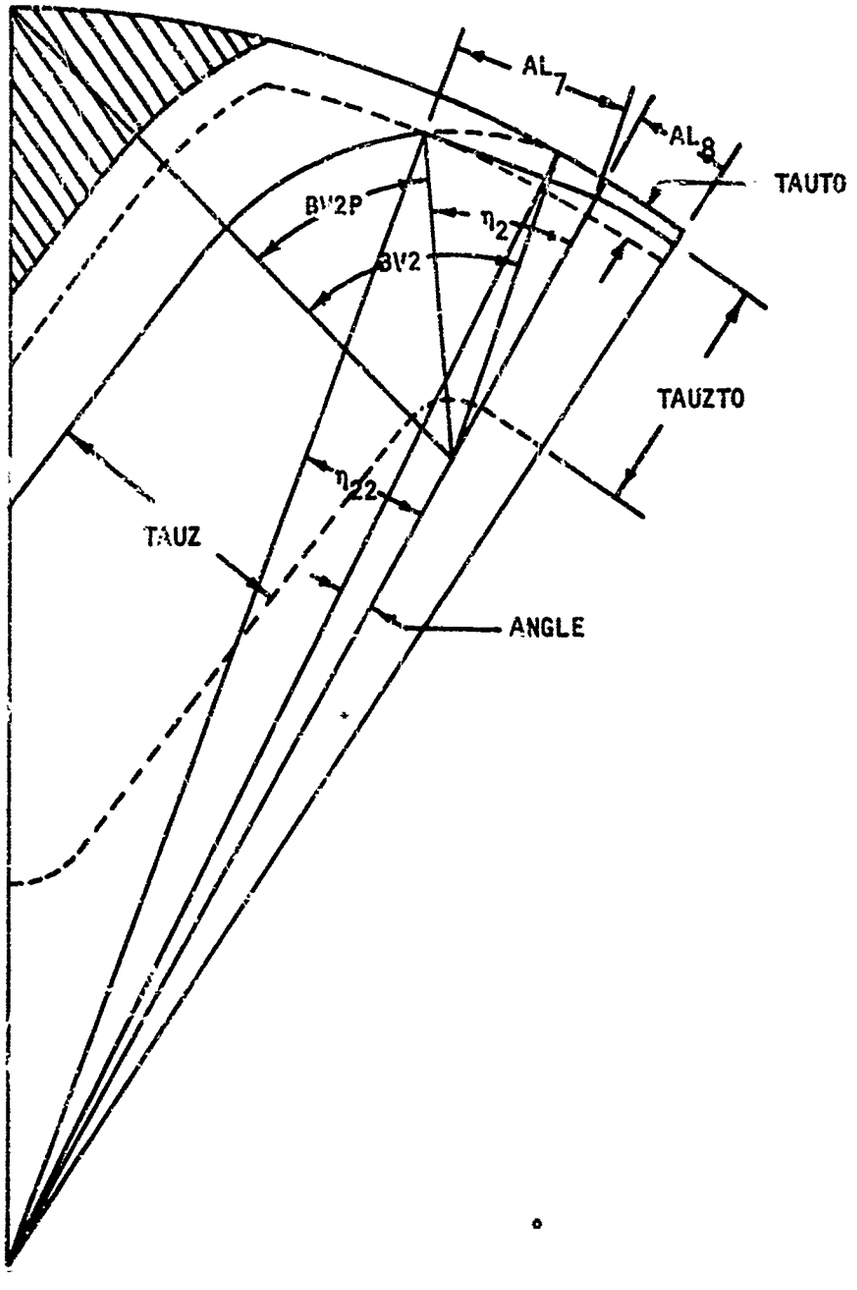


Figure 4.4. Anisotropic Propellant Burning Configuration Near Case Wall Before Web Burnout

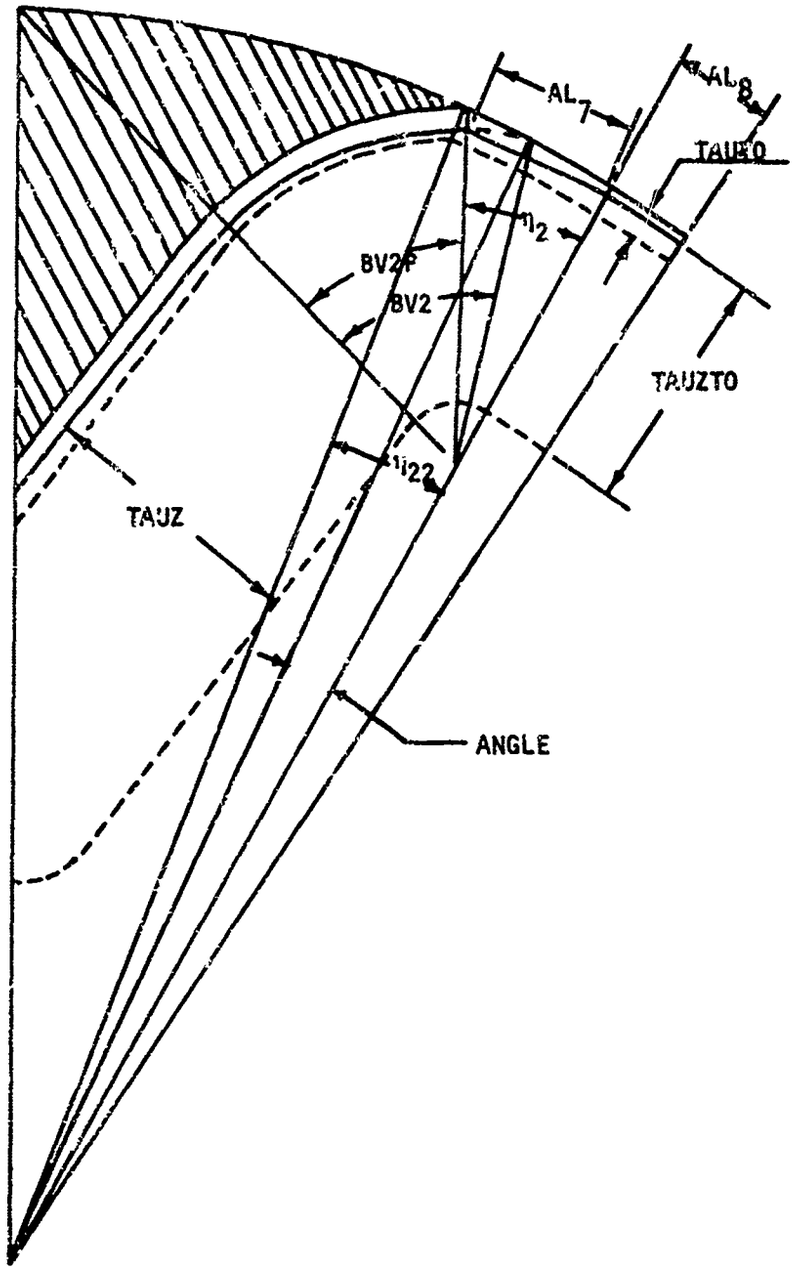


Figure 4.5. Anisotropic Propellant Burning Configuration Near Case Wall and Inert Sliver Before Web Burnout

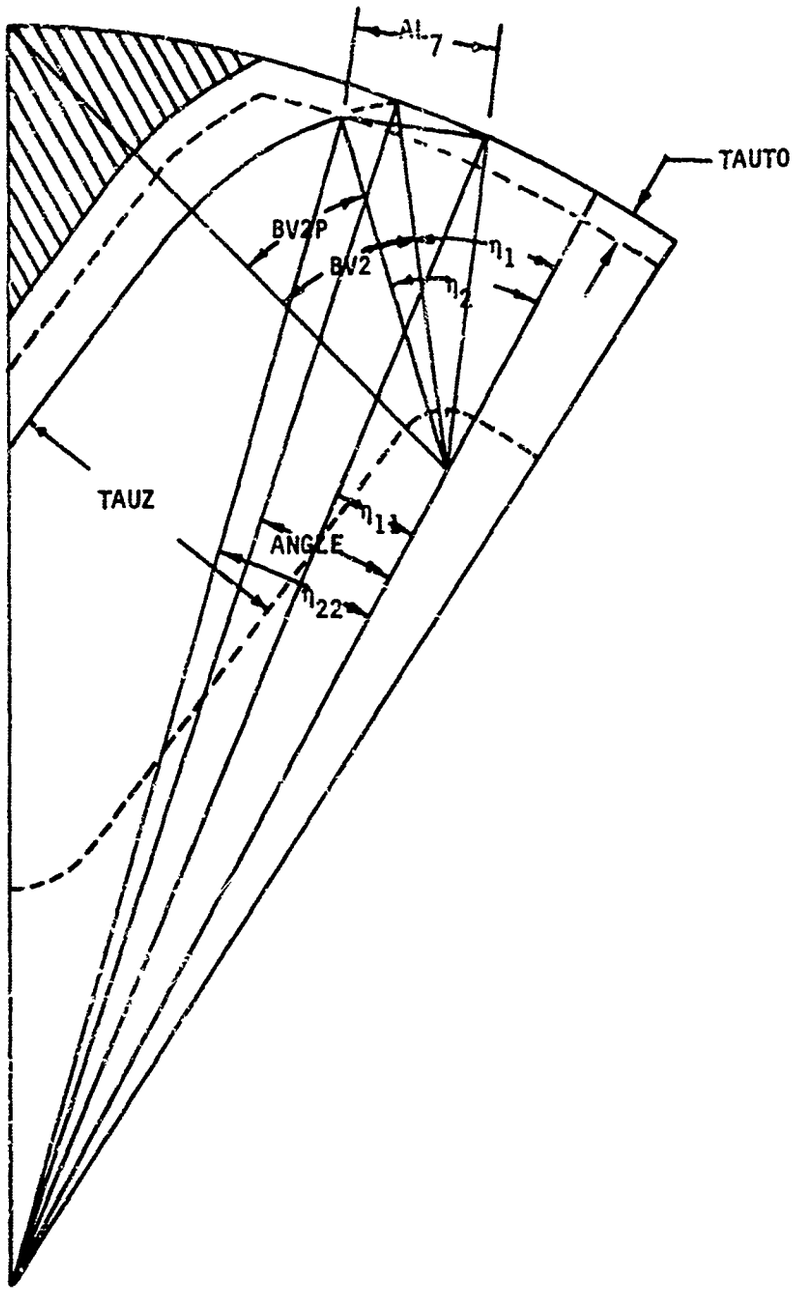


Figure 4.6. Anisotropic Propellant Burning Configuration Near Case Wall After Web Burnout

5.0 GEOMETRICAL DEFINITION OF PROPELLANT GRAIN

For geometrical analysis, the motor is divided longitudinally into three sections: fore-head section, cylindrical section, and aft-head section. The fore-head section may incorporate a head-end with web or it may be defined in a manner similar to the aft-head section which is a straight through grain. The following describes subroutines and equations used to calculate burning surface area, port cross sectional area, propellant volume, center of gravity and moment of inertia for the fore-head, cylindrical, and aft-head sections.

5.1 Grain Cross Section Geometry

Propellant grain cross section options which are programmed for the computer are shown in Figure 5.1. The grain design may vary from the more complicated forked wagon wheel to the standard star, or to the circular port. The slotted-cone grain design is a modification of the standard star. Variations in the input parameters for the forked wagon wheel, which are shown in Figure 5.2, will produce the five basic grain design patterns. The basic parameters required to describe the grain cross section are input for reference planes located at specified distances from the forward tangent plane of the motor, Figure 4.3. The reference planes describing the propellant cross section may be placed at any desired location within the cylindrical section, thus allowing accurate descriptions of the propellant configuration for either monolithic or segmented motors.

5.1.1 General Forked Wagon Wheel

Cross-sectional geometry constants are required to determine the perimeter length and port area of each input reference plane. These basic geometry constants are determined in the first core load. Once these plane constants have been computed and stored for each input reference plane, the perimeter length for all values of distance burned and the initial port area are determined for each reference plane in the second core load and stored in tables for use during the internal ballistic solution in the fourth core load. The reference plane constants for the forked wagon wheel grain configuration are determined by subroutine PLNCNS from the geometry inputs, Figure 5.2. These plane constants are shown in Figures 5.3 and 5.4. A total of 45 constants are generated and stored for each reference plane:

Subroutine PLNCNS Reference Plane Constants

$$R_1 = R_f - \tau_w - L_{S1}$$

$$R_9 = R_f - \tau_w - L_{S2}$$

5.1.1 General Forked Wagon Wheel (Continued)

$$\theta_1 = \frac{\pi}{N0}$$

$$\tau_{2max} = R_2 + L_A \frac{\sin \alpha_{01}}{\cos \alpha_{01}}$$

$$\tau_{4max} = \tau_{2max} + L_B \frac{\sin \alpha_{02}}{\cos \alpha_{02}}$$

$$\tau_{5max} = (\tau_{4max} + R_4) \frac{\cos \alpha_{02}}{\cos \alpha_{03}} - R_4$$

$$X_{45} = (\tau_{5max} + R_5) \cos \alpha_{03}$$

$$Y_{45} = R_1 + R_2(1-\sin \alpha_{01}) + L_A \cos \alpha_{01} + \tau_{2max}(\sin \alpha_{01} - \sin \alpha_{02}) + L_B \cos \alpha_{02} + R_4(\sin \alpha_{03} - \sin \alpha_{02}) - R_5 \sin \alpha_{03}$$

$$L_C = \left[(R_f - \tau_w - R_5)^2 - (X_{45} \cos \alpha_{03} - Y_{45} \sin \alpha_{03})^2\right]^{1/2} - X_{45} \sin \alpha_{03} - Y_{45} \cos \alpha_{03}$$

$$X_{03} = (\tau_{2max} - R_3) \left[\cos \alpha_{01} + \operatorname{Tan} \left(\frac{(\alpha_{01} - \alpha_{02})}{2}\right) \sin \alpha_{01}\right]$$

$$Y_{03} = R_1 + R_2 + (R_3 - R_2) \sin \alpha_{01} + \left[(\tau_{2max} - R_3) \operatorname{Tan} \frac{\alpha_{01} - \alpha_{02}}{2} + L_A\right] \cos \alpha_{01}$$

$$R_{03} = \left[X_{03}^2 + Y_{03}^2\right]^{1/2}$$

$$X_{05} = (\tau_{5max} + R_4) \cos \alpha_{03}$$

5.1.1 General Forked Wagon Wheel (Continued)

$$Y_{05} = Y_{45} + (R_5 - R_4) \sin \alpha_{03}$$

$$R_{05} = \left[X_{05}^2 + Y_{05}^2 \right]^{1/2}$$

$$X_{07} = X_{45} + L_C \sin \alpha_{03}$$

$$Y_{07} = Y_{45} + L_C \cos \alpha_{03}$$

$$R_{07} = \left[X_{07}^2 + Y_{07}^2 \right]^{1/2}$$

$$\tau_{6max} = \tau_{5max} + L_C \frac{\sin \alpha_{03}}{\cos \alpha_{03}}$$

$$\tau_{7max} = \left[X_{07}^2 + (R_f - Y_{07})^2 \right]^{1/2} - R_5$$

$$\tau_{12max} = R_8 + L_E \frac{\sin \alpha_{05}}{\cos \alpha_{05}}$$

$$X_{76} = (\tau_{12max} + R_6) \cos \alpha_{04}$$

$$Y_{76} = R_9 + R_8(1-\sin \alpha_{05}) + L_E \cos \alpha_{05} + \tau_{12max}(\sin \alpha_{05} - \sin \alpha_{04}) - R_6 \sin \alpha_{04}$$

$$L_D = \left[(R_f - \tau_w - R_6)^2 - (X_{76} \cos \alpha_{04} - Y_{76} \sin \alpha_{04})^2 \right]^{1/2} - X_{76} \sin \alpha_{04} - Y_{76} \cos \alpha_{04}$$

$$X_{09} = X_{76} + L_D \sin \alpha_{04}$$

$$Y_{09} = Y_{76} + L_D \cos \alpha_{04}$$

5.1.1 General Forked Wagon Wheel (Continued)

$$R_{09} = \left[X_{09}^2 + Y_{09}^2 \right]^{1/2}$$

$$X_{011} = (\tau_{12max} - R_7) \left[\tan \frac{\alpha_{05} - \alpha_{04}}{2} \sin \alpha_{05} + \cos \alpha_{05} \right]$$

$$Y_{011} = R_9 + R_8 + (R_7 - R_8) \sin \alpha_{05} + \left[(\tau_{12max} - R_7) \tan \left(\frac{\alpha_{05} - \alpha_{04}}{2} \right) + L_E \right] \cos \alpha_{05}$$

$$R_{011} = \left[X_{011}^2 + Y_{011}^2 \right]^{1/2}$$

$$\tau_{10max} = \tau_{12max} + L_D \frac{\sin \alpha_{04}}{\cos \alpha_{04}}$$

$$\tau_{9max} = \left[X_{09}^2 + (R_f - Y_{09})^2 \right]^{1/2} - R_6$$

$$\theta_2 = \arccos \left(\frac{Y_{07}}{R_{07}} \right)$$

$$\theta_3 = \arccos \left(\frac{Y_{09}}{R_{09}} \right)$$

$$\theta_4 = \theta_1 - \theta_2 - \theta_3$$

$$\beta_{71max} = \arccos \left[(\tau_{7max} + R_5)^2 - (R_f - Y_{07})^2 \right]^{1/2} / (\tau_{7max} + R_5) - \alpha_{03}$$

$$\beta_{72max} = \frac{\pi}{2} + \theta_2 - \beta_{71max} - \alpha_{03}$$

$$\beta_{91max} = \arccos \left[(\tau_{9max} + R_6)^2 - (R_f - Y_{09})^2 \right]^{1/2} / (\tau_{9max} + R_6)$$

5.1.1 General Forked Wagon Wheel (Continued)

$$\beta_{92max} = \frac{\pi}{2} + \theta_3 - \beta_{91max} - \alpha_{04}$$

$\tau_{max} = \tau_{7max}$, or τ_{9max}, whichever is larger.

If θ_0 is input, determine τ_{max} for slotted-cone geometry as follows (Figure 5.7):

$$\angle AJB = \arcsin\left[\frac{(R_f - R_5 - \tau_w)\sin(\theta_2)}{T_{6M} + R_5}\right]$$

$$\angle ABC = \pi - \theta_2 - \angle AJB$$

$$\angle ACB = \arcsin\left[\frac{(R_f - R_5 - \tau_w)\sin(\angle ABC)}{R_f}\right]$$

$$\angle BAC = \pi - \angle ABC - \angle ACB$$

$$\angle GFE = \frac{\pi}{2} - \alpha_{01}$$

$$\angle AFE = \frac{\pi}{2} + \alpha_{01}$$

$$\angle AEF = \arcsin\left[\frac{(R_1 + R_2)\sin(\angle AFE)}{R_f}\right]$$

$$\angle GAE = \pi - \angle AFE - \angle AEF$$

If $\theta_0 \geq \angle GAE$, $\tau_{max} = R_f - R_1$

If $\theta_0 < \angle GAE$,

$$BH = \left[R_f^2 + (R_f - R_5 - \tau_w)^2 - 2R_f(R_f - R_5 - \tau_w)\cos(\theta_0 + \theta_2)\right]^{\frac{1}{2}}$$

If $(\theta_0 + \theta_2) \geq \angle BAC$,

$$\angle AHB = \arcsin\left[\frac{(R_f - R_5 - \tau_w)\sin(\theta_0 + \theta_2)}{BH}\right]$$

$$\angle ABH = \pi - \angle AHB - \theta_0 - \theta_2$$

$$\angle HBC = \angle ABC - \angle ABH$$

$$BH' = BH \cos(\angle HBC)$$

A

A

5.1.1 General Forked Wagon Wheel (Continued)

τ_{max} = $(R_f - R_1)$ or $(BH' - R_5)$, whichever is smaller.

If $(\theta_0 + \theta_2) < \angle BAC$,

τ_{max} = $(R_f - R_1)$ or $(BH - R_5)$, whichever is smaller.

The calculated plane constants appear on the printout and allow the user a means of checking if the proper grain design is being analyzed. Although the program is designed to solve the general configuration shown in Figure 5.2, there are certain variations of this configuration that exceed the mathematical limits of the analysis. To obtain a program solution, all of the following conditions must exist for each reference plane used:

R_1	must be greater than or equal to zero
R_3	must be less than or equal to τ_{2max}
R_7	must be less than or equal to τ_{12max}
R_9	must be greater than or equal to zero
L_C	must be greater than or equal to zero
L_D	must be greater than or equal to zero
β_{71M}	must be greater than or equal to zero
β_{91M}	must be greater than or equal to zero
α_{01}	must be less than 90°
α_{02}	must be greater than or equal to zero
α_{03}	must be less than 90°
α_{04}	must be greater than or equal to zero
α_{05}	must be less than 90°
θ_4	must be greater than or equal to zero

If any of these restrictions are exceeded for any of the input reference planes, the program will automatically stop and print the reference plane dimensions along with a statement of the exceeded restriction. Although the program is self-checking for these mathematically invalid configurations, there are some physically invalid configurations for which there is no such check.

Special attention should be given to the manner in which input lengths L_A, L_B, and L_E are defined. The length L_A is measured along a common tangent to the arcs generated by radii R_2 and R_3 (Figure 5.2). One of the points that defines this length is the point of tangency with the arc generated by the radius R_2. How-

5.1.1 General Forked Wagon Wheel (Continued)

ever, the other point that defines length L_A is not the point of tangency with the arc generated by radius R_3. This end limit of length L_A is determined by bisecting the included angle between lengths L_A and L_B, and extending this bisector until it intersects the axis of symmetry of the grain sector. From this intersection point, a line perpendicular to L_A is drawn. The intersection of this perpendicular and the line L_A is the point which defines the end of length L_A. Line lengths L_B and L_E are defined in a similar manner.

The perimeter length and initial port area of the grain cross section for each reference plane are determined in the second core load for incremental distances burned before and after web burnout specified by input. The geometry plane constants of each reference plane are moved from storage into working locations in subroutine LPDAPS and the perimeter length and initial port area are determined for each sector of the cross section (shown in Figures 5.2, 5.3, and 5.4) at the specified DTAU increments by subroutine AFPSUB.

Subroutine LPDAPS

Subroutine LPDAPS sets up the parameters required to determine the perimeter length, L_p, and the cross-sectional propellant area, A_{FF}, for both the primary and secondary propellant tips of the forked wagon wheel. Initially, the parameters required to determine the secondary propellant tip are set and subroutine AFPSUB is used to evaluate the perimeter length and the area of propellant for each sector, and then the parameters for the primary propellant tip are set. Figure 5.5 shows the boundaries of the sectors for the forked wagon wheel grain.

The perimeter length and propellant area of sector 8 are then determined and summed with the values determined from sectors 1-7 and 9-13. The total perimeter of the grain configuration is obtained by multiplying the sum by 2NO. The port area is obtained by summing the cross sectional area of the propellant sectors, multiplying by NO, and subtracting the result from the area of a circle of radius R_f.

Subroutine AFPSUB

Subroutine AFPSUB determines the port perimeter length of one-

5.1.1 General Forked Wagon Wheel (Continued)

half of a symmetrical section and propellant cross sectional area of a symmetrical section of all sectors except sector 8. The plane constants required for each sector are set by subroutines MNCHN2 and LPDAPS.

The perimeter and area of the cross section for all grain configurations are calculated from basic trigonometric formulas. Required angles and line lengths are computed from known dimensions using the law of sines and the law of cosines. Propellant cross sectional area is determined by adding and subtracting areas of circular sectors and triangles. All configurations contain only straight lines and circular arcs.

Initially, the constants to determine the initial area and perimeter length for sectors 9 through 13, Figure 5.5, are set by subroutine LPDAPS, and then the sectors 1 through 7 are set such that $L_{13} = L_1$, $L_{12} = L_2$, $L_{11} = L_3$, $L_{10} = L_4$, and $L_9 = L_7$. The sector perimeter length, L, and initial propellant cross sectional areas, AFP, are determined as follows:

1. If $\tau < R_2$,

$$L_1 = (R_2 - \tau)\left(\frac{\pi}{2} - \alpha_{01}\right)$$

$$AFP_1 = (R_2 - \tau)L_1$$

2. If $\tau \geq R_2$,

$$L_1 = 0$$

$$AFP_1 = 0$$

3. If $\tau < R_3$,

$$\Delta L_3 = (\tau_{2max} - R_3) \operatorname{Tan}\left(\frac{\alpha_{01} - \alpha_{02}}{2}\right)$$

$$AFD = (R_3 + \tau_{2max} - 2\tau)\,\Delta L_3$$

5.1.1 General Forked Wagon Wheel (Continued)

4. If $\tau \geq R_3$ and if $\tau < \tau_{2max}$

$$\Delta L_3 = (\tau_{2max} - \tau) \text{ Tan } \left(\frac{\alpha_{01} - \alpha_{02}}{2}\right)$$

$$AFD = (\tau_{2max} - \tau)\, \Delta L_3$$

5. If $\tau \geq R_3$ and if $\tau \geq \tau_{2max}$

$$L_2 = 0$$

$$\Delta L_3 = 0$$

$$AFD = 0$$

6. If $\tau \leq R_2$,

$$L_2 = L_A + \Delta L_3$$

$$AFP_2 = (R_2 - 2\tau + \tau_{2max})\, L_A + AFD$$

7. If $\tau > R_2$,

$$L_2 = L_A \left[\frac{(\tau_{2max} - \tau)}{(\tau_{2max} - R_2)}\right] + \Delta L_3$$

$$AFP_2 = (\tau_{2max} - \tau)(L_2 + \Delta L_3) + AFD$$

8. If $\tau < R_3$,

$$L_3 = (R_3 - \tau)(\alpha_{01} - \alpha_{02})$$

$$AFP_3 = L_3 (R_3 - \tau)$$

9. If $\tau \geq R_3$,

$$L_3 = 0$$

$$AFP_3 = 0$$

5.1.1 General Forked Wagon Wheel (Continued)

10. If $\tau < \tau_{2max}$

$$L_4 = L_B + \Delta L_3$$

$$AFP_4 = (\tau_{2max} - 2\tau + \tau_{4max})\, L_B + AFD$$

11. If $\tau_{2max} \leq \tau < \tau_{4max}$

$$L_4 = (\tau_{4max} - \tau)\, L_B / (\tau_{4max} - \tau_{2max})$$

$$AFP_4 = (\tau_{4max} - \tau)\, L_4$$

12. If $\tau_{2max} \leq \tau \geq \tau_{4max}$,

$$L_4 = 0$$

$$AFP_4 = 0$$

13. If $\tau < \tau_{4max}$

$$L_5 = (R_4 + \tau)(\alpha_{03} - \alpha_{02})$$

$$AFP_5 = (R_4 + \tau_{5max})(R_4 + \tau_{4max})\sin(\alpha_{03} - \alpha_{02}) - L_5(R_4 + \tau)$$

14. If $\tau_{4max} \leq \tau < \tau_{5max}$,

$$L_5 = (R_4 + \tau)\ \alpha_{03} - \text{arc cos}\left[\frac{(R_4+\tau_{4max})\cos(\alpha_{02})}{(R_4 + \tau)}\right]$$

$$AFP_5 = (R_4 + \tau_{5max})(R_4 + \tau)\ \sin\left[\frac{L_5}{(R_4 + \tau)}\right] - (R_4 + \tau)\, L_5$$

15. If $\tau_{4max} \leq \tau \geq \tau_{5max}$,

$$L_5 = 0$$

$$AFP_5 = 0$$

5.1.1 General Forked Wagon Wheel (Continued)

16. If $\tau \leq \tau_{5max}$,

$$L_6 = L_C$$

$$AFP_6 = (\tau_{5max} - 2\tau + \tau_{6max})\, L_C$$

17. If $\tau_{5max} < \tau < \tau_{6max}$, L_C

$$L_6 = L_C(\tau_{6max} - \tau)/(\tau_{6max} - \tau_{5max})$$

$$AFP_6 = (\tau_{6max} - \tau)\, L_6$$

18. If $\tau_{5max} < \tau \geq \tau_{6max}$,

$$L_6 = 0$$

$$AFP_6 = 0$$

19. If $\tau \leq \tau_{6max}$,

$$\beta_{71} = \beta_{71max}$$

$$AFP = (R_5 + \tau_{7max})(R_5 + \tau_{6max})\sin(\beta_{71}) - \beta_{71}(R_5 + \tau)^2$$

20. If $\tau_{6max} < \tau < \tau_{7max}$,

$$\beta_{71} = \beta_{71max} + \alpha_{03} - \arccos\left(\frac{X_{07}}{(\tau + R_5)}\right)$$

$$AFP = (R_5 + \tau_{7max})(R_5 + \tau)\sin(\beta_{71}) - \beta_{71}(R_5 + \tau)^2$$

21. If TSLVR > 0,

$$\beta_{VX} = \arcsin\left[\frac{R_7 \sin(\theta_2)}{R_5 + \tau_{7max}}\right] - \arcsin\left[\frac{R_7 \sin(\theta_2 - \theta_{SLV})}{(R_5 + \tau_{SLVR})}\right] - \theta_{SLVR}$$

$$Temp = \tau_w^2 + (R_5 + \tau_{7max})^2 - 2\tau_w(R_5 + \tau_{7max}) \cos\left[\arcsin\left(\frac{R_7 \sin\theta_2}{R_5 + \tau_{7max}}\right)\right]$$

5.1.1 General Forked Wagon Wheel (Continued)

$$Temp_a = \arcsin\left[\frac{R_7 \sin\theta_2}{R_5 + \tau_{7max}}\right]$$

$$Temp_b = \pi - \arcsin\left[\frac{R_7 \sin\theta_2}{Temp}\right]$$

$$Temp_c = \arcsin\left[\frac{Temp \sin(Temp_b)}{(T_{SLVR} + R_5)}\right]$$

$$\beta_{VXX} = Temp_c - Temp_a$$

$$A_{SLVR} = \theta_2 R_f^2 - (R_f - \tau_w)R_7 \sin\theta_2 - (\theta_2 - \theta_{SLV})R_f^2 + (TSLVR + R_5)R_7 \sin\{\pi - \theta_2 + \theta_{SLV} - \arcsin[R_7 \sin(\theta_2 - \theta_{SLV})/(T_{SLVR} + R_5)]\} - Temp(T_{SLVR} + R_5)\sin(\pi - Temp_c - Temp_b) - (\beta_{VXX} + \beta_{VX})(T_{SLVR} + R_5)^2$$

22. If $\tau \leq \tau_w$,

$$\beta_{72} = \beta_{72max}$$

$$AFP_7 = AFP + \theta_2 R_f^2 - R_f R_7 \sin\theta_2 - \beta_{72}(R_5 + \tau)^2$$

$$L_7 = (\beta_{71} + \beta_{72})(R_5 + \tau)$$

23. If $\tau > \tau_w$,

$$\beta_{72} = \arccos\left\{\frac{(\tau + R_5)^2 + (R_f - \tau_w - R_5)^2 - R_f^2}{2(\tau + R_5)(R_f - \tau_w - R_5)}\right\} - \beta_{71max} - \alpha_{03} - \frac{\pi}{2} + \theta_2$$

5.1.1 General Forked Wagon Wheel (Continued)

$$AFP_7 = AFP + \theta_2 R_f^2 - R_f R_7 \sin\theta_2 + R_7(R_5 + \tau)\sin(\beta_{72max} - \beta_{72})$$

$$- R_f^2 \arccos\left\{1 - \left(\frac{R_5 + \tau(\sin(\beta_{72max} - \beta_{72})}{R_f}\right)^2\right\}^{1/2}$$

$$- \beta_{72}(R_5 + \tau)^2$$

$$L_7 = (\beta_{71} + \beta_{72})(R_5 + \tau)$$

24. If $\tau < \tau_{SLVR}$,

$$L = L_1 + L_2 + L_3 + L_4 + L_5 + L_6 + L_7$$

$$AFP = AFP_1 + AFP_2 + AFP_3 + AFP_4 + AFP_5 + AFP_6 + AFP_7 - ASLVR$$

25. If $\tau \geq \tau_{SLVR}$,

$$L = 0$$

$$AFP = 0$$

5.1.2 Slotted-Cone

The slotted-cone configuration is an addition to the standard star in which a segment of propellant, represented by angle θ_6, has been inserted as shown in Figure 5.6. The insert of propellant results in additions to the perimeter and area calculations for a standard star which requires the determination of three basic angles, QAG, RAG, and SAG, shown in Figures 5.9, 5.10, and 5.11, respectively. Nine points, A, B, C, C', E, F, G, J, and H are defined in Figure 5.7, and are used in the following analysis to determine line lengths and angles. Four moving points, P, Q, R, and S on the burning perimeter are identified in Figures 5.8 through 5.13.

Point A lies on the motor axis (Figure 5.7). Point B coincides with the center of the input radius R_5 and point F coincides with the center of the input radius R_2. Point G is located on the case

5.1.2 Slotted-Cone (Continued)

wall at the point where a line through points A and F intersect the case. Points C and E are located on the case wall where a line perpendicular to side L_c at the intersection of side L_c with radius R_5 intersects the case and where a line perpendicular to side L_c at the intersection of side L_c with radius R_2 intersects the case. Point H lies on the case wall at the angle θ_0 from point G. Point C' defines the point where side L_c of the standard star disappears as a result of the progression of the burning surface of the slotted cone insert.

Perimeter length QR, Figure 5.9, defines the addition to side L_c of the standard star, resulting from the addition of the central angle θ_0 of the slotted-cone. Perimeter length PQ defines the length of the arc subtended from the radius, $(R_1 + \tau)$, and intersecting with length QR. When the burning distance, τ, is less than or equal to the input radius R_2, only the perimeter length PQ is present. When the burning distance is greater than R_2, but less than or equal to the geometry constant T_{6max}, as shown in Figure 5.9, both perimeter lengths PQ and QR are present.

Perimeter length RS defines the addition to the arc subtended from the point of the input radius R_5 (geometry point B). Whenever T'_{V7} is greater than T_{7max}, and T_{7max} is greater than T_{6max} (Figure 5.10), and τ is greater than T_{6max} but less than or equal to T_{7max}, geometry point S lies on the line AG and perimeter lengths PQ, QR, and RS are present.

Whenever τ is greater than T_{7max} but less than T'_{V7}, perimeter length RS is defined as in Figure 5.11.

Whenever τ is greater than T'_{V7}, as shown in Figures 5.12 and 5.13, geometry point R and perimeter length QR do not exist and only perimeter lengths PQ and QS remain.

The angle θ_0 is allowed to vary on input between 0° and 90°. Should θ_0 be less than the angle QAG shown in Figure 5.9, then the perimeter length PQ does not exist and point Q then lies on the line AH. Should θ_0 be less than the angles QAG and RAG, then the perimeter lengths PQ and QR and the points P and Q do not

5.1.2 Slotted-Cone (Continued)

exist and the point R lies on the line AH. When angle SAG exceeds θ_0, complete burnout has occurred.

The following are the port perimeter and propellant cross sectional area equations for this addition to the standard star configuration. Figures 5.8 through 5.13 show the progression of the burning surface and the geometric figures required for each equation.

1. If $\tau \leq R_2$ (Figure 5.8),

$$\text{Perimeter} = \theta_0(R_1 + \tau)$$

$$\text{Area} = \theta_0 \left[R_f^2 - (R_1 + \tau)^2\right]$$

2. If $\tau > R_2$ (Figure 5.9),

$$\angle AJB = \arcsin \left[\frac{(R_f - R_5 - \tau_w)}{T_{6max} + R_5} \sin \theta_2\right]$$

$$\angle ABC = \pi - \theta_2 - \angle AJB$$

$$\angle ACB = \arcsin \left[\frac{(R_f - R_5 - \tau_w)}{R_f} \sin \angle ABC\right]$$

$$\angle BAC = \pi - \angle ABC - \angle ACB$$

$$BC = R_f \frac{\sin \angle BAC}{\sin \angle ABC}$$

$$T'_{V6} = BC - R_5$$

$$T'_{V7} = \frac{(R_f - R_5 - \tau_w)^2 - R_1^2 - R_5^2 - 2(R_f - R_5 - \tau_w)R_5 \cos \angle ABC}{2R_1 - 2R_5 + 2(R_f - R_5 - \tau_w) \cos \angle ABC}$$

$$Temp_{76} = \text{minimum of } T'_{V7} \text{ and } T'_{V6}$$

5.1.2 Slotted-Cone (Continued)

3. If $R_2 < Temp_{76}$, and if $\tau \leq T_{6max}$ (Figure 5.3),

$$FR = \frac{(\tau - R_2)}{\sin \alpha_{01}}$$

$$AR = R_1 + R_2 + FR$$

$$\angle RQA = \pi - \arcsin \left[\frac{AR \sin \alpha_{01}}{R_1 + \tau}\right]$$

$$\angle QAR = \pi - \angle RQA - \alpha_{01}$$

$$QR = (R_1 + \tau) \frac{\sin \angle QAR}{\sin \alpha_{01}}$$

$$\angle QAG = \arcsin \left[\frac{QR \sin \alpha_{01}}{(R_1 + \tau)}\right]$$

a. and $\angle QAG \geq \theta_0$,

$$\text{Perimeter} = \frac{AR \sin \theta_0}{\sin(\pi - \alpha_{01} - \theta_0)}$$

$$\text{Area} = \theta_0 R_f^2 - (\text{Perimeter}) AR \sin \alpha_{01}$$

b. Or $\angle QAG < \theta_0$,

$$PQ = (R_1 + \tau)(\theta_0 - \angle QAG)$$

$$\text{Perimeter} = PQ + QR$$

$$\text{Area} = \theta_0 R_f^2 - (\theta_0 - \angle QAG)(R_1+\tau)^2 - QR\ AR \sin \alpha_{01}$$

5.1.2 Slotted-Cone (Continued)

4. If $R_2 < \tau < Temp_{76}$ and if $T_{6max} < \tau \leq T_{7max}$ (Figure 5.10),

$$\angle ASB = \arcsin\left[\frac{(R_f - R_5 - \tau_w)\sin\theta_2}{(R_5 + \tau)}\right]$$

$$\angle SBA = \pi - \theta_2 - \angle ASB$$

$$Area_1 = \theta_0 R_f^2 + (R_f - R_5 - \tau_w)(R_5 + \tau)\sin\angle SBA$$

a. And $\angle RAG \geq \theta_0$

$$\angle BRA = \arcsin\left[\frac{(R_f - R_5 - \tau_w)\sin(\theta_2 + \theta_0)}{(R_5 + \tau)}\right]$$

$$\angle RBA = \pi - \angle BRA - \theta_2 - \theta_0$$

$$\angle RBS = \angle SBA - \angle RBA$$

$$RS = \angle RBS(R_5 + \tau)$$

$$Perimeter = RS$$

$$Area = Area_1 - (R_f - R_5 - \tau_w)(R_5 + \tau)\sin\angle RBA - \angle RBS(R_5 + \tau)^2$$

b. Or $\angle RAG < \theta_0$

$$Area_2 = Area_1 - \angle RBS(R_5 + \tau)^2 - (R_f - R_5 - \tau_w)(R_5 + \tau)\sin\angle ABC$$

(1) And if $\angle QAG \geq \theta_0$

$$\angle QAR = \theta_0 - \angle RAG$$

$$\angle AQR = \pi/2 + \angle ARB - \angle QAR$$

$$QR = \frac{AR \sin\angle QAR}{\sin\angle AQR}$$

$$Perimeter = QR + RS$$

5.1.2 Slotted-Cone (Continued)

$$\text{Area} = \text{Area}_2 - QR\ AR \sin(\pi/2 - \angle ARB)$$

(2) Or if $\angle QAG < \theta_0$

$$\angle PAQ = \theta_0 - \angle QAG$$

$$PQ = \angle PAQ(R_1 + \tau)$$

$$QR = \frac{(R_1 + \tau) \sin \angle RAQ}{\sin(\pi/2 - \angle ARB)}$$

$$\text{Perimeter} = PQ + QR + RS$$

$$\text{Area} = \text{Area}_2 - QR\ AR \sin(\pi/2 - \angle ARB) - \angle PAQ(R_1+\tau)^2$$

5. If $R_2 < \tau < \text{Temp}_{76}$, and if $T_{6max} < \tau > T_{7max}$ (Figure 5.11),

$$\angle SAB = \arccos \left[\frac{R_f^2 + (R_f - R_5 - \tau_w)^2 - (R_5+\tau)^2}{2 R_f (R_f - R_5 - \tau_w)} \right]$$

$$\angle SAG = \angle SAB - \theta_2$$

$$AR = \left[(R_5+\tau)^2 + (R_f - R_5 - \tau_w)^2 - 2(R_5+\tau)(R_f - R_5 - \tau_w) \cos \angle ABC \right]^{1/2}$$

$$\angle RAB = \arcsin \left[\frac{(R_5+\tau) \sin \angle ABC}{AR} \right]$$

$$\angle RAG = \angle RAB - \theta_2$$

$$\angle ARB = \pi - \angle ABC - \angle RAB$$

$$\angle ARQ = \frac{\pi}{2} - \angle ARB$$

$$\angle AQR = \pi - \arcsin \left[\frac{AR \sin \angle ARQ}{(R_1 + \tau)} \right]$$

$$\angle QAR = \pi - \angle AQR - \angle ARQ$$

$$\angle QAG = \angle QAR + \angle RAG$$

5.1.2 Slotted-Cone (Continued)

a. And $SAG \geq \theta_0$

Complete burnout has occurred.

Perimeter = 0.0
Area = 0.0

b. Or $SAG < \theta_0$

$$\angle ASB = \arcsin\left[\frac{(R_f - R_5 - \tau_w)\sin(\theta_2 + \angle SAG)}{(R_5+\tau)}\right]$$

$$\angle SBA = \pi - \theta_2 - \angle SAG - \angle ASB$$

$$Area_1 = (\theta_0 - \angle SAG)R_f^2 + R_f(R_f - R_5 - \tau_w)\sin(\theta_2 + \angle SAG)$$

$$\angle RQA = \pi - \arcsin\left[\frac{AR\sin(\pi/2 - \angle ARB)}{(R_1 + \tau)}\right]$$

$$\angle RAQ = \frac{\pi}{2} + \angle ARB - \angle RQA$$

$$\angle QAG = \angle RAQ + \angle RAG$$

$$\angle RBS = \angle SBA - \angle ABC$$

$$RS = \angle RBS(R_5 + \tau)$$

(1) and If $\angle RAG \geq \theta_0$ go to 4a

(2) or If $\angle RAG < \theta_0 \leq \angle QAG$ go to 4b(1)

(3) or If $\angle RAG < \theta_0 > \angle QAG$ go to 4b(2)

6. If $R_2 < \tau \geq Temp_{76}$, and if $T'_{V6} = T'_{V7}$

Complete burnout has occurred.

Perimeter = 0.0
Area = 0.0

5.1.2 Slotted-Cone (Continued)

7. if $R_2 < \tau \geq TEMP_{76}$, and if $T_{V6}' > T_{V7}'$, and $\tau \leq \tau_w$ (Figure 5.12),

$$\angle QAB = \arccos\left[\frac{(R_{V1} + \tau)^2 + (R_f - R_5 - \tau_w)^2 - (R_5 + \tau)^2}{2(R_1 + \tau)(R_f - R_5 - \tau_w)}\right]$$

$$\angle AQB = \arcsin\left[\frac{(R_f - R_5 - \tau_w)\sin(\angle QAB)}{(R_5 + \tau)}\right]$$

$$\angle ABQ = \pi - \angle AQB - \angle QAB$$

$$\angle ASB = \arcsin\left[\frac{(R_f - R_5 - \tau_w)\sin(\theta_2)}{(R_5 + \tau)}\right]$$

$$\angle ABS = \pi - \theta_2 - \angle ASB$$

$$\angle QAG = \angle QAB - \theta_2$$

a. and $\angle QAG \geq \theta_0$

$$\angle AQB = \arcsin\left[\frac{(R_f - R_5 - \tau_w)\sin(\theta_2 + \theta_0)}{(R_5 + \tau)}\right]$$

$$\angle ABQ = \pi - \theta_2 - \theta_0 - \angle AQB$$

$$\angle QBS = \angle ABS - \angle ABQ$$

$$PERIM = \angle QBS(R_5 + \tau)$$

b. or $\angle QAG < \theta_0$

$$PERIM = (\angle ABS - \angle ABQ)(R_5 + \tau) + (\theta_0 - \angle QAG)(R_1 + \tau)$$

5.1.2 Slotted-Cone (Continued)

g. If $R_2 < T \geq Temp_{76}$, and if $T'_{V6} > T'_{V7}$ and $\tau > \tau_w$ (Figure 5.12), A

$$\angle SAB = \arccos\left[\frac{R_f^2 + (R_f - R_5 - \tau_w)^2 - (R_5+\tau)^2}{2R_f(R_f - R_5 - \tau_w)}\right]$$

$$\angle SAG = \angle SAB - \theta_2$$

a. and $\angle SAG \geq \theta_0$

Complete burnout has occurred.

Perimeter = 0.0
Area = 0.0

b. Or $\angle SAG < \theta_0$

$$\angle QAB = \arccos\left[\frac{(R_1+\tau)^2 + (R_f - R_5 - \tau_w)^2 - (R_5+\tau)^2}{2(R_1+\tau)(R_f - R_5 - \tau_w)}\right]$$

$$\angle QAG = \angle QAB - \theta_2$$

$$\angle ABS = \arccos\left[\frac{(R_f - R_5 - \tau_w)^2 + (R_5+\tau)^2 - R_f^2}{2(R_f - R_5 - \tau)(R_5+\tau)}\right]$$

(1) and If $\angle QAG \geq \theta_0$

$$\angle AQB = \arcsin\left[\frac{(R_f - R_5 - \tau_w)\sin(\theta_2+\theta_0)}{(R_5+\tau)}\right]$$

$$\angle ABQ = \pi - \theta_2 - \theta_0 - \angle AQB$$

$$\angle QBS = \angle ABS - \angle ABQ$$

$$QS = \angle QBS(R_5+\tau)$$

Perimeter = QS

$$\text{Area} = (\theta_2+\theta_0 - \angle SAB)R_f^2 + R_f(R_f - R_5 - \tau_w)\sin\angle SAB - (R_5+\tau)^2\angle QBS - (R_f - R_5 - \tau_w)(R_5+\tau)\sin\angle ABQ$$

5.1.2 Slotted-Cone (Continued)

(2) Or if $\angle QAG < \theta_0$

$$\angle ABQ = \arccos \left[\frac{(R_f - R_5 - \tau_w)^2 + (R_5 + \tau)^2 - (R_1 + \tau)^2}{2(R_f - R_5 - \tau_w)(R_5 + \tau)} \right]$$

$$\angle QBS = \angle ABS - \angle ABQ$$

$$QS = \angle QBS \, (R_5 + \tau)$$

$$\angle PAQ = \theta_2 + \theta_0 - \angle QAB$$

$$PQ = \angle PAQ \, (R_1 + \tau)$$

$$\text{Perimeter} = PQ + QS$$

$$\text{Area} = (\theta_2 + \theta_0 - \angle SAB) R_f^2 + R_f (R_f - R_5 - \tau_w) \sin \angle SAB - (R_5 + \tau)^2 \angle QBS - (R_1 + \tau)(R_f - R_5 - \tau_w) \sin \angle QAB - (\theta_2 + \theta_0 - \angle QAB)(R_1 + \tau)^2$$

5. If $R_2 < \tau \geq \text{Temp}_{76}$, and if $T_{V6} < T_{V7}$ (Figure 5.13), A

$$AT = \left[(R_f - R_5 - \tau_w)^2 + (R_5 + \tau)^2 - 2(R_f - R_5 - \tau_w)(R_5 + \tau) \cos \angle ABC \right]^{1/2}$$

$$\angle ATB = \arcsin \left[\frac{(R_f - R_5 - \tau_w) \sin \angle ABC}{AT} \right]$$

$$\angle STA = \pi/2 - \angle ATB$$

$$\angle AST = \pi - \arcsin \left[\frac{AT \sin \angle STA}{R_f} \right]$$

$$\angle TAB = \pi - \angle ABC - \angle ATB$$

$$\angle SAT = \pi - \angle AST - \angle STA$$

$$\angle SAG = \angle SAT + \angle TAB - \theta_2$$

a. And $\angle SAG \geq \theta_0$

Complete burnout has occurred.

5.1.2 Slotted-Cone (Continued)

Perimeter = 0.0
Area = 0.0

b. Or $\angle SAG < \theta_0$

$$\angle QSA = \pi - \angle AST$$

$$\angle AQS = \pi - \arcsin \left[\frac{R_f \sin \angle QSA}{(R_1 + \tau)} \right]$$

$$\angle QAS = \pi - \angle AQS - \angle QSA$$

$$\angle QAG = \angle SAG + \angle QAS$$

(1) And if $\angle QAG \geq \theta_0$

$$\angle QAS = \theta_0 - \angle SAG$$

$$\angle AQS = \pi - \angle QAS - \angle QSA$$

$$QS = \frac{R_f \sin \angle QAS}{\sin \angle AQS}$$

Perimeter = QS

Area = $\angle QAS \, R_f^2 - R_f \, QS \sin \angle QSA$

(2) Or if $\angle QAG < \theta_0$

$$\angle PAQ = \theta_0 - \angle QAG$$

$$PQ = (R_1 + \tau) \angle PAQ$$

$$QS = R_f \frac{\sin \angle QAS}{\sin \angle AQS}$$

Perimeter = PQ + QS

Area = $(\angle PAQ + \angle QAS) R_f^2 - QS \, R_f \sin \angle QSA - \angle PAQ \, (R_1 + \tau)^2$

5.2 Grain Longitudinal Geometry

Representative longitudinal configurations which can be accommodated by the computer program have been shown in Figure 2.2. Many configurations are possible: monolithic or segmented grains in the cylindrical section of the motor; head-end with web or a straight through grain in the fore-head section; straight through grain in the aft-head; external and internal taper; and elliptical contour fore-head and aft-head motor sections are examples. Grain cross sectional geometry can be varied within the cylindrical section of the motor.

5.2.1 Head-End with Web, Fore-Head Section

This section describes the analysis of the head-end with web which is solved in the third core load of the computer program. Description of the head-end with web calculations are based on the motor fore-head section shown in Figure 5.14. Grain geometry within the fore-head section is based on the input geometrical cross section at the forward tangent plane.

The burning surface area for all distances burned and the initial propellant volume are obtained by separating the analysis into four blocks. Each block performs the following function:

Block 1 calculates the surface area versus distance burned and the initial volume of the propellant tip. The volume and area are obtained by integrating elemental areas and volumes consisting of trapezoids and parallelograms.

Block 2A calculates the surface area of the pseudoellipsoid minus the igniter opening using the Theorem of Pappus. Block 2B calculates the volume of propellant between the inner and outer ellipsoids and the surface area on the pseudo ellipsoid which is covered by the propellant tip. The volume and area are obtained by integrating elemental areas and volumes using the Theorem of Pappus.

Block 3 calculates the initial total propellant volume. The volume between the inner and outer ellipsoids is determined from the difference in volume of two oblate spheroids. The volume of the tip is obtained by adding the volumes of cylindrical segment elements.

Total surface area, A, versus distance burned is obtained by combining the blocks:

$$A = A_{\text{Block 1}} + A_{\text{Block 2A}} - A_{\text{Block 2B}}$$

The initial propellant volume is calculated in two ways, one

5.2.1 Head-End with Web, Fore-Head Section (Continued)

method as in Block 3 and the other by:

$$\text{Volume} = V_{\text{Block 1}} + V_{\text{Block 2B}}$$

The initial volumes are compared in subroutine VOLSUB and a correction factor, A_R, is obtained which is added to the total burning surface area. This is due to the assumption that the difference is caused by the integration method in the Block 1 analysis.

Subroutine HDNSUB

Subroutine HDNSUB is the control routine which sets up the correct variables and equations to perform the block 1, 2A, 2B, and 3 analysis.

5.2.1.1 Block 1 Analysis

The generalized forked wagon wheel grain configuration is divided into 13 sectors (1, 2, 3, 3A, 3B, 4, 5, 6, 7, 9, 10, 11, 11A, 11B, 12, 13) as shown in Figure 5.15. Sectors (1, 2, 4, 5, 6, 7, 9, 10, 12 and 13) share a common analysis, as do sectors (3 and 11) and (3A, 3B, 11A, and 11B); however, some of the sectors have special equations for line segments and angles. The sector boundaries used for the head-end with web analysis, Figure 5.15, are different than sector boundaries used for the straight through grain analysis, Section 5.2.3 and Figure 5.32 .

Subroutine SCI is the control routine to determine the surface area versus distance burned and initial volume of the propellant tip for the block 1 analysis and is called from subroutine HDNSUB with an argument L to indicate the sector to be computed. The analysis for sectors 1 and 3 will be explained in detail since the analysis for the other sectors is similar.

Figure 5.16 shows geometric constructions and calculation control planes used to obtain elemental burn surface areas and propellant volumes in the propellant tip. Also shown is part of a forked wagon wheel grain and the required constructions. For clarity, only one tip is shown. Two planes, "A" and "B", control volume and area calculations for the propellant tip. These two planes are generated as follows: The intersection of the surface of the propellant tip with the forward tangent plane, i.e., the tangent plane perimeter, Figure 5.16b, is divided into incremental lengths, $\Delta L0$. Lines, spaced $\Delta L0$ apart, perpendicular to the tangent plane, are run from the tangent plane along the side of the propellant tip to intersect the inner ellipsoid. These intersections locate points P_{oa} and P_{ob}.

5.2.1.1 Block 1 Analysis (Continued)

Perpendiculars to the side of the propellant tip from points P_{oa} and P_{ob} locate points P_{1a} and P_{1b} on the plane of symmetry or on the outer ellipsoid depending on the initial location of each $\Delta L0$ along the propellant tip perimeter in the tangent plane. Figure 5.16a shows P_{1a} and P_{1b} on the plane of symmetry. Perpendiculars to the inner ellipsoid at points P_{oa} and P_{ob} locate points P_{2a} and P_{2b} on the outer ellipsoid. Points P_{oa}, P_{1a}, P_{2a}, P_{ob}, P_{1b}, and P_{2b} define the A and B planes. Points P_{3a} and P_{3b} lie in the A and B planes and are located on the outer ellipsoid.

The trapezoid formed by $\Delta L0$ on the perimeter of the tip at the tangent plane and points P_{oa} and P_{ob} is the area calculation element.

Perpendiculars, in "x-z" planes, for these same four points form the volume calculation elements which are bounded by the trapezoidal area elements as shown in Figure 5.16. The $\Delta L0$ spacing on the propellant tip perimeter which governs plane placement varies in value along the perimeter as follows:

The $\Delta L0$ spacing, Figure 5.16b, is calculated first as:

a) $\Delta L0_1$ of each sector is:

$$\Delta L0_1 = \left(\frac{\Delta L}{R_f}\right) R_f$$

where $\frac{\Delta L}{R_f}$ is an input parameter.

b) $\Delta L0$ is then modified by:

$$\Delta L0 = \frac{K(\Delta L0_{previous})}{(D_{pr} + D_{ps})}$$

where

D_{pr} and D_{ps} are the distances between planes A and B, Figure 5.17.

The starting value of $\Delta L0$ previous is $\Delta L0_1$.

5.2.1.1 Block 1 Analysis (Continued)

The factor K, an input variable, is the major parameter in determining the distance between the two planes. The incremental distance $\Delta L0$ is stepped along the sector perimeters from $L_x = 0$ to $L_x = L_p$.

5.2.1.1.1 Sector 1 (Figure 5.15)

Subroutines ASUBC, BSUBC, RASUBB, XRSUBB, THETAR, GAMSUB, GAMA2S, POSUB, P1SUB, P3SUB, ROPSB, and VSTRSB are used to obtain the surface area and initial volume for sector 1.

The distance D_{03} between the points P_0 and P_3 on the inner ellipsoid are shown in Figure 5.18 for planes that are located at increments of one-tenth the perimeter length of a sector. A minimum perimeter length, HOLDR, is set equal to the perimeter length in which the distance D_{03} for the plane is greater than the burn distance, τ. The first plane is located at the perimeter length HOLDR and subsequent planes are spaced the distance $\Delta L0$ apart. HOLDR is initialized to the perimeter length for plane B on subsequent iterations.

After the minimum perimeter length, HOLDR, is determined, the distance D_{03} for a plane located at the total perimeter AL(1) for the sector is determined. The parameter TDMAX is initialized to the maximum value of TDMAX or D_{03} for the sector and then checked with the maximum permissible burn distance, TAUM. If TDMAX equals or exceeds TAUM, an error condition exists and execution is terminated. If all D_{03}'s are less than TAUM, the radial burning surface area between the planes and the burning surface area on the propellant tip are determined.

Radial burning surface area, Figure 5.17:

$$ASI = \frac{(L_{TA} + L_{TB})(D_{pr} + D_{ps})}{4}$$

Propellant tip burning surface area:

$$ASI = \frac{(L_p - HOLDR)(R_2 - \tau)(Y_{0A} + Y_{0B})}{2R_2}$$

where Y_0 is defined in Figure 5.21.

5.2.1.1.1 Sector 1 (Figure 5.15) (Continued)

L_P is the perimeter length along the initial grain perimeter measured from the beginning of a sector to a general point. HOLDR is the prior incremental value of L_P.

The initial volume is determined from the following equation:

$$V_{STR} = \frac{(Y_{OA} + Y_{OB})(L_P - HOLDR)R_2}{4}$$

Subroutine ASUBC

Subroutine ASUBC sets up the correct variables and equations to determine the coordinates (X, Y, and Z) of the points P_{oa}, P_{1a}, and P_{3a} for planes located at increments of one-tenth L_p along the perimeter of the sector. Subroutines RASUBB, XRSUBB, THETAR, GAMSUB, GAMA2S, POSUB, P1SUB, P3SUB, and TRAN are called to determine the coordinates.

Subroutine RASUBB

Subroutine RASUBB determines the length of the radius vector, R_{aT}, from the motor axis to a general point in a sector. The perimeter length from the beginning of the sector to a general point is required in calculating a value of R_{aT} for each sector, Figure 5.19.

Subroutine XRSUBB

Subroutine XRSUBB determines the X-coordinate, X_{ra}, for a point located on the perimeter of a sector. The parameter R_{aT} from the RASUBB subroutine is required to obtain the coordinate. A separate equation is required for each sector, Figure 5.15.

Subroutine THETAR

Subroutine THETAR determines the angle, θ_r, between the Z-axis and the line segment R_{aT}. The parameters X_{ra} and R_{aT} are required to obtain θ_r, Figure 5.15.

Subroutine GAMSUB

Subroutine GAMSUB determines the angle γ_1 between the line normal to the perimeter in the XZ-plane, and a line normal to the line segment R_{aT}, Figure 5.19. The perimeter length of the sector and the angle θ_r are required to obtain γ_1. A separate equation for each of the 16 individual sectors is required. γ_1 for sector 3A is not equal to γ_1 for sector 3B (also true for sectors 11A and 11B).

5.2.1.1.1 Sector 1 (Figure 5.15) (Continued)

Subroutine GAMA2S

Subroutine GAMA2S determines the angle γ_2 between the Y-axis and a line normal to the ellipse $\left(\frac{Y}{B_{oe}}\right)^2 + \left(\frac{Z'}{A_{oe}}\right)^2 = 1$, which is defined by the ellipse ratio β_{oe}, at the point $Z' = RAT$. Although γ_2 is in the rotated YZ'-plane and not in the YZ-plane, because of the symmetry of the ellipsoid about the Y-axis, computation can occur in the YZ-plane, Figure 5.20.

Subroutine POSUB

Subroutine POSUB determines the coordinates X, Y, and Z of the point P_0 which is located at the intersection of the inner ellipse and a line extended along the propellant surface parallel to the tip from a general point on the perimeter, Figures 5.16 and 5.21.

The parameters R_{aT} and θ_r are required to determine the coordinates. The coordinates X_o and Z_o are obtained by trigonometry from R_{aT} and θ_r, Figure 5.21. The equation of the ellipsoid:

$$\left(\frac{Y_o}{B_{oe}}\right)^2 + \left(\frac{X_o^2 + Z_o^2}{A_{oe}^2}\right) = 1$$

yields the coordinate Y_o.

The remaining points defining the plane (P_1, P_2, and P_3) are obtained from P_o. Radial burning in the plane originates at P_o.

Subroutine P1SUB

Subroutine P1SUB determines the coordinates (X_1, Y_1, and Z_1) of the point P_1 which is located on the Y-Z plane or on the outer ellipse along a line through point P_o and normal to the sector perimeter as shown in Figure 5.22. P_1 is normally located on the Y-Z plane; however, for sectors 7 and 9, when the angle γ_1 exceeds β_{71max} in sector 7 or β_{91max} in sector 9, the point P_1 is located on the outer ellipse and is coincident with P_3. The line segment Z_{1aT} shown in Figure 5.19 is used to flag subroutine P3SUB that P_1 is coincident with P_3 whenever Z_{1aT} is non-zero.

5.2.1.1.1 Sector 1 (Figure 5.15) (Continued)

β_{91max} and β_{71max} are geometry plane constants discussed in Section 5.1.1.

Subroutine P3SUB

Subroutine P3SUB determines the coordinates (X_3, Y_3, and Z_3) of the point P_3 that is located on the outer ellipse. If Z_{1aT}, determined in subroutine P1SUB, is not equal to zero, P_3 is coincident with P_1 and the coordinates of P_3 are set equal to the coordinates of P_1. If Z_{1aT} is equal to zero, then P_3 is in the Y-Z plane and the coordinates of P_3 are determined from the angle Φ shown in Figure 5.22.

Subroutine ROPSB

Subroutine ROPSB sums the values of the Y axis coordinate of P_o (Y_{0A} and Y_{0B}) or P_o' (Y_{0A}' and Y_{0A} or Y_{0B}' and Y_{0B}) in planes A and B which are used in subroutine SCI to compute the surface area along the grain face. If the burn distance τ is greater than the maximum permissible burn distance for the sector, then the value of the sum is set to zero.

Subroutine BSUBC

Subroutine BSUBC sets up the correct variables and equations to determine the coordinates (X, Y, and Z) of the points P_{ob}, P_{1b}, and P_{3b} located at increments of $\Delta L0$ along the perimeter of sector 1, Figure 5.15. The A plane coordinates are initialized to the prior B plane coordinates during the integration along the perimeter.

Subroutine VSTRSB

Subroutine VSTRSB determines the initial volume of the sectors. The incremental volume for each sector is determined from the incremental cross-sectional areas of the sectors and the average of the P_o point Y-coordinates of the A and B planes.

5.2.1.1.2 Sector 3

Subroutines HASUBC, HBSUBC, HAPSBC, HBPSBC, STUPRS, STUPPS, DPRASB, RASUBB, XRSUBB, THETAR, GAMSUB, GAMA2S, POSUB, P1SUB P3SUB, and ROPSB are used to obtain the surface area and initial

5.2.1.1.2 Sector 3 (Continued)

volume for sectors 3, 3A, and 3B. As in sector 1, two planes are used to obtain the surface area. The distance between the planes A and B is determined by $\Delta L0$ in the same manner as for sector 1. The analysis for the surface area in sector 3 is similar to the analysis for the surface area in sector 1 except that the A and B planes will cross as shown in Figure 5.23 for sectors 3 and 11 and in Figure 5.24 for sectors 3A, 3B, 11A, and 11B.

The perimeter length of sector 3A (AL3A) is determined from the geometry constants, and the coordinates of points P_0, P_1, and P_3 for both planes A and B. Since the surface area of sector 3B is identical with the surface area of sector 3A, the grain surface areas of both sectors between the planes are determined simultaneously by stepping the B plane an increment $\Delta L0$ along the sector 3A perimeter. The surface area along the grain between the planes is determined from the following equation:

$$ASI = \frac{(Y_0 + Y_0')}{2} \left[(X_0 - X_0')^2 + (Z_0 - Z_0')^2\right]^{1/2}$$

The surface area along the tip for sector 3 is determined from the following equation after the integration for sector 3A is complete:

$$ASI = L_3 \frac{(R_2 - \tau)}{R_2} \frac{(Y_{0A} + Y_{0B})}{2}$$

where L_3 is the initial sector 3 perimeter length.

The initial volume of sector 3, and sectors 3A and 3B, is determined at the beginning of subroutine SCTOR1 after completion of the block 1 analysis as follows:

$$V_{STR} = \frac{(Y_{0A}+Y_{3A}+Y_{0B}+Y_{3B})(\tau_{2max}+R_3)}{4.} + \frac{(\alpha_{01}-\alpha_{02})(Y_{0B}+Y_{3B})R_3^2}{4.}$$

Subroutines RASUB3, XRSUBB, THETAR, GAMSUB, CAMA2S, POSUB, P1SUB, P3SUB, and ROPSB have been explained in Section 5.2.1.1.1 for sector 1. Therefore, only the subroutines unique to sector 3 are explained in this section.

5.2.1.1.2 Sector 3 (Continued)

Subroutines HASUBC, HBSUBC, HAPSUBC, and HBPSUBC

The function of these subroutines is the same as the function of subroutines ASUBC and BSUBC for sector 1; the correct variable and equations are set up to determine the coordinates (X, Y, and Z) of the points P_o, P_1, and P_3 for planes located at increments of $\Delta L0$ along the perimeter of the sector. Subroutine HASUBC deals with plane A, subroutine HBSUBC deals with plane B, subroutine HAPSBC deals with plane A', and subroutine HBPSBC deals with plane B', Figure 5.24.

Subroutines STUPRS and STUPPS

These subroutines store the variables that define the planes produced in sector 3A. Subroutine STUPRS is called in subroutine SCI after the A and B planes have been defined by subroutines HASUBC and HBSUBC. Subroutine STUPPS is called in subroutine SCI after the A' and B' planes have been defined by subroutines HAPSBC and HBPSBC. The stored variables are then used in subroutine SCI to determine the area along the grain face.

Subroutine DPRASB

Subroutine DPRASB determines the distance between the points P_{ra} and P'_{ra} and between P_{sa} and P'_{sa} that lie on the planes produced in sector 3A as shown in Figure 5.24. These distances DP_{ra} and DP_{sa} are used in subroutine SCI to alter the distance between the planes ($\Delta L0$) for each successive iteration as explained in Section 5.2.1.1 for sector 1.

5.2.1.2 Block 2A Analysis

Subroutine SCTOR1 is the control routine to determine the surface area of the pseudoellipsoid for the block 2A analysis and is called from subroutine HDNSUB. The initial volume of propellant for sectors 3A, 3B, 11A, and 11B is determined prior to the integration for the pseudoellipsoid surface area.

Points P_o and P_1 that are used in Block 2A are not the same plane points used in the Block 1 analysis. Points P_o and P_1 lie on the inner ellipsoid and are spaced a distance DS along the ellipsoid, Figure 5.25, starting at the igniter opening. The spacing of P_o and P_1 are determined as follows:

5.2.1.2 Block 2A Analysis (Continued)

First

$$\Delta R = \left(\frac{\Delta R_v}{R_f}\right) R_f$$

where

$\frac{\Delta R_v}{R_f}$ is an input parameter

R_f grain radius at the forward tangent plane.

Then each successive increment is

$$\Delta R = \frac{KK}{DS} \Delta R$$

where KK is an input.

Initially, if the motor has an igniter hole in the head end, Z_{P0}, which is the Z-coordinate of the point, P_0, is set equal to R_{ig}. Otherwise, Z_{P0} is set equal to zero. ΔR is then added to Z_{P0} to obtain Z_{P1}, which is the Z coordinate of the point P1. Subroutine YPSUB is then called to obtain the Y coordinate of points P_0 and P_1. The radius of curvature ρ_1 at the point P_1 on the pseudoellipsoid, the length, b, of the Y-intercept of the normal line to the ellipse at P_0, and the Z coordinate Z_i are then determined to obtain the arc length, L_Q. Using these values, the incremental strip surface area is determined. This procedure is then repeated by setting $Z_{P0} = Z_{P1}$, and $Z_{P1} = Z_{P0} + \Delta R$ until $Z_{P1} = R_f - \tau_w$. The area adjacent to the igniter hole is then determined and added to the incremental sum.

Subroutines YPSUB, POEISB, LBSUB, ZISUB, and AIGSUB are used to determine the surface area of the pseudoellipsoid. The surface area for an incremental strip, as shown in Figure 5.25, is determined by the following equation:

$$ASI = \frac{\pi L_Q}{2NO} (Z_{P1} + \tau \sin \alpha_{rc1} + Z_{P0} + \tau \sin \alpha_{rc0})$$

5.2.1.2 Block 2A Analysis (Continued)

The surface area for the entire pseudoellipsoid, including the igniter hole, is obtained by summing the incremental areas. The surface area around the igniter hole is added to the sum of the incremental areas. The lateral surface area of the igniter hole is assumed to be a non-burning inhibited surface.

Subroutine YPSUB

Subroutine YPSUB determines the Y coordinate of a point on the pseudoellipsoid. The angles α_{rc0} and α_{rc1} of the points P_{0a} and P_{0b} as shown in Figure 5.25 are also determined.

Subroutine ROE1SB

Subroutine ROE1SB determines the radius of curvature ρ_1 at the point P_0 on the inner ellipsoid. The radius of curvature is determined by the standard equation:

$$\rho_1 = \frac{\left|1 + (Z')^2\right|^{3/2}}{Z''} \quad , \text{ where}$$

$$Z' = \frac{dZ}{dy} \quad , \qquad Z'' = \frac{d^2Z}{dy^2}$$

Subroutine LBSUB

Subroutine LBSUB determines the length b of the Y-intercept of the line normal to the inner ellipse at P_0, Figure 5.25. The length is used in subroutine ZISUB to obtain the coefficients of the ellipse equation which defines the pseudoellipsoid.

Subroutine ZISUB

Subroutine ZISUB determines the Z-coordinate produced by the intersection of the outer ellipse:

$$\left(\frac{Y}{B_{ie}}\right)^2 + \left(\frac{Z}{A_{ie}}\right)^2 = 1$$

and the normal line to the ellipse at P1.

5.2.1.2 Block 2A Analysis (Continued)

Subroutine AIGSUB

Subroutine AIGSUB determines the surface area around the igniter opening. The area is obtained by finding the surface area of revolution which requires an angle $\pi/N0$, an arm length $\frac{\tau \sin \alpha_{rN}}{2} + R_{Ig}$, and an arc length $\tau \alpha_{rN}$, Figure 5.26.

Initially, the Y-intercept of a line normal to the inner ellipse at the igniter radius is obtained,

$$Y_{N0} = \left[B_{OE}^2 - \frac{R_{Ig}^2}{\beta_{OE}^2} \right]^{1/2}$$

from which the angle between the Y-axis and the igniter opening on the inner ellipse is obtained,

$$\alpha_{rN} = \frac{\pi}{2} - \arccos \left[\frac{R_{Ig}}{\left[(\beta_{OE}^2 Y_{N0})^2 + R_{Ig}^2 \right]^{1/2}} \right]$$

and then the surface area of revolution is determined (Theorem of Pappus)

$$A_{Ig} = (2B_{Ig} + \tau \sin \alpha_{rN}) \frac{\pi \tau \alpha_{rN}}{2 N_0}$$

5.2.1.3 Block 2B Analysis

Subroutine SCTOR2 is the control routine to determine the surface area on the pseudoellipsoid that is covered by the propellant tips for the block 2B analysis. The surface area is determined by dividing the cross-sectional grain configuration into 12 sectors in subroutine HDNSUB, as shown in Figure 5.27. The surface area on the pseudoellipsoid for each sector is then determined by subroutine S2SK. Summing the surface areas for all sectors, and subtracting this area from the area obtained in blocks 1 and 2A, yields the total surface area of the head-end with web for any value of τ.

5.2.1.3 Block 2B Analysis

Subroutine S2SK

Subroutine S2SK determines the sector surface area on the pseudoellipsoid and is called from subroutine SCTOR2 with an argument to indicate the current sector. Each sector is set up to determine the incremental surface area contributed by that sector. Thus, in sector 3, Z_{P0} is set equal to R_{P2}, then R_{P3} is obtained and θ_{r0} is set equal to θ_{r1}. ΔR is then added to Z_{P0} to obtain Z_{P1} as shown in Figure 5.28. Y_{P0}, Y_{P1} and DS are then determined. The spacing for ΔR is calculated in the same manner as was done in Block 2A.

Finally, the parameters L_{PP}, X_{r1}, θ_{r0}, θ_{r1}, α_{rc0}, α_{rc1}, ρ_1, b, Z_1, and L_Q are determined and the incremental surface area for the sector is obtained from the equation, Figure 5.25:

$$L_Q = (\rho_1 + \tau)(\alpha_{rc1} - \alpha_{rc0})$$

and

$$AS = L_Q(Z_{P1} + \tau \sin \alpha_{rc1} + Z_{P0} + \tau \sin \alpha_{rc0}) \frac{(\theta_{r1} + \theta_{r0})}{4}$$

Z_{P0} is then set to Z_{P1} and the procedure repeated until Z_{P1} equals maximum radius of the sector.

The initial volume between the inner and outer ellipsoids for each sector is determined as follows (see Figure 5.25):

$$V_{STO} = \left[(\rho_1 + D_{WB})^2 - \rho_1^2\right](\theta_{r1} + \theta_{r0})(\alpha_{rc1} - \alpha_{rc0}) \frac{Z_G N_0}{2}$$

where:

$$D_{WB} = \frac{Z_1 - Z_{P1}}{\sin \alpha_{rc1}}$$

$$D_{S1} = \rho_1(\alpha_{rc1} - \alpha_{rc0})$$

$$D_{S2} = (\rho_1 + D_{WB})(\alpha_{rc1} - \alpha_{rc0})$$

5.2.1.3 Block 2B Analysis (Continued)

$$X_{WB} = \frac{(2D_{S2} + D_{S1})\ D_{WB}}{3(D_{S2} + D_{S1})}$$

$$Z_G = \frac{(Z_{P0} + Z_{P1})}{2} + X_{WB} \sin\left[\frac{\alpha_{rc1} + \alpha_{rc0}}{2}\right]$$

Subroutines YPSUB, XRTHR, ROE1SB, LBSUB, and ZISUB are used to obtain the surface area. All of these subroutines except XRTHR have been explained in Section 5.2.1.2 for the block 2A analysis.

Subroutine XRTHR

Subroutine XRTHR is a set-up subroutine that uses subroutine XRSUBB to obtain the X-coordinate of a point located on the perimeter of a sector shown in Figure 5.28. The angle θ_{r1} between the Z axis and a line from the motor axis to the point on the sector is also determined.

5.2.1.4 Block 3 Analysis

Subroutine VOLSUB is the control routine which determines the initial propellant volume for the block 3 analysis. Initially, the volume present in the web region is determined from the volume produced by the difference of volumes of two oblate spheroids minus the volume of the igniter hole as follows:

$$V_{EH} = \frac{2}{3}\pi\ (B_{ie}\ A_{ie}^{\ 2} - B_{oe}\ A_{oe}^{\ 2}) - \pi\ R_{ig}^{\ 2}(B_{ie} - B_{oe})$$

Next, the volume of the propellant tips is determined by dividing the grain configuration into 12 sectors as was done in block 2B, Figure 5.27. The volume contributed by each sector (subroutine VSEC) is then added to V_{EH} to obtain the total volume of propellant in the head-end, V_{FH}. Finally, the surface area generated by radial burning from the line of intersection of the propellant tip with the head-end web, A_R, is approximated in the following manner:

The propellant volume in the radial burning portion is determined,

$$V_R = V_{FH} - V_{EH} + V_{STO} - 2\ V_{STR}\ N_0$$

5.2.1.4 Block 3 Analysis (Continued)

The value for thickness burned at which the maximum surface area of this radial burning portion occurs is assumed to be the thickness at which the initial burnout of the web portion of the head-end web begins (for most cases this is very nearly correct). The curve for surface area versus thickness burned for this fuel volume is assumed to have the following equations (Figure 5.29):

$$A_R = \begin{cases} \dfrac{(TDMAX - \tau_{WH})^q \, \tau}{\tau_{WH}} & \text{for } \tau \leq \tau_{WH} \\ (TDMAX - \tau)^q & \text{for } \tau_{WH} < \tau < TDMAX \\ 0 & \text{for } \tau \geq TDMAX \end{cases}$$

where

TDMAX = maximum burn distance in the head-end section

τ_{WH} = maximum web thickness in the head-end section

q = calculated exponent

The maximum thickness burned in the head-end web is determined,

If $B_{IE} - B_{OE} > \tau_W$, $\tau_{WH} = \tau_W$

If $B_{IE} - B_{OE} \leq \tau_W$, $\tau_{WH} = B_{IE} - B_{OE}$

The radial burning volume is matched to the following integral ($V_R = V_{RX}$) by an iteration process to determine the exponent q,

$$V_{RX} = \int_0^{\tau_{WH}} \frac{(TDMAX - \tau_{WH})^q}{\tau_{WH}} \tau d\tau + \int_{\tau_{WH}}^{TDMAX} (TDMAX - \tau)^q \, d\tau$$

or

5.2.1.4 Block 3 Analysis (Continued)

$$V_{RX} = \frac{(TDMAX - \tau_{WH})^{q} \tau_{WH}}{?} + \frac{(TDMAX - \tau_{WH})^{q+1}}{q+1}$$

The above integra represents the area beneath the curve shown in Figure

The radial burning area A_R is added to the total surface area, ASI, at the completion of the block 3 analysis in subroutine VOLSUB.

Subroutine VSEC

Subroutine VSEC determines the initial volume of the tips that are present in the fore-head and is called from subroutine VOLSUB with an argument to indicate the sector to be computed. The same subroutines used in the block 2B analysis to obtain the incremental surface area of a pseudoellipsoid are used in this subroutine to obtain the incremental sector volumes. An arc length L_Q is obtained from the expression

$$L_Q = Z_{P1} - Z_{P0}$$

and the incremental volume within a sector is obtained from the expression

$$\Delta V = NO\ L_Q (Z_{P1} + Z_{P0})(\theta_{r1} + \theta_{r0})(Y_{P0} + Y_{P1})/4$$

5.2.2 Cylindrical Section

The longitudinal cylindrical section is that portion of the motor between the forward and aft tangent planes, Figure 4.3. Its length is designated as h_{co} and the radius as R_f as shown in Figure 5.30. It may be either straight or tapered and may contain either a monolithic or segmented grain with or without a tapered port..

The longitudinal cylindrical section is first divided into incremental mass addition regions by locating increment dividing planes every delta Z distance, starting at the forward tangent plane and proceeding to the aft tangent plane. A maximum of 100 increment dividing planes is allowed.

The longitudinal cylindrical section is then divided by a number of reference planes. A minimum of two is required, one at each of the tangent planes. A maximum of eleven, A through K, is allowed to indicate changes in the cross-sectional grain geometry at specified locations within the section as shown in Figure 4.3. The cross sectional grain geometry is described at each reference plane used, by the port perimeter, L_p, the case radius, R_f, the port area, A_p, the propellant area, A_{FF}, the radius of gyration, K_{GY}, and the distance to the inert sliver, T_{SLVR}, if the inert

5.2.2 Cylindrical Section (Continued)

sliver option is used.

In segmenting propellant grains, the location of the slots, which separates the grain segments, is determined by defining the distance of the slot forward and aft interfaces from the forward tangent plane of the motor. This is shown by the values S1A, S1B, S2A, S2B, etc., Figure 4.3. The increment dividing planes, in this case, are determined as above, but with each segment treated as having a forward and aft tangent plane. The reference planes may be located within a slot, within a grain segment, or on a slot interface. The restrictions on the number of increment dividing planes and reference planes is also 100 and 11 respectively.

The following describes the subroutines which determine the longitudinal geometry for the cylindrical section:

Subroutine MNCHN4

Subroutine MNCHN4 contains the program control logic required to obtain the internal ballistic solution and the control logic used to initialize the working reference planes for subroutine SEGSUB. During burning, the distance burned at each reference plane for each time increment is determined by linear interpolation between adjacent increment dividing planes. When the reference plane is located within a slot, the increment dividing planes located within the grain segment are used for extrapolation to obtain the reference plane distance burned. When the distance burned has been determined for each input reference plane, the perimeter length, port area, and radius of gyration for each reference plane, and the burn area and CG location for each head section is determined from a table look-up procedure in the geometry tables.

During the internal ballistic solution for each time point the cylindrical section working reference planes (X and Y) are set up for successive input reference planes (A-B, B-C, etc.).

Subroutine SEGSUB

Subroutine SEGSUB contains the program control logic which determines the perimeter length, cross sectional propellant and port area, propellant volume, and mass generation at each increment dividing plane or mass addition region. The control logic is set to check for the existance of a slot forward interface between adjacent increment dividing planes, to check the location of the current upstream (X) and downstream (Y) working reference planes, and to set the parameters required in performing the gas dynamic solution for the slots and mass addition regions. Each increment dividing plane case radius, perimetar length, sliver radius, fuel area and port area and radius of gyration are obtained by linear interpolation between each reference plane.

5.2.3 Straight Through Grain, Motor End Sections

The following is applicable to motor aft-head or fore-head sections with straight through grains. A straight through grain is shown in Figure 5.31. The E subscript shown is set to N for analysis of the aft-head and to H for the fore-head.

Basic geometry constants required for analysis are calculated prior to determination of burn surface area versus distance burned and propellant volume. These constants are calculated in subroutine ENDCSB and are shown in Figure 5.30.

5.2.3.1 Geometry Constants

Subroutine ENDCSB

Initially, the case opening radius is determined from the input parameter DE1:

$$R_{E1} = \frac{D_{E1}}{2}$$

Then the angle between the tangent to the ellipse section at the radius R_{E1} and the motor axis is determined:

$$\alpha_{ER} = \text{arc cos } R_{E1} / \left[(R_f^2 - R_{E1}^2)\ \beta_E^2 + R_{E1}^2 \right]^{1/2}$$

where R_f and β_E are input parameters.

If α_{ER} is less than or equal to the maximum allowable angle, α_{0Emax}, defined by input, then α_{0Emax} is set to α_{ER}, R_{E2} is set to R_{E1} and h_{E1} is set to zero. If, however, α_{ER} is greater than α_{0Emax}, then

$$R_{E2} = \frac{\cos\ (\alpha_{0Emax})\ R_f\ \beta_E}{\left[\cos(\alpha_{0Emax})^2\ \beta_E^2 - \cos\ (\alpha_{0Emax})^2 + 1.0\right]^{1/2}}$$

and

$$h_{E1} = (R_{E2} - R_{E1})\ \frac{\sin\ (\alpha_{0Emax})}{\cos\ (\alpha_{0Emax})}$$

Next, the length of the head elliptical section is determined:

$$h_{E2} = \left[R_f^2 - R_{E2}^2\right]^{1/2} / \beta_E$$

5.2.3.1 Geometry Constants, Subroutine ENDCSB (Continued)

and the length of the end section is computed:

$$h_{E0} = h_{E1} + h_{E2}.$$

If h_{E0} is less than the maximum burn distance at the adjacent tangent plane, τ_{max}, determined in Section 5.1, Geometry Constants, the end section is lengthened to the maximum burned distance:

$$h_{ER} = \tau_{max}$$

If, however, h_{E0} is greater than or equal to τ_{max}, then $h_{ER} = h_{E0}$. Finally, the maximum burn distance in the conical section and the end section is determined:

$$\tau_{E1} = [(R_{E2} - R_{E1})^2 + h_{E1}^2]^{1/2}$$

$$\tau_{E0} = [(R_f^2 - R_{E1})^2 + h_{E0}^2]^{1/2}$$

The complete end section case volume is determined from:

$$V_{CE} = (h_{ER} - h_{E0})\,\pi R_f^2 + \frac{1}{3}\left[3\frac{R_f}{\beta_E}^2 - h_{E2}^2\right]\left[\pi h_{E2}\beta_E^2\right] + (R_{E2}R_{E1} + R_{E1}^2 + R_{E2}^2)\,\pi\frac{h_{E1}}{3}$$

The following coefficients are calculated for use in subroutine RCSUB when the burning distance $\tau > \tau_{E1}$. They are the coefficients of a fourth degree equation of the intersection of an ellipse and a circle and are used to compute the location of intersection of the burning surface and the case wall.

$$CAE = (\beta_E^2 - 1)^2$$

$$CBE = -(\beta_E^2 - 1)^2\,\beta_E^2\,R_{E1}\,4$$

$$CCCE = [\beta_E^4 R_{E1}^2\,3 + (\beta_E^4 + \beta_E^2)\,h_{E0}^2 + R_f^2(\beta_E^2 - 1) - R_E^2\beta_E^2\,]\,2$$

$$CCVE = 2(\beta_E^4 - \beta_E^2)$$

$$CDCE = [\,(h_{E0}^2 + R_{E1}^2)\,\beta_E^2 + R_f^2\,\beta_E^2\,]\,4R_{E1}$$

5.2.3.1 Geometry Constants, Subroutine ENDCSB (Continued)

$$COVE = 4 R_{E1} \beta_E^4$$

$$CECE = R_f^4 + (R_{E1}^2 - h_{E0}^2) \beta_E^2 R_f^2 2 + (R_{E1}^2 + h_{E0}^2) \beta_E^4$$

$$CEVE = (h_{E0}^2 \beta_E^2 + R_{E1}^2 \beta_E^2 + R_f^2) 2 \beta_E^2$$

5.2.3.2 Calculation Sectors and Zones

The cross-sectional grain geometry in motor end sections is based on the geometry at the forward and aft tangent planes. Figures 5.32 and 5.33 define sectors and zones used for burn-surface area and propellant volume calculations. The general forked wagon wheel grain in Figure 5.32 is divided into 13 sectors. Depending on the exact grain geometry, more than one sector may exist in a zone. This is the case for zone A, Figure 5.33 and initial sectors 1, 2, 3, and 4 in Figure 5.32. The opposite may exist where only a portion of a sector is bounded by a zone boundary.

Four zones can exist in the end section. Their boundaries are defined as:

Zone A is that region between the minimum propellant radius, R_1, and the case opening, R_{E1}. Burning will occur along the side of the propellant tip and on the end face.

Zone B is that region between the case opening, R_{E1}, and where the end-burning surface intersects the case, R_c. Burning will occur along the propellant tip and on the toroidal end face.

Zone C is that region between where the end-burning surface intersects the case, R_c, and the web, $\tau_w - \tau$. Burning will occur only along the side of the propellant tip or in the valley.

Web Zone is that region between the radius $R_f - \tau_w + \tau$ and the radius of the case R_f. Burning will occur along the perimeter of sector 8 and along the end face if the case opening, R_{E1}, is greater than the radius to the web, $R_f - \tau_w + \tau$.

The sectors that are in zones B, C, and web are subdivided into smaller elements. The sectors in zone A are not subdivided. Sector boundaries and zones which the sectors occupy are recalculated as the burning surface regresses.

5.2.3.2 Calculation Sectors and Zones (Continued)

Subroutine ASESUB

Subroutine ASESUB is the control routine to determine the total burning surface area and initial volume of the end sections. The grain cross-section at the adjacent tangent plane is divided into sectors, Figure 5.32. The correct equations from subroutines XRSUB and RASUB are set up and the proper values for the coordinates of the origin of the circular arc, X_{0V}, Y_{0V}, the radius of curvature of the sector, R_T, the angle between the bisector of the propellant tip and the straight side sectors, α_V, and the perimeter length, L_x, are assigned for each sector. After the required parameters have been set for a sector, the sector burning area and volume are determined in subroutine AESUB.

Subroutine AEPSUB

Subroutine AEPSUB tests for the existence of a sector and is called from subroutine ASESUB. If a sector has burned out or was not present in the initial grain configuration, control is returned to subroutine ASESUB; otherwise, control proceeds to subroutine AESUB. After the sector burning area and volume have been determined in subroutine AESUB, the sector values are added to the sum of the values for the previous sector and control is returned to subroutine ASESUB.

Subroutine AESUB

Subroutine AESUB determines the total burning surface area and initial volume of the sectors. A test is made at the beginning of each zone to determine if the sector exists in that zone.

The parameters X_{R0}, R_{A0}, and Y_{A0} are associated with the beginning coordinates of a sector perimeter, and the parameters X_{RX}, R_{AX}, Y_{AX} and L_X are associated with the end coordinates of a sector perimeter as shown in Figure 5.32. These parameters are determined by subroutines XRSUB and RASUB from the Pythagorean Theorem. The beginning and end points of a sector may not be the beginning and end points of the area to be computed should a sector exist in more than one zone. The beginning coordinates of an area are then subscripted min and the end coordinates are subscripted max instead of 0 and X, respectively. The perimeter length is then defined as L_R. Figure 5.34 shows an example of the min and max coordinates that are used in the following zone A analysis. When an integration scheme is employed, zones B, C, and Web, the min and max coordinates of each increment are determined to compute sector surface area.

5.2.3.2 Calculation Sectors and Zones (Continued)

Subroutine RCSUB

Subroutine RCSUB obtains the radius vector from the motor axis to the intersection of the aft burning surface with the case wall, R_c, Figure 5.33. The intersection is determined from the equation of a straight line when $\tau \leq \tau_{E1}$, and from the equation for the aft-dome configuration (circle or ellipse) when $\tau > \tau_{E1}$, where:

$$\tau_{E1} = [(R_{E2} - R_{E1})^2 - h_{E1}^2]^{1/2}$$

Subroutine ARSSUB

Subroutine ARSSUB determines the chord length, L_{RS}, between the minimum point of a sector and a general point along the perimeter of a sector as shown in Figure 5.35. The required parameters are R_{A0}, X_{R0}, R_A, and X_R.

Subroutine ALRSUB

Subroutine ALRSUB determines the arc length of a sector, L_R, from the minimum point of a sector to a general point along the perimeter as shown in Figure 5.35. The required parameters are L_{RS} and R_T.

Subroutine XRSUB

Subroutine XRSUB determines the X-coordinate of a general point on the perimeter of a sector. A separate equation is used for each sector. The required parameters are R_A and τ.

Subroutine RASUB

Subroutine RASUB determines the length of a radius vector from the motor axis to a general point on the perimeter of a sector. A separate equation is used for each sector. The perimeter length along the sector and the distance burned τ are required.

Subroutine HESUB

Subroutine HESUB determines the length of the trapezoidal elements, h_E, used to determine the incremental volumes and areas, Figure 5.36.

5.2.3.2.1 Zone A Calculations

When $R_{A0} < R_{E1}$, the surface area is computed in Zone A. When $R_{A0} \geq R_{E1}$, the analysis proceeds to the next zone and R_{Amax} is set to the smaller value of R_{AX} and R_{E1}.

The following Zone A analysis applies to sectors 1 through 7 and 9 through 13. Figure 5.35 is used as an example to define calculation parameters. It illustrates sector 3.

The burning surface area in zone A is determined from an algebraic composition of simple geometric figures such as shown in Figure 5.35.

The value of γ_T, L_R, and L_{RS} are determined as follows:

$$\gamma_T = 2 \arccos \left(\frac{[(2R_T)^2 - L_{RS}^2]^{1/2}}{2R_T} \right)$$

$$L_R = \gamma_T |R_T|$$

$$L_{RS} = \left\{ \left[R_{Amax}^2 - X_{Rmax}^2 \right)^{1/2} - (R_{Amin}^2 - X_{Rmin}^2)^{1/2} + (X_{Rmax} - X_{Rmin})^2 \right\}^{1/2}$$

where $R_T = R_3 - T$ for sector 3

A_{T0} is the area between the chord L_{RS} and the circular arc L_R and is determined by subtracting the area of the inscribed triangle from the area of the circular sector, abg:

$$A_{T0} = |R_T| L_R - L_{RS} \left[R_T^2 - \frac{(L_{RS})^2}{2} \right]^{1/2}$$

A_{TT} is equal in magnitude to A_{T0} and is positive if R_T is positive, negative if R_T is negative, and zero if R_T is zero. A_{FF} is the area of the trapezoid, abof:

$$A_{FF} = \left\{ [R_{Amax}^2 - X_{Rmax}^2]^{1/2} - [R_{Amin}^2 - X_{Rmin}^2]^{1/2} \right\} \frac{(X_{Rmax} - X_{Rmin})}{2}$$

5.2.3.2.1 Zone A Calculations (Continued)

A_R is the area bcd determined by subtracting the triangular area obd from the circular sector obc:

$$A_R = \frac{R_{Amax}^2 \gamma_R - X_{Rmax} [R_{Amax}^2 - X_{Rmax}^2]^{1/2}}{2}$$

where

$$\gamma_R = \text{arc sin} \left(\frac{X_{Rmax}}{R_{Amax}} \right)$$

A_{RO} is the area aef determined by subtracting the triangular area oaf from the area of circular sector oae:

$$A_{RO} = \frac{R_{Amin}^2 \gamma_{RO} - X_{Rmin} [R_{Amin}^2 - X_{Rmin}^2]^{1/2}}{2}$$

where

$$\gamma_{RO} = \text{arc sin} \left(\frac{X_{Rmin}}{R_{Amin}} \right)$$

The burning area along the side of the propellant tip is $h_E(L_R)$ and the total sector area A_{EE} is:

$$A_{EE} = 2 NO [L_R h_E + A_{TT} + A_{FF} + A_R - A_{RO}]$$

The sector volume is:

$$DV = (A_{FF} + A_R - A_{RO} + A_{TT}) h_E NO 2$$

If the maximum point of the sector, R_{Amax} is within zone A, then control is returned to subroutine AEPSUB; otherwise, computation will proceed to zone B.

5.2.3.2.2 Zone B Calculations

When R_{AO} for a sector is less than R_C, surface area is computed in zone B. When R_{AO} is greater than or equal to R_C, computation proceeds to Zone C.

Initially, R_{Amax} is set to the smallest value of R_{AX} and R_C from which L_{Rmax} is determined by subroutine ARSSUB and ALRSUB. L_{R1}

5.2.3.2.2 Zone B Calculations (Continued)

is determined in the same manner from R_{Amin}. The burning surface area is then computed in increments of ΔL where $\Delta L = R_f$ (DLRF) by integrating over the perimeter length, L_{Rmax}. DLRF is an input parameter. For each increment, R_{Amax} is determined from $L = L_{R1} + \Delta L$, and R_{Amin} is determined from $L = L_{R1}$. Figure

The X-coordinate, X_R, of the centroid, Figure 5.36, is obtained from subroutine XRSUB and the radius vector R_A is obtained from subroutine RASUB. The angle γ_R is:

$$\gamma_R = \text{arc sin} \left(\frac{X_R}{R_A}\right)$$

The cross sectional area of the end face is equal to the product of the incremental arc length $(\lambda - \lambda_{min})\tau$, and the arc length, $\gamma_R R_A$, through which the centroid is rotated.

The surface area along the side of the propellant tips are approximated by trapezoidal increments and is added to the area of the end face. The burning surface areas and volumes of each increment are added to the sum of the previous increment values. They are determined for an increment as follows:

$$A_{EE} = 2\,NC \left[(L-L_{R1}) \frac{h_E + h'_E}{2} + R_A\,\gamma_R\,(\lambda - \lambda_{min})\tau\right]$$

where

$$h_E = \left|h_{ER} - [\gamma^2 - (R_{Amax} - R_{E1})^2]^{1/2}\right|$$

$$h'_E = \left|h_{ER} - [\gamma^2 - (R_{Amin} - R_{E1})^2]^{1/2}\right|$$

$$DV = 2\,NO\,(R_{Amax} - R_{Amin}) \frac{h_E + h'_E}{2}\,\gamma_R\,R_A$$

The next increment in the sector is determined by setting $L_{R1} = L$, $h'_E = h_E$, $R_{Amin} = R_{Amax}$, and $L_{R1} = L_{R1} + \Delta L = L$. L is set to L_{Rmax} for the last iteration for a sector.

5.2.3.2.2 Zone B Calculations (Continued)

The parameters R_A, R_{Amax}, L, and h_E are determined for each increment.

The toroidal end burning area is formed by revolving an arc about the motor axis, and is equal to the product of the length of the arc increment and the arc length through which the centroid of the arc increment is rotated (Theorem of Pappus). The area along the side of the propellant tip is determined from the trapezoids.

The radial vector, R_A, to the centroid of the arc increment, as shown in Figure 5.36, is:

$$R_A = \frac{2\tau}{\lambda - \lambda_{min}} \sin\left(\frac{\lambda - \lambda_{min}}{2}\right) \sin\left(\frac{\lambda + \lambda_{min}}{2}\right) + R_{El}$$

where $\frac{2\tau}{\lambda - \lambda_{min}} \sin\left(\frac{\lambda - \lambda_{min}}{2}\right)$ is the distance from the centroid of the arc increment to the origin of the circle about which the arc increment is revolved.

The angles λ and λ_{min} are determined as follows:

$$\lambda = \text{arc sin}\left(\frac{R_{Amax} - R_{El}}{\tau}\right)$$

$$\lambda_{min} = \text{arc sin}\left(\frac{R_{Amin} - R_{El}}{\tau}\right)$$

If R_{AX} is less than R_C, computation will proceed to the next sector. If R_{AX} is greater than or equal to RC, computation will proceed to zone C.

5.2.3.2.3 Zone C Calculations

The burning surface area in Zone C consists only of the surface along the side of the propellant tip, and is determined from trapezoidal elements. If a sector exists in zones B and C, R_A is set equal to R_{Amax} of zone B; otherwise, $R_A = R_{A0}$. With R_A, L_{A1} is determined from subroutines ARSSUB and ALRSUB. The length of the initial edge, h_E', of the trapezoidal element is determined in subroutine HESUB as follows:

5.2.3.2.3 Zone C Calculations (Continued)

If $R_A \leq R_{E2}$,

$$h_E' = h_{ER} - h_{E1}\left(\frac{R_A - R_{E1}}{R_{E2} - R_{E1}}\right)$$

Or if $R_A > R_{E2}$,

$$h_E' = h_{ER} + \frac{(R_f^2 - R_A^2)^{1/2}}{\beta_E} - h_{E0}$$

An incremental length ΔL is added to L_{R1} and a corresponding R_A is determined from subroutine RASUB. The length of the top edge h_E of the trapezoidal element is determined from the above equations in subroutine NESUB and the elemental trapezoidal area and volume are added to the previous sectors as follows:

$$A_{EE} = 2\ NO\ (L - L_{R1})\left(\frac{h_E + h_E'}{2}\right)$$

where

$$R_A = \frac{R_{Amax} + R_{Amin}}{2}$$

$$DV = 2\ NO\ (R_{Amax} - R_{Amin})\ \frac{(h_E + h_E')}{2}\ \gamma_R$$

5.2.3.2.4 Web Zone Calculations

Subroutine AWESUB determines burning surface area and initial volume of the web zone.

The burning surface area of sector 8 is determined first from the trapezoidal element of length h_E, which is determined from $R_{A0} = R_f - \tau_w + \tau$, as follows:

$$AWE = 2\ NO\ h_E\ L_8$$

L_8 is the perimeter length of sector 8.

The volume of propellant in the web zone is determined as follows: (geometric symbols are given in Figures 5.33 and 5.36)

5.2.3.3.4 Web Zone Calculations (Continued)

If $R_{E2} > (R_f - \tau_2 + \tau)$, calculate the parameter,

$$h_{EFC} = \frac{(R_{E2} - R_f + \tau_w - \tau)}{R_{E2} - R_{E1}} h'_E$$

and the volume as:

$$DV = \left\{ \left[\left(\frac{R_f}{\beta_E} \right)^2 h_{E2} - \frac{h_{E2}^3}{3} \right] \beta_E^2 + (h_{ER} - h_{E0}) R_f^2 + \left[(R_f - \tau_w + \tau)^2 + R_{E2}(R_f - \tau_w + \tau) + R_{E2}^2 \right] \frac{h_{EFC}}{3} - (h_{EFC} + h_{ER} - h_{E1})(R_f - \tau_w + \tau)^2 \right\} \pi$$

If $R_{E2} \leq (R_f - \tau_w)$, calculate the parameter,

$$Z_1 = \frac{\left[R_f^2 - (R_f - \tau_w + \tau)^2 \right]^{1/2}}{\beta_E}$$

and the volume as:

$$DV = \left\{ \left[\left(\frac{R_f}{\beta_E} \right)^2 Z_1 - \frac{Z_1^3}{3} \right] \beta_E^2 + (h_{ER} - h_{E0}) R_f^2 - (Z_1 + h_{ER} - h_{E0})(R_f - \tau_w + \tau)^2 \right\} \pi$$

The additional end burning area and initial propellant volume, when $R_{E1} > R_f - \tau_w + \tau$, are determined as follows:

When $R_{E1} < R_C$

$$A_{WE} = 2 NO \theta_1 (R_{E1}^2 - R_{A0}^2)$$

$$DV = \pi \theta_E (R_{E1}^2 - R_{A0}^2)$$

The toroidal end burning surface exists when $R_C > R_{E1}$. The re-

5.2.3.2.4 Web Zone Calculations (Continued)

volved area is a product of the arc length and the circumference of the circle described by the centroid of the arc length. The radial vector to the centroid of the arc increment, Figure 5.36, is:

$$R_A = \frac{2\tau}{\lambda - \lambda_{min}} \sin\left(\frac{\lambda - \lambda_{min}}{2}\right) \sin\left(\frac{\lambda + \lambda_{min}}{2}\right) + R_{E1}$$

The toroidal surface area is determined from the product of the arc length, $(\lambda - \lambda_{min})\tau$, and the circumference of the circle, $2\ NO\ \theta_1\ R_A$, described by the centroid of the curve:

$$A_{WE} = 2(\lambda - \lambda_{min})\ \tau\ NO\ R_A\ \theta_1$$

5.3 Moments of Inertia and CG Location

Pitch and roll moments of inertia (MOI) and the center of gravity (CG) location during motor burning can be calculated. The roll moment (J-ROLL) is taken about the longitudinal axis of the motor. The pitch moment (J-X-Y) is taken about an axis passing through the motor CG and centerline. The center of gravity is measured from the aft tangent plane. The value is positive when the CG is forward of the aft tangent plane. The moments about the pitch and yaw axes are assumed to be equal. This assumption is valid for any configuration with an even multiple of 4 propellant tips.

The MOI and CG location of the motor are based on the combined values of each section; fore-head, cylinder, and aft-head.

The pitch MOI of the fore-head is initially determined about the forward tangent plane and then transferred to the aft tangent plane, the cylindrical and aft-head section MOI's are initially determined about the aft tangent plane. These values about the aft-tangent plane are then transferred to the motor CG. The transfer formula is:

$$J_{CG} = J_{\text{aft tangent plane}} + d^2 W/g_o$$

where d is the distance between the motor CG and aft tangent plane.

The MOI of a body with respect to a given axis is defined as the product of the mass and the square of the distance from the axis. If $dm = dW/g_o$ represents an elemental mass and Y its distance from an axis, the MOI, J, of the object about this axis will be equal to $\int Y^2\, dW/g_o$, Reference 8.

The CG is that point at which the mass of an object is concentrated so that the moment of the concentrated mass about any axis or plane is the same as the sum of the moments of all the elements of the mass about the same axis or plane. The sum of the moments from a plane is $\int \frac{x dW}{g_o}$

and the CG is defined as: $\bar{x} = \frac{\int x dW}{W}$

where

$\bar{x}$ = distance to the CG location from a plane.

The MOI and CG location for each section are determined from a summation of incremental volumes and areas about the desired axis. The incremental volumes are hollow circular cylinders for the cylindrical section and thin shells for the head-end sections. The radius of gyration for the cylindrical section is determined from the roll MOI of the grain cross-sectional area. The incremental rectangular MOI s are first taken about the CG of the incremental volume and then transferred to the desired axis. The transfer formula is $I = I_{CG} + d^2 m$, where I_{CG} is the MOI about the CG and d is the distance to the reference axis.

5.3.1 Roll Moment of Inertia

The roll MOI of an incremental thin shell for the head sections are determined from the fundamental equation; Figure 5.37:

$$J_p = \frac{W}{g_o} r^2, \text{ slug-in}^2$$

The thin shells are based on a subdivision of sector boundaries.

The roll MOI of the cross sectional area of an incremental hollow circular cylinder, Figure 5.38, is determined from the fundamental equation:

$$J_p = \frac{(\theta_{r1} + \theta_{ro})}{4} (r_o^4 - r_i^4) \text{ NO, in}^4$$

where

r_0 = outer incremental radius, in

r_i = inner incremental radius, in

The radius of gyration is determined from:

$$K = \left(\frac{J_p}{AFP}\right)^{1/2}, \text{ in}$$

where AFP is the cross sectional area of propellant, in^2.

5.3.1.1 Motor End Sections

The roll MOI s for the motor end sections are determined in subroutines PT1AA and SD1D13 from a summation of thin shells of each sector and the web region as follows:

$$AJPP = \sum_1^{11} \ldots X] + (R_{A0}^2 + R_A^2)(R_A^2 - R_{A0}^2) \pi \frac{(h_E + h_E')}{2} \frac{\rho_f}{2g_o}$$

where, $J_{PX} = \ldots_A^2 + R_{A0}^2) \frac{W_i}{2g_o}$

$$W_i = (\theta_{r1} + \theta_{ro}) \text{ NO } \rho_f (R_A^2 - R_{A0}^2) \frac{(h_E + h_E')}{4}$$

R_{A0} is the minimum radius of the increment

R_A is the maximum radius of the increment

5.3.1.2 Cylindrical Section

The roll MOI for the cylindrical section is determined in subroutine SEGSUB using the radius of gyration of the propellant cross section. The radius of gyration of the cross section is determined in subroutines PT1AA and SD1D13 from a summation of the roll MOI for the elementary hollow circular cylinders of each sector and the web region as follows:

$$J_{PP} = \sum_{1}^{13} \left[\frac{(\theta_{ri}+\theta_{ro})}{4} (R_A^4 - R_{AO}^4)\ NO \right] + \frac{\pi}{2} (R_A^4 - R_{AO}^4)$$

$$W_T = \sum_{1}^{13} \left[\frac{(\theta_{ri}+\theta_{ro})}{2} (R_A^2 - R_{AO}^2)\ NO \right] + \pi (R_A^2 - R_{AO}^2)$$

$$K_{GY} = \left[\frac{J_{PP}}{W_T} \right]^{1/2}$$

The radius of gyration is calculated only at the input reference planes and linearly interpolated at each increment dividing plane. The cylindrical section total roll MOI is determined from a summation of individual mass addition region roll MOI values as follows, Figure 4.3:

$$I_{PCYL} = \sum_{1}^{NI} \left[(\pi R_{fHI}^2 - A_{PHI}) K_{GYHI}^2 + (\pi R_f^2 - A_p) K_{GY}^2 \right] \frac{\Delta Z\, \rho_f}{2\, g_o}$$

The subscripted HI parameters are the values at the adjacent upstream increment dividing plane. NI is the total number of increment dividing planes.

5.3.2 Pitch MOI

The pitch MOI s of the head sections are taken with reference to the adjacent tangent plane such that:

$$J_B = \frac{W}{g_o} \left(\frac{r^2}{2} + \frac{L^2}{12}\right) + \frac{W}{g_o} R_{CG}^2$$

where

r = radius to CG of cross section, in

L = incremental length of shell, in

R_{CG} = distance from reference axes (tangent plane) to the CG, in

5.3.2 Pitch MOI (Continued)

For the incremental hollow circular cylinders of the cylindrical section the calculations are taken with reference to the CG of the incremental cylinder and then transferred to the aft tangent plane such that:

$$J_B = \frac{W}{g_o}\left(\frac{K^2}{2} + \frac{L^2}{12}\right) + \frac{W}{g_o} d^2$$

where

K = radius of gyration of cross section, in^2

d = distance from the CG to aft tangent plane, in

5.3.2.1 Motor End Sections

The pitch MOI for the motor end sections are determined in subroutines PT1AA and SD1D13 from a summation of MOI s for elemental thin shells of each sector and the web region as follows:

$$AJBB = \sum_{1}^{13} \left\{ \left[\frac{(h_E + h'_E)}{2} \right]^2 \frac{W_i}{12 g_o} + \frac{J_{PX}}{2} + \frac{W_i R_{CG}^2}{g_o} \right\}$$

$$+ \frac{R_{CG}^2 W_i}{g_o} + \left[\frac{(h_E + h'_E)^2}{12} + (R_A^2 + R_{AO}^2) \right] \frac{W_i}{4 g_o}$$

where

$$R_{CG} = \begin{cases} h_{EO} + \dfrac{(h_E + h'_E)}{4} & \text{for the fore-head and} \\ \dfrac{h_E + h'_E}{4} & \text{for the aft-head} \end{cases}$$

$$J_{PX} = (R_A^2 + R_{AO}^2) \frac{W_i}{2 g_o}$$

5.3.2.2 Cylindrical Section

The MOI is determined in subroutine SEGSUB from a summation of individual mass addition region values as follows:

$$I_{BCYL} = \sum_{1}^{NI} \left\{ \frac{(\pi R_{FHI}^2 - A_{PHI})}{2} \left[K_{GYHI}^2 + 2\left(\frac{3}{4}(AINCW - AINCHI) + h_{CO} - AINCW\right)^2 \right. \right.$$

5.3.2.2 Cylindrical Section (Continued)

$$+ \frac{2(AINCW-AINCHI)^2}{12} \Big] + \Big[K_{GY}^2 + 2\left(\frac{AINCW-AINCHI}{4} + h_{CO} - AINCW\right)^2 \Big]$$

$$\frac{(\pi R_f^2 - A_p)}{2} \Bigg\} \frac{\rho_f \ (AINCW-AINCHI)}{2\, g_o} \Bigg]$$

5.3.3 CG of Sections

The CG for each section is determined from a summation of the moments of incremental volumes about the desired axis. The CG for the cylindrical section is determined from a summation of the moments of incremental hollow circular cylinders about the aft tangent plane, Figure 5.38, and the CG for the head sections are determined from a summation of the moments of thin shells about the adjacent tangent plane, Figure 5.37. Thus:

$$\overline{MX} = \frac{W}{g_o} \overline{X} = \Sigma X_I \frac{dW}{g_o}$$

therefore

$$\overline{X} = \Sigma X_I \, dW/W$$

where

X_I = moment arm of incremental volume, in

dW = incremental volume weight, lb

W = total weight, lb

5.3.3.1 Head Sections

The CG is determined in subroutines PT1AA and SD3013 from a summation of moments for elemental thin shells of each sector and the web region as follows:

$$\overline{X}_I = \sum_1^{13} \left[\left(W_T \overline{X}_{I \text{ previous}} + (h_E + h'_E) \frac{W_I}{4}\right) \Big/ (W_I + W_T) \right]$$

where $W_T = \sum_1^{13} W_I$

subscript I is N for aft-head,

H for fore-head.

5.3.3.2 Cylindrical Section CG Location

The CG location is determined in subroutine SEGSUB from a summation of the individual mass addition region moments as follows, Figure 5.38:

$$AOMCYL = \sum_{1}^{NI} \left\{ \left[\left(\frac{3(AINCW-AINCHI)}{4} + h_{CO} - AINCW \right) (\pi R_{fHI}^2 - A_{PHI}) + \left(\frac{AINCW-AINCHI}{4} + h_{CO} - AINCW \right) (\pi R_f^2 - A_p) \right] \frac{(AINCW-AINCHI)}{2} \rho_f \right\}$$

5.3.4 Motor MOI and CG

Motor Roll MOI:

$$J_{PP} = J_{PHed} + J_{PNoz} + I_{Pcyl}$$

The motor CG location and pitch MOI are determined by a transfer of axes of the MOI of each section as follows:

Motor CG:

$$\bar{X}_{IH} = \frac{(\bar{X}_H + h_{CO})\ V_{fH}\ \rho_f + AOMCYL - \bar{X}_N\ V_{fN}\ \rho_f}{W_f}$$

Fore-Head Section Pitch MOI:

$$J_{BHed} = (J_{BHed})_{Aft} - \left[\bar{X}_H^2 - (\bar{X}_H + h_{CO} - \bar{X}_{IH})^2 \right] \frac{V_{fH}\ \rho_f}{g_o}$$

Aft-Head Section Pitch MOI:

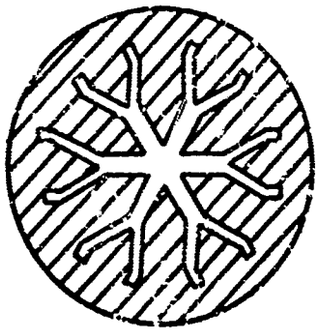
$$J_{BNoz} = (J_{BNoz})_{Aft} - \left[\bar{X}_N^2 - (\bar{X}_N + \bar{X}_{IH})^2 \right] \frac{V_{fN}\ \rho_f}{g_o}$$

Cylindrical Section Pitch MOI:

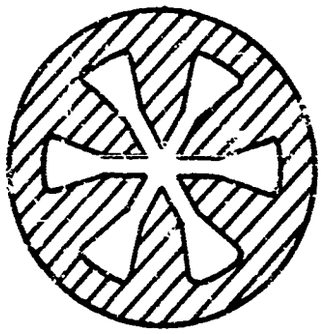
$$I_{Bcyl} = (I_{Bcyl})_{Aft} - \left\{ \left(\left[\bar{X}_{IH}\ W_f - (\bar{X}_H + h_{CO})\ V_{fH}\ \rho_f + \bar{X}_N\ V_{fN}\ \rho_f \right] \Big/ \left[W_f - (V_{fH} + V_{fN})\ \rho_f \right] \right)^2 \right\} \left[W_f - (V_{fH} + V_{fN})\ \rho_f \right] \Big/ g_o$$

Motor Pitch MOI:

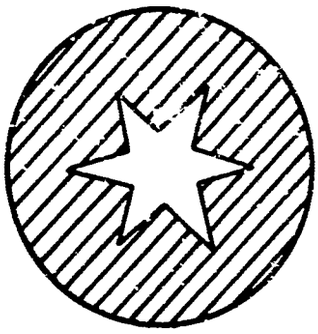
$$J_{BB} = J_{BHed} + J_{BNoz} + I_{Bcyl}$$



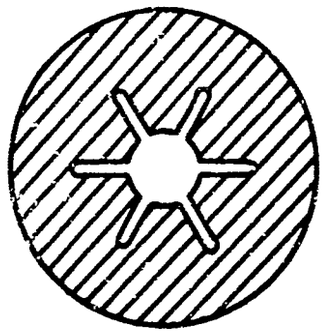
Forked Wagon Wheel



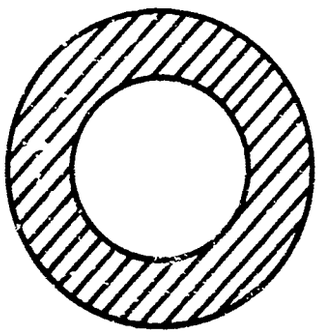
Conventional Wagon Wheel



Standard Star

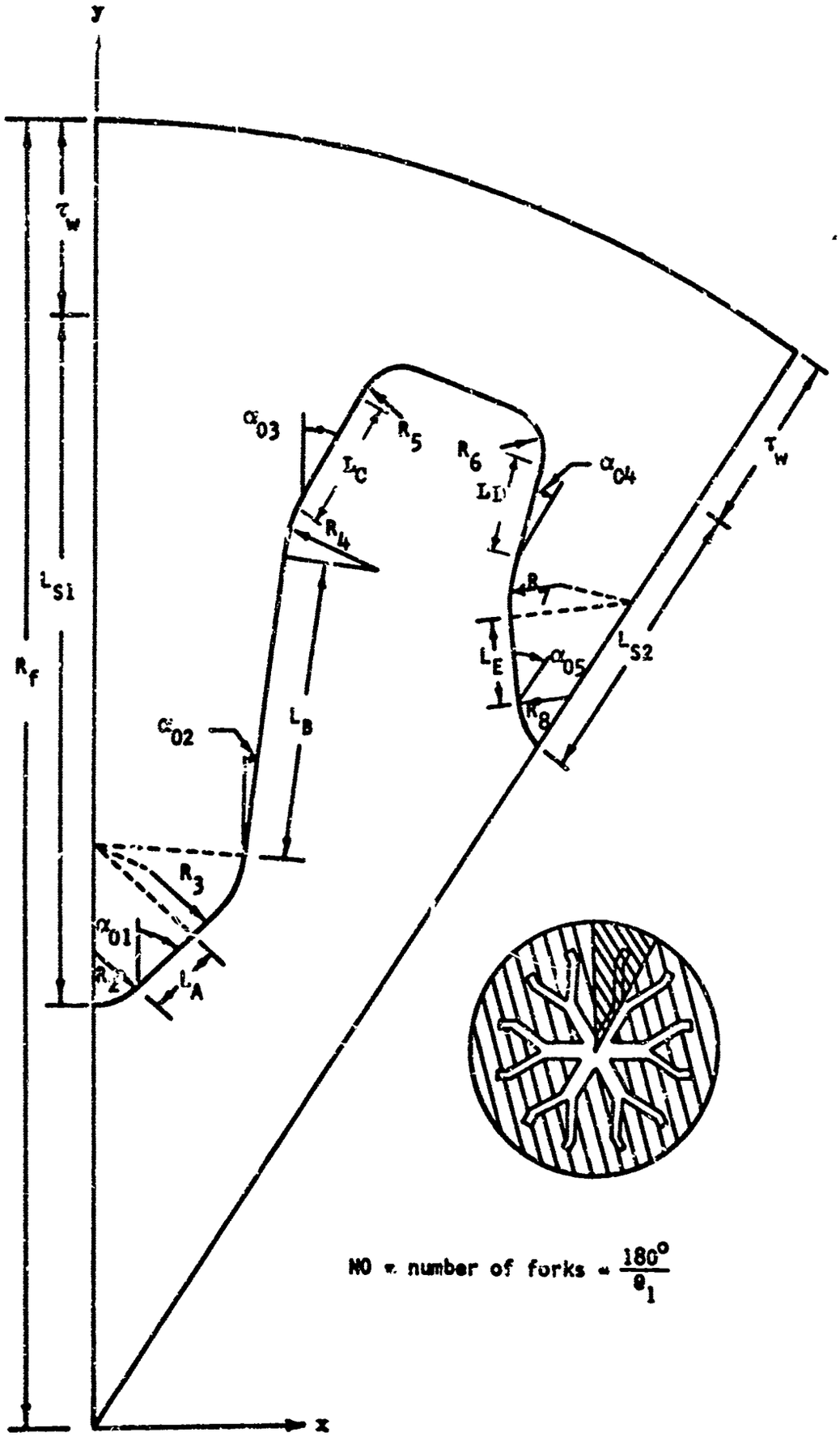


Slotted-Cone



Circular Port

Figure 5.1. Grain Design Options



NO = number of forks = $\frac{180^\circ}{\theta_1}$

Figure 5.2 One-Half Fork of General Modified Wagon Wheel Configuration

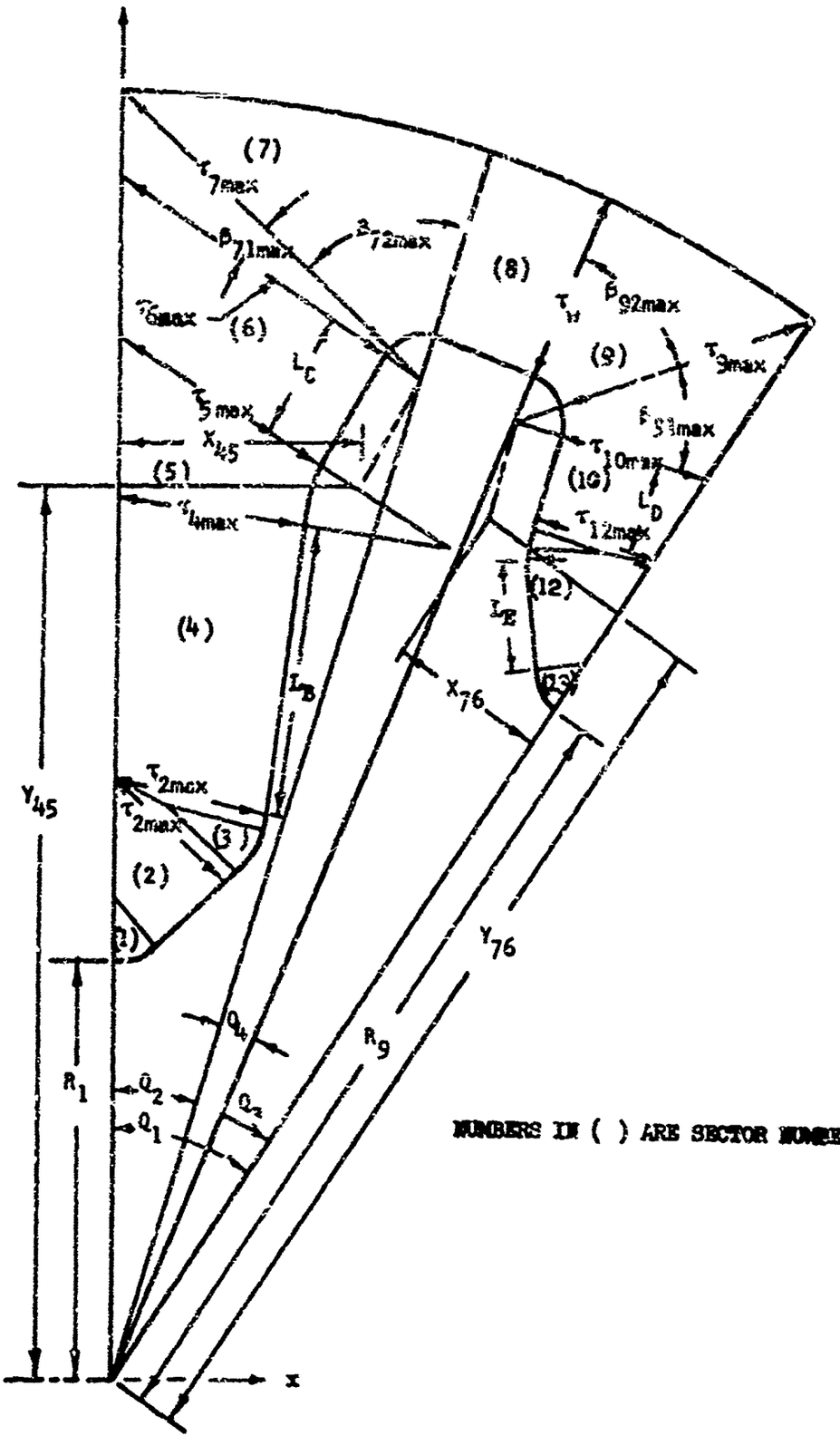


Figure 5.3 Part of Calculated Constants for One-Half Fork of General Modified Wagon Wheel Configuration Produced by PLNCNS Subroutine

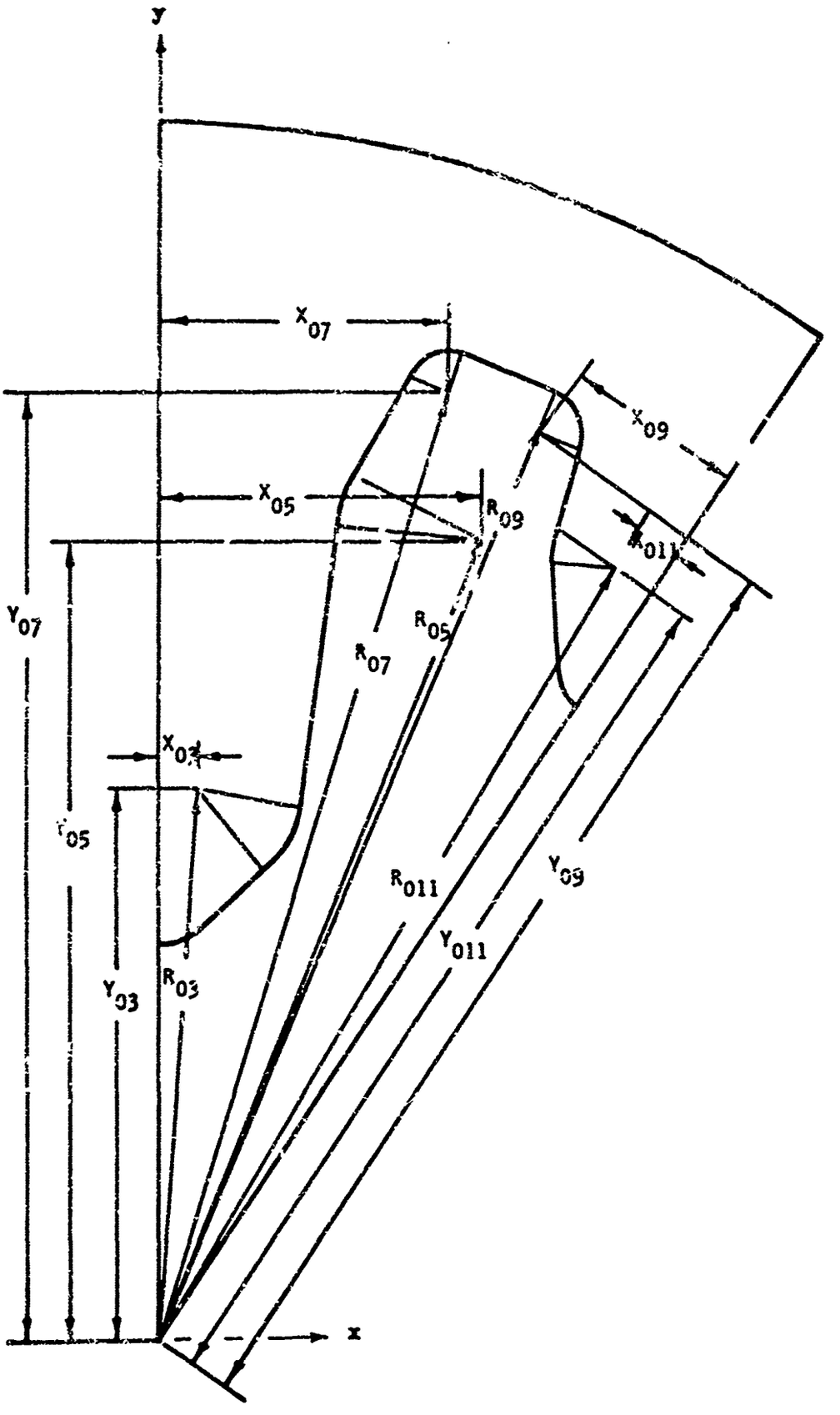


Figure 5.4 Part of Calculated Constants for One-Half Fork of General Modified Wagon Wheel Configuration Produced by FLNCNS Subroutine

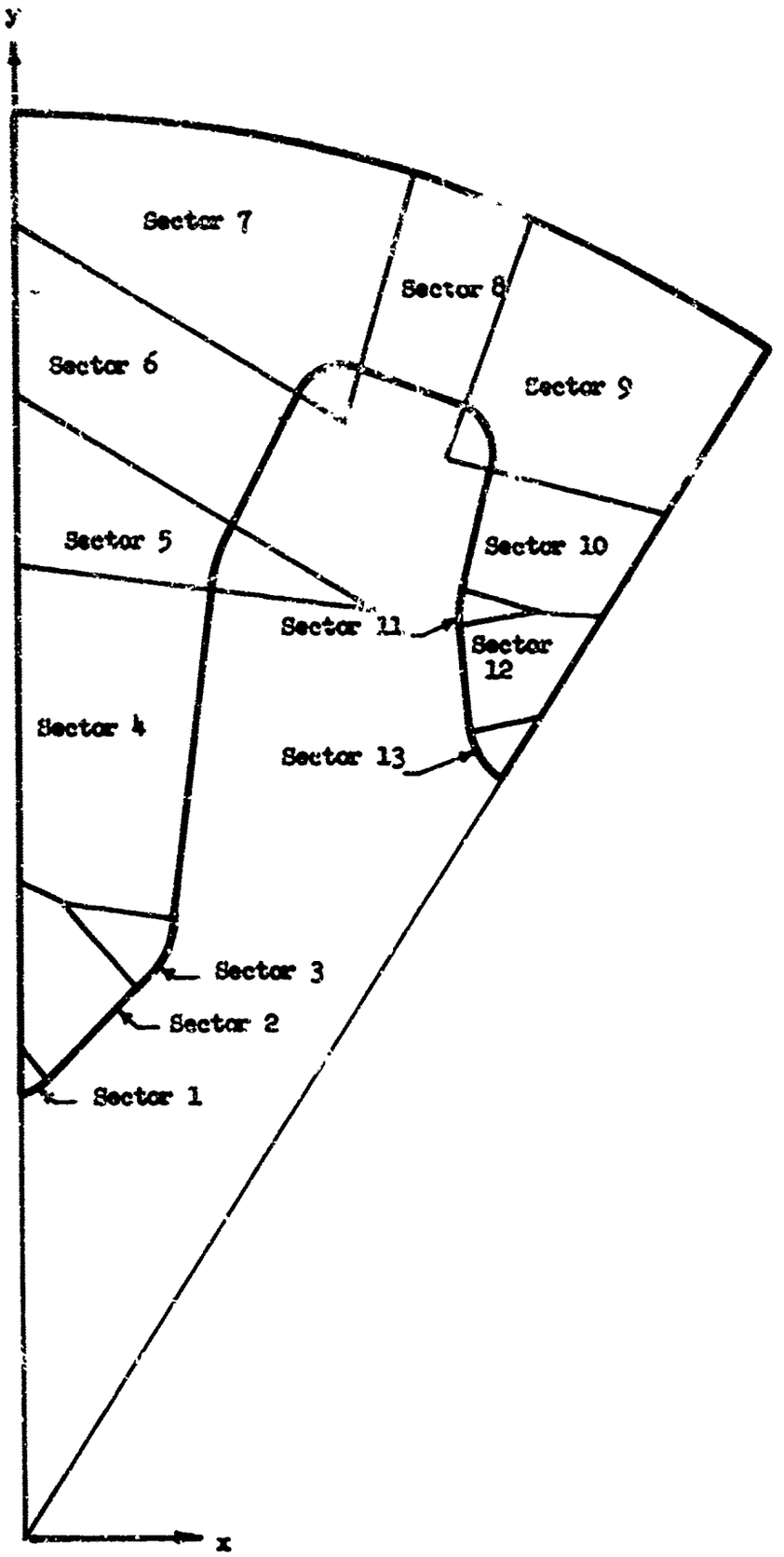


Figure 5.5 Sector Definition

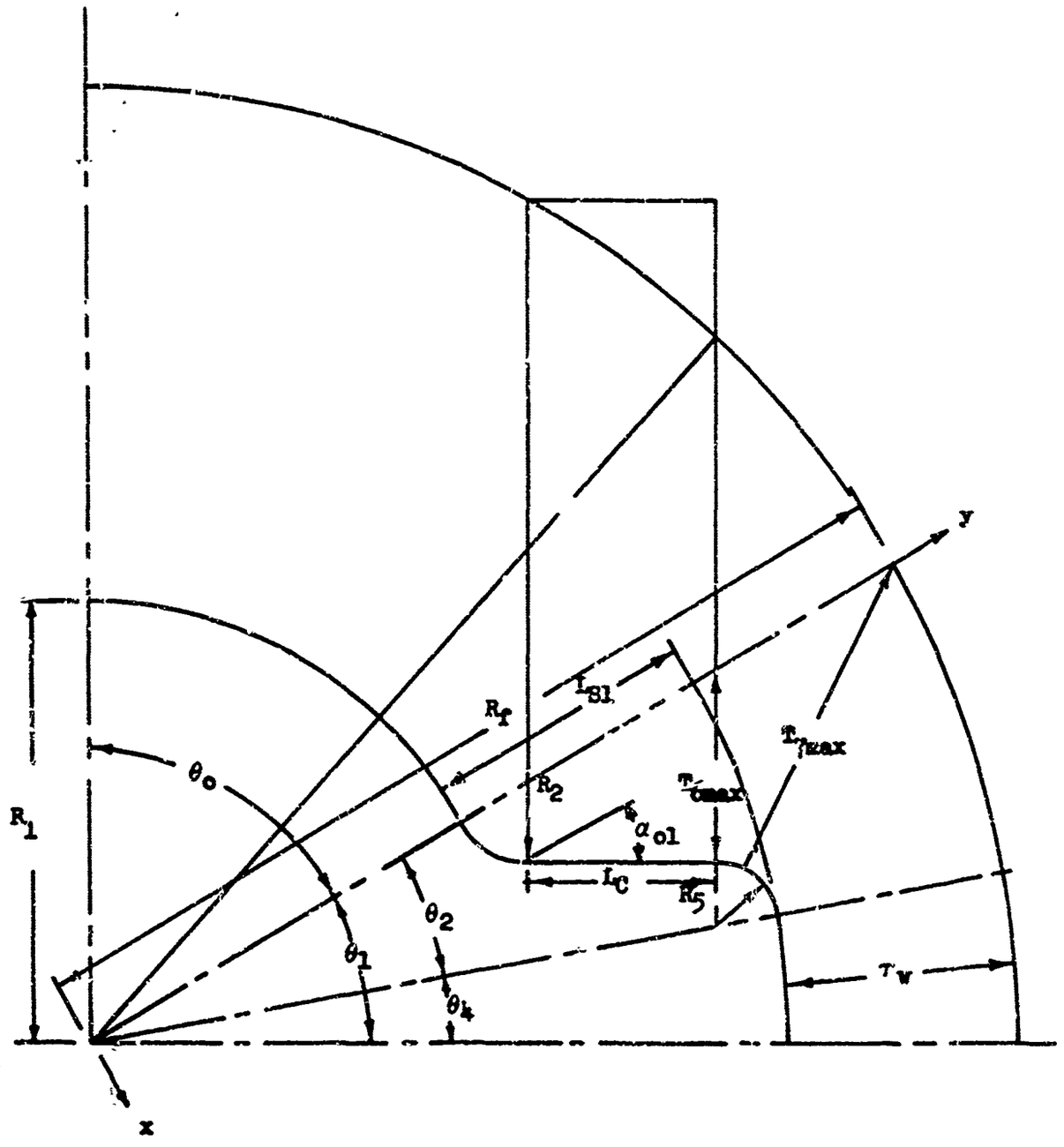


Figure 5.6 Slotted-Cone

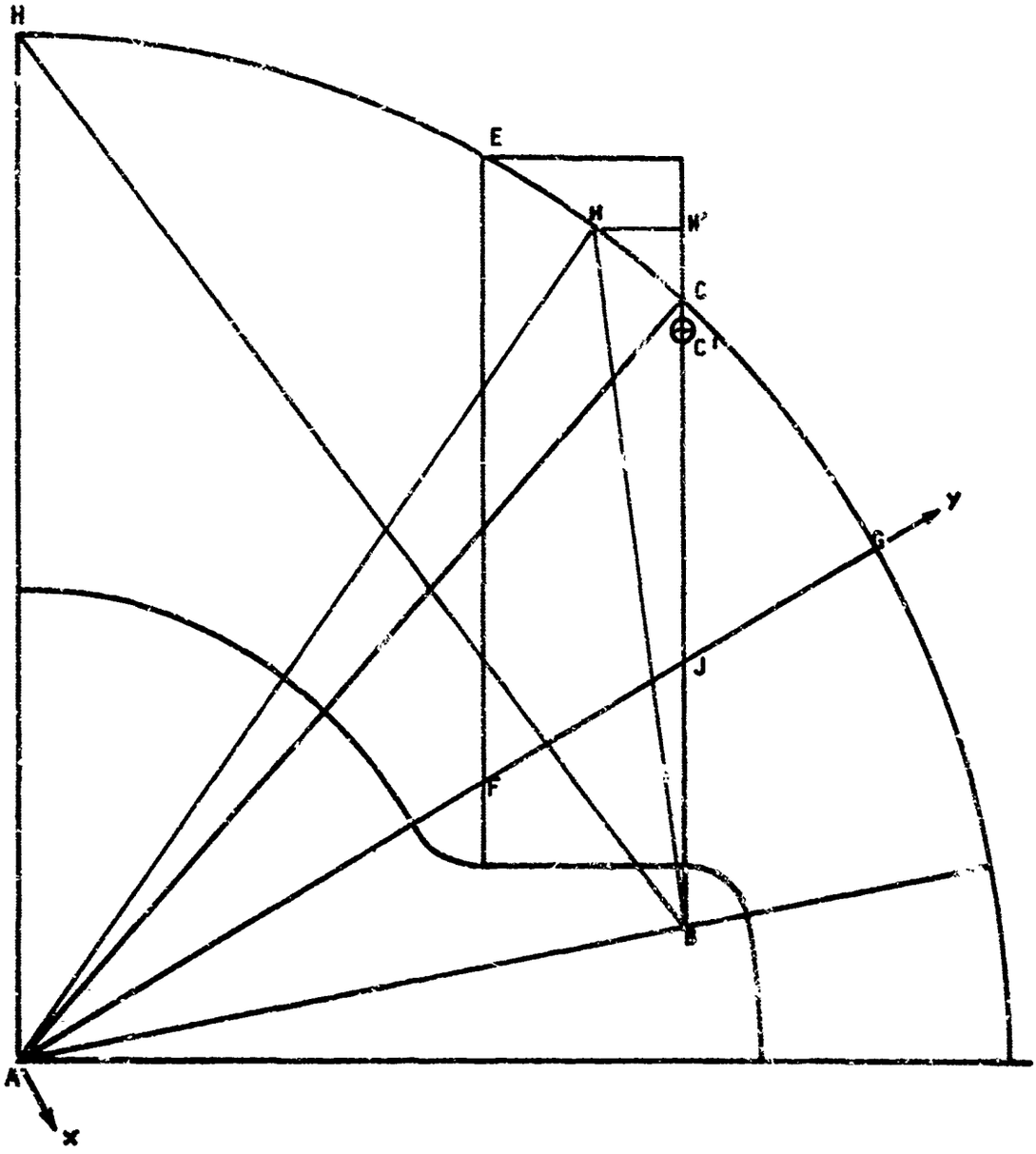


Figure 5.7 Slotted-Cone Addition to Standard Star Showing Location of Fixed Geometry Points

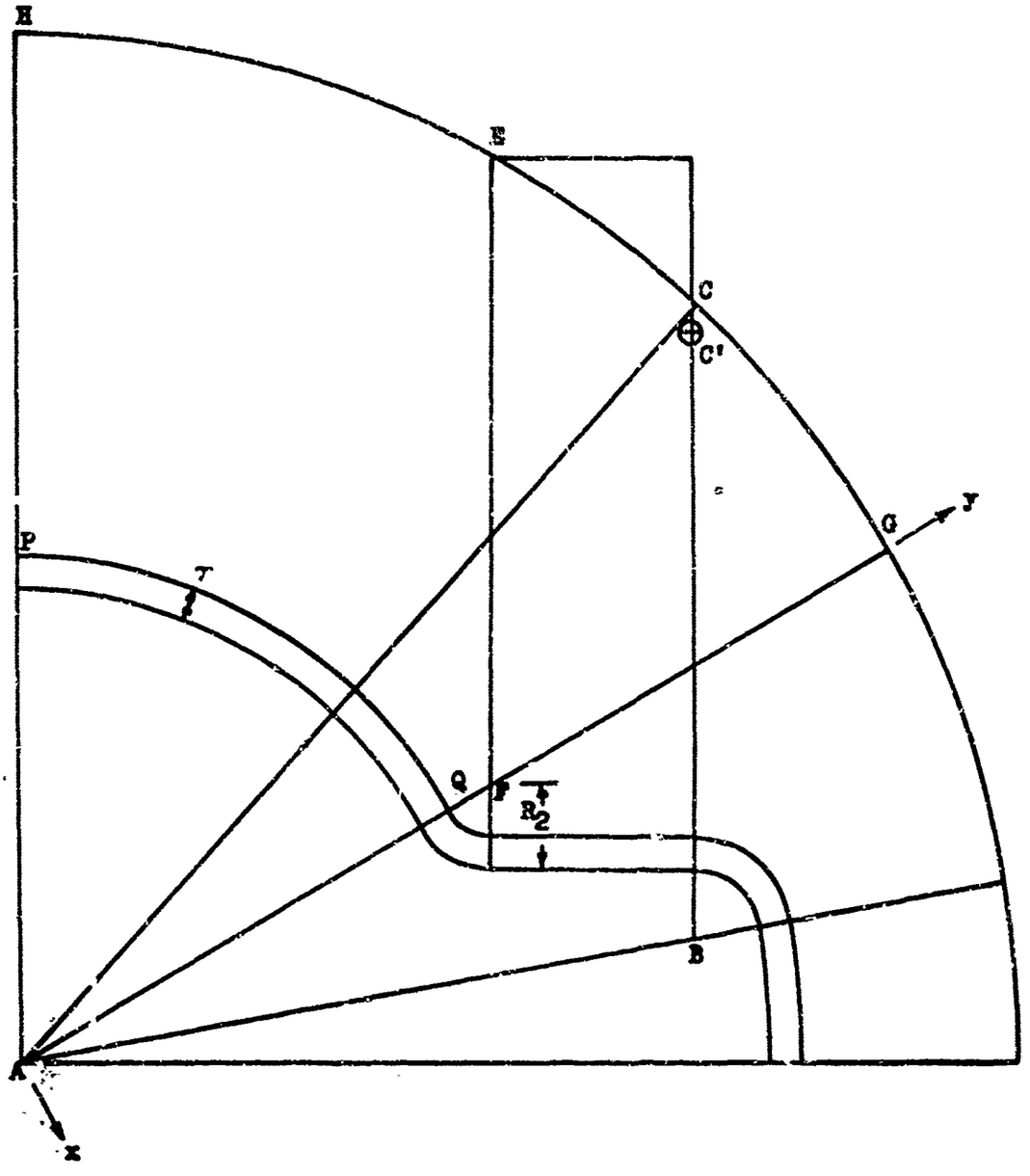


Figure 5.8 Complete Slotted-Cone Burning Surface for τ less than R_2

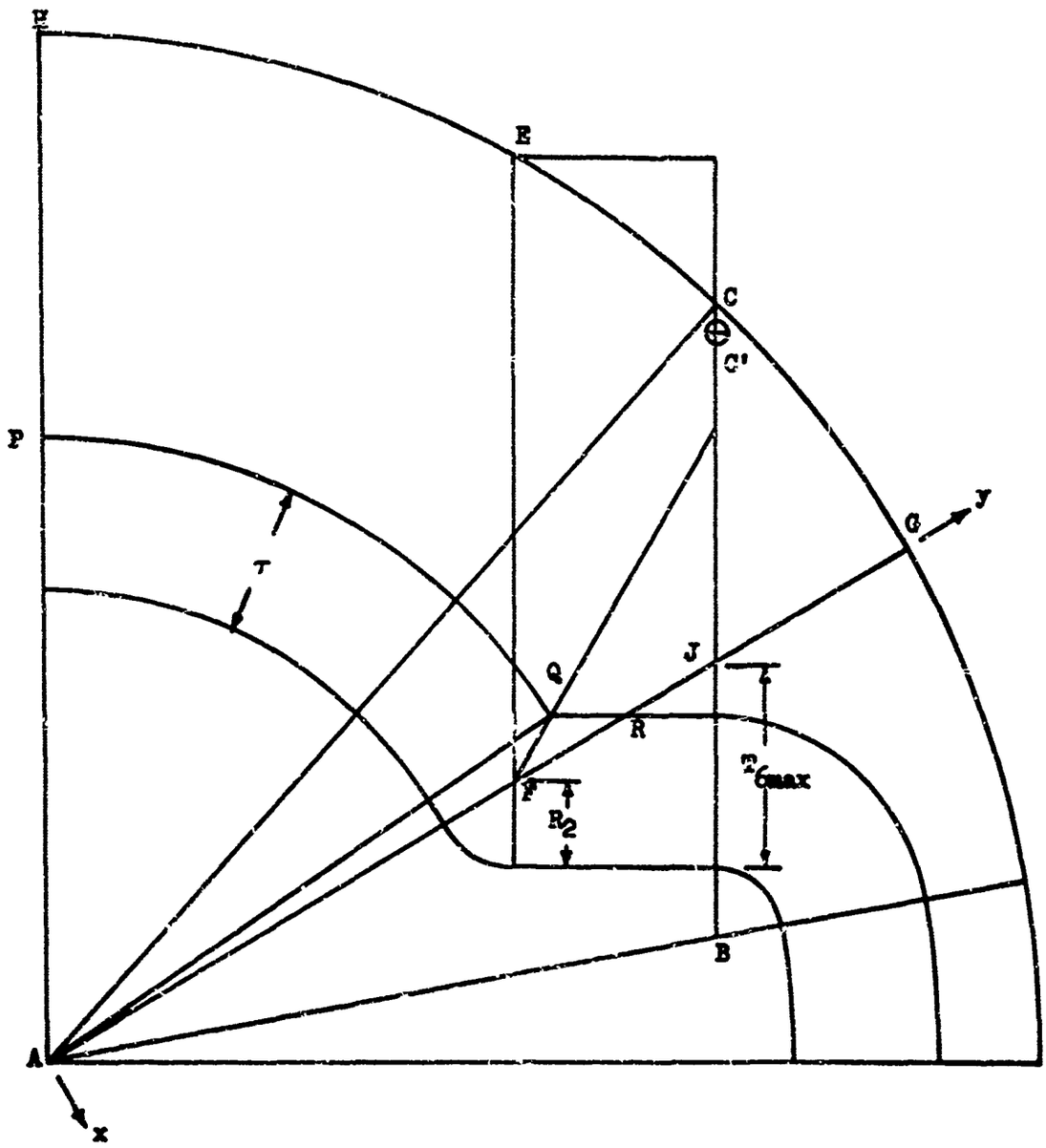


Figure 5.9 Slotted-Cone Burning Surface Addition for τ Greater than R_2 and Less than τ_{6max}

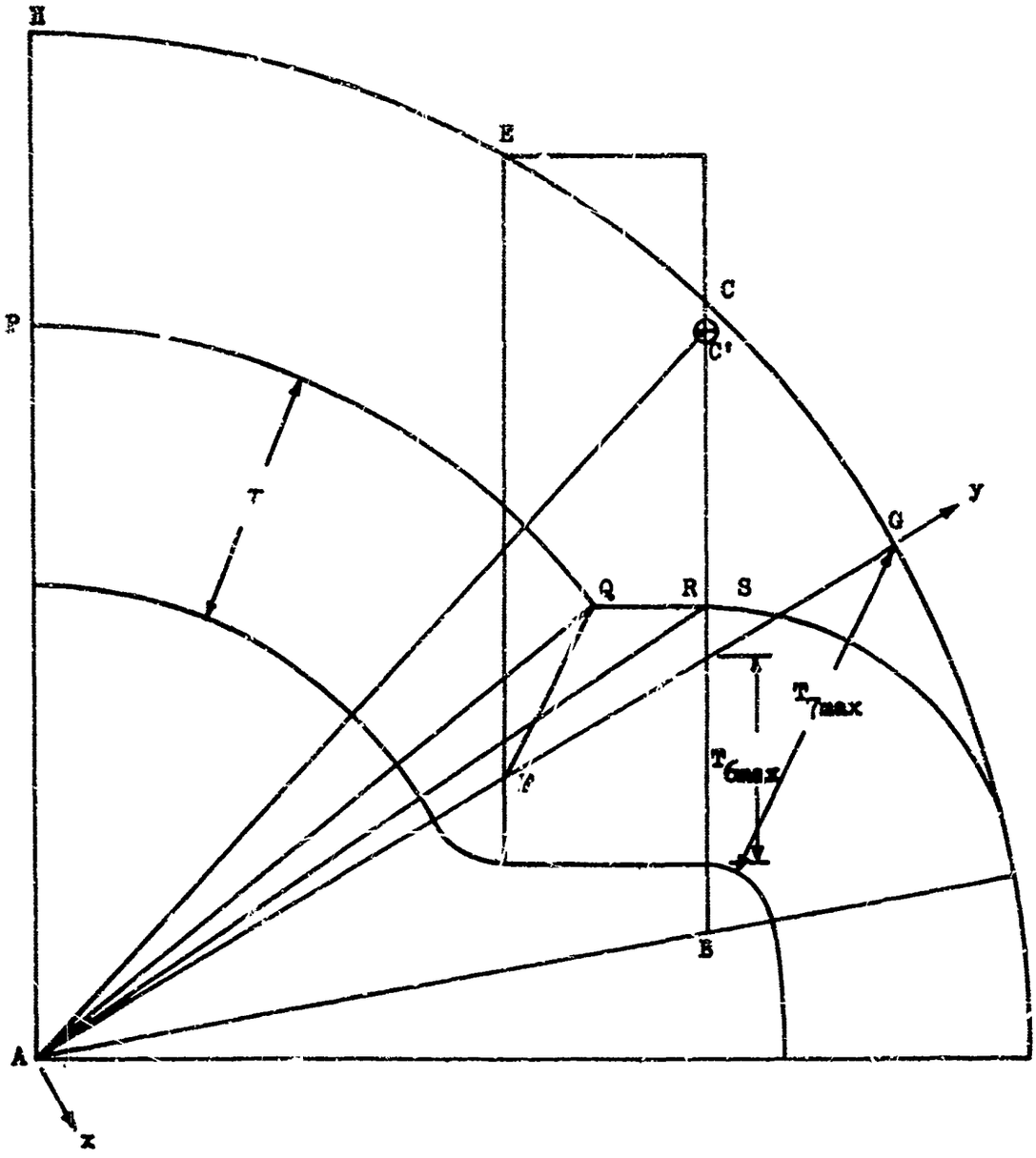


Figure 5.10 Slotted-Cone Burning Surface Addition For τ Greater than $T_{\sigma max}$ and less than $T_{\tau max}$

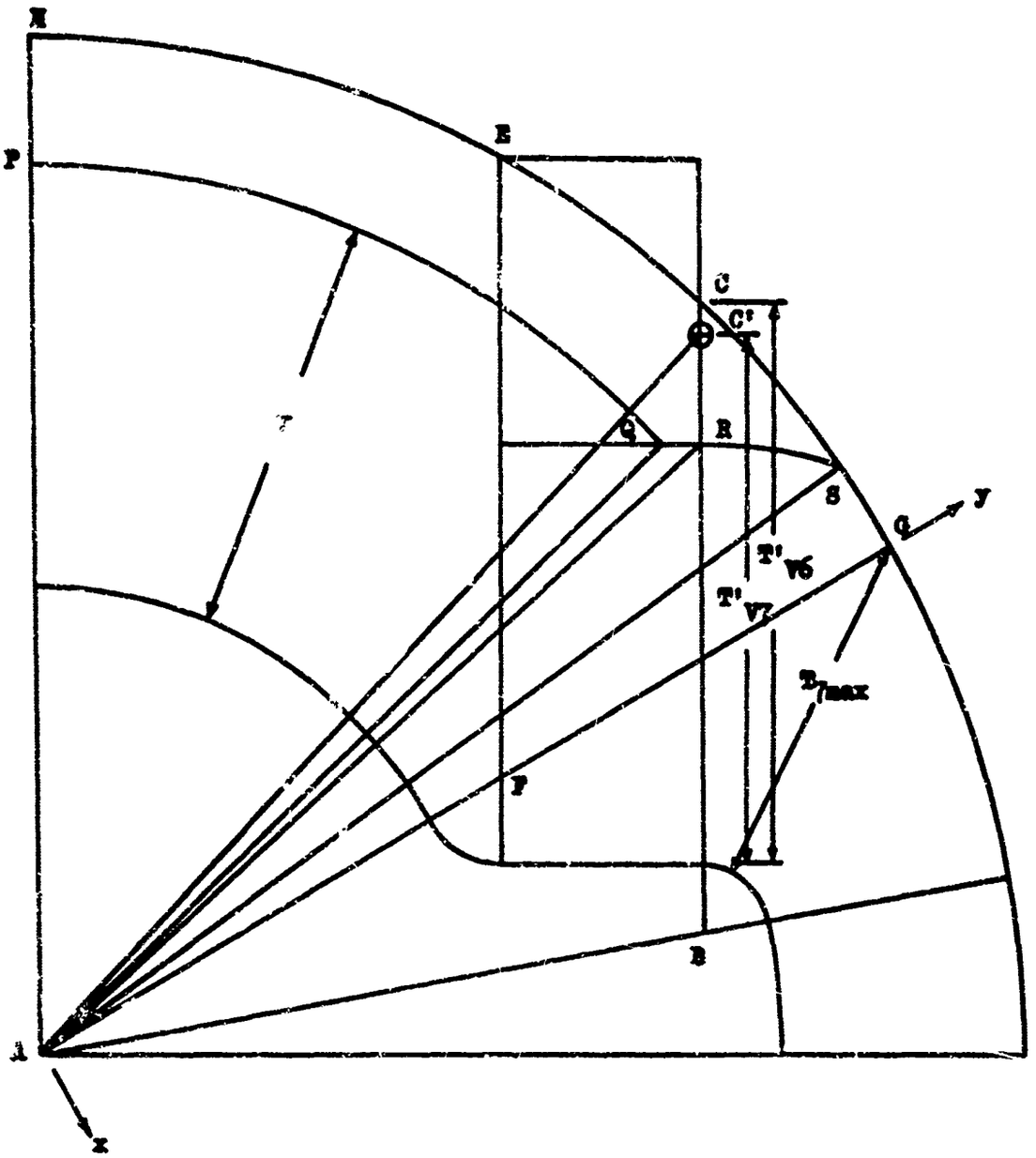


Figure 5.11 Slotted-Cone Burning Surface Addition for r Greater than r_{max} and Less than r'_{W7}, with T'_{W7} less than T'_{WC}

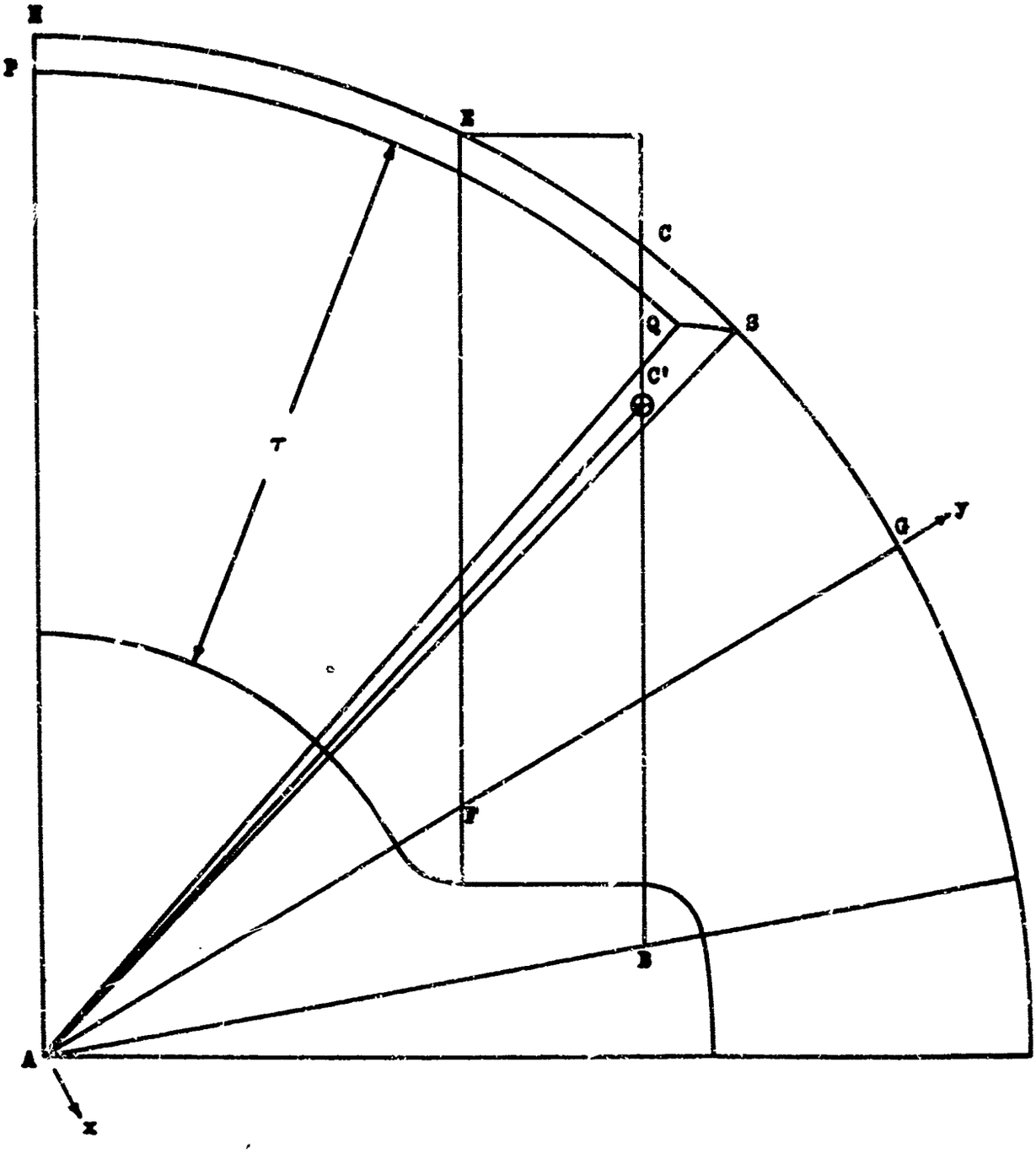


Figure 5.12 Slotted-Cone Burning Surface For τ Greater than T'_{V7} with T'_{V7} Less than T'_{V6}

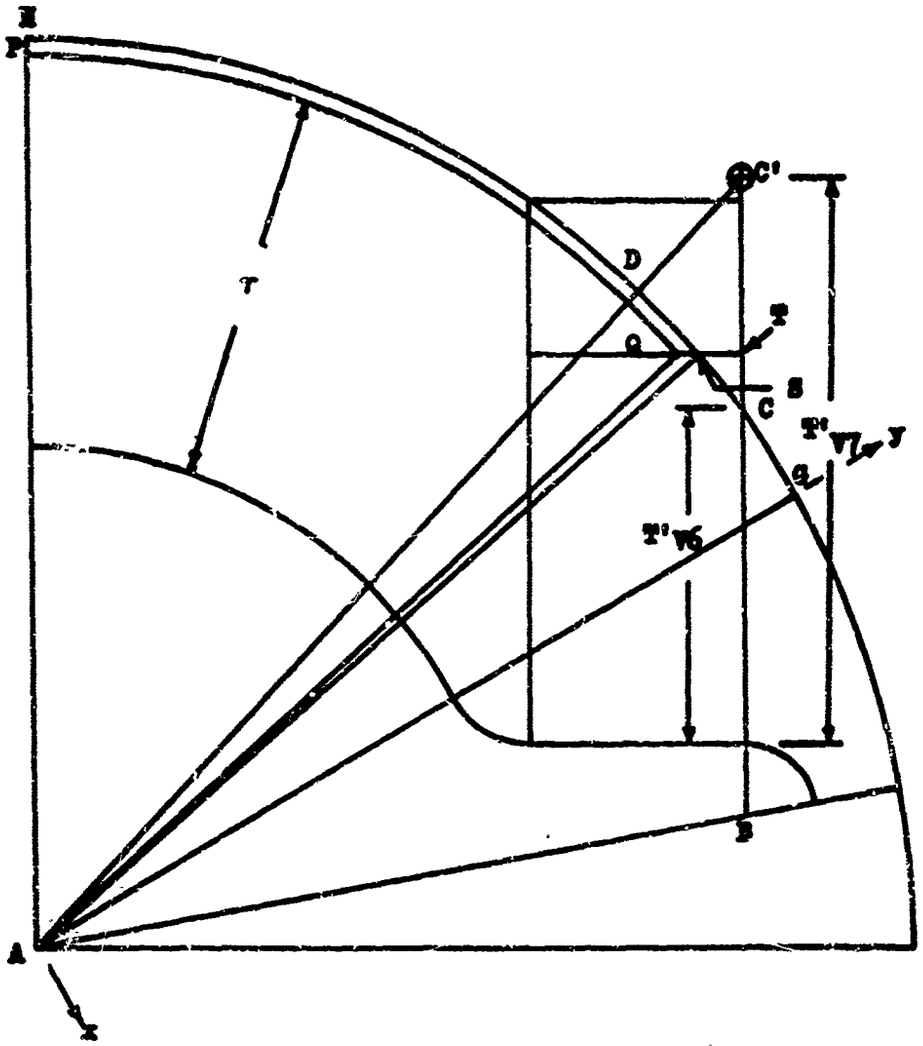


Figure 5.13 Slotted-Cone Burning Surface For τ Greater than T'_{V6} with T'_{V5} Less than T'_{V7}

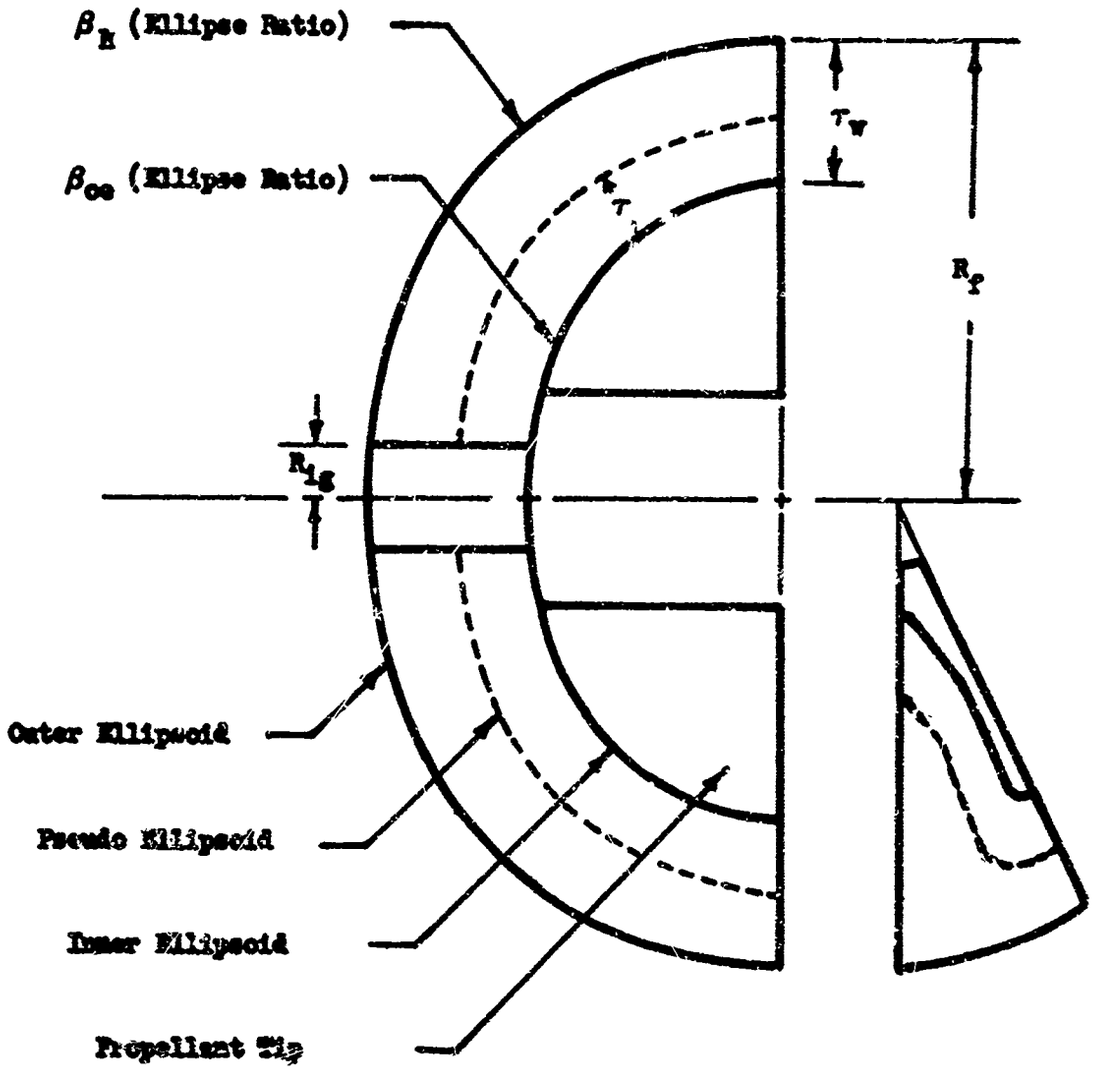


Figure 5.14 Head-End with Web, Motor Fore-Head

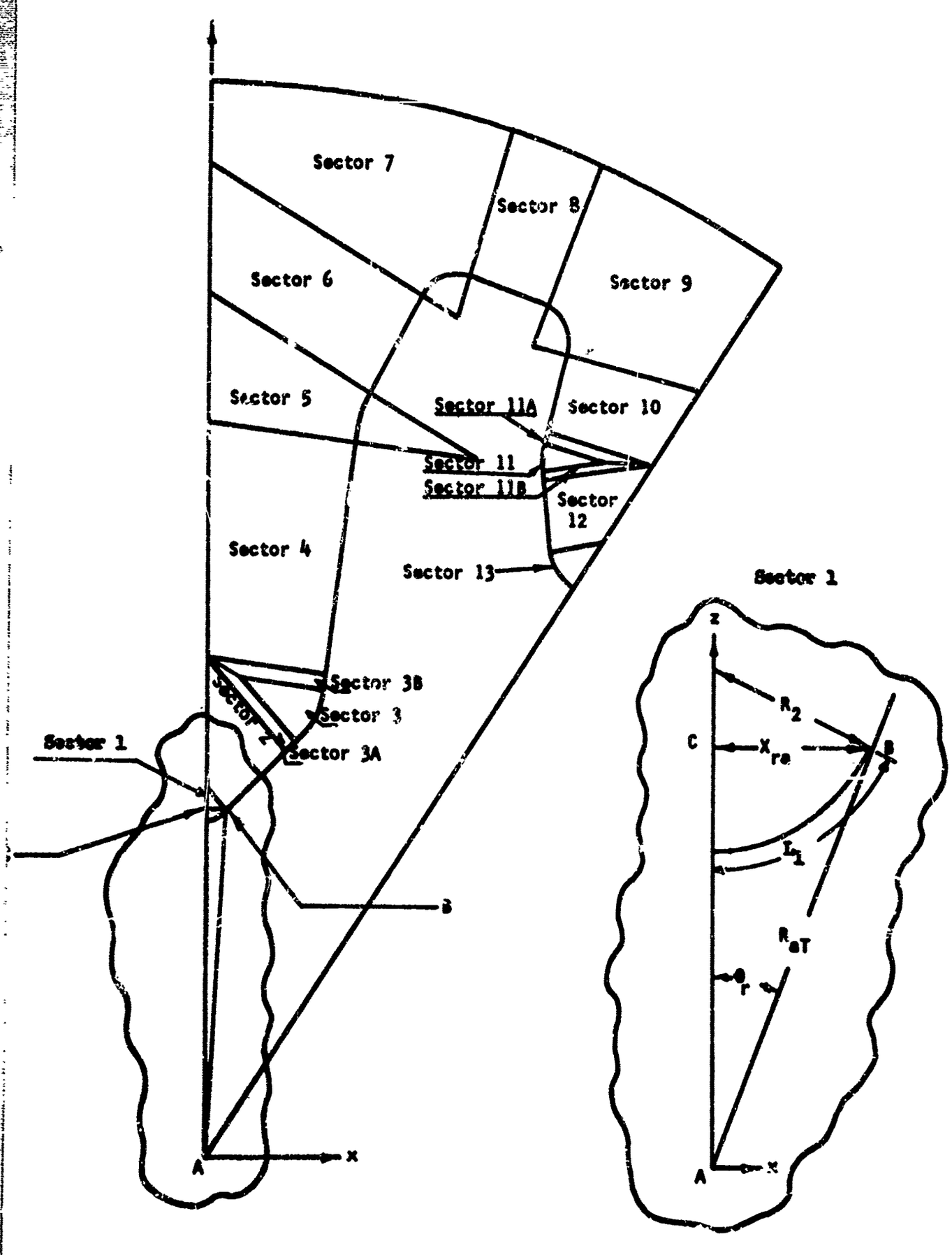


Figure 5.15 Sectors for Block No. 1

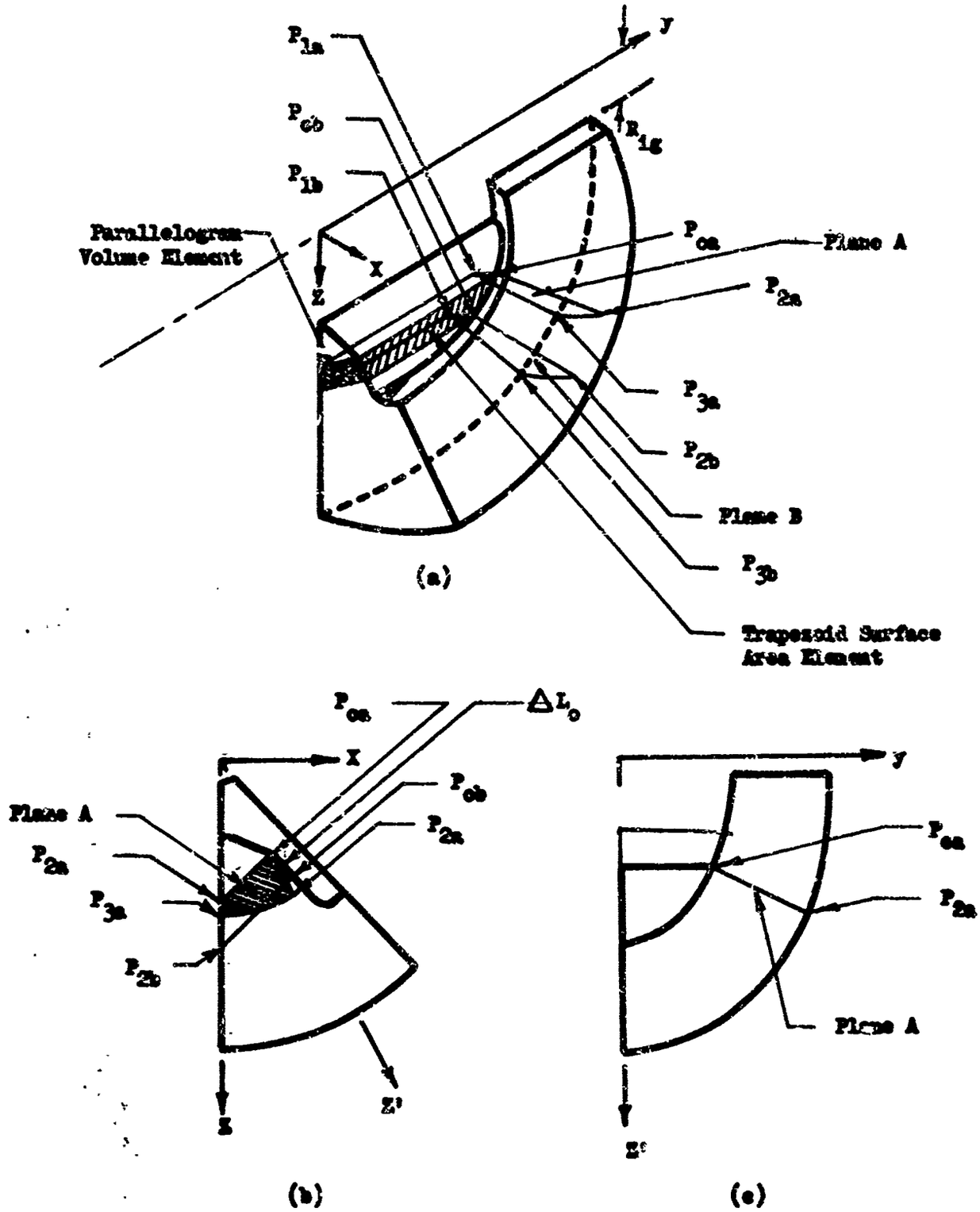


Figure 5.16 Head-End with Web Plane Definition

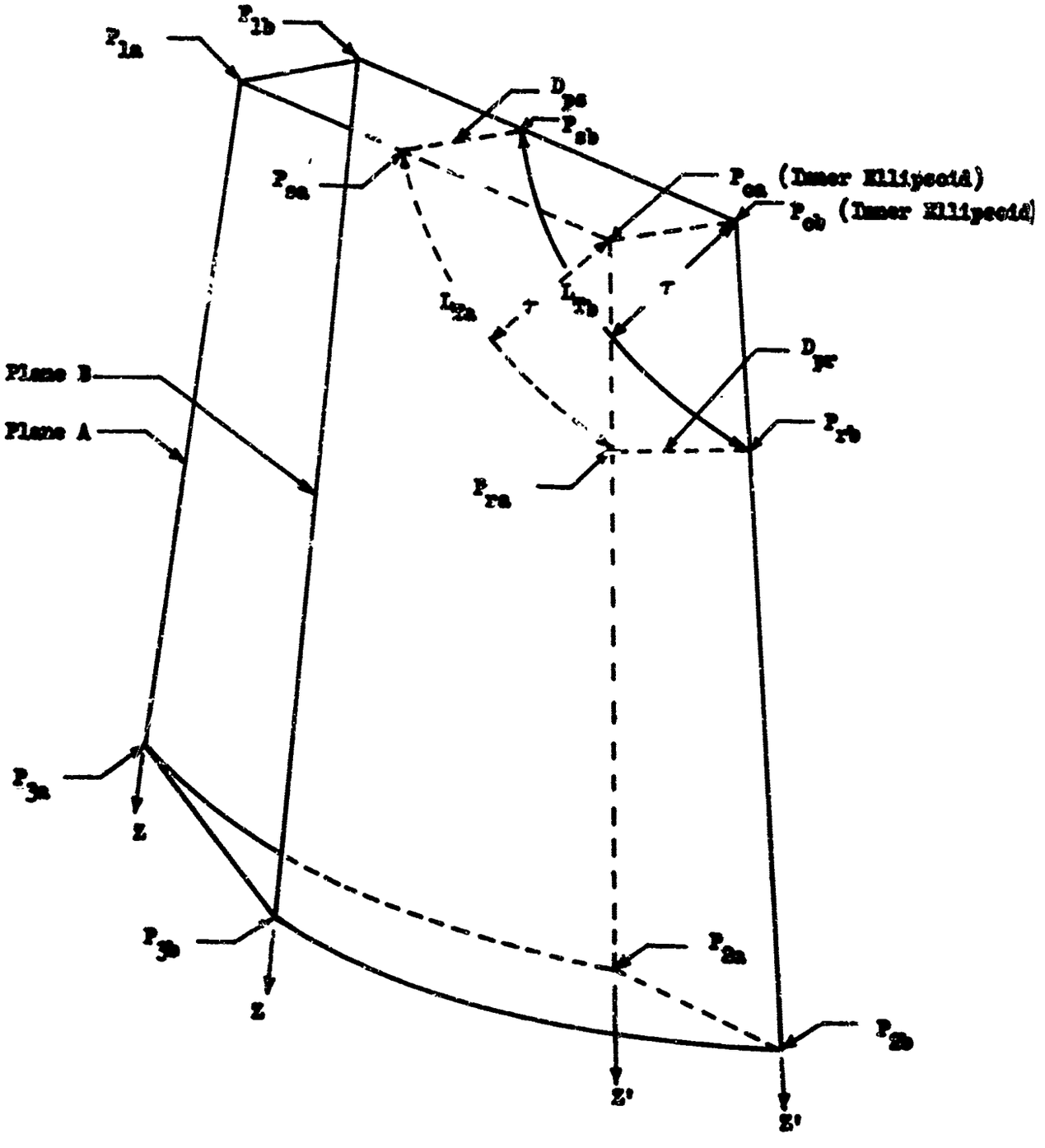


Figure 5.17 Hood-End with Web, Block 1 Plane Definition

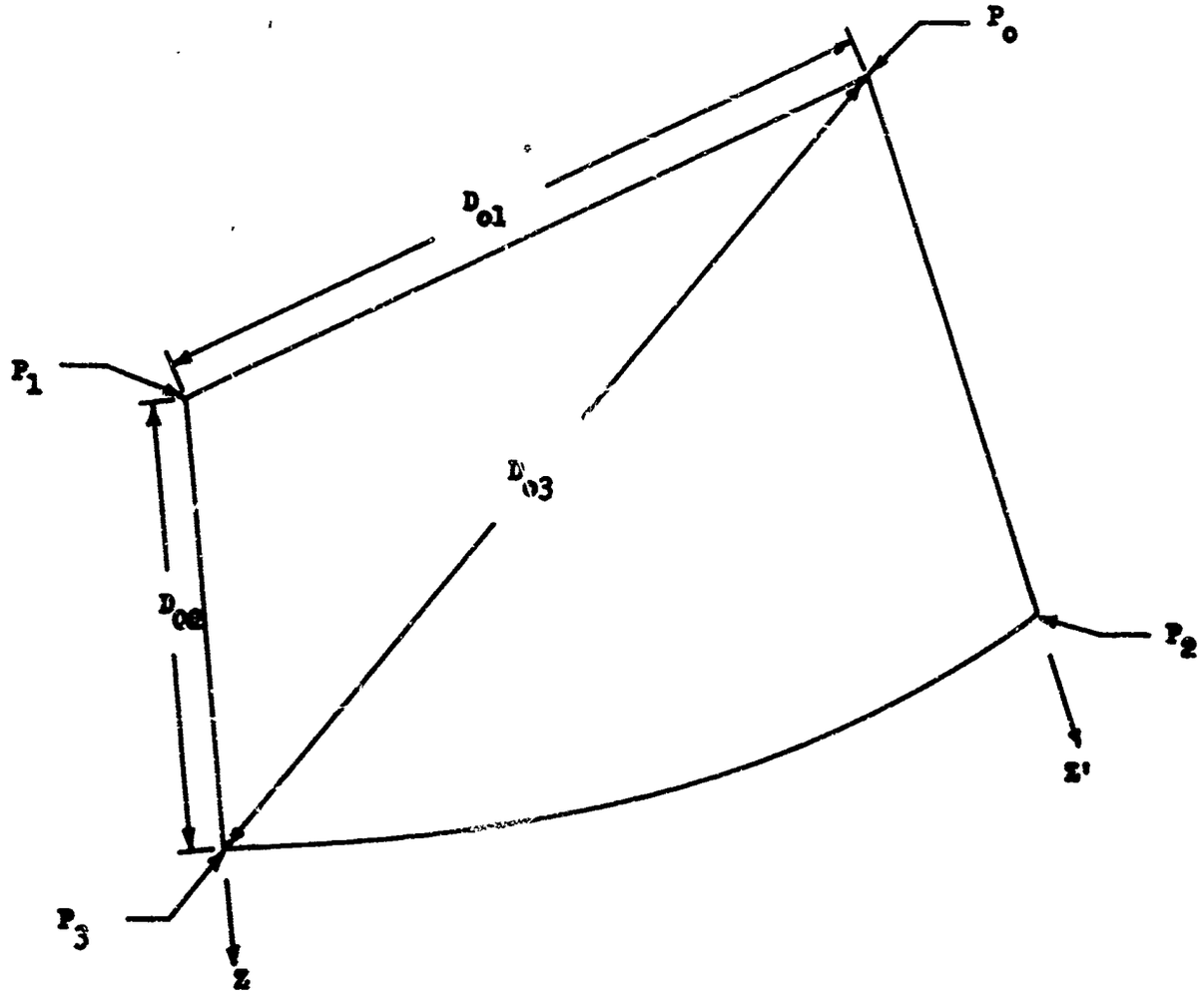


Figure 5.18 Plane for Block 1 Analysis

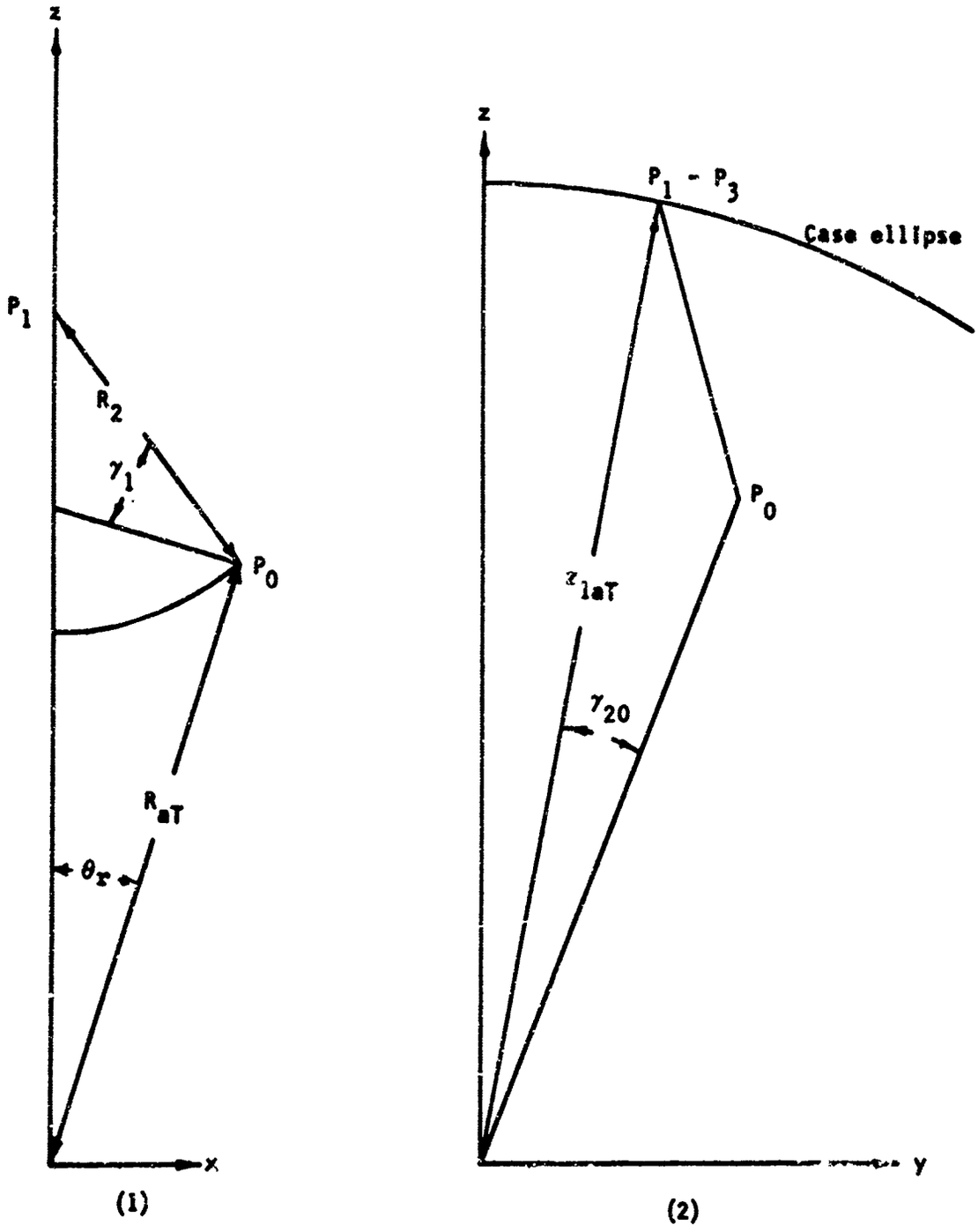


Figure 5.19 γ_1 for Subroutine GAMSUB

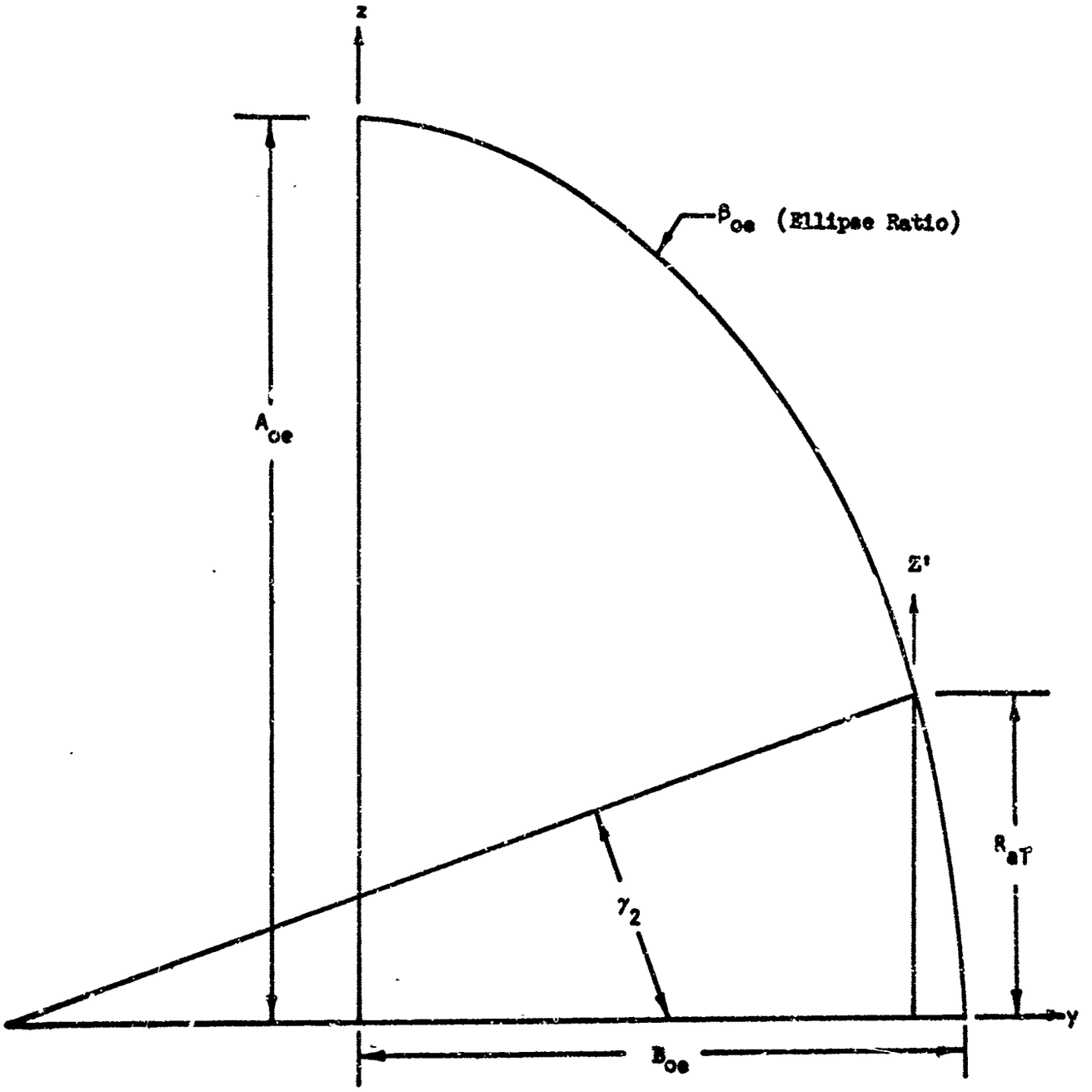


Figure 5.20 γ_2 for Subroutine GAM2S

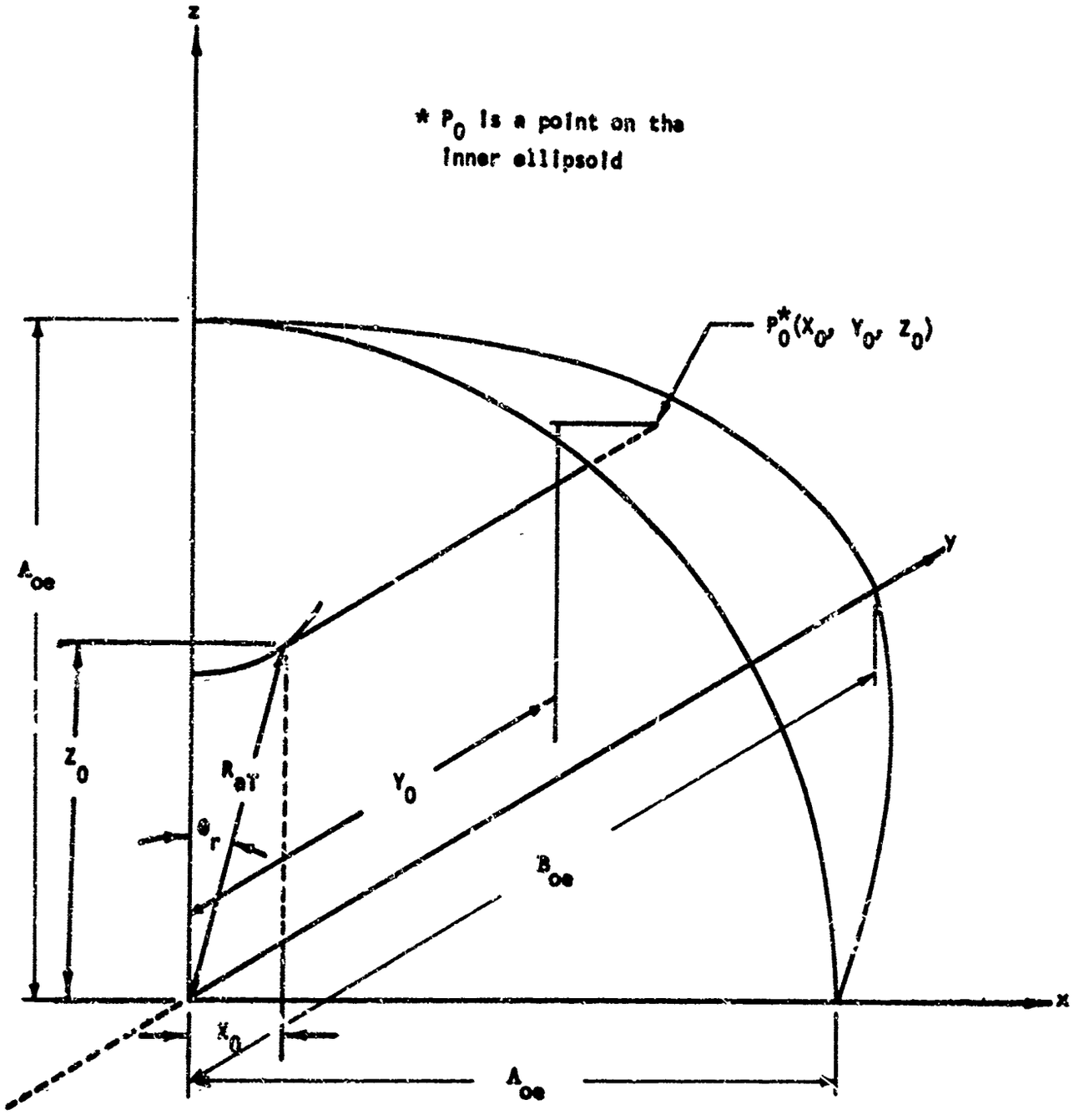


Figure 5.21 P_0 for Subroutine POSUB

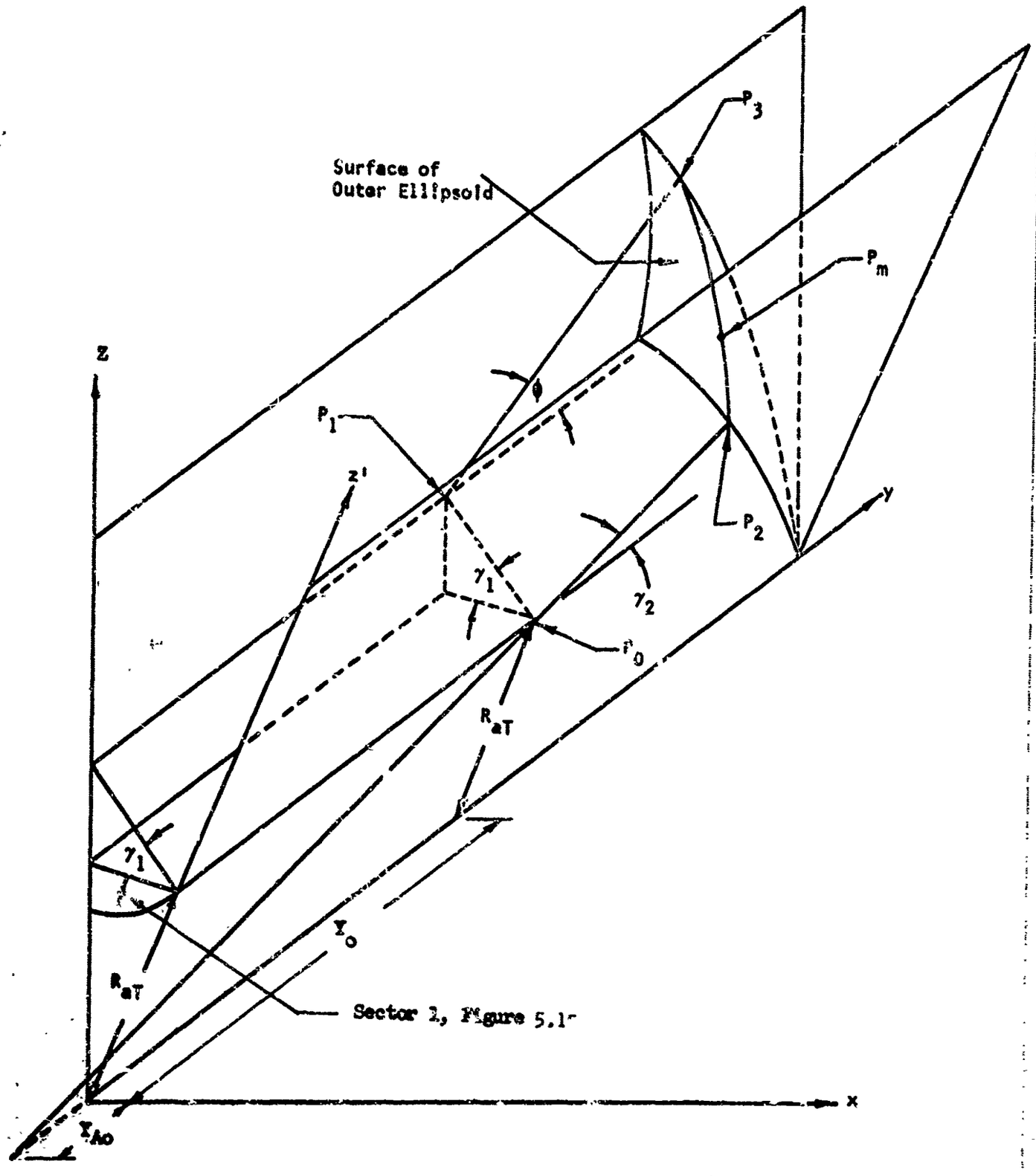


Figure 5.22 P_3 for Subroutine P3SUB

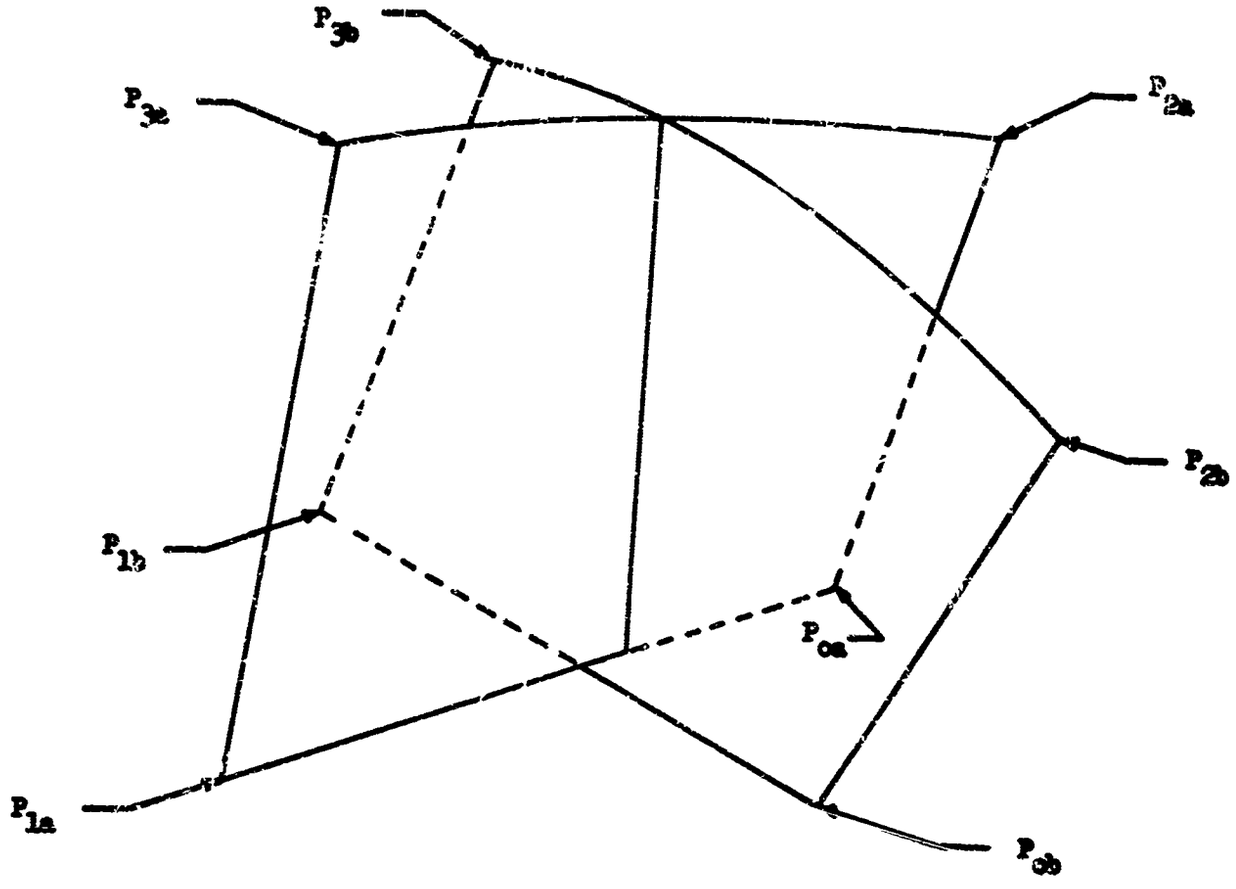


Figure 5.23 Planes for Block 1 Analysis

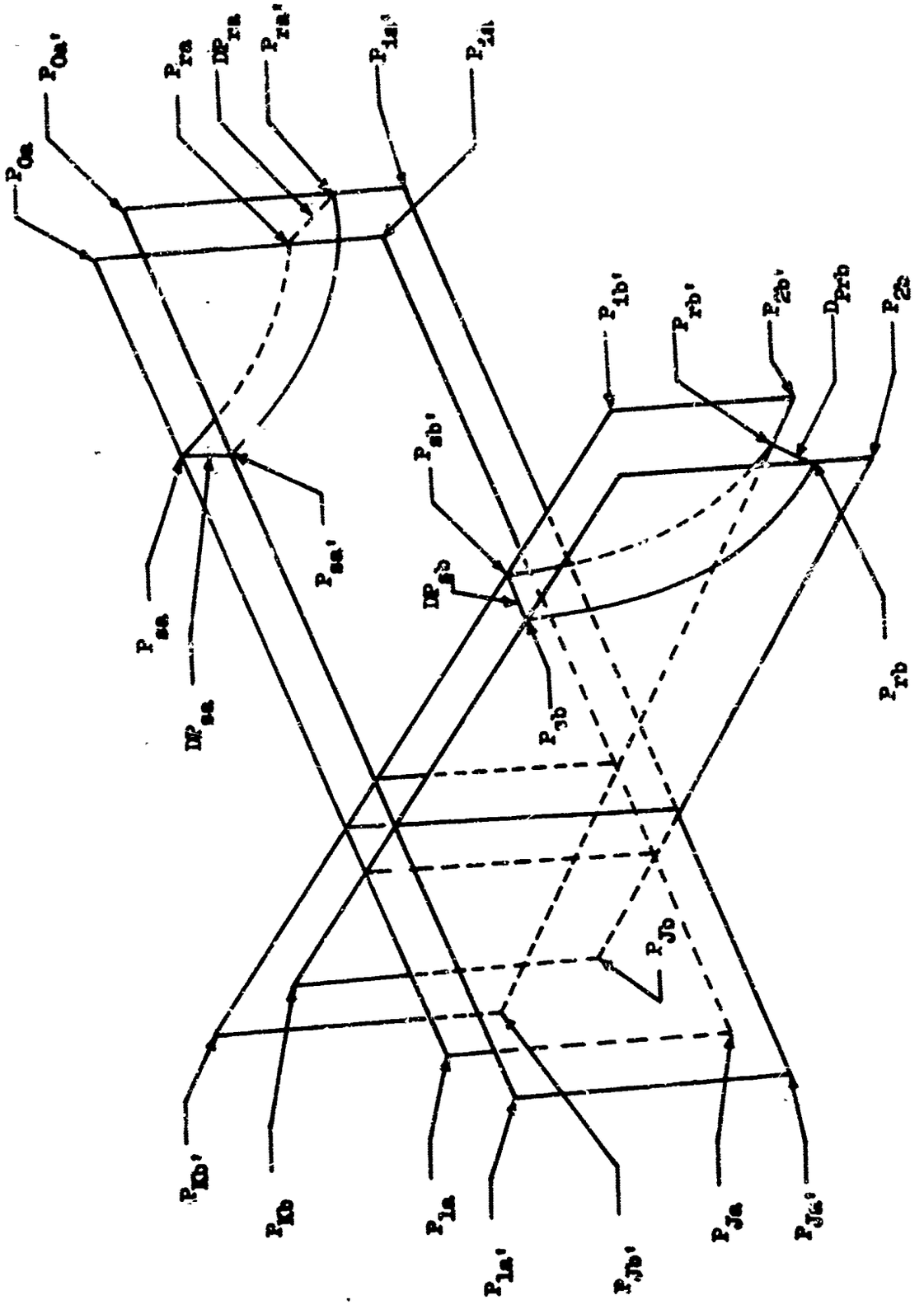
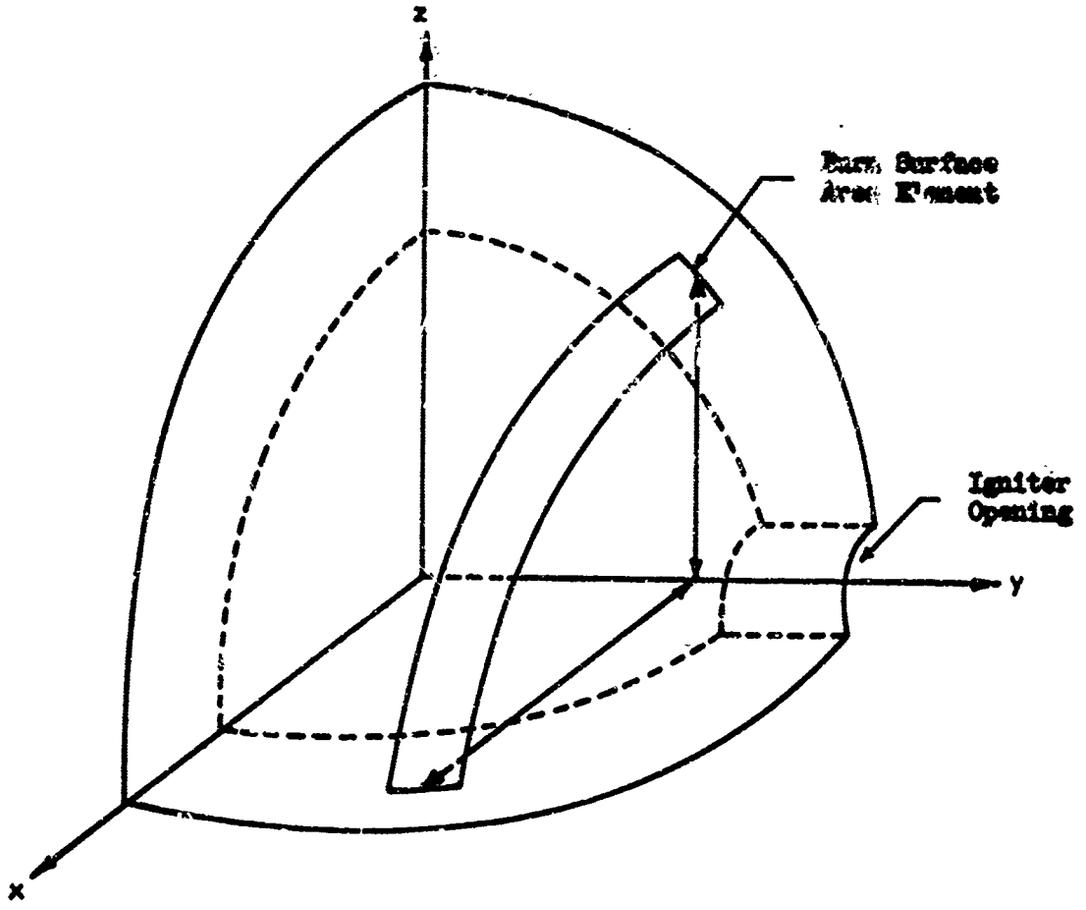


Figure 5.24 Planes Produced in Sectors 3A and 3B or 1A Sectors 11A and 11B



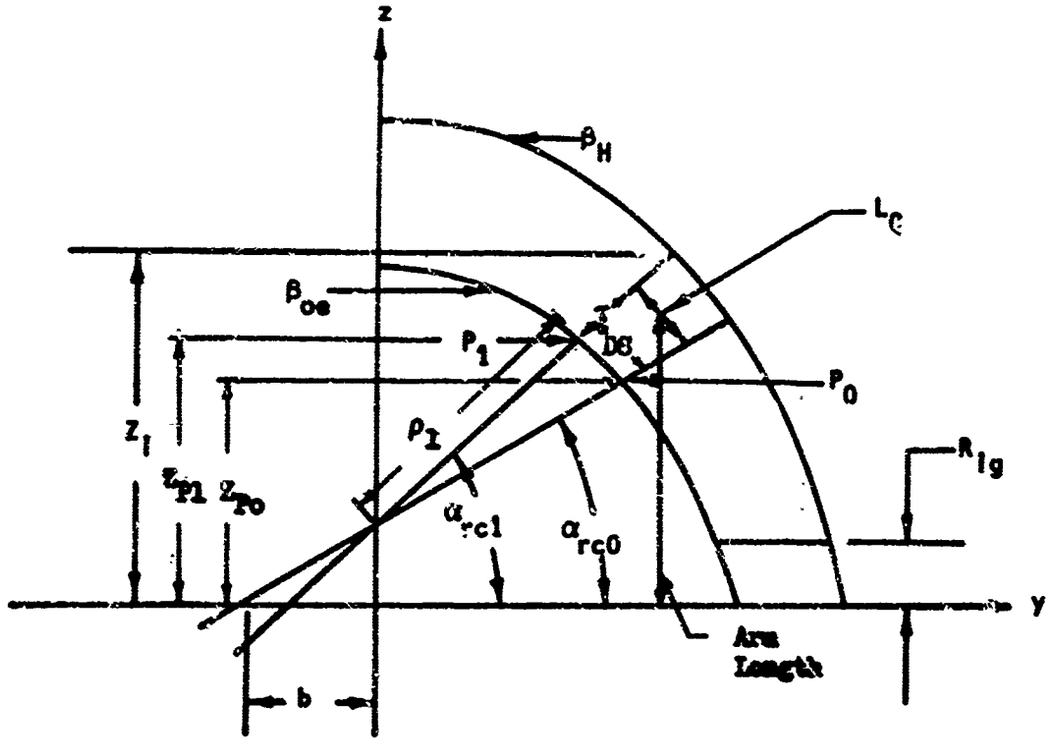
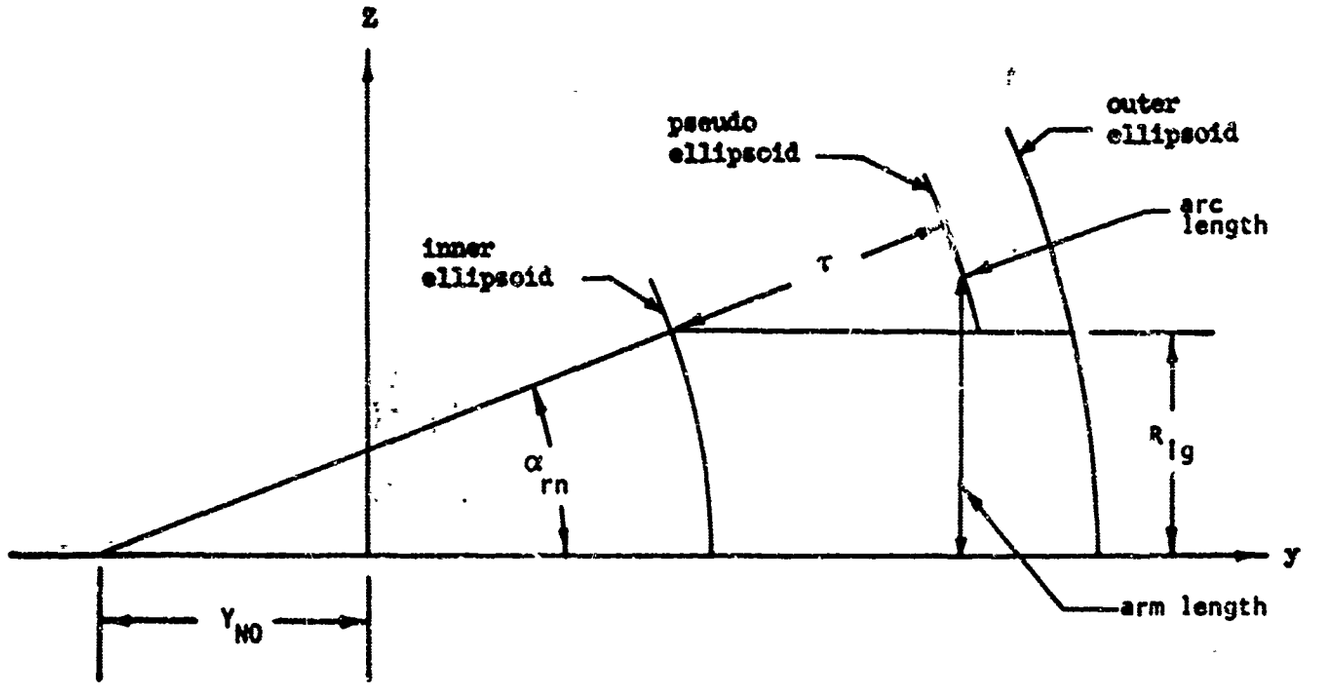


Figure 5.25 Areas for Block No. 2A and 2B



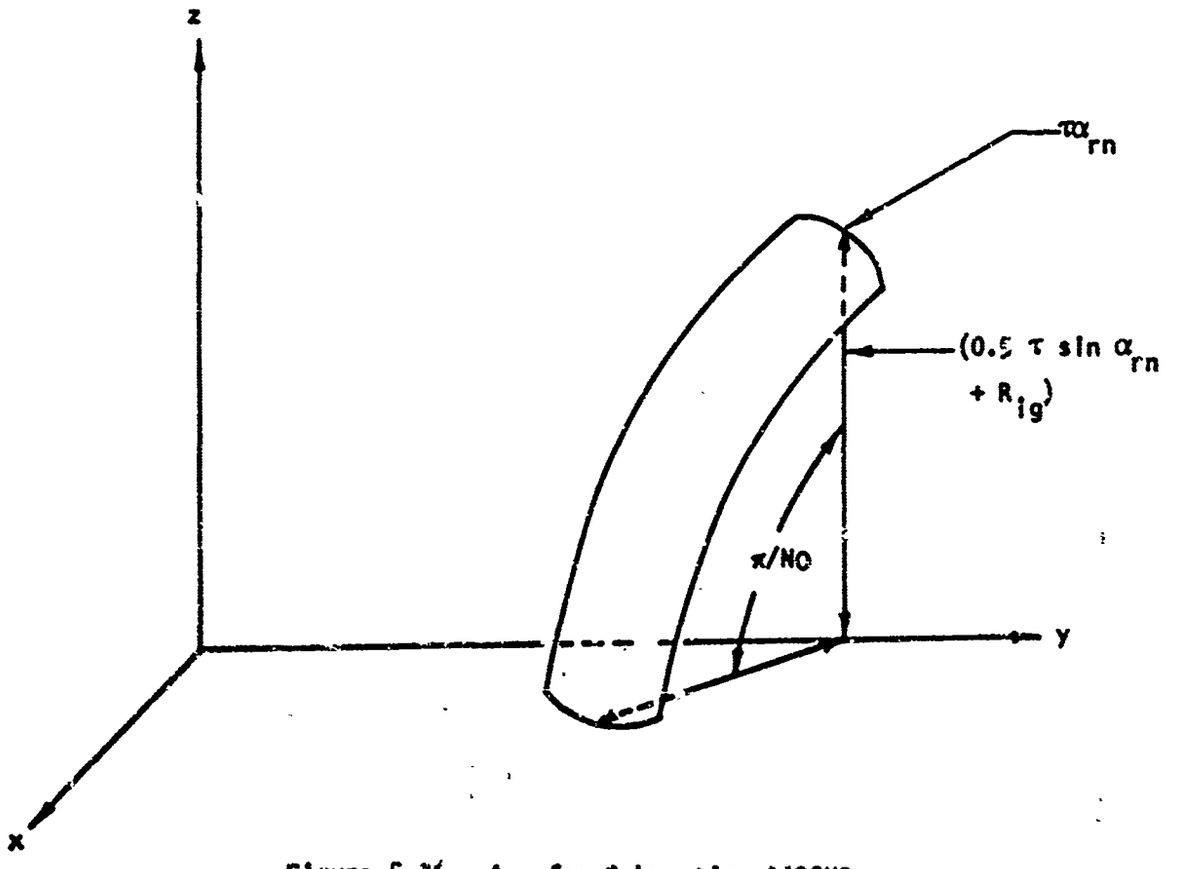


Figure 5.26 A_{ig} for Subroutine AIGSUB

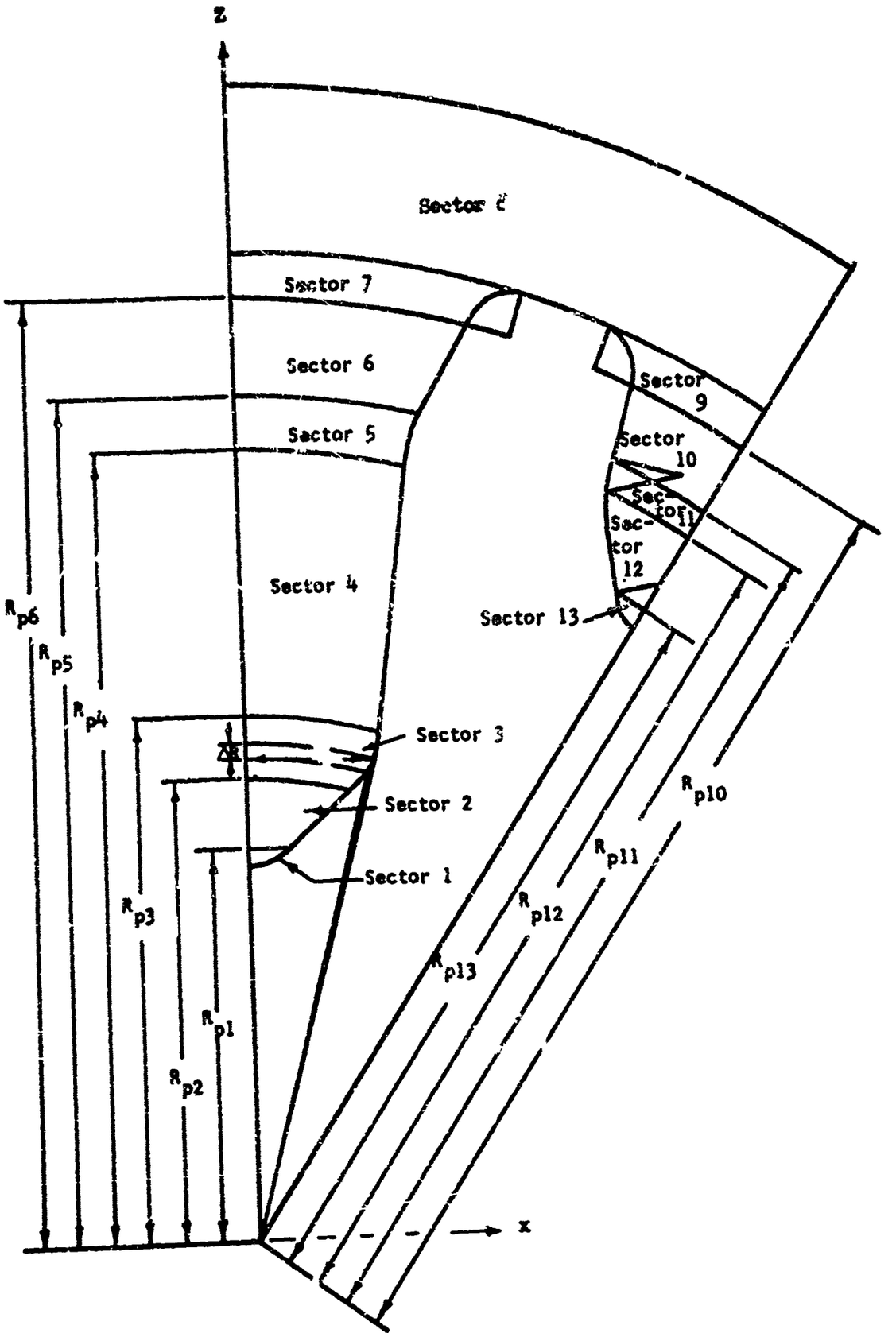


Figure 5.27 Sectors for Block 2B of Fore-Head Section

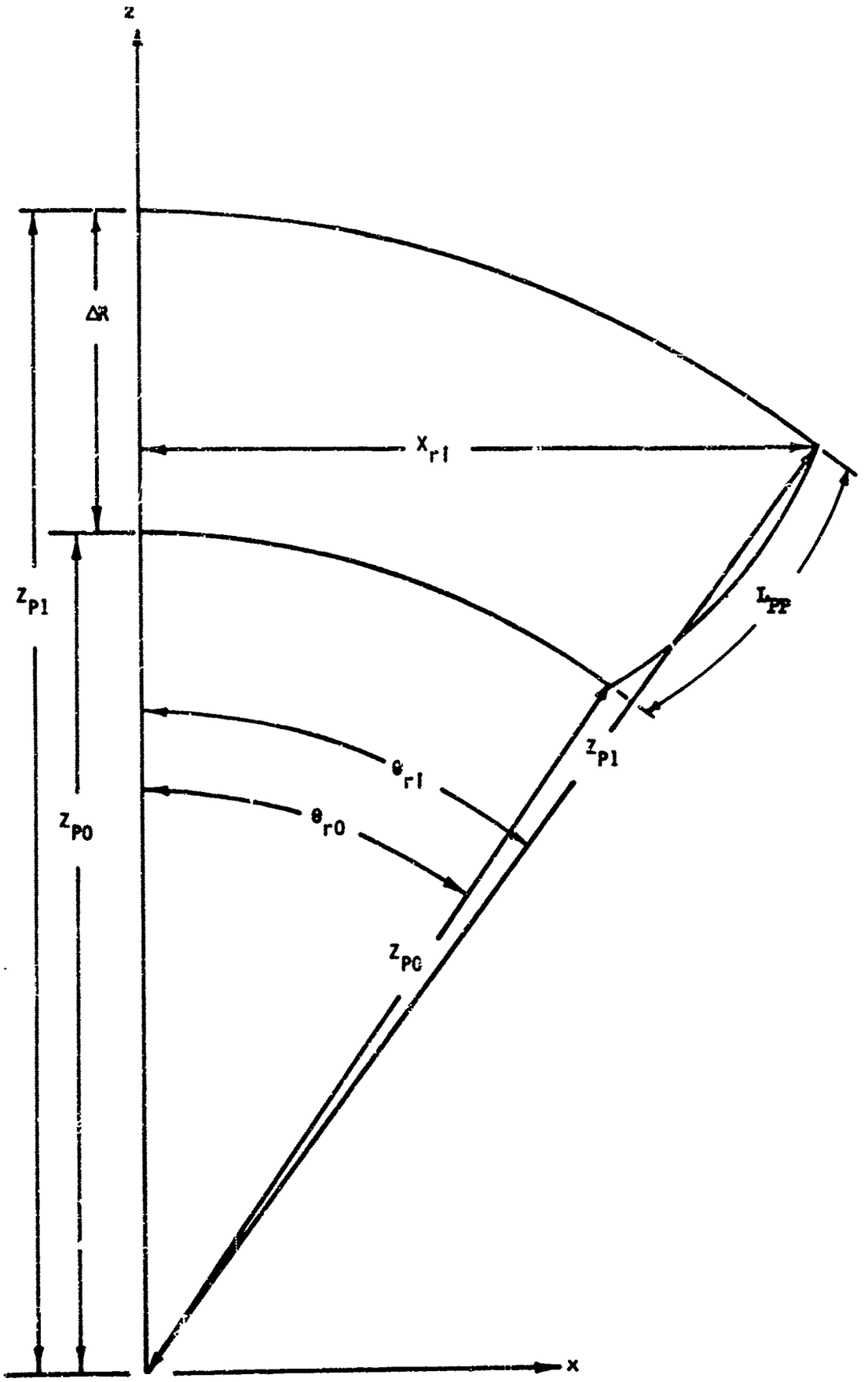


Figure 5.28 Sector for Block 2B

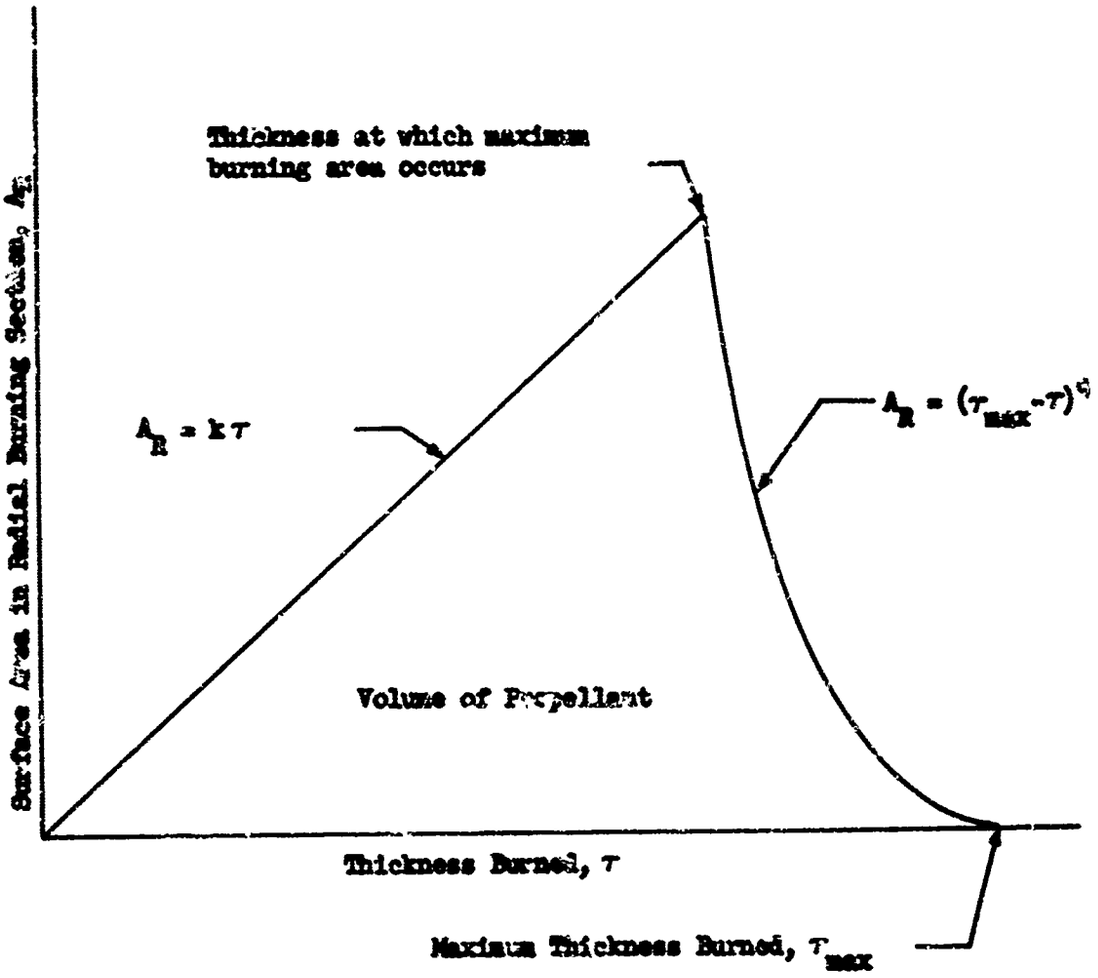


Figure 5.29 Distribution of Volume in Radial Burning Section

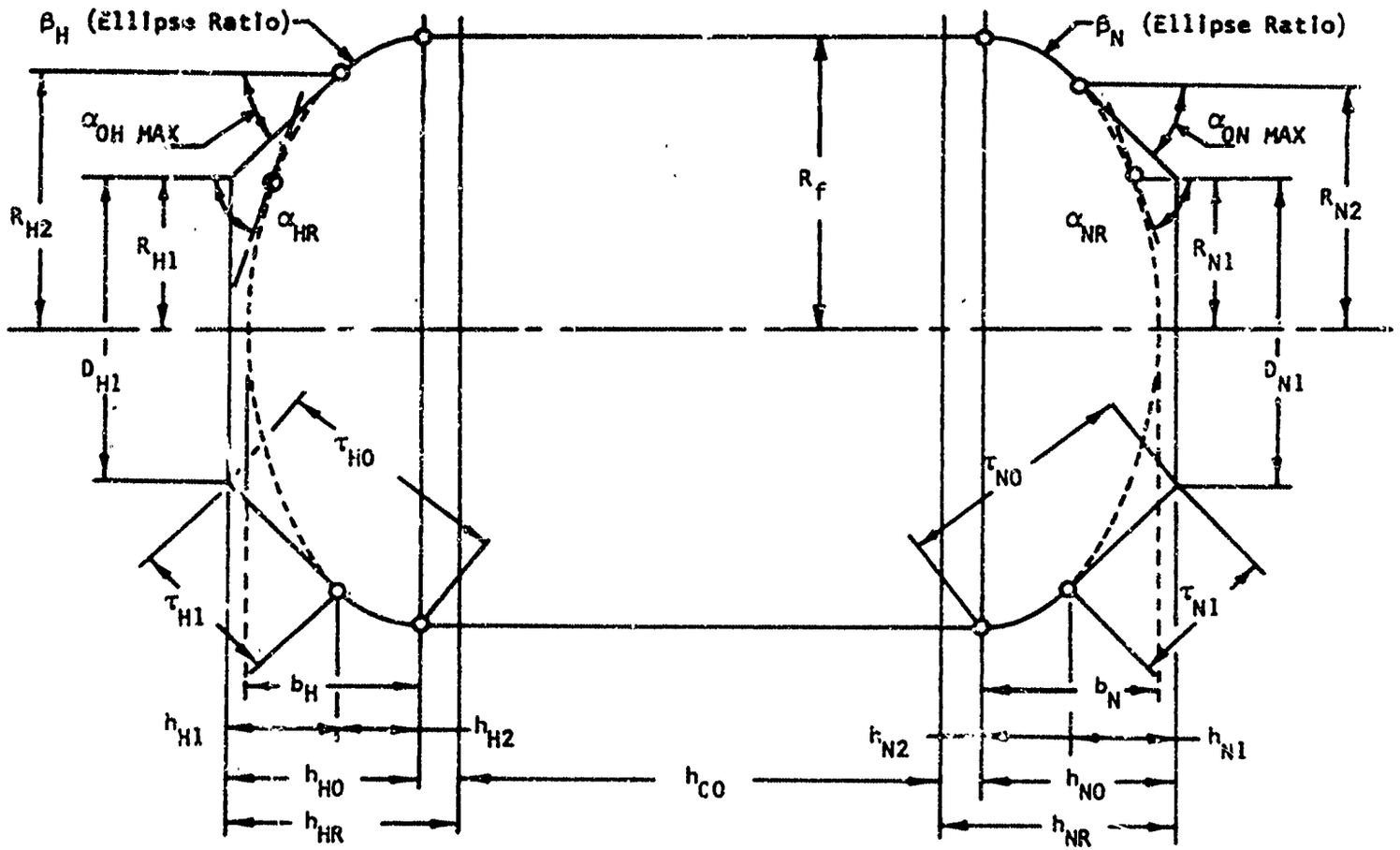


Figure 5.30 Motor Case Longitudinal Constants

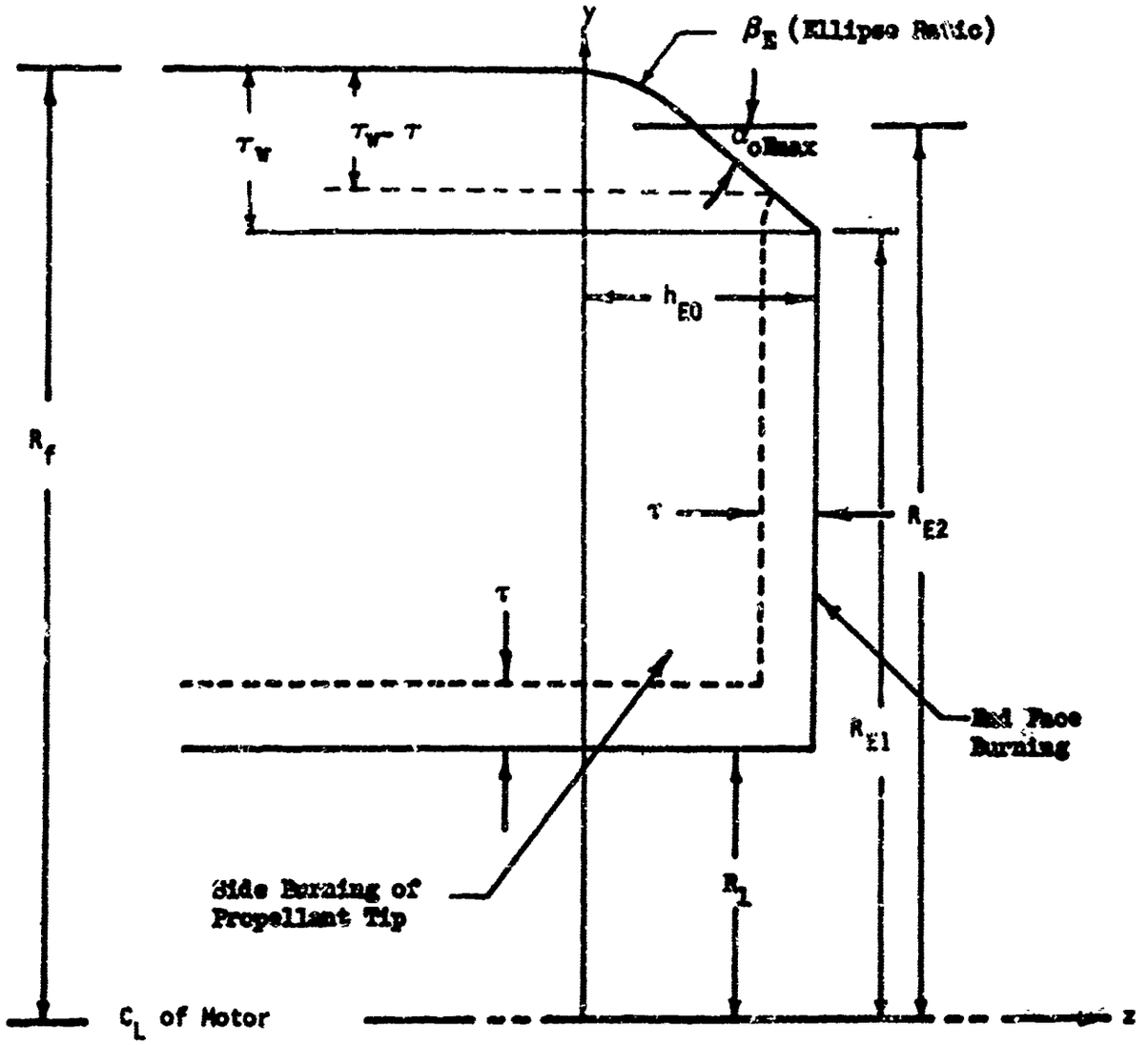


Figure 5.31 Straight Through Grain Configuration

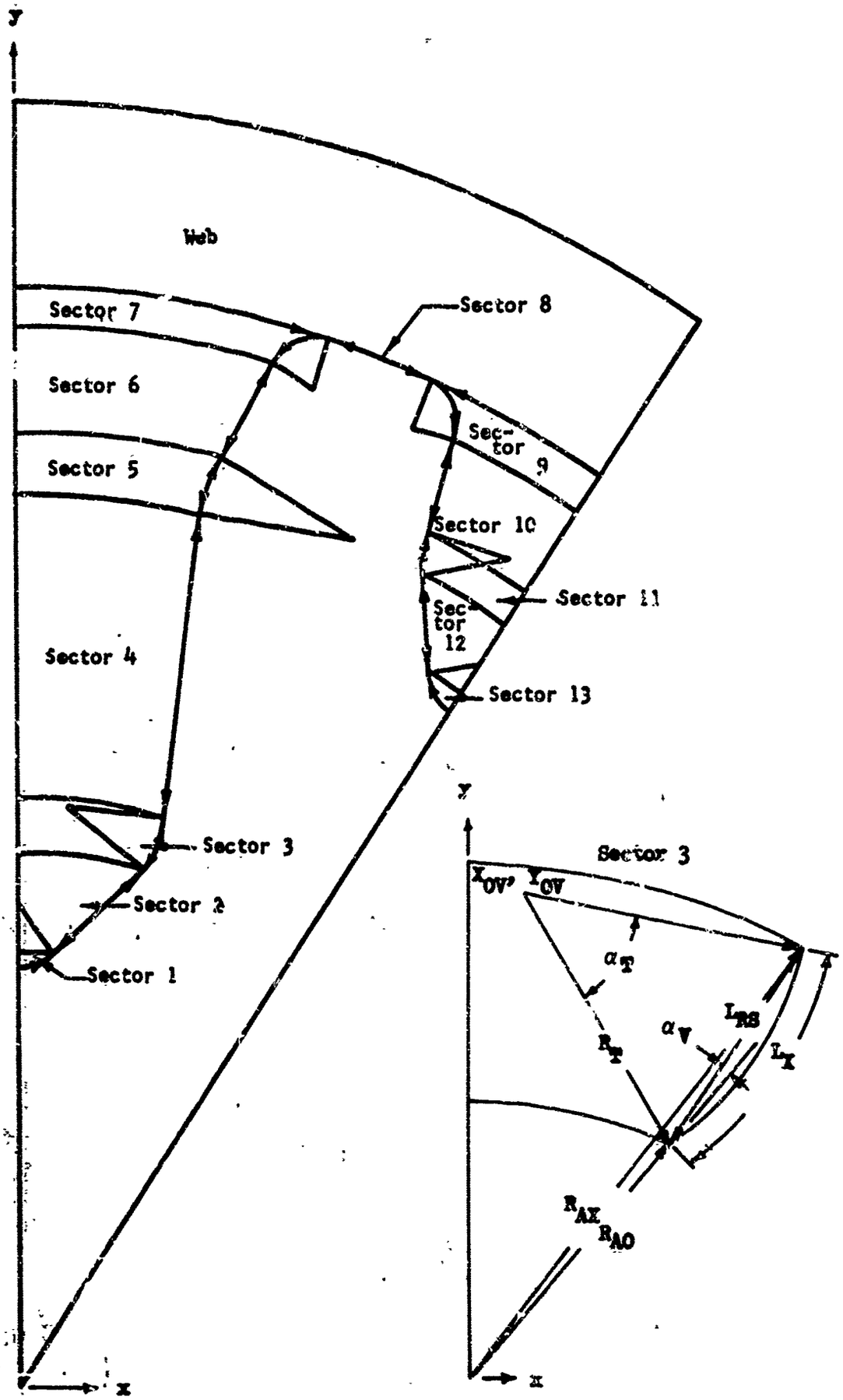


Figure 5.32 Sector Definition

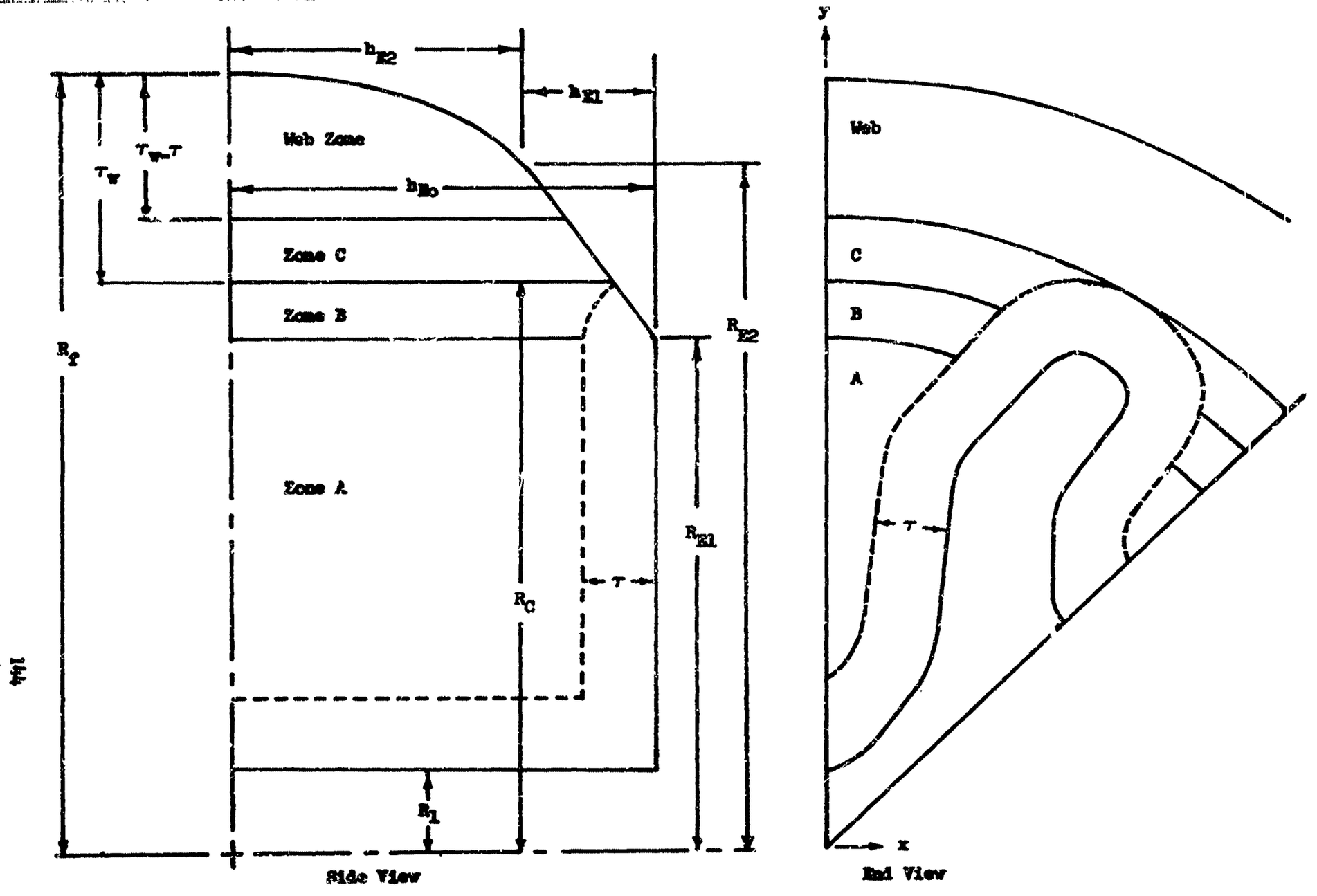
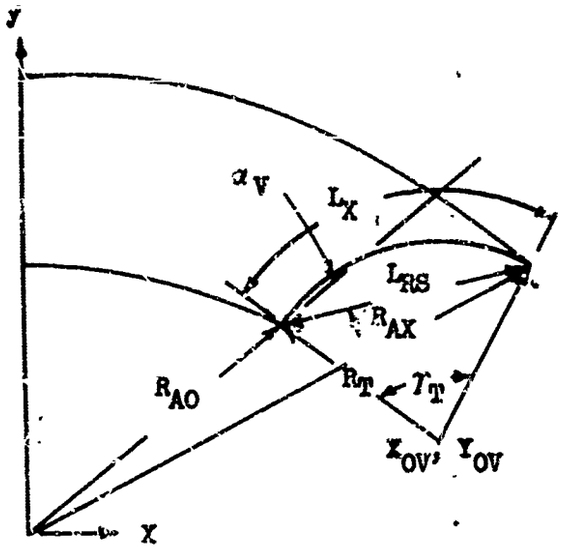
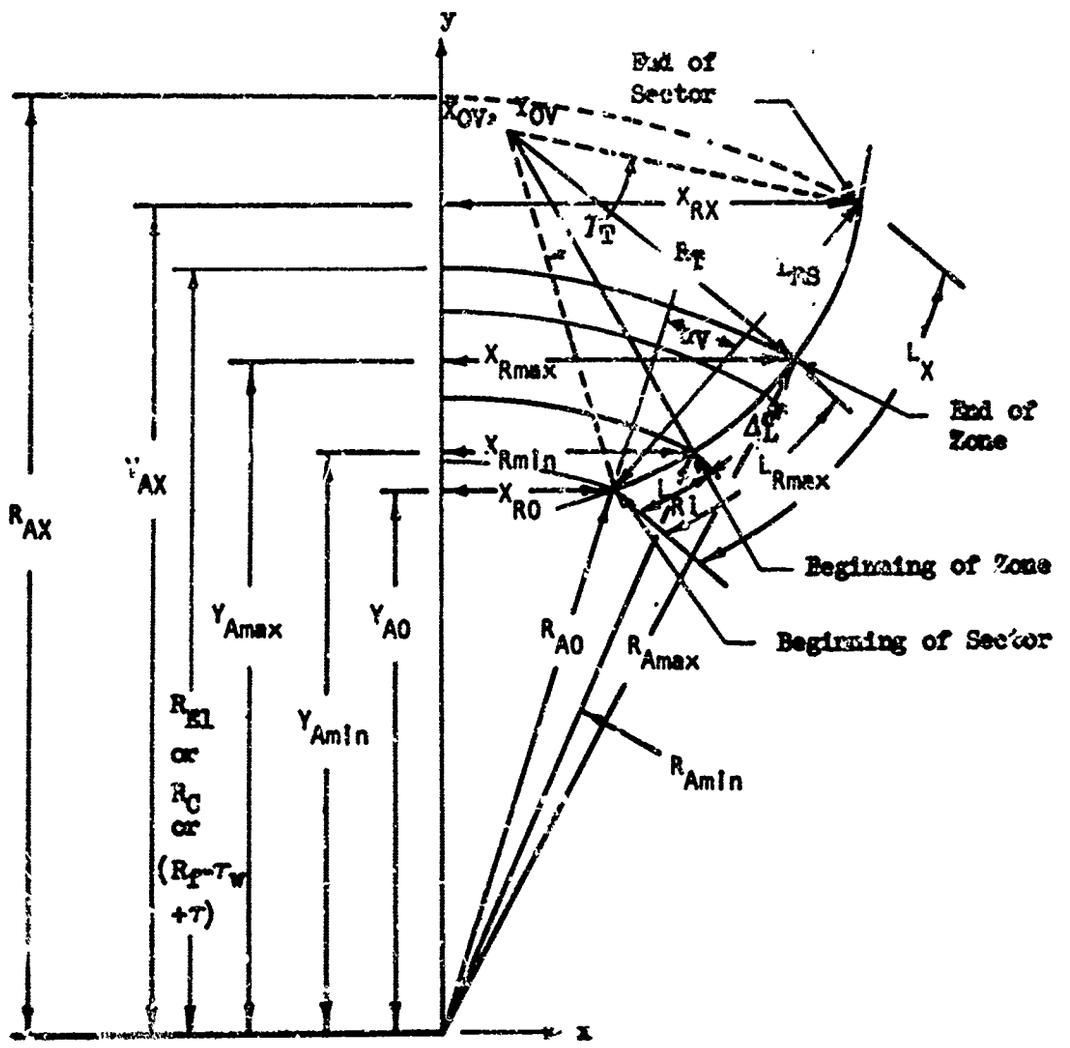


Figure 5.33 Zone Definition



Sectors 5, 7, 9



Sectors 1, 3, 11, 13

Figure 5.34 Sector Parameters, Zones B, C, and Web

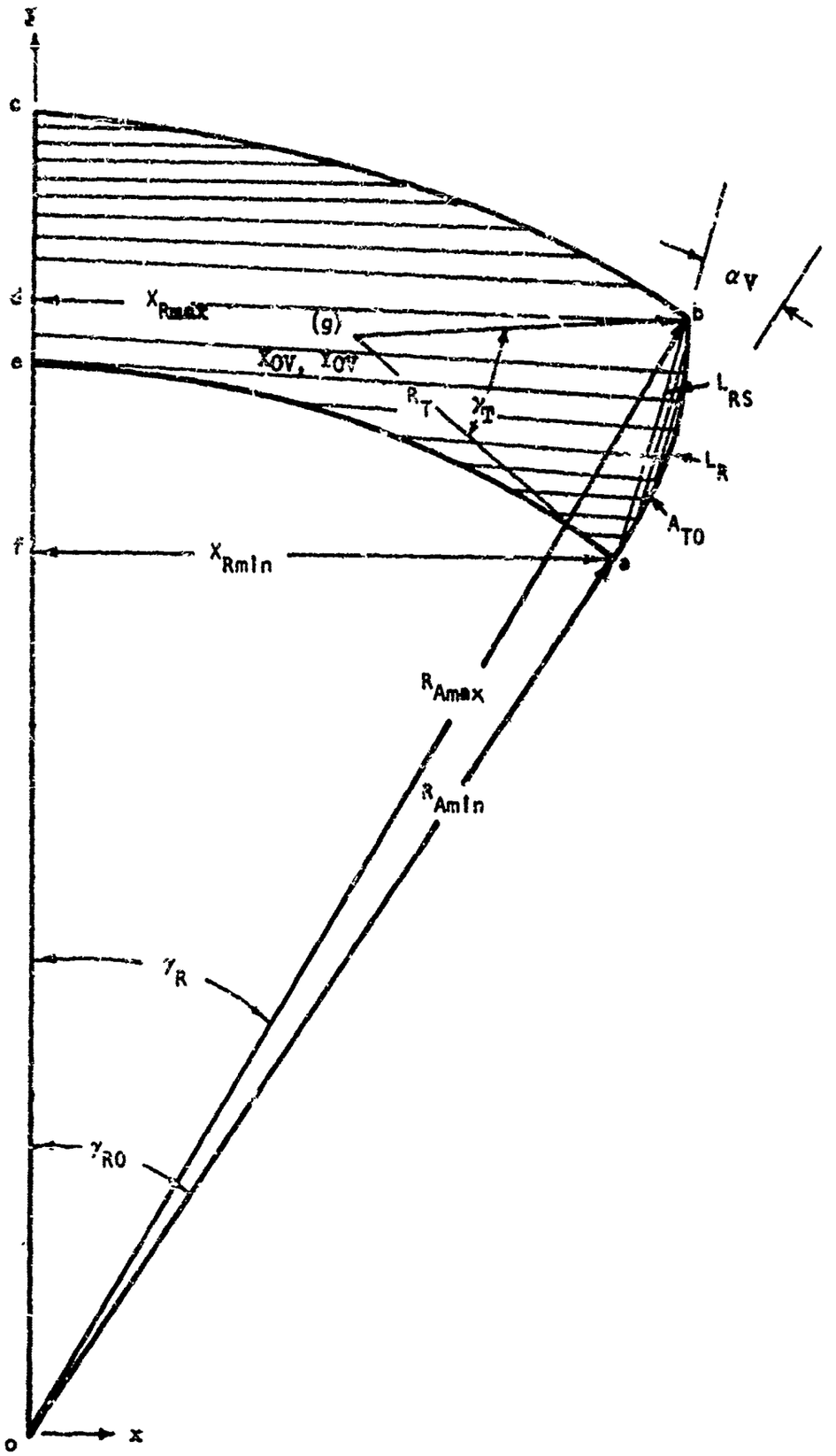


Figure 5.35 Circular Arc Sector 3 Zone A

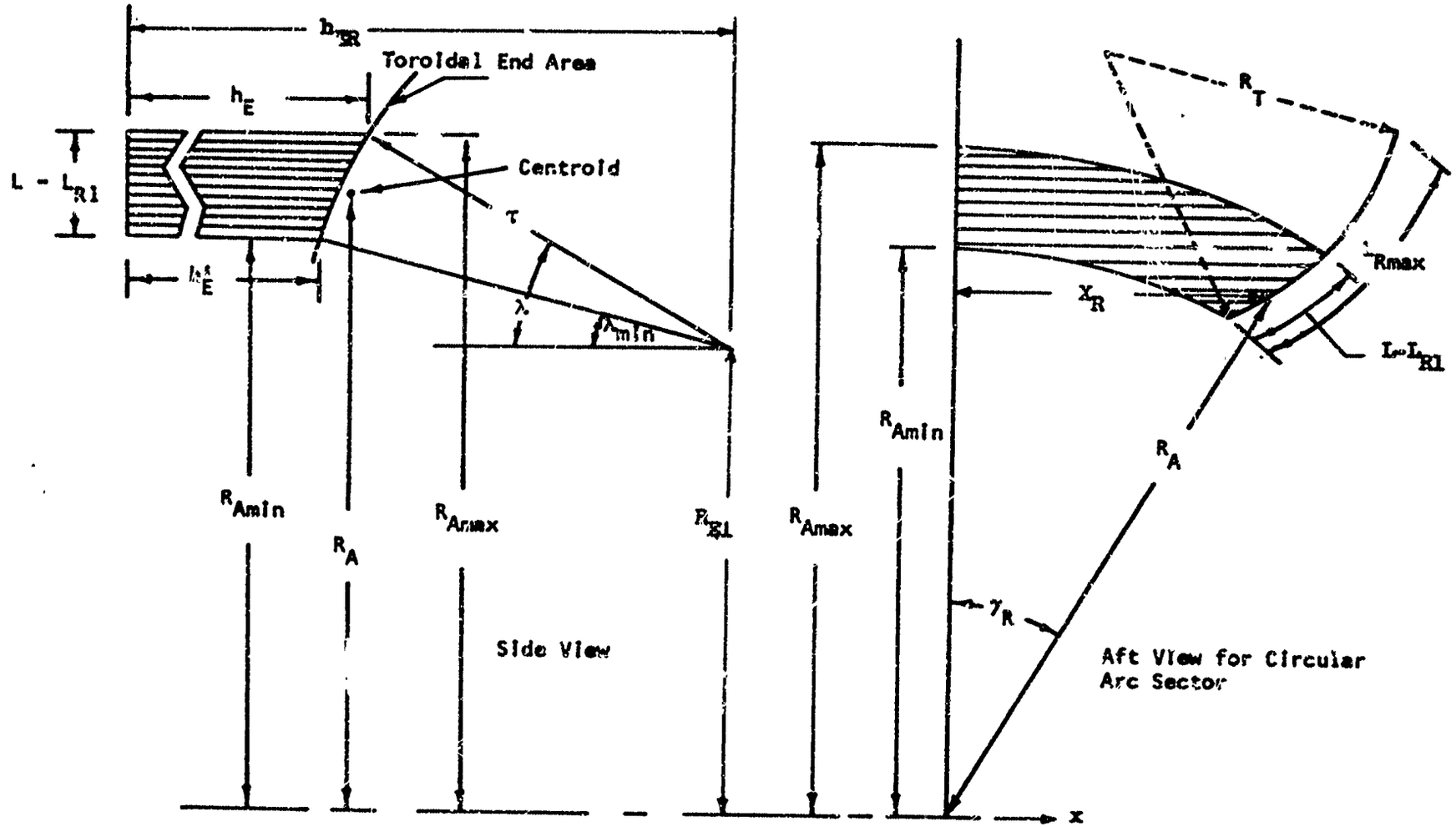


Figure 5.36 Element of Incremental Area for Zone B

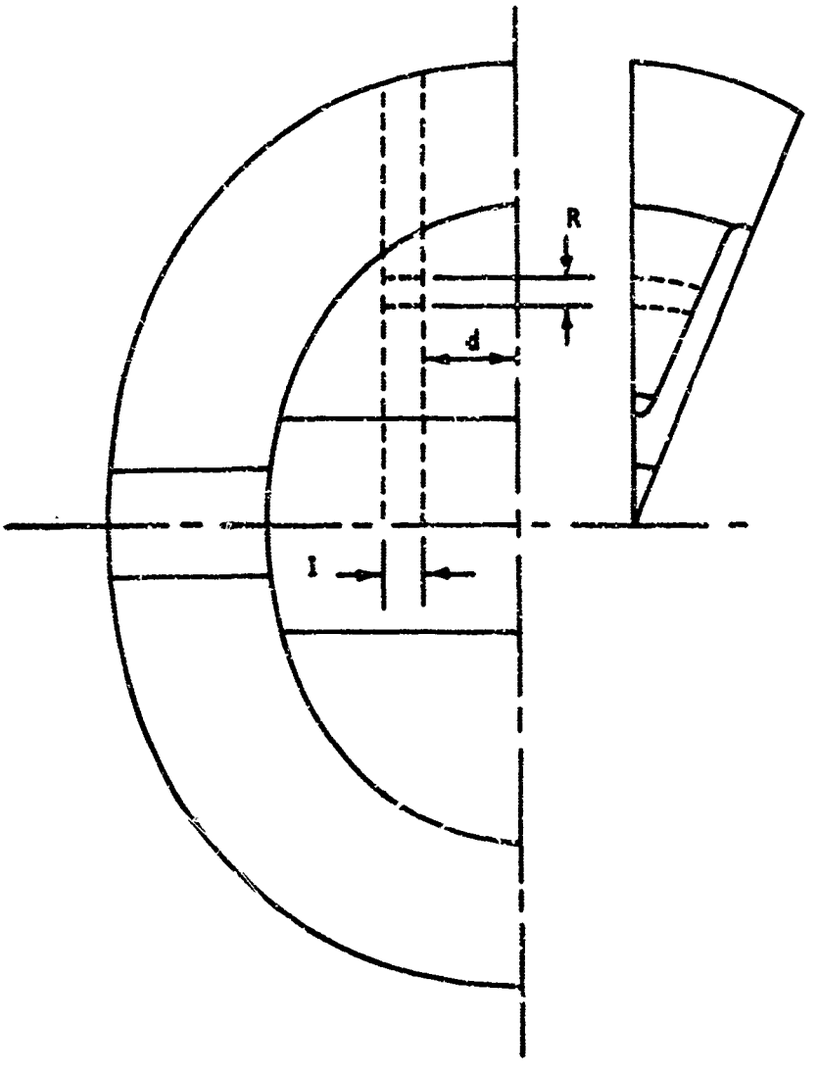
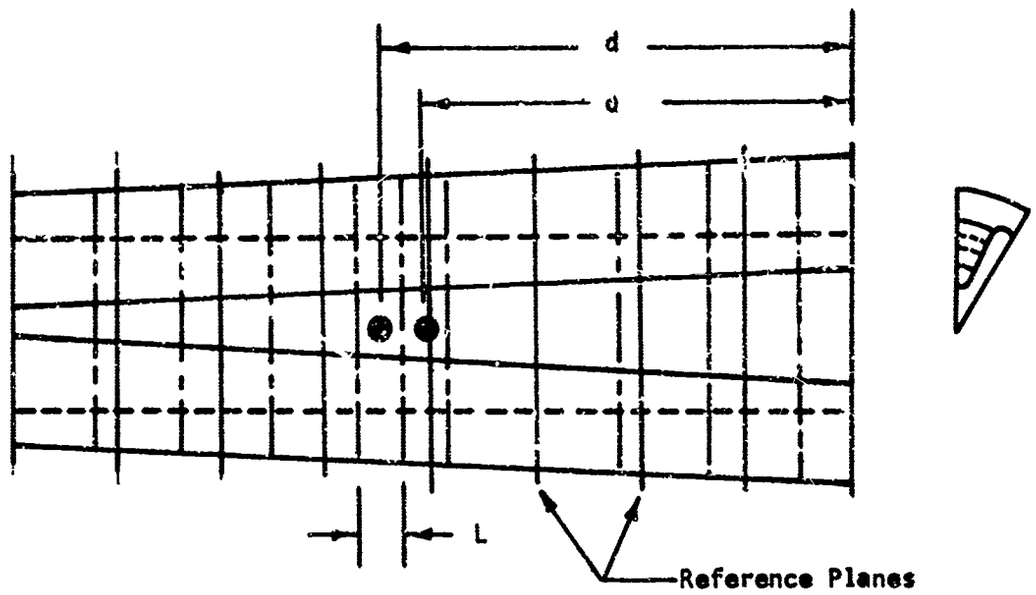


Figure 5.37 Head-End Section Elemental Volumes for MOI and CG Calculations



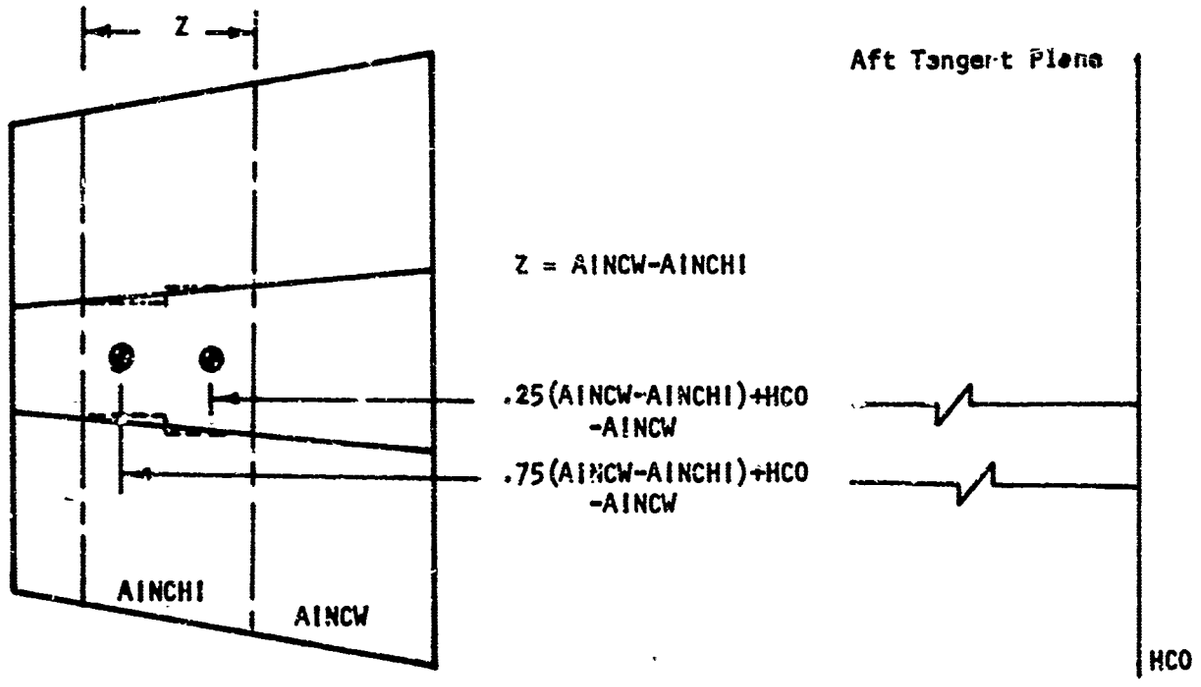


Figure 5.38 Cylindrical Section Elemental Volumes for MOI and CG Calculations

6.0 DETAILED PROGRAMMING INFORMATION

Information required to maintain and revise the program is presented in this section. A brief description of all program subroutines, macroscopic program logic flow charts, the program storage allocation, a description of the computing system, program diagnostic aids, and a list of the program nomenclature are included.

As stated in Section 3.0 on the method of solution, the primary purpose of this computer program is to obtain the performance characteristics of solid propellant rocket motors, which requires the solution of the internal ballistics. In order to obtain the performance characteristics, the computer solution is separated into two major sections. One section obtains the propellant burning surface area and volume (geometry calculations), and the other section obtains the solution of the gas dynamic equations (internal ballistic solution). The computer solution of the geometry equations requires three separate core loads and the computer solution of the gas dynamic equations requires a fourth core load. Each computer core load contains a control subroutine which calls the required subroutines and computes values of control parameters. A common data region named COM and dimensioned 6600, which resides in the machine memory core at all times during program execution, contains all of the computed variables so that each core load may be linked to all other core loads. Another common section named TBLK and dimensioned 2580 is used to store the geometry tables which are calculated in core loads 1-3 and which are used in core load 4. The individual core load control subroutines are linked through the MAIN program by a control variable named ICHN. The control subroutine for the first computer core load is MNCHN1, for the second computer core load - MNCHN2, for the third computer core load - MNCHN3, and for the fourth computer core load - MNCHN4.

The first computer core load (ICHN = 1) contains the subroutines required to read the input data, initialize the data cells, compute the input reference plane constants, locate the increment dividing planes, check for input data errors, and print the program inputs and computed constants. The second computer core load (ICHN = 2) contains the geometry subroutines required to compute the initial propellant area, perimeter length, and radius of gyration for the cylindrical section reference planes; and to compute the initial propellant volume, burn area, center of gravity location, and moments of inertia for the aft-head and straight through grain fore-head section. The third computer core load (ICHN = 3) contains the geometry subroutines required to compute the initial propellant volume, burn area, center of gravity, and moments of inertia for the fore-head with web. The fourth computer core load (ICHN = 4) contains the subroutines required to obtain the internal ballistic solution.

6.1 Subroutine Description

This subsection is divided into two parts. Part one (6.1.1) contains a verbal description of the purpose of each subroutine and includes cross-references to other sections which give additional, detailed explanations of particularly complex or important subroutines. Part two (6.1.2) contains a tabular description of the subroutine linkage. The table identifies all lower level subroutines called by a particular routine plus all routines which call that particular subroutine.

6.1.1 Subroutine Descriptions

ACOS - Subroutine ACOS determines the arc cosine for arguments between 0 and 2π radians.

AEPSUB - Subroutine AEPSUB tests for the existence of a sector for the end sections. If a sector is burned out or does not exist, program control is returned to subroutine ASESUB, otherwise computation proceeds to subroutine AESUB. The sector areas are then summed and program control is returned to subroutine ASESUB (Section 5.2.3.2).

AESUB - Subroutine AESUB determines the surface area and initial volume of a sector for the zones in the end sections (Section 5.2.3.2).

AFPSUB - Subroutine AFPSUB determines the perimeter length and cross-sectional area of all sectors, except sector 8, in the cylindrical section (Section 5.1.1).

AIBST - Subroutine AIBST determines the pressure loss and changes in the gas properties between increment dividing planes due to mass addition and area change for the non-steady flow solution of the internal ballistics (Section 4.1.2.1).

AIBSUB - Subroutine AIBSUB determines the pressure loss and changes in the gas properties between increment dividing planes due to mass addition and area change for the solution of the internal ballistics neglecting transient effects (Section 4.1.1).

AIGSUB - Subroutine AIGSUB determines the surface area around the igniter opening in the head end section (Section 5.2.1.2).

ALRSUB - Subroutine ALRSUB determines the arc length of a sector in the end sections from the minimum point of a sector to a general point along the perimeter of the sector (Section 5.2.3.2).

6.1.1 Subroutine Descriptions (Continued)

ARSSUB - Subroutine ARSSUB determines the chord length between the minimum point of a sector and a general point along the perimeter of the sector (Section 5.2.3.2).

ASESUB - Subroutine ASESUB sets up the correct equations for subroutines XRSUB and RASUB and assigns for each sector the proper values for the coordinates of the origin of the circular arc (RAO, XAO), the radius of curvature of the sector (RT), and the perimeter length (AL) of the sector (Section 5.2.3.2).

ASTSUB - Subroutine ASTSUB sets up the correct equations for subroutine PTIAA to determine the moments of inertia for the block 1 analysis of the head end with web (AJSTP and AJSTB).

ASUBC - Subroutine ASUBC sets up the correct variables and equations to determine the coordinates (X, Y, and Z) of the points POA, P1A, and P3A for the block 1 analysis in subroutine SC1 (Section 5.2.1.1).

AWESUB - Subroutine AWESUB determines the total burning surface area of the web zone at thickness TAU and the burning surface area of sector 8 for the end sections (Section 5.2.3.2.4).

BRAKSB - Subroutine BRAKSB determines the length of the diagonal of the parallelogram that is formed by the intersection of two planes in the block 1 analysis (See Figure 5.2?).

BSUBC - Subroutine BSUBC sets up the correct variables and equations to determine the coordinates (X, Y, and Z) of the points POB, P1B, and P3B on the pseudoellipsoid for the block 1 analysis in subroutine SC1 (Section 5.2.1.1.1).

COMPSC - Subroutine COMPSC determines the sine and cosine for the reference plane geometry angles A(1) thru A(5).

CONV - Subroutine CONV determines new iterations value for either AKRST or PCTAB during the start transient calculations for the internal ballistic solution.

6.1.1 Subroutine Descriptions (Continued)

CSTRSB - Subroutine CSTRSB determines the propellant gas properties, CSTAR, molecular weight, specific heat ratio, gas constant, and combustion temperature as a function of the chamber pressure during the internal ballistic solution (Section 4.3.3).

DFRASB - Subroutine DFRASB determines the distance between the points P_{ra} and P'_{ra}; P_{sa} and P'_{sa}; P_{rb} and P'_{rb}; and P_{sb} and P'_{sb} that lie on the planes produced in sectors 3A and 3B or 11A and 11B in the block 1 analysis of subroutine SCI (Section 5.2.1.1.2).

ENDCSB - Subroutine ENDCSB determines the coefficients of a fourth degree polynomial equation obtained by the intersection of an ellipse and a circle, CAE, CBE, CCCE, CCVE, CDCE, CDVE, CECE, and CEVE and determines the constants RE1, RE2, ALFE, ALFEM, HE1, HE2, and HE0 that define the geometry of the fore-head and aft-head sections (Section 5.2.3.1).

FDGRE - Subroutine FDGRE solves for the roots of a fourth degree polynomial equation by reducing to the form

$$X^4 + A X^2 + BX + C = 0$$

by the substitution

$$Y = (X - P/R)$$

and then solving the resultant cubic

$$T^3 + \frac{A}{2} T^2 + \frac{(A^2 - 4C)}{16} T - \frac{B^2}{64} = 0$$

GAMA2S - Subroutine GAMA2S determines the angle between the Y-axis and a line normal to the ellipse

$$\left(\frac{Y}{B0E}\right)^2 + \left(\frac{Z'}{A0E}\right)^2 = 1$$

(which is defined by the ellipse ratio β_{0E}) at the point $Z' = RAT$ (Section 5.2.1.1.1).

GAMSUB - Subroutine GAMSUB determines the angle γ_1 between a line normal to the perimeter in the X-Z plane, and a line normal to the line segment RAT which is a radial vector from the motor axis to a point on a sector perimeter (Section 5.2.1.1.1).

6.1.1 Subroutine Descriptions (Continued)

HAPSBC - Subroutine HAPSBC sets up the correct equations to determine the coordinates (XOP, YOP, ZOP) of the points POA', P1A', and P3A' on the pseudoellipsoid for the block 1 analysis of the intersecting planes for sectors 3 and 11 in subroutine SCI (Section 5.2.1.1.2).

HASUBC - Subroutine HASUBC sets up the correct variables to determine the coordinates (XO, YO, ZO) of the points POA, P1A, and P3A that lie on the pseudoellipsoid produced in the block 1 analysis of the intersecting plane for sectors 3 and 11 in subroutine SCI (Section 5.2.1.1.2).

HBPSBC - Subroutine HBPSBC sets up the correct equations and variables to determine the coordinates (XOP, YOP, ZOP) of the points POB', P1B', and P3B' that lie on the pseudoellipsoid produced in the block 1 analysis of the intersecting planes for sectors 3 and 11 in subroutine SCI (Section 5.2.1.1.2).

HDNSUB - Subroutine HDNSUB sets up the correct variables to perform the block 1, 2A, 2B, and 3 analysis of the head end with web (Section 5.2.1).

HESUB - Subroutine HESUB determines the length of the zones in the end sections from which the incremental surface areas in subroutine AESUB are determined (Section 5.2.3.2).

LBSUB - Subroutine LBSUB determines the length (b) of the Y intercept produced by the intersection of the line Y = 0 and the line normal to the ellipse at PO (Section 5.2.1.2).

LPDAPS - Subroutine LPDAPS sets up the correct variables to determine the perimeter length, ALP, and the cross-sectional fuel area, AFP, of the propellant tips in subroutine AFPSUB for the cylindrical section reference planes (Section 5.1.1).

LPTO - Subroutine LPTO determines the perimeter length AL7 and AL8 of the anisotropic propellant in sectors 7 and 8 during the motor tail-off interval (Section 4.3.3).

6.1.1 Subroutine Descriptions (Continued)

MNCHN1 - Subroutine MNCHN1 is the control routine for the first core load which reads the input data, computes the constants that define the geometry of the grain cross-section and longitudinal configuration for use by the second and third core loads, checks for data errors, and prints the program inputs and geometry constants.

MNCHN2 - Subroutine MNCHN2 is the control routine for the second core load which determines the initial fuel area (AFF) and port area (AP) for the cylindrical section reference planes and determines the burn area and initial fuel volume of the straight through grain fore-head and aft-head sections as a function of distance burned.

MNCHN3 - Subroutine MNCHN3 is the control routine for the third computer core load which determines the initial fuel volume and burn area as a function of time for the head end with web.

MNCHN4 - Subroutine MNCHN4 is the control routine for the fourth computer core load which obtains the internal ballistic solution (Section 5.2.2).

MODTSB - Subroutine MODSTB modifies the value of TIME and the value of the nozzle throat diameter after convergence of the ballistic solution iteration and initializes X and Y reference planes for interpolation of the increment dividing planes in subroutine TISUB.

MSISUB - Subroutine MSISUB determines the location of the center of gravity and the polar and rectangular moment of inertia for the block 2A analysis of the head-end with web.

MTISUB - Subroutine MTISUB determines the location of the center of gravity and the polar and rectangular moment of inertia for the block 2B analysis of the head end with web.

PCHGIS - Subroutine PCHGIS prints the program inputs for the propellant properties and the burning rate equation constants.

PCHPLI - Subroutine PCHPLI prints the geometry constants calculated for each reference plane.

6.1.1 Subroutine Descriptions (Continued)

PLNCNS - Subroutine PLNCNS calculates the geometry constants of each cylindrical section reference plane (Section 5.1.1).

PLNLCS - Subroutine PLNLCS checks for reference plane input data errors, prints appropriate diagnostic comments, and flags the program for case termination if an error exists.

POSUB - Subroutine POSUB determines the coordinates (XO, YO, ZO) of the point PO that is located on the intersection of the inner ellipsoid with the core (Section 5.2.1.1.1).

PT1AA - Subroutine PT1AA determines the polar and rectangular moment of inertia for the cylindrical section, straight through grain end sections, and the block 1 analysis of the head end with web (Section 5.3).

P1SUB - Subroutine P1SUB determines the coordinates (X1, Y1, and Z1) of the point P1 that is located on the Z axis along a line through point PO and normal to the sector perimeter (Section 5.2.1.1.1).

P3SUB - Subroutine P3SUB determines the coordinates (X3, Y3, and Z3) of the point P3 that is located in the Y-Z plane and on the outer ellipse (Section 5.2.1.1.1).

RASUB - Subroutine RASUB determines the length of a radius vector from the motor axis to a point on the perimeter for each sector in the end sections with a straight through web (Section 5.2.3.2).

RASUBB - Subroutine RASUBB determines the length of a radius vector from the motor axis to a general point in a sector for the block 1 analysis of the head end with web (Section 5.2.1.1.1).

RBSTSB - Subroutine RBSTSB determines the initial estimate of the burn rate coefficient, AKRST, for each time increment during the start transient interval and performs the table look-ups for PH and AKRST (Section 4.3.3).

RBSUB - Subroutine RBSUB determines the propellant burning rate at each increment dividing plane (Section 4.3.2).

RBVSUB - Subroutine RBVSUB checks the validity of the burning rate equation constants and prints appropriate diagnostic comments.

6.1.1 Subroutine Descriptions (Continued)

RCSUB - Subroutine RCSUB determines the value of the radial distance from the motor axis to the intersection of the aft-end burning surface and the motor case for any configuration (Section 5.2.3.2).

RGISUB - Subroutine RGISUB determines the radius of gyration for the incremental thin shells of the head end with web.

ROEISB - Subroutine ROEISB determines the radius of curvature, ρ_1, at the point P_1 on the pseudoellipsoid for the block 2A analysis in subroutine SCI (Section 5.2.1.2).

ROPSB - Subroutine ROPSB sums the values of the Y coordinates PC (YOA and YOB) or PC' (YOA' and YOB') for the A and B planes from which the block 1 surface area is obtained in subroutine SCI (Section 5.2.1.1-1).

RSSPLN - Subroutine RSSPLN determines the coefficients of the piecewise cubics that are used for the spline interpolation procedure.

SCI - Subroutine SCI is the control routine to determine the surface area and initial volume of the propellant tip for the block 1 analysis of the head end with web (Section 5.2.1.1).

SCTOR1 - Subroutine SCTOR1 is the control routine to determine the surface of the pseudoellipsoid for the block 2A analysis of the head end with web (Section 5.2.1.2).

SCTOR2 - Subroutine SCTOR2 is the control routine to determine the surface area on the pseudoellipsoid of the projected propellant core in the block 2B analysis of the head-end with web (Section 5.2.1.3).

SDIDI3 - Subroutine SDIDI3 determines the center of gravity and moments of inertia of the straight through grain end sections (Section 5.3).

SEGSUB - Subroutine SEGSUB is the cylindrical section control routine to determine the mass generation rate, port area, perimeter length, and cross-sectional fuel area for each increment dividing plane and mass addition region during the internal ballistic solution (Section 5.2.2).

6.1.1 Subroutine Descriptions (Continued)

SETPH - Subroutine SETPH is the internal ballistic solution control routine to obtain convergence on the fore head pressure by matching the grain discharge flow with the nozzle flow determined from the nozzle pressure. The performance calculations for thrust, total impulse, thrust coefficient, etc., are included in subroutine SETPH (Section 4.2).

SLOT - Subroutine SLOT determines the gas properties at the discharge section of a slot between grain segments for the non-steady flow solution of the internal ballistics (Section 4.1.2.2).

SPLN1A - Subroutine SPLN1A sets up subroutine RSSPLN to perform the initialization for the spline interpolation procedure.

SPLN2A - Subroutine SPLN2A sets up subroutine RSSPLN to determine the functional values and derivatives for the arguments of the spline interpolation functions after SPLN1A has been executed.

SPLN3A - Subroutine SPLN3A sets up subroutine RSSPLN to determine the coefficients of the interpolating function for the spline interpolation procedure.

SQRT - Subroutine SQRT is a modification of the IBSYS-13 monitor library routine to determine the square root of negative numbers. Only the positive value of the argument is transferred to the designated register.

STUPPS - Subroutine STUPPS stores the variables defining the plane A produced in sectors 3A or 11A for the block 1 analysis in subroutine SCI of the head end with web (Section 5.2.1.1.2).

STUPRS - Subroutine STUPRS stores the variables defining plane B produced in sectors 3A or 11A for the block 1 analysis in subroutine SCI of the head end with web (Section 5.2.1.1.2).

S2SK - Subroutine S2SK determines the sector surface area on the pseudoellipsoid of the projected grain cross-section for the block 2B analysis in subroutine SCTOR2 of the head end with web (Section 5.2.1.3).

TDGRE - Subroutine TDGRE determines the largest real root of a third degree polynomial for the argument X.

6.1.1 Subroutine Descriptions (Continued)

THETAR - Subroutine THETAR determines the angle between the Z-axis and the line segment RAT for the block 1 analysis in subroutine SCI of the head end with web (Section 5.2.1.1.1).

TISUB - Subroutine TISUB determines the value of DELT for the steady state internal ballistic solution neglecting transient effects and modifies the values of thickness burned in each increment dividing plane after the ballistic solution is converged for each time point.

TRAN - Subroutine TRAN transfers the geometry constants from the permanent common storage location to the working array common storage location.

VFPPSB - Subroutine VFPPSB determines the port volume of each cylindrical section segment and sums the segment port volumes to obtain the total cylindrical section port volume.

VOLSUB - Subroutine VOLSUB is the control routine which determines the initial volume for the block 3 analysis of the head-end with web (Section 5.2.1.4).

VSEC - Subroutine VSEC determines the volume produced by the difference of volumes of two oblate spheroids, minus the volume of the igniter hole in the block 3 analysis of the head end with web (Section 5.2.1.4).

VSTRSB - Subroutine VSTRSB determines the initial core volume that is present in the head end with web for the block 3 analysis (Section 5.2.1.4).

XRSUB - Subroutine XRSUB determines the X-coordinate of a general point on the perimeter of a sector in the end sections (Section 5.2.3.2).

XRSUBB - Subroutine XRSUBB determines the X-coordinate of the RAT line segment which is a radial vector from the motor axis to a point on a sector perimeter for the analysis of the head end with web (Section 5.2.1.1.1).

XRTHR - Subroutine XRTHR is a set up subroutine that uses subroutine XRSUBB to obtain the X-coordinate of a point located on the perimeter of a sector in the block 2B analysis of the head end with web. The angle θ_{rl} between the Z axis and a line from the motor axis to a general point in a sector is also determined (Section 5.2.1.3).

6.1.1 Subroutine Descriptions (Continued)

YPSUB - Subroutine YPSUB determines the Y-coordinate of the points P0 and P3 which are located on the surface of the inner and outer ellipsoids respectively for the block 2 analysis of the head end with web (Section 5.2.1.2).

ZISUB = Subroutine ZISUB determines the Z-coordinate produced by the intersection of the outer ellipse and the line normal to the ellipse at P1 (Section 5.2.1.2).

6.1.2 Subroutine Linkage Table

NAME	LOWER-LEVEL CALLS	CALLED BY		
ACØS	SQRT	AESUB	GAMA2A	RASUBB
		AFPSUB	LPTØ	SD1D13
		AIGSUB	MNCHN2	THETAR
		ALRSUB	PLNCNS	XRTHR
		AWESUB	P1SUB	YPSUB
		ENDCSB	P3SUB	
		FDGRE	RASUB	
AEPSUB	AESUB	ASESUB		
AESUB	ACØS	AEPSUB		
	ALRSUB			
	ARSSUB			
	HESUB			
	RASUB			
	SQRT			
	XRSUB			
AFPSUB	ACØS	LPDAPS		
	SQRT			
AIBST	AIBSUB	AIBSUB		
	SQRT	MNCHN4		
AIBSUB	AIBST	AIBST		
	SQRT	MNCHN4		
		SEGSUB		
AIGSUB	ACØS	SCTØR1		
	SQRT			
ALRSUB	ACØS	AESUB		
	SQRT			
ARSSUB	SQRT	AESUB		
ASESUB	AEPSUB	ENDCSB		
	AWESUB			
	RCSUB	MNCHN2		

6.1.2 Subroutine Linkage Table (Continued)

NAME	LOWER LEVEL CALLS		CALLED BY
ASTSUB	PT1AA		MNCHN3
ASUBC	GAMA2S	THETAR	SC1
	GAMSUB	TRAN	
	PØSUB	XRSUBB	
	P1SUB		
	P3SUB		
	RASUBB		
AWESUB	ACØS		ASESUB
	HESUB		
	SQRT		
BRAKSB	SQRT		SC1
BSUBC	GAMA2S	THETAR	SC1
	GAMSUB	TRAN	
	PØSUB	XRSUBB	
	P1SUB		
	P3SUB		
	RASUBB		
CØMPSC			LPTØ
			MNCHN1
			MNCHN2
			MNCHN3
CØNV			SETPH
CSTRSB	SPLN1A		MNCHN4
	SPLN2A		RBSTSB
DPRASB	SQRT		SC1
ENDCSB	ACØS		MNCHN1
	ASESUB		
	LPDAPS		
	SQRT		

6.1.2 Subroutine Linkage Table (Continued)

NAME	LOWER-LEVEL CALLS		CALLED BY
FDGRE	ACØS		RCSUB
	SQRT		
GAMA2S	ACØS		ASUBC
	SQRT		BSUBC
			HAPSBC
			HASUBC
			HBPSBC
			HBSUBC
GAMSUB			ASUBC
			BSUBC
			HABSBC
			HASUBC
			HBPSBC
			HBSUBC
HAPSBC	GAMA2S	THETAR	SCI
	GAMSUB	TRAN	
	PØSUB	XRSUBB	
	P1SUB		
	P3SUB		
	RASUBB		
HASUBC	GAMA2S	THETAR	SCI
	GAMSUB	TRAN	
	PØSUB	XRSUBB	
	P1SUB		
	P3SUB		
	RASUBB		
HBPSBC	GAMA2S	THETAR	SCI
	GAMSUB	TRAN	
	PØSUB	XRSUBB	
	P1SUB		
	P3SUB		
	RASUBB		
HBSUBC	GAMA2S	THETAR	SCI
	GAMSUB	TRAN	
	PØSUB	XRSUBB	
	P1SUB		
	P3SUB		
	RASUBB		

6.1.2 Subroutine Linkage Table (Continued)

NAME	LOWER-LEVEL CALLS		CALLED BY
HDNSUB	SCI		MNCHN3
	SCTØR1		
	SCTØR2		
	VØLSUB		
HESUB	SQRT		AESUB
			AWESUB
			PT1AA
			SD1D13
INPT			MAIN
LBSUB			SCTØR1
			S2ØK
LPDAPS	AFPSUB		ENDCSB
	PT1AA		MNCHN2
			MNCHN3
LPTØ	ACØS		SEGSUB
	CØMPSC		
	SQRT		
	TRAN		
MAIN	INPT		
	MNCHN1		
	MNCHN2		
	MNCHN3		
	MNCHN4		
MNCHN1	CØMPSC	RBVSUB	MAIN
	ENDCSB		
	PCHGIS		
	PCHPLI		
	PLNCMS		
	PLNLCS		

6.1.2 Subroutine Linkage Table (Continued)

NAME	LOWER-LEVEL CALLS		CALLED BY
MNCHN2	ACØS		MAIN
	ASESUB		
	CØMPSC		
	LPDAPS		
	PTIAA		
	RCSUB		
	TRAN		
MNCHN3	ASTSUB		MAIN
	CØMPSC		
	HDNSUB		
	LPDAPS		
	RCSUB		
	RGISUB		
	SQRT		
	TRAN		
MNCHN4	AIBST	SETPH	MAIN
	AIBSUB	SQRT	
	CSTRSB	TRAN	
	ØUTPUT		
	RBSTSB		
	RBSUB		
	STRSUB		
MØDTSB	TISUB		ØUTPUT
MSISUB	SQRT		SCTØR1
MTISUB	SQRT		S2SK
ØUTPUT	MØDTSB		MNCNN4
PCHGIS			MNCHN1
PCHPL1			MNCHN1
PLNCNS	ACØS		MNCHN1
	SQRT		

6.1.2 Subroutine Linkage Table (Continued)

NAME	LOWER-LEVEL CALLS	CALLED BY
PLNLCS		MNCHN1
PØSUB	SQRT	ASUBC BSUBC HAPSBC HASUBC HBPSBC HBSUBC SCTØR1
PT1AA	HESUB SD1D13 SQRT	ASTSUB LPDAPS MNCHN2 RG1SUB
P1SUB	ACØS SQRT	ASUBC BSUBC HAPSBC HASUBC HBPSBC HBSUBC
P3SUB	ACØS SQRT TDORE	ASUBC BS1BC HAPSBC HASUBC HBPSBC HBSUBC
RAS1B	ACØS SQRT	AESUB SD1D13
RASUBB	ACØS SQRT	ASUBC BSUBC HAPSBC HASUBC HBPSBC HBSUBC SCTØR1
RBSTSB	CSTRSB	RBSUB

6.1.2 Subroutine Linkage Table (Continued)

NAME	LOWER-LEVEL CALLS		CALLED BY
RBSUB	RBETSB		MNCHN4 SEGSUB SLØT
RBVSUB			MNCHN1
RCSUB	FDGRE TDGRE		ASESUB MNCHN2 MNCHN3
RGISUB	PT1AA SQRT		MNCHN3
RØE1SB			SCTØR1 S2SK
RØPSB			SCI
RSSPLN			SPLN1A SPLN2A SPLN3A
SCI	ASUBC BRAKSB BSUBC DPRASB HAPSBC HASUBC HBPSBC	HBSUBC RØPSB SQRT STUPPS STUPRS TRAN VSTRSB	HDNSUB
SCTØR1	AIGSUB LBSUB MSISUB PØSUB RASUBB	RØE1SB SQRT YPSUB ZISUB	HDNSUB
SCTØR2	S2SK		HDNSUB

6.1.2 Subroutine Linkage Table (Continued)

NAME	LOWER-LEVEL CALLS	CALLED BY
SD1D13	ACØS HESUB RASUB SQRT XRSUB	PT1AA
SEGSUB	AIBSUB LPTØ RBSUB SLØT SQRT	MNCHN4
SETPH	CØNJ SQRT VFPPSB	MNCHN4
SLØT	RBSUB SQRT	SEGSUB
SPLN1A	RSSPLN	CSTRSB
SPLN2A	RSSPLN	CSTRSB
SPLN3A	RSSPLN	(For Diagnostic Use)
SQRT		ACØS AESUB AFPSUB AIBST AIBSUB AIGSUB ALRSUB ARSSUB AWESUB BRAKSB DPRASB ENDCSB FDGRE GAMA2S HESUB LPTØ MNCHN3 MNCHN4 MSISUB MTISUB PLNCNS PØSUB PT1AA P1SUB P3SUB RASUB RASUBB RGISUB SCI SCTØRJ SD1D13 SEGSUB SETPH SLØT S25K TDGRE THETAR VØLSUB VSEC VSTRSB XRSUB XRSUBB XRTHR YPSUB

6.1.2 Subroutine Linkage Table (Continued)

NAME	LOWER-LEVEL CALLS	CALLED BY	
STUPPS		SC1	
STUPRS		SC1	
S2SK	LBSUB MT1SUB RØE1SB SQRT XRTHR YPSUB Z1SUB	SCTØR2	
TDGRE	SQRT	P3SUB RCSUB Z1SUB	
THETAR	ACØS SQRT	ASUBC BSUBC HAPSBC HASUBC HBPSBC HBSUBC	
T1SUB		MØØTSB	
TRAN		ASUBC BSUBC HAPSBC HASUBC HBPSBC HASUBC	LPTØ MNCHN2 MNCHN3 MNCHN4 SC1
VFPPSB		SETPH	
VØLSVB	SQRT VSEC	HDNSUB	
VSEC	SQRT XRTHR YPSUB	VØLSUB	

6.1.2 Subroutine Linkage Table (Continued)

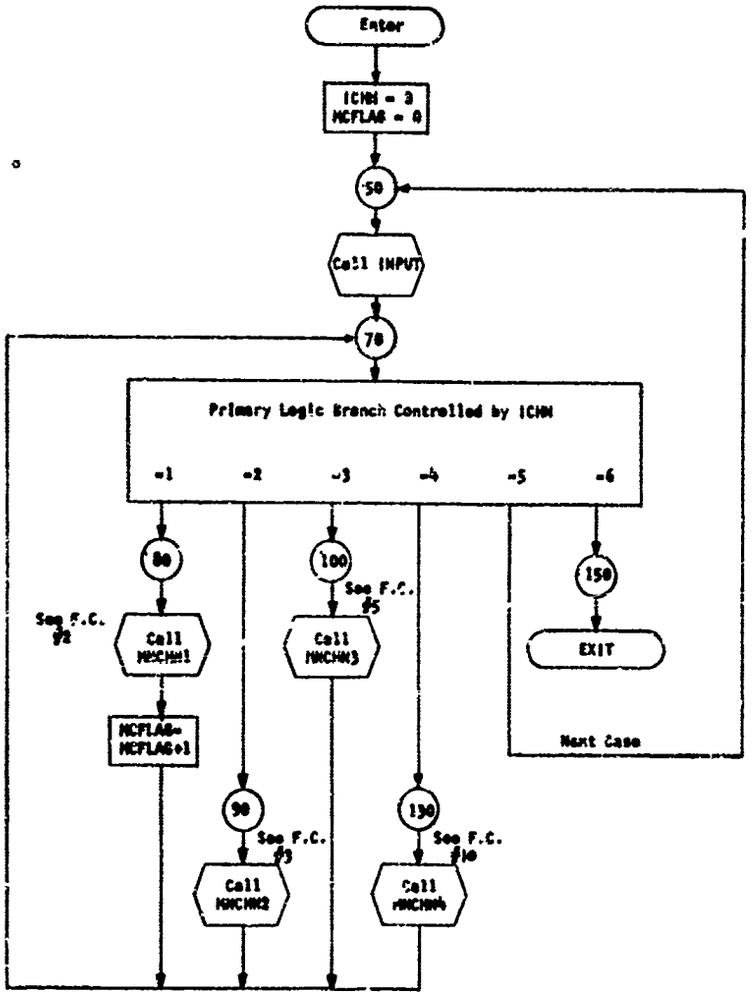
NAME	LOWER-LEVEL CALLS	CALLED BY
VSTRSB	SQRT	SCI
XRSUB	SQRT	AESUB SD1D13
XRSUBB	SQRT	ASUBC [illegible]UBC HAPSBC HASUBC HBPSBC HBSUBC XRTHR
XTHR	ACØS SQRT XRSUBB	S2SK VSEC
YPSUB	ACØS SQRT	SCTØR1 S2SK VSEC
ZISUB	TDGRE	SCTØR1 S2SK

6.2 Flow Charts

This section contains macro-scopic flow charts in schematic form of the first, second and third level subroutines. The Fortran listings themselves are considered to be the flow charts for the lower level subroutines. In order to facilitate their use each routine has been processed by a special program which re-numbers all statement numbers in steps of ten. These routines are also annotated by comment cards which define the computational blocks and locate important logic branches.

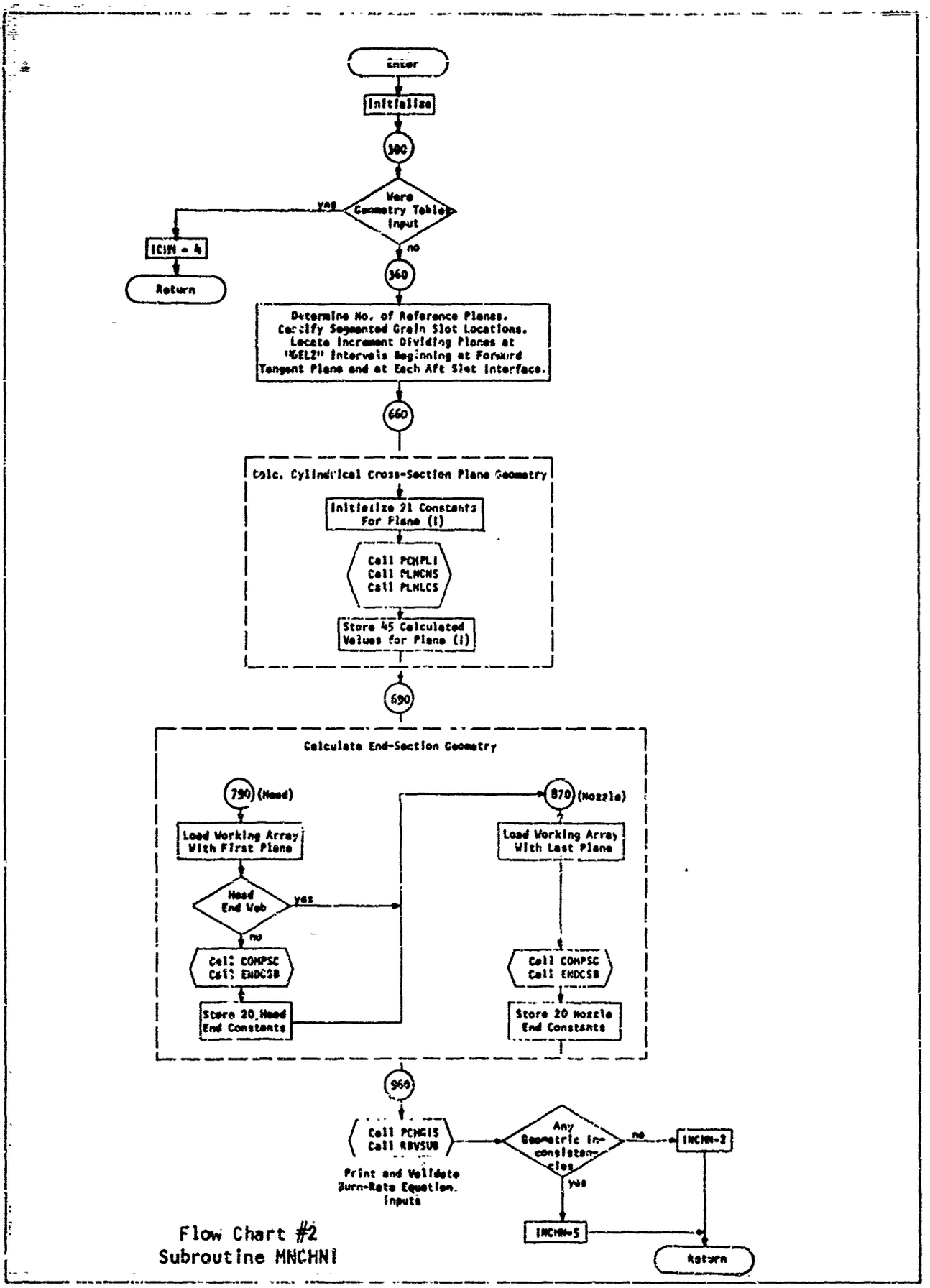
The following schematic flow charts are included:

Name	Flow Chart No.
MAIN Program	1
Subroutine MNCHN1	2
Subroutine MNCHN2	3
Compute Plane Constants	4
Subroutine AESUB	5
Subroutine MNCHN3	6
Subroutine SCI	7
Subroutine SCTOR1	8
Subroutine SCTOR2	9
Subroutine MNCHN4	10
Subroutine SEGSUB	11
Subroutine SETPH	12
Subroutine TISUB	13
Check For Case Termination	14

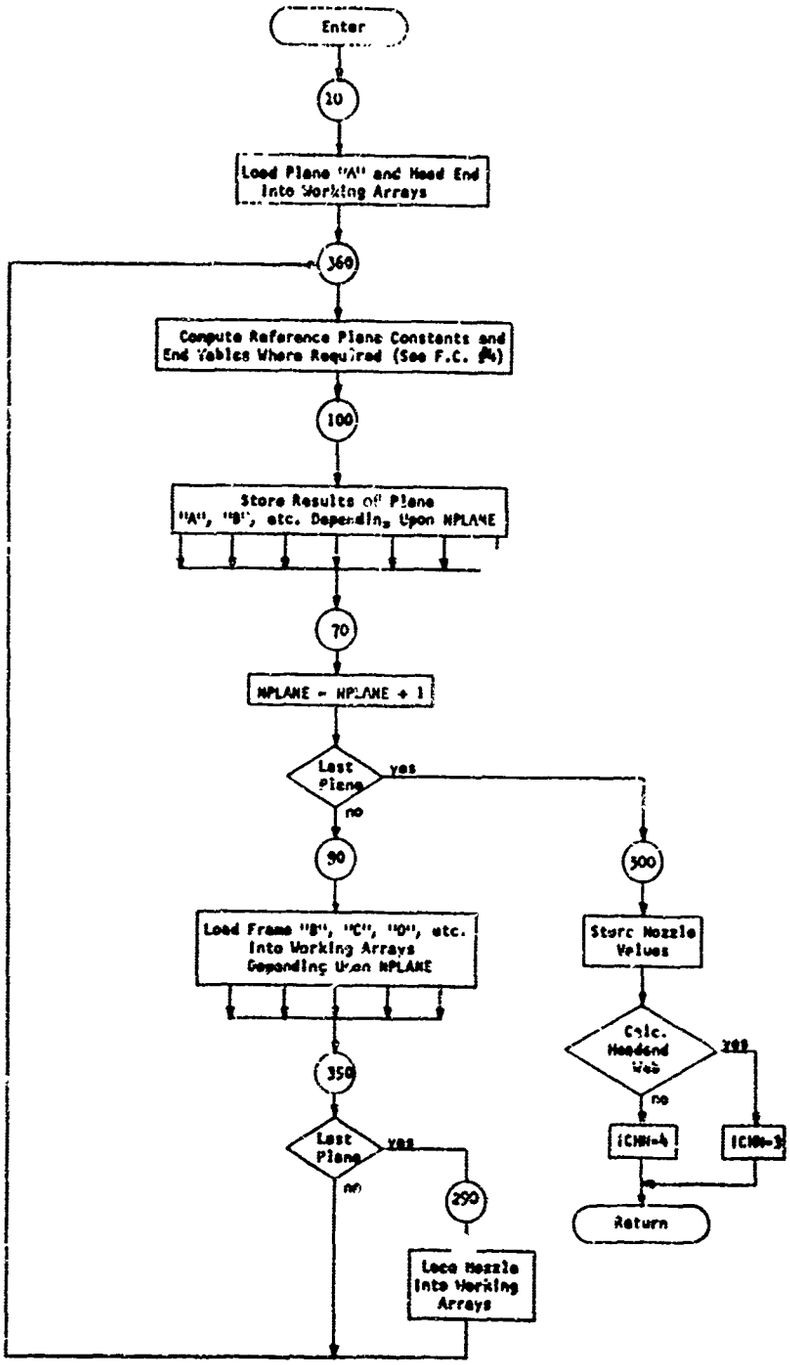


Flow Chart #1
MAIN Program

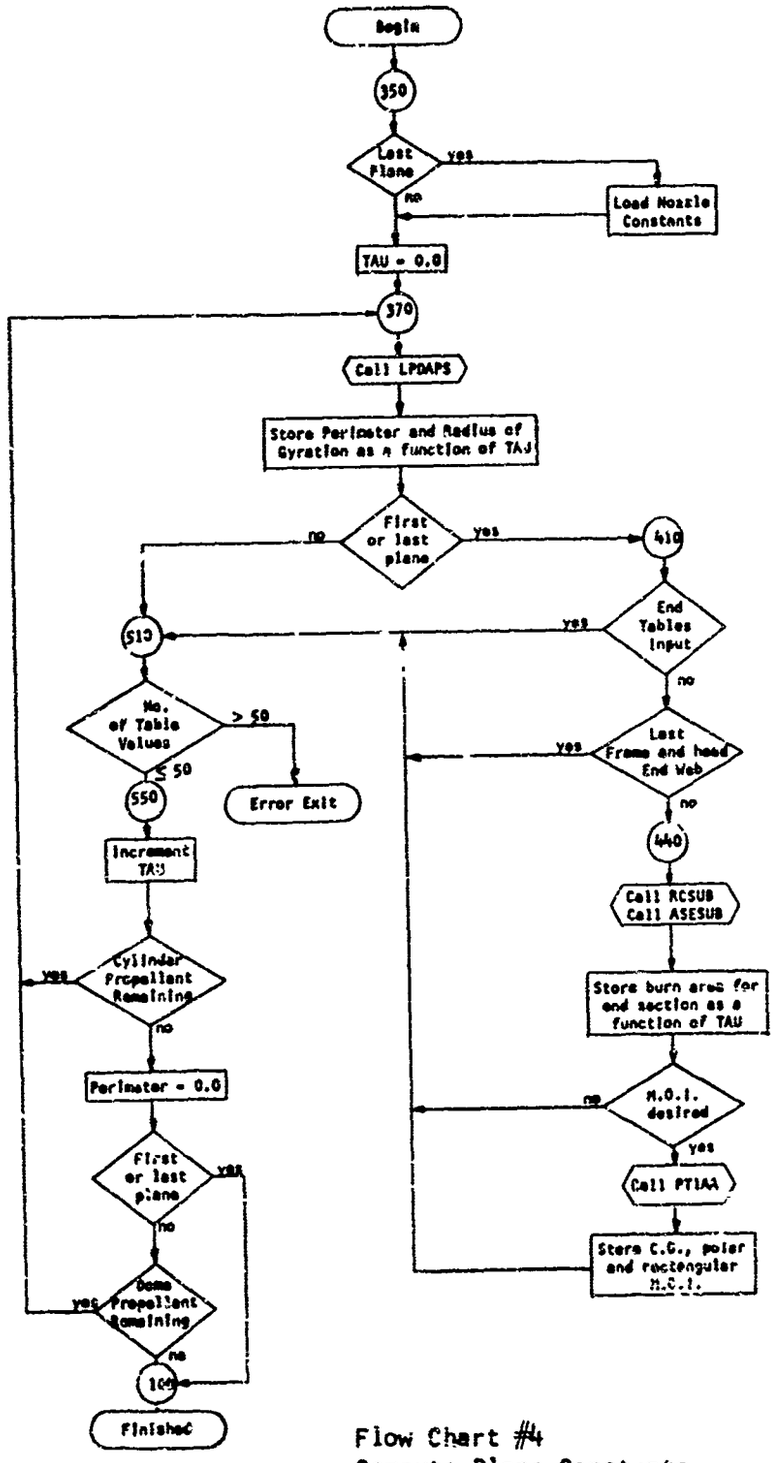
A



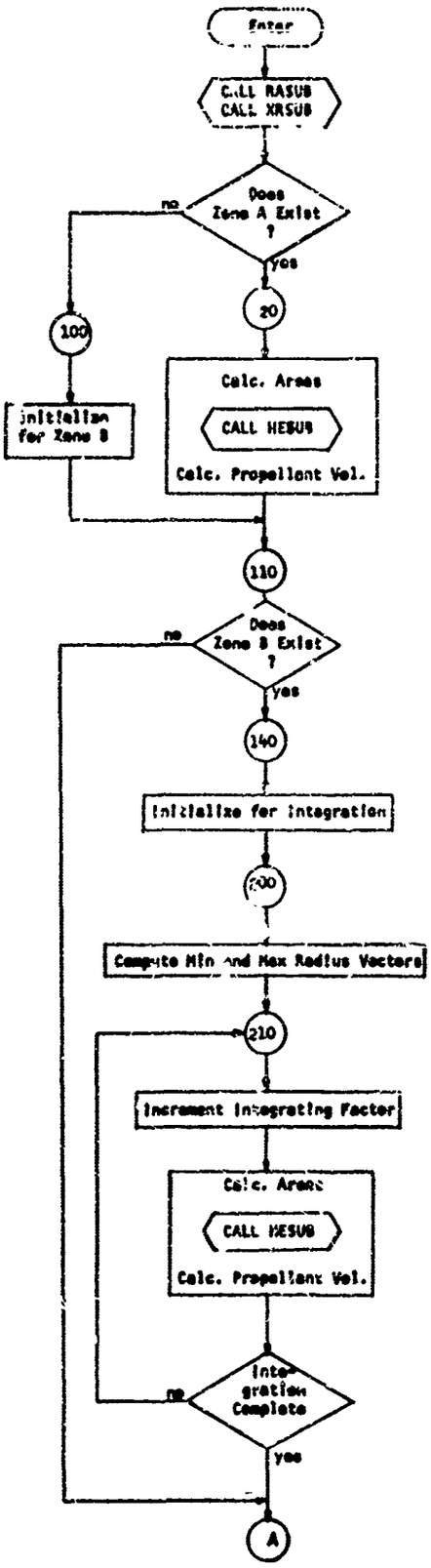
Flow Chart #2
Subroutine MNCHNI



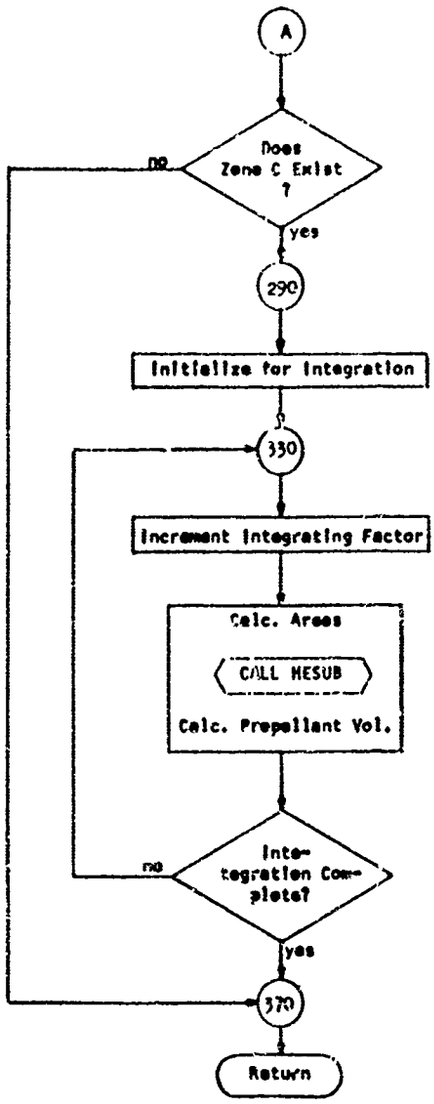
Flow Chart #3
Subroutine MNCHN2



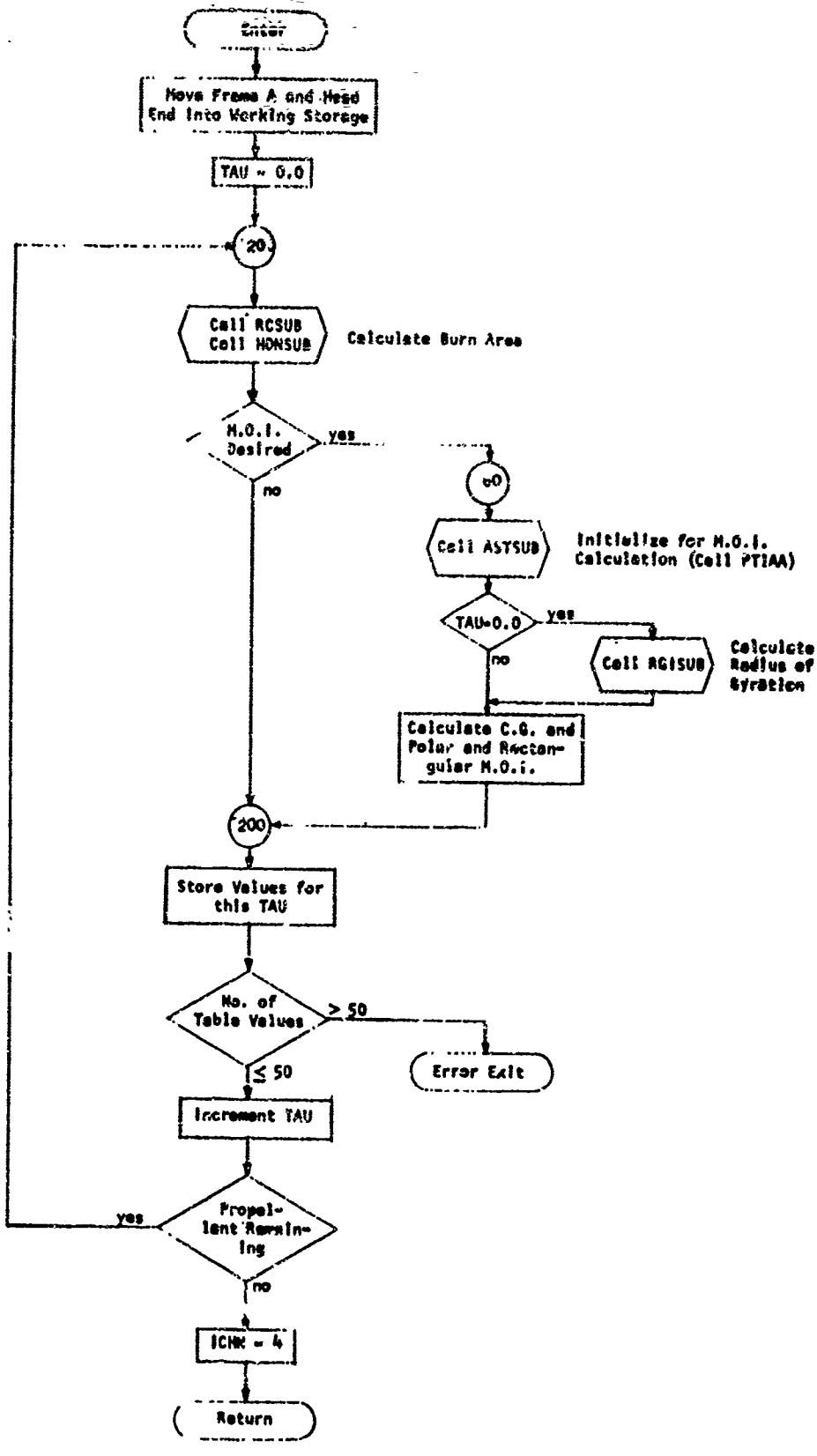
Flow Chart #4
Compute Plane Constants



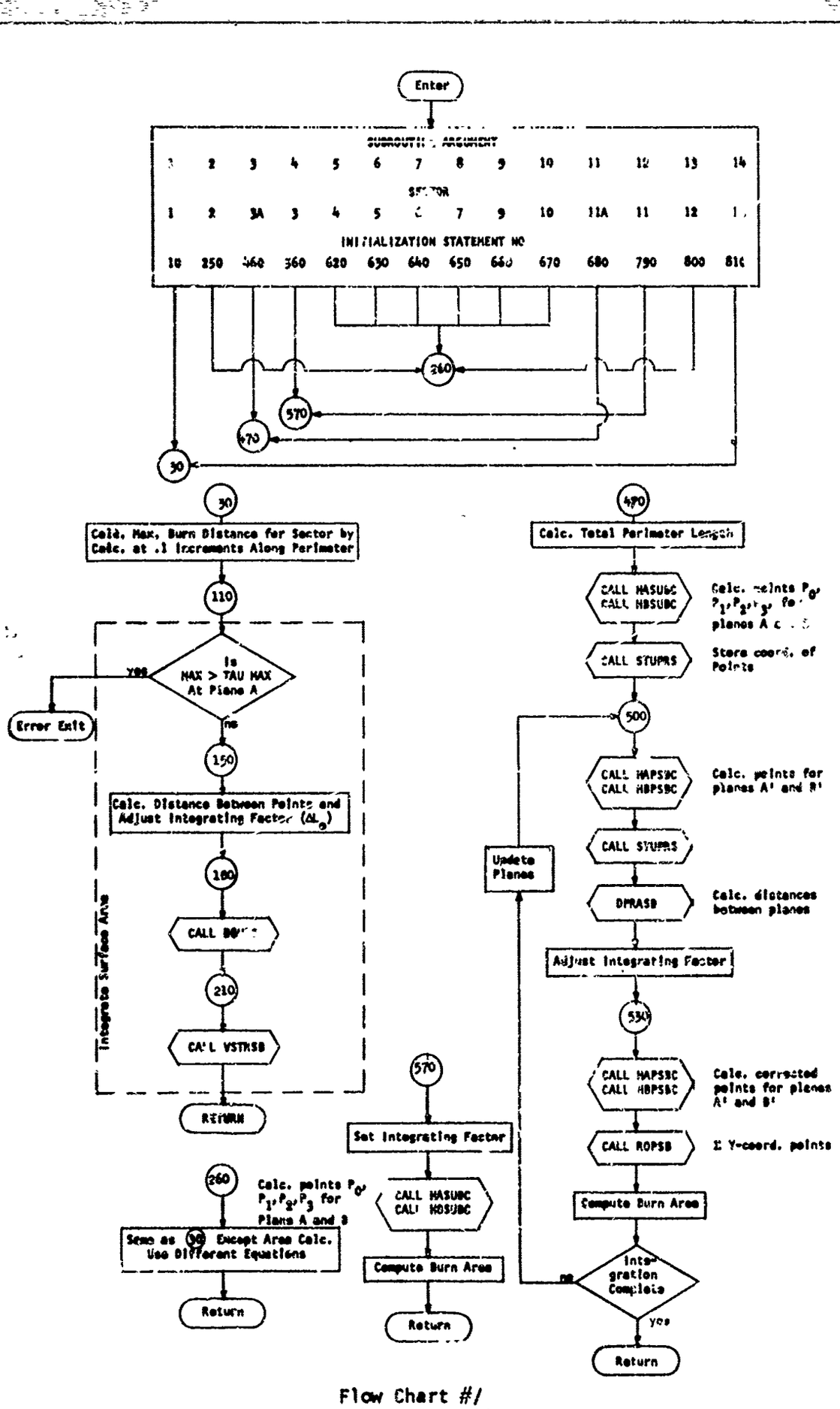
Flow Chart #5
Subroutine AESUB (1 of 2)



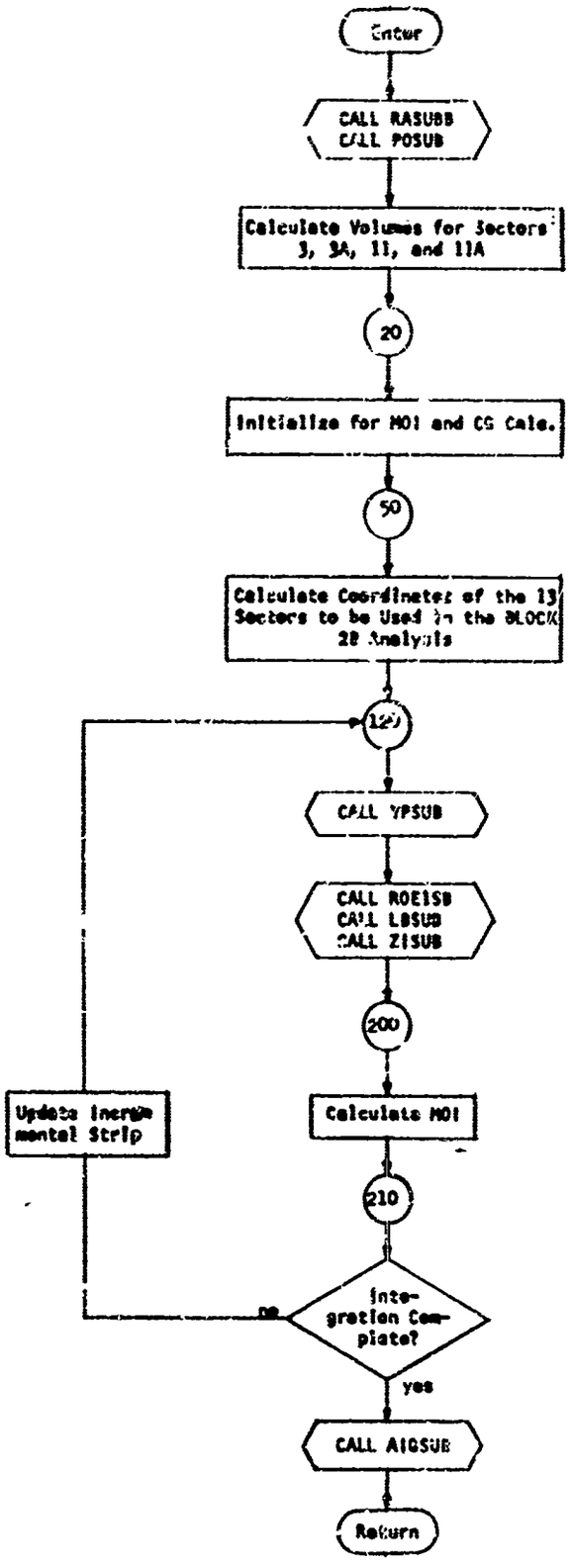
Flow Chart #5
Subroutine AESUB (2 of 2)



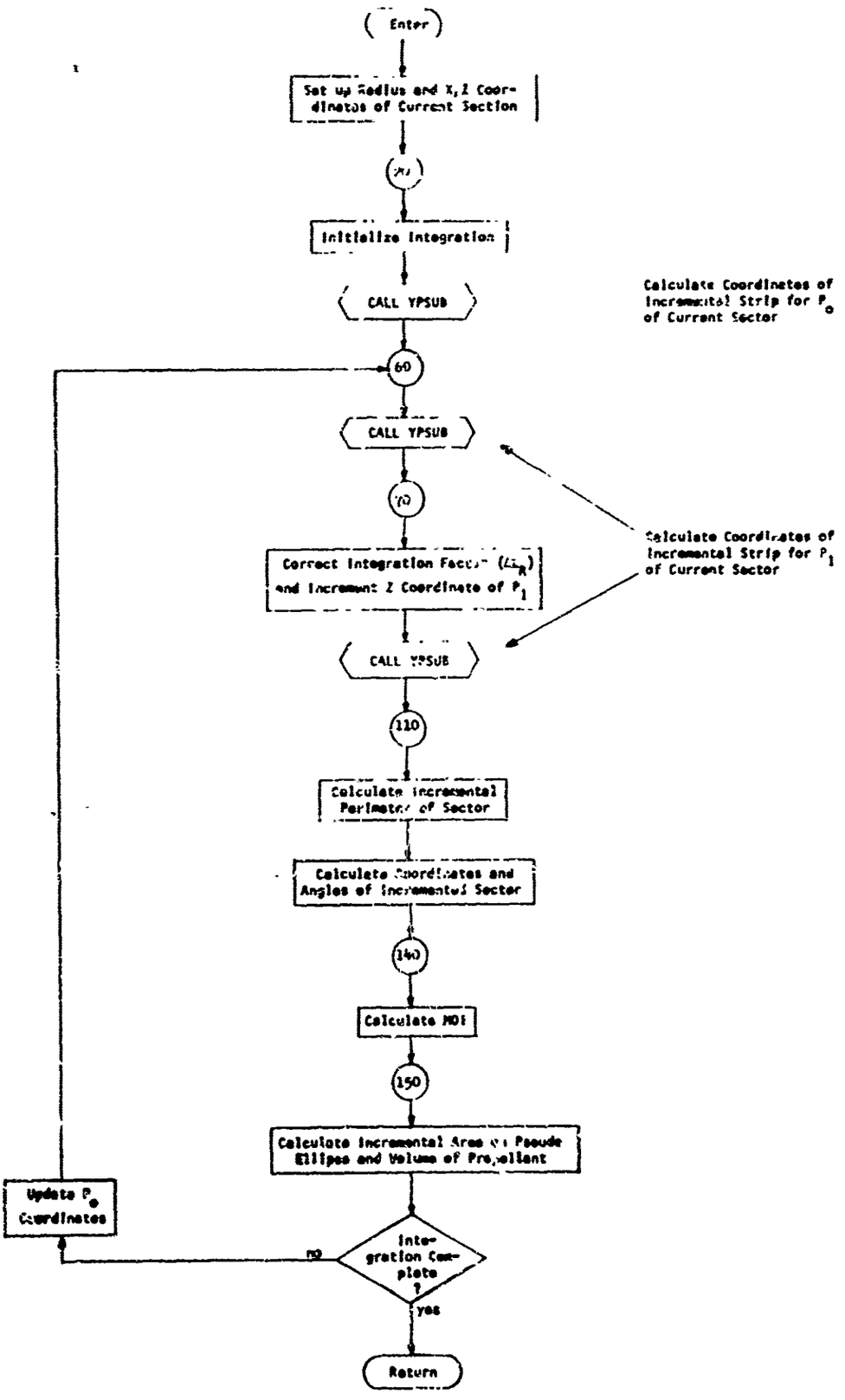
Flow Chart #6
Subroutine MNCHN3



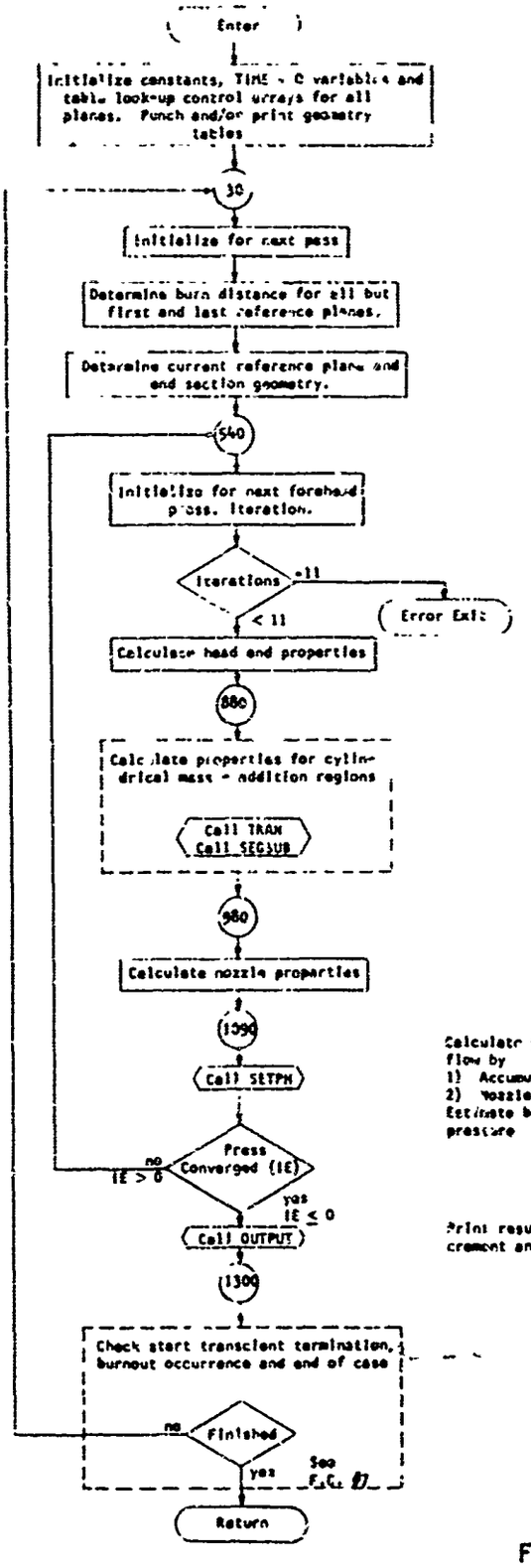
Flow Chart #/
Subroutine SCI



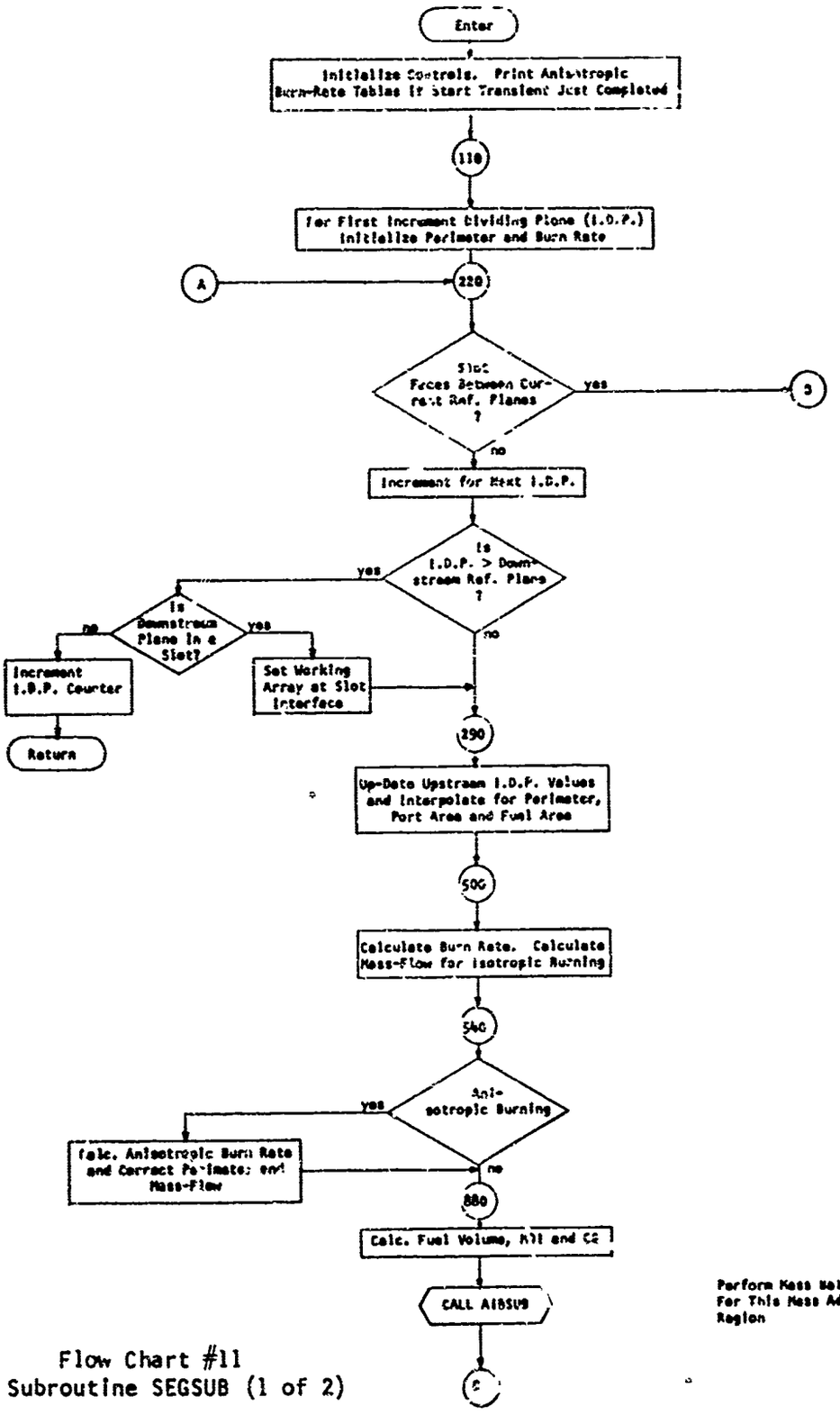
Flow Chart #8
Subroutine SCT@R1



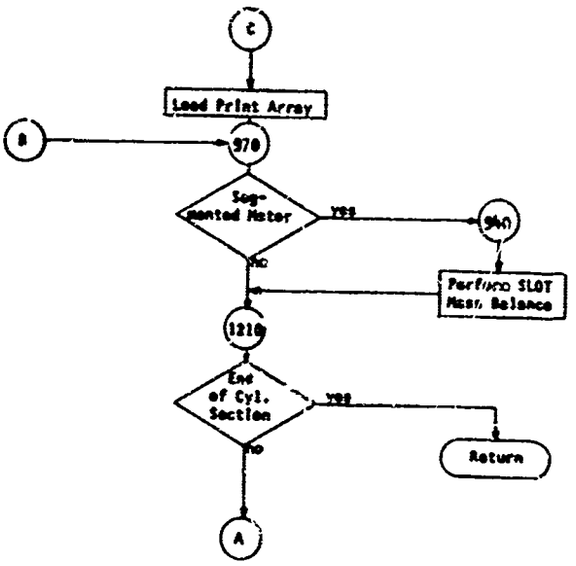
Flow Chart #9
Subroutine SCTØR2



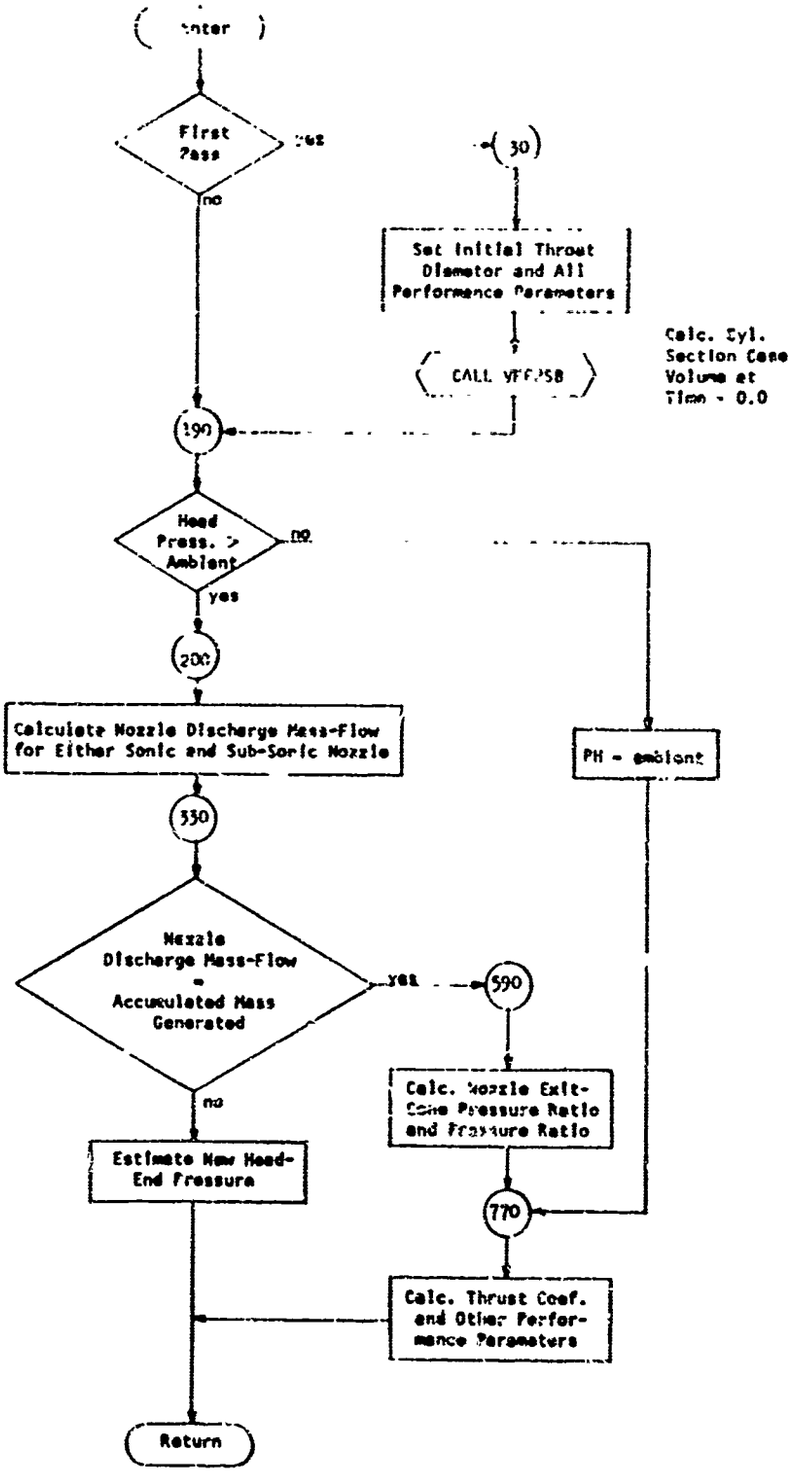
Flow Chart #10
Subroutine MNCHN4



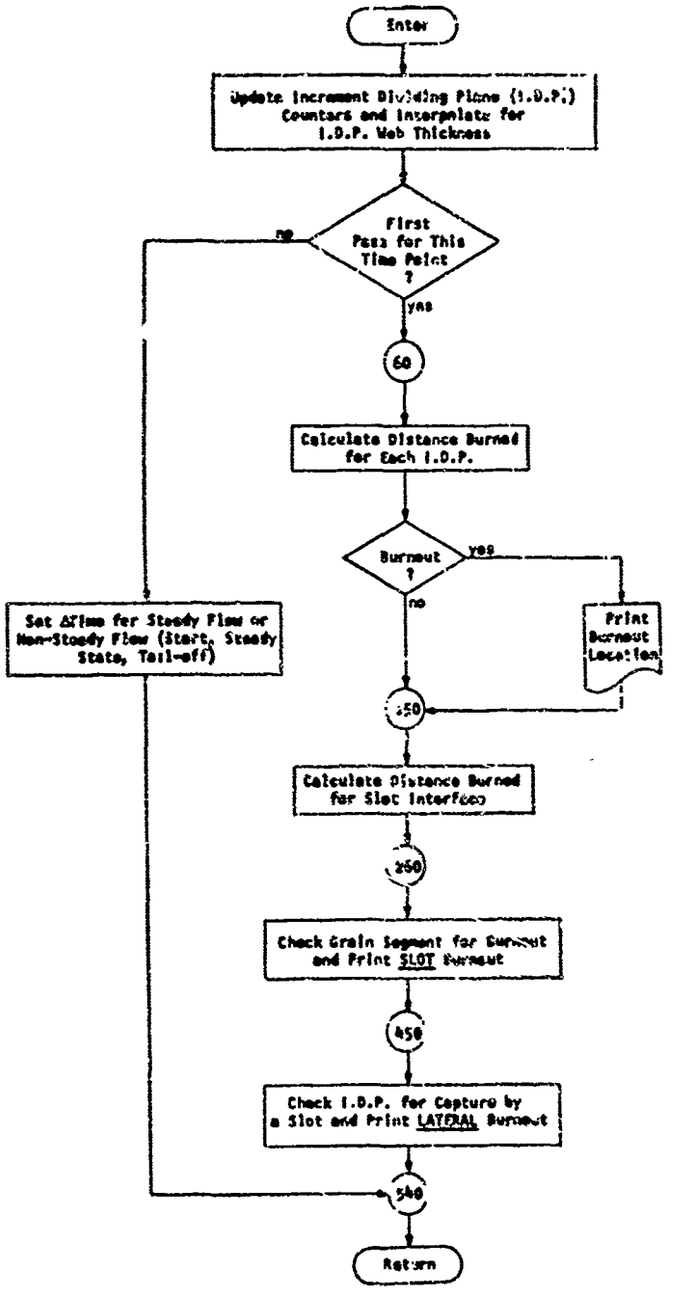
Flow Chart #11
Subroutine SEGSUB (1 of 2)



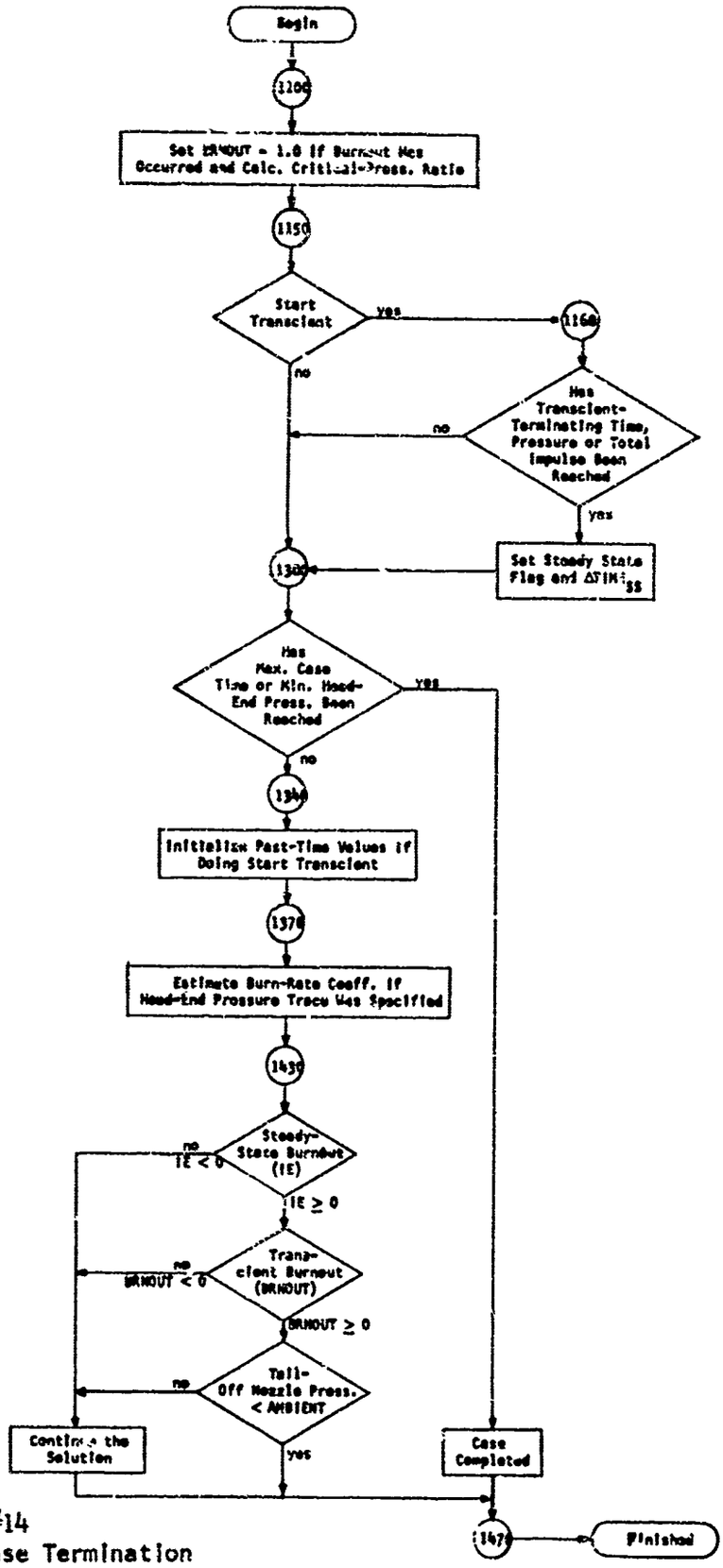
Flow Chart #11
Subroutine SEGSUB (2 of 2)



Flow Chart #12
Subroutine SETPH



Flow Chart #13
Subroutine TISUB



Flow Chart #14
Check for Case Termination

6.3 Storage Allocation and Computer System

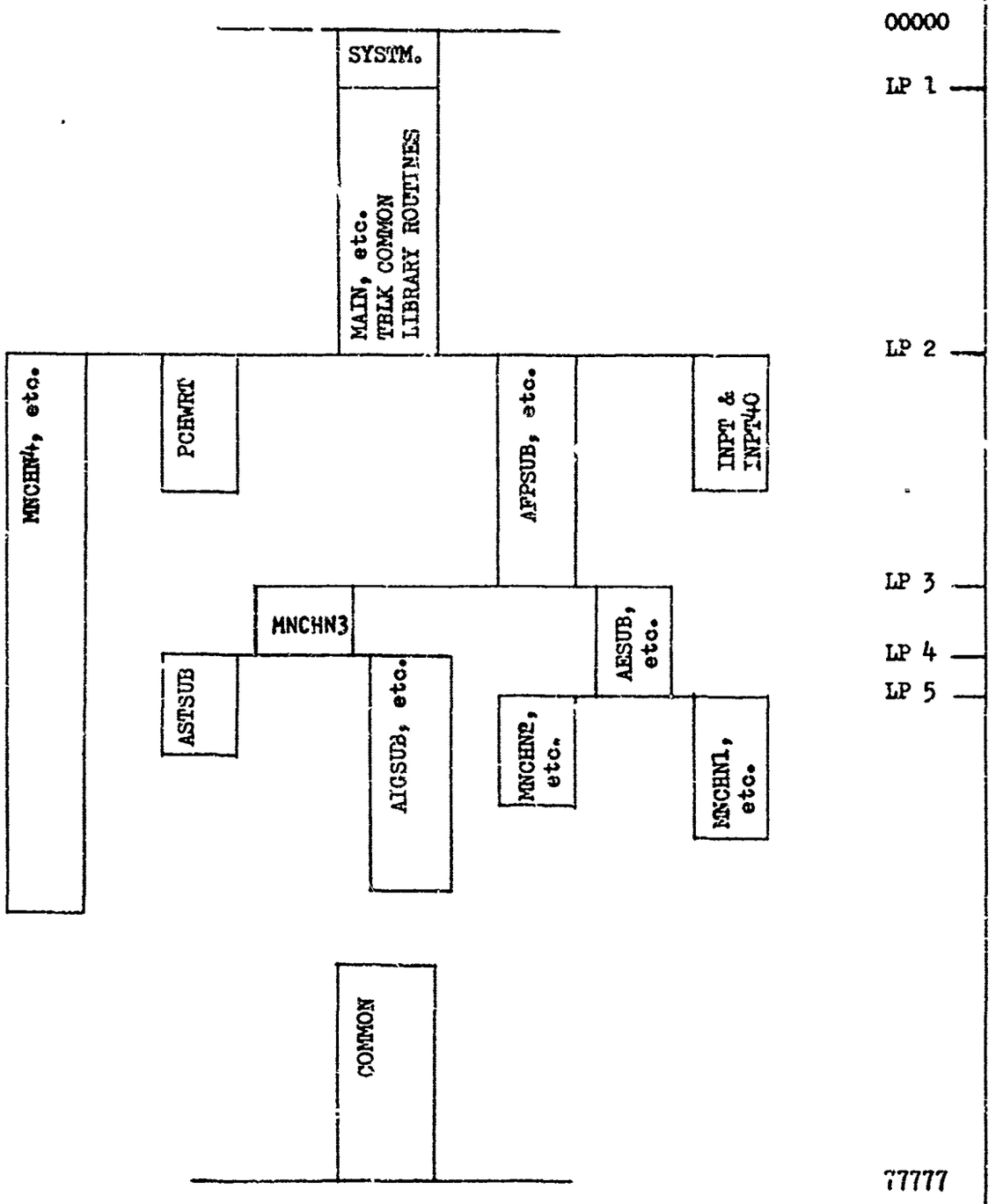
6.3.1 Storage Allocation

The program is divided into four core loads. Subsection 6.3.1.1 consists of a table showing which routines are required in each core load. Subsection 6.3.1.2 contains a diagram explaining the computer allocation of the program code and geometry tables. Subsection 6.3.1.3 contains both an alphabetical and a numerical listing of COMMON allocation. Subsection 6.3.1.4 contains a table which defines the labeled COMMON allocation of the geometry tables. Subsection 6.3.1.5 consists of the allocation map printed out by the computer system.

6.3.1.1 Subroutine Requirements for Each Core Load

	Core Load					Core Load					Core Load			
Name	1	2	3	4	Name	1	2	3	4	Name	1	2	3	4
ACOS	X	X	X	X	LBSUB			X		SCI			X	
AEPSUB	X	X			LPDAPS	X	X	X		SCTOR1			X	
AESUB	X	X			LPTO			X		SCTOR2			X	
AFPSUB	X	X	X		MAIN	X	X	X	X	SDID13	X	X	X	
AIBST				X	MNCHN1	X				SEGSUB				X
AIBSUB				X	MNCHN2		X			SETPH				X
AIGSUB			X		MNCHN3			X		SLOT				X
ALRSUB	X	X			MNCHN4				X	SPLN1A				X
ARSSUB	X	X			MODTSB				X	SPLN2A				X
ASESUB	X	X			MSISUB			X		SPLN3A				X
ASTSUB			X		MTISUB			X		SORT	X	X	X	X
ASUBC			X		OUTPUT				X	STUPPS			X	
AWESUB	X	X			PCHGIS	X				STUPRS			X	
BRAKSB			X		PCHPLI	X				S2SK			X	
BSUBC			X		PLNCNS	X				TDGRE	X	X	X	
COMPSC	X	X	X	X	PLNLCS	X				THETAR			X	
CONV				X	POSUB			X		TISUB				X
CSTRSB				X	PTIAA	X	X	X		TRAN		X	X	X
DPRASB			X		PISUB			X		VFPPSB				X
ENDCSB	X				P3SUB			X		VOLSUB			X	
FDGRE	X	X	X		RASUB	X	X	X		VSEC			X	
GAMA2S			X		RASUBB			X		VSTRSB			X	
GAMSUB			X		RBSTSB				X	XRSUB	X	X	X	
HAPSBC			X		RBSUB				X	XRSUBB			X	
HASUBC			X		RBVSUB		X	X		XRTHR			X	
HBPSBC			X		RCSUB	X	X	X		YPSUB			X	
HBSUBC			X		RGISUB			X		ZISUB			X	
HDNSUB			X		ROEISB			X						
HESUB	X	X	X		ROPSB			X						
INPT	X				RSSPLN				X					

6.3.1.2 Schematic Diagram of Computer Storage Allocation



Notes:

1. Storage locations are in octal numbers.
2. Load points are located as follows:

LP 1 - 4252	LP 4 - 37625
LP 2 - 23672	LP 5 - 41563
LP 3 - 36743	

6.3.1.3 COMMON Allocation

The following pages contain output from a special Boeing Company pre-compiler which lists numerically and alphabetically those variables which are assigned to unlabled COMMON through equivalence statements.

There are, in addition, two blocks of labeled common.

1) "TBLX" contains the geometry tables and is explained on page 199.

2) "CRITVM" contains the three convergence criteria CRP, CRT and CRW in cells 1-3 respectively.

NUMERIC LISTING OF PROGRAM VARIABLES IN COM ARRAY

1	AINC	2	AMO	3	RF	4	TAUW	5	R2	6	R3
7	R4	8	R5	9	R6	10	R7	11	R8	12	ALSI
13	ALS2	14	ALA	15	ALB	16	ALE	17	AO	22	AINCA
24	RFA	25	TAUWA	43	AINCB	45	RFB	46	TAUWB	64	AINCC
66	RFC	67	TAUWC	85	AINCD	87	RFD	88	TAUWD	106	AINCE
108	RFE	109	TAUWE	122	AOE	127	AINCF	129	RFF	130	TAUWF
148	AINCG	150	RFG	151	TAUWG	169	AINCH	171	RFH	172	TAUWH
190	AINCI	192	RFI	193	TAUWI	211	AINCJ	213	RFJ	214	TAUWJ
232	AINCK	234	RFK	235	TAUWK	253	AINCN	274	RE1	275	ALFEM
276	ALFE	277	RE2	278	HE1	279	HE2	280	HEO	281	HER
282	VFEO	283	VCE	284	TAUEO	285	TAUE1	286	CAE	287	CBE
288	CCCE	289	CCVE	290	CDCE	291	CDVE	292	CECE	293	CEVE
294	RH1	299	HH2	301	HHR	302	VFHO	303	VCH	314	RN1
320	HHO	323	VCH	334	A	339	R1	340	R9	341	TH1
342	T2M	343	T4M	344	T5M	345	X45	346	Y45	347	ALC
348	X03	349	Y03	350	R03	351	X05	352	Y05	353	R05
354	X07	355	Y07	356	R07	357	T6M	358	T7M	359	T12M
360	X76	361	Y76	362	ALD	363	X09	364	Y09	365	R09
366	X011	367	Y011	368	R011	369	T10M	370	T9M	371	TAUM
372	TH2	373	TH3	374	TH4	375	B71M	376	B72M	377	B91M
378	B92M	379	AC	424	AB	469	AC	514	AD	559	AE
604	AF	649	AG	694	AH	739	AI	784	AJ	829	AK
874	AN	919	DE1	920	BE	921	AUEM	922	DH1	923	BH
925	DN1	928	BTADE	929	RIG	930	ANI	931	HCO	932	GAMA
933	R	934	TO	935	AKK	936	DLRF	937	DLORF	938	DRRF
939	DRVRF	940	DELT	941	DELF	942	AKG	947	AKU	952	AKR
991	PA	992	DT	993	DE	994	DELLA	995	DELLM	996	AN2
997	DELIS	998	EM	999	AAK	1029	SPOP	1030	STOT	1031	ANSIG
1032	PYPHY	1033	SC	1034	SCULT	1035	WP	1036	DELC	1037	DELLL
1038	DELIN	1039	PIL	1040	SIGK	1041	THI	1042	TLO	1043	TREF
1044	ANN	1045	SPE	1046	SN	1047	AN1	1048	BETA	1049	DELN
1050	DELNE	1051	DELI	1052	PHI	1053	AMTJ	1054	AMTI	1056	AMSJ
105	AJPHO	1058	AJBHO	1059	WBE	1060	WLE	1061	WIG	1062	XBARIE
1063	WTE	1064	RHOLD	1065	TAUHD	1066	RHOLD	1067	RGF	1068	RGI
1069	YBARST	1070	AJSTP	1071	AJSTB	1072	WTST	1073	RGFB	1074	RGIB
1075	XBARRI	1076	XBARRF	1077	YV7	1078	TAUWEI	1079	XCGA	1080	XCGB
1081	ZRO	1082	ACGA	1083	ACGB	1084	RCGO	1085	ZCC	1086	YCG
1087	AMSI	1088	TAUZ	1189	RBZ	1290	TAUZTO	1391	RBZTO	1492	TAUWOP
1593	PO	1694	PDPD	1795	V	1896	VPR	1997	AKRTAU	2097	TAUAKR
2197	CMPTME	2199	MACCEL	2200	ACCELT	2250	TIMEAS	2300	TIMEPS	2350	EPCA
2400	EPCN	2450	PPESS	2470	TCOMB	2490	AMWG	2510	CSTR	2530	GAMAG
2550	TIMEPH	2620	PHST	2690	S1A	2691	S2A	2692	S3A	2693	S4A
2695	S5A	2696	S6A	2697	S7A	2698	S8A	2699	S9A	2700	S10A
2701	S11A	2702	S1B	2703	S2B	2704	S3B	2705	S4B	2706	S5B
2707	S6B	2708	S7B	2709	S8B	2710	S9B	2711	S10B	2712	S11B
2760	ABSLTA	2771	ABSLTF	2782	APA	2790	TABHA	2793	APF	2804	DWSLTA
2815	DWDTS	2826	TABHV	2826	DWSLTF	2837	PSA	2848	PSF	2850	TABNW
2859	PQA	2870	PQF	2881	RBSLTA	2892	RBSLTF	2903	RBRPL	2910	TABNV
2914	TSA	2925	TSF	2936	APORTX	2937	AFHI				
2939	DELZ	2940	TITL	2952	CKNUMP	2960	KNUMP	3050	AKRH	3051	AKRN
3052	MAXRST	3053	PCTAB	3054	TAUTOZ	3055	RSLVRN	3055	TSLVRN	3056	APORTA
3057	APORTB	3058	APORTC	3059	APORTD	3060	APORTE	3061	APORTF	3062	APORTG
3063	APORTH	3064	APORTI	3065	APORTJ	3066	APORTK	3067	TSLVRA	3068	TSLVRB
3069	TSLVRC	3070	TSLVRD	3071	TSLVRE	3072	TSLVRF	3073	TSLVRG	3074	TSLVRH
3075	TSLVRI	3076	TSLVRJ	3077	TSLVRK	3078	THSLVA	3079	THSLVY	3080	TSLVRX
3080	PSLVRX	3081	RSLVRY	3081	TSLVRY	3082	PO	3082	THSLV	3083	PSLVR

3083	TSLVR	3084	THSLVV	3085	TSLVRV	3086	ASLVR	3087	VFHPR	3088	STFLAG
3089	TMAX	3102	DELL	3103	DELLO	3104	DELLR	3106	ALITBE	3107	TAU
3108	VRX	3109	ALITG	3110	COUNT	3111	VFREWI	3112	VSTR	3113	VSTO
3114	VEX	3115	VR	3116	ASTO	3117	ASCHEK	3118	APO	3121	HEFC
3124	RC	3125	SUMOV	3126	XR	3131	DV	3132	HE	3133	SINA
3138	COSA	3143	AV1	3144	AV2	3145	AV3	3146	BV1M	3147	BV2M
3148	THV	3149	TV2	3150	TV4	3151	TV5	3152	TV6	3153	TV7
3154	ALVA	3155	ALVB	3156	ALVC	3157	RV2	3158	RV3	3159	RV4
3160	RV5	3161	RV7	3162	XV7	3163	AFP	3164	AL	3177	AP
3178	DELL3	3179	DEL3	3180	DEL7	3181	B71	3182	B91	3183	AFD
3184	TAUSQ	3185	AER	3186	DELRV	3187	BV1	3188	BV2	3189	KRASUB
3190	KXRSUB	3215	AJOB	3216	RCG	3217	DELLI	3219	RVI	3240	XBARIM
3241	XBARIN	3242	HCR	3243	KWIT1	3244	KWIT2	3245	LSWIT1	3246	LSWIT2
3247	AY	3284	TAUMX	3292	AY	3329	TAUMY	3337	AINCX	3339	RFX
3340	TAUMX	3358	AINCY	3360	RFY	3361	TAUMY	3379	PMIN	3380	PMAX
3381	RB	3383	PH	3384	TAUHT	3385	TAUNT	3386	AHO	3388	TIME
3389	ASE	3390	AHH	3391	VFH	3392	VF	3393	APHI	3394	AINCW
3395	T	3396	P	3397	DELTA	3398	DWDOT	3400	U	3401	AAN
3402	VFN	3403	ALPHI	3404	RBHI	3405	RFHI	3406	THOLD	3407	TAUMW
3408	ALPX	3409	APX	3410	ALPY	3411	APY	3412	WDOTI	3413	WDOT
3414	CAA	3415	CAB	3416	CC	3417	RAD	3418	ANIBO	3419	ANIBW
3420	TIMEW	3421	GCR	3422	UCR	3423	G	3424	THE	3425	HPB
3426	RT	3427	XRO	3428	RAX	3429	RAMAX	3430	ALRS	3431	ALR
3432	ATT	3433	ATO	3434	AFF	3435	GAMAR	3436	AR	3437	GAMARO
3438	ARO	3439	AFE	3440	RAMIN	3441	ALRI	3442	HEI	3443	ALAMIN
3444	AXE	3445	GAMAT	3446	AFX	3447	AFY	3448	PLIT	3449	QLIT
3450	RLIT	3451	SLIT	3452	RIE	3453	BOE	3454	ALRMAX	3455	UT
3458	TAILST	3462	ARIGR	3463	ASHOLD	3467	PHOLD	3468	DLTMP	3469	PTMP
3470	TTMP	3471	UTMP	3472	AJBH	3473	AJBH	3474	XBARI	3475	WI
3476	VT	3477	PA	3478	RAO	3479	THR1	3480	ALL	3481	ALSX
3482	AKGY	3483	AJPP	3484	XDIH	3485	AOMCYL	3486	AIBCYL	3487	AIPCYL
3488	AKGYHI	3489	AKGYX	3490	AKGYY	3491	WTH	3492	WTN	3493	AKRIP
3494	AKRFP	3495	AKRIB	3496	AKRFB	3497	AJPH	3498	AJPH	3499	TAUAO
3500	AJPHP	3501	AJBHN	3502	AJPHED	3503	AJBHED	3504	AJPNOZ	3505	AJBNOZ
3506	AJPHEW	3507	AJBHEW	3508	XRH	3509	XBN	3510	XBHEW	3511	AJPX
3512	FHOF	3513	DTINT	3514	ALAMN	3516	CEMPC	3517	TSS	3518	AMBSS
3519	CFC	3520	AMBSU	3521	EXP1	3522	PSOPO	3525	GP1	3524	GM1
3525	CODET	3526	WIS	3527	VIS	3528	CODEB	3529	AIT	3530	PHMAX
3531	SPHOT	3532	SPOIDT	3533	WR	3534	VFINT	3535	VPINT	3536	VFPP
3537	POW	3538	DIS	3539	AMBSE	3540	SDIS	3541	DELLP	3544	AMPN
3545	AT	3546	F	3547	EPG	3548	EPS	3549	EP1	3550	PEPO
3551	PEPO2	3552	CFOL	3553	VE	3554	FAVG	3555	FAVGWB	3556	VFWEB
3557	YAWER	3558	PHAVWB	3559	PONAWB	3560	ATAVG	3561	AISPWB	3562	CFVL
3563	FX	3564	PHR	3565	PONX	3566	TX	3567	ATMAX	3568	GNOY
3570	FD	3571	DEED	3573	DISB	3574	DISC	3576	WOB	3588	CLOPS
3589	RSSTOR	3590	DTMAX	3591	DTMIN	3592	ANITW	3593	CODTI	3594	CSTAR
3595	TIMEHO	3596	DTWBR	3597	DTTOR	3598	AANN	3599	TOMAX	3600	DOIA
3601	DOIB	3602	XMAX	3603	ZMAX	3604	YMAX	3605	DWB	3606	DSI
3607	DS2	3608	XWB	3609	ZG	3610	ALHO	3613	TWH	3614	X11A
3615	X11B	3616	Y11A	3617	Y11B	3618	BX	3619	RXX	3620	ASI1
3644	POLOR	3645	DELLRI	3648	ALSX	3654	GAMA20	3655	THRX	3656	QI
3657	Q2	3658	RPZ	3659	XP	3660	AZ	3662	DELLOI	3664	ASI
3665	ALSURX	3669	VFH	3670	ALLO	3674	RAT	3675	XRAT	3676	THR
3677	GAMA1	3678	GAMA2	3679	DPR	3680	DPS	3681	DPRA	3682	DPSA
3683	DPRB	3684	DPSB	3685	ROPE1	3686	ROPE2	3687	ROPE3	3688	ROPE4
3689	AL3A	3690	BRAK	3691	AL11A	3692	AS	3694	RPX	3697	A1E
3700	ZIAT	3702	PHII	3703	YA1	3712	C03	3789	ALDP	3792	YRO
3798	AAA	3799	BOB	3800	CCC	3814	YI	3838	ZPO	3839	YPO

3840	ZP1	3841	YP1	3842	DS	3843	ARCO	3844	ARC1	3845	ROE1
3846	ALITYL	3847	ZI	3848	ALO	3849	AIG	3850	THRI	3851	ALP
3852	THRO	3853	THRZ	3854	YNO	3855	ARN	3856	XP1	3857	YP1
3858	RP1	3859	XP2	3860	YP2	3861	RP2	3862	XP3	3863	YP3
3864	RP3	3865	XP4	3866	YP4	3867	RP4	3868	XP5	3869	YP5
3870	RP5	3871	XP6	3872	YP6	3873	RP6	3874	XP13	3875	YP13
3876	RP13	3877	XP12	3878	YP12	3879	RP12	3880	XP11	3881	YP11
3882	RP11	3883	XP10	3884	YP10	3885	RP10	3927	KRASB8	3928	KXRSB8
3929	KGAM	3930	KBRAK	3931	ANRAA	3932	ANYOB	3933	ANYOA	3934	ANY2A
3935	ANZ1A	3936	ANRAB	3937	ANX2A	3939	ANXOB	3940	ANY1B	3941	ANZOB
3942	ANX1B	3943	ANZ1B	3944	ANX2B	3945	ANY2B	3946	ANZ2B	3947	ANXOA
3948	ANZOA	3949	ANX1A	3950	ANY1A	3951	ATANG2	3952	ASINTR	3953	ACOSTR
3954	BSINTR	3955	BCOSTR	3956	BTANG2	3957	ATANP1	3958	BTANP1	3959	ANAA
3960	ANAB	3961	ANBA	3962	ANBB	3963	ANCA	3964	ANCB	3965	ANDA
3966	ANDB	3967	ANBTAO	3968	BNBTAO	3971	KVSTR	3972	RAA	3973	XRATA
3974	THRA	3975	GAMA1A	3976	GAMA2A	3977	XOA	3978	YOA	3979	ZOA
3980	X2A	3981	Y2A	3982	Z2A	3983	X1A	3984	Y1A	3985	Z1A
3986	X3A	3987	Y3A	3988	Z3A	4001	TANG2A	4002	SINTRA	4003	COSTRA
4004	TANP1A	4005	AAAA	4006	BA	4007	CA	4008	DA	4009	BTAOA
4014	ALTA	4018	RAB	4019	XRATB	4020	THRB	4021	GAMA1B	4022	GAMA2B
4023	XOB	4024	YOB	4025	ZOB	4026	X2B	4027	Y2B	4028	Z2B
4029	X1B	4030	Y1B	4031	Z1B	4032	X3B	4033	Y3B	4034	Z3B
4047	TANG2B	4048	SINTRB	4049	COSTRB	4050	TANP1B	4051	ABB	4052	BB
4053	CB	4054	DB	4055	BTAOB	4060	ALTB	4064	RAAP	4065	XRATAP
4066	THRAP	4067	GAM1AP	4068	GAM2AP	4069	XOAP	4070	YOAP	4071	ZOAP
4072	X2AP	4073	Y2AP	4074	Z2AP	4075	X1AP	4076	Y1AP	4077	Z1AP
4090	X3AP	4093	TG2AP	4094	STRAP	4095	CTRAP	4096	TP1AP	4097	AAP
4098	BAP	4099	CAP	4100	DAP	4101	BTAOAP	4106	ALTAP	4110	CABP
4111	XRATBP	4112	THRBP	4113	GAM1BP	4114	GAM2BP	4115	XOBP	4116	YOBP
4117	ZOBP	4118	X2BP	4119	Y2BP	4120	Z2BP	4121	X1BP	4122	Y1BP
4123	Z1BP	4139	TG2BP	4140	STRBP	4141	CTRBP	4142	TP1BP	4143	ABP
4144	BBP	4145	CBP	4146	DBP	4147	BTAOBP	4152	ALTBP	4156	XO
4157	YO	4158	ZO	4162	X1	4163	Y1	4164	Z1	4165	X3
4166	Y3	4167	Z3	4180	TANGM2	4181	SINTHR	4182	COSTHR	4183	TANPH1
4189	SINGM2	4190	COSGM2	4191	SINGM1	4192	COSGM1	4255	ALX	4266	ALAMDA
4361	[illegible]	4362	IIJ	4363	ANLOPS	4364	PFPO1	4365	FPO1	4366	PPO2
4367	WF	4368	RETAIN	4369	IIZ	4370	NZPLAN	4371	NTABH	4372	NTABN
4373	VOLCH	4374	VOLCN	4375	PCTTAU	4376	WOOTO	4377	TAUWPN	4378	VOLCHO
4379	VOLCNO	4380	RGYPA	4381	RGYPB	4382	RGYPC	4383	RGYPD	4384	RGYPE
4385	RGYPF	4386	RGYPG	4387	RGYPH	4388	RGYPI	4389	RGYPJ	4390	RGYPK
4391	RBSLOT	4392	RSLOTA	4393	RSLOTF	4394	SLTFLG	4395	NSLOT	4396	NTABE
4397	ICNN	4398	NTME	4399	TAUTO	4400	AL7	4401	AL8	4402	TMFLAG
4403	TAUTOV	4404	VPH	4405	VPN	4406	CFO	4407	AMW	4408	VCHINP
4409	VCHINP	4410	NTOH	4411	NTOH	4412	BVX	4413	BVXX	4414	NINCPL
4415	ACCEL	4416	VSLVR	4417	CFIT	4418	TPR	4419	KDEG	4420	NPH
4421	PRTOUT	4422	STOYST	4423	DELTSS	4424	DELTTO	4425	PRTFLG	4426	VP
4427	VEI	4428	DPO	4429	ABTOT	4430	ABLVL	4431	TST	4432	PST
4433	DELTST	4434	RRFLAG	4435	IFLAG	4436	AITST	4437	AKRST	4438	PITER
4439	NEPS	4440	NCSTR	4441	UA	4452	UF			4463	WSLOTO
4474	WSLOTI	4485	AFRPLA	4486	AFRPLB	4487	AFRPLC	4488	AFRPLD	4489	AFRPLE
4490	AFRPLF	4491	AFRPLG	4492	AFRPLH	4493	AFRPLI	4494	AFRPLJ	4495	AFRPLK
4496	AFRPLX	4497	AINCPL	4498	AKSLOT	4500	ALPRPA	4501	ALPRPB	4502	ALPRPC
4503	ALPRPD	4504	ALPRPE	4505	ALPRPF	4506	ALPRPG	4507	ALPRPH	4508	ALPRPI
4509	ALPRPJ	4510	ALPRPK	4511	ALPRPO	4512	DTAU	4513	DTAUA	4514	DTAUB
4515	DTAUC	4516	DTAUD	4517	DTAUE	4518	DTAUF	4519	DTAUG	4520	DTAUH
4521	DTAUI	4522	DTAUJ	4523	DTAUK	4524	DTAUW	4525	DTAUWA	4526	DTAUWB
4527	DTAUWC	4528	DTAUWD	4529	DTAUWE	4530	DTAUWF	4531	DTAUWG	4532	DTAUWH
4533	DTAUWI	4534	DTAUWJ	4535	DTAUWK	4536	DVDT	4537	IIS	4538	IPLANE

NUMERIC LISTING (CONTINUED)

4539	IS1	4540	IS2	4541	KPLANE	4542	TAURPL	4555	NPLANE	4556	PI
4557	PIO2	4558	TH0	4559	TH0A	4560	TH0B	4561	TH0C	4562	TH0D
4563	TH0E	4565	TH0F	4565	TH0G	4566	TH0H	4567	TH0I	4568	TH0J
4569	TH0K	4570	TH0W	4571	TSLOTA	4582	TSLOTF	4593	WDSLOT	4594	WISLOT
4595	NI	4596	NABRNH	4604	NABRNN	4612	NKGYPA	4620	NKGYPB	4628	NKGYPC
4636	NKGYPD	4644	NKGYPE	4652	NKGYPF	4660	NKGYPG	4668	NKGYPH	4676	NKGYPI
4684	NKGYPJ	4692	NKGYPK	4708	NLPPLA	4716	NLPPLB	4724	NLPPLC	4732	NLPPLD
4740	NLPPLE	4744	AMUG	4748	NLPPLF	4756	NLPPLG	4764	NLPPLH	4772	NLPPLI
4780	NLPPLJ	4788	NLPPLK	4796	NPMOIN	4804	NPMOIN	4812	NRMOIN	4820	NRMOIN
4845	PRNT	6360	MCFLAG	6361	ISET	6371	TH0W	6441	GEOM	6442	AKRFLG
6443	PPTAGR	6444	WGPORT	6445	WGTOT	6446	SWDOTN	6447	AINCHI	6448	AMACH
6449	AMACHO	6450	PSAPR	6460	PSFPR	6470	SCUR	6498	PRCRIT	6499	ZCALC

NUMBER OF VARIABLES = 1104

ALPHABETIC LISTING OF PROGRAM VARIABLES IN COM ARRAY

A	334	AA	379	AAA	3798	AAAA	4005	AAK	999	AAN	3401
AANN	3598	AAP	4097	AB	424	ABB	4051	ABCYL	4430	ABIGR	3462
ABP	4143			ABSLTA	2760	ABSLTF	2771	ABTOT	4429	AC	469
ACCEL	4415	ACCELT	2200	ACOA	1082	ACOB	1083	ACOSTR	3953	AD	514
AE	559	AEE	3439	AER	3185	AF	604	AFD	3183	AFF	3434
AFHI	2937	AFP	3163	AFRPLA	4485	AFRPLB	4486	AFRPLC	4487	AFRPLD	4488
AFRPLE	4489	AFRPLF	4490	AFRPLG	4491	AFRPLH	4492	AFRPLI	4493	AFRPLJ	4494
AFRPLK	4495	AFRPLX	4496	AFX	3446	AFY	3447	AG	649	AH	694
AHH	3390	AHO	3386	AI	739	AIBCYL	3486	AIG	3849	AINC	1
AINCA	22	AINCB	43	AINCC	64	AINCD	85	AINCE	106	AINCF	127
AINCG	148	AINCH	169	AINCHI	6447	AINCI	190	AINCJ	211	AINCK	232
AINCN	253	AINCPL	4497	AINCW	3394	AINCX	3437	AINCY	3358	AIPCYL	3407
AISPWS	3561	AIT	3529	AITST	4436	AJ	794	AJBB	3215	AJBH	3473
AJBHED	3503	AJBHEW	3507	AJBHN	3501	AJBHO	1058	AJBN	3472	AJBNOZ	3505
AJPH	3498	AJPHED	3502	AJPHEW	3506	AJPHN	3500	AJPHO	1057	AJPN	3497
AJPNOZ	3504	AJPP	3483	AJPX	3512	AJST8	1071	AJSTP	1070	AK	829
AKG	942	AKGY	3482	AKGYHI	3488	AKGYX	3489	AKGYY	3490	AKK	935
AKR	952	AKREB	3496	AKRELG	6442	AKREP	3494	AKRH	3050	AKRIB	3495
AKRIP	3493	AKRN	3051	AKRST	4437	AKRTAU	1997	AKSLOT	4498	AKU	947
AL	3164	ALA	14	ALAMDA	4266	ALAMIN	3443	ALAMN	3514	ALB	15
ALC	347	ALD	762	ALDP	3789	ALE	16	ALFE	276	ALFEM	275
ALHO	3610	ALITBE	3106	ALITO	3109	ALITTL	3846	ALL	3480	ALLO	3670
ALP	3851	ALPHI	3403	ALPRPA	4500	ALPRPB	4501	ALPRPC	4502	ALPRPD	4503
ALPRPE	4504	ALPRPF	4505	ALPRPG	4506	ALPRPH	4507	ALPRPI	4508	ALPRPJ	4509
ALPRPK	4510	ALPRPO	4511	ALPX	3408	ALPY	3410	ALQ	3846	ALR	3431
ALRI	5401	ALRMAX	3454	ALRS	3430	ALSI	12	ALSUBX	3665	ALSX	3481
ALS2	13	ALTA	4014	ALTAP	4106	ALTB	4060	ALTBP	4152	ALVA	3154
ALVB	3155	ALVC	3156	ALX	4255	ALXX	3648	AL11A	3691	AL3A	3669
AL7	4400	AL8	4401	AMACH	6448	AMACHO	6449	AMBSE	3539	AMBSS	3518
AMBSU	3520	AMPN	3544	AMSI	1087	AMSJ	1056	AMTI	1054	AMTJ	1053
AMUG	4744	AMW	4407	AMWG	2490	AN	874	ANAA	3959	ANAB	3960
ANBA	3961	ANBB	3962	ANBTAO	3967	ANCA	3963	ANCB	3964	ANDA	3965
ANDB	3966	ANI	930	ANIBO	3418	ANIBW	3419	ANITW	3592	ANLOPS	4363
ANN	1044	ANO	2	ANRAA	3931	ANRAB	3936	ANSIG	1031	ANXOA	3947
ANXOB	3939	ANX1A	3949	ANX1B	3942	ANX2A	3937	ANX2B	3944	ANYOA	3933
ANYOB	3932	ANY1A	3950	ANY1B	3946	ANY2A	3934	ANY2B	3945	ANZOA	3948
ANZOB	3941	ANZ1A	3935	ANZ1B	3943	ANZ2B	3946	ANI	1047	AN2	996
AO	17	AOE	122	AOEM	921	AOMCYL	3485	AP	3177	APA	2782
APF	2793	APHI	3393	APO	3118	APORTA	3056	APORTB	3057	APORTC	3058
APORTD	3059	APORTE	3060	APORTF	3061	APORTG	3062	APORTH	3063	APORTI	3064
APORTJ	3065	APORTK	3066	APORTX	2936	APX	3409	APY	3411	AR	3436
ARCO	3843	ARC1	3844	ARN	3855	ARO	3438	AS	3692	ASCHEK	3117
ASE	3389	ASHOLD	3463	ASI	3664	ASINTR	3952	ASP1	3620	ASLVR	3086
ASTO	3116	AT	3545	ATANG2	3951	ATANP1	3957	ATAVG	3560	ATMAX	3567
ATO	3433	ATSLOT	2938	ATT	3432	AV1	3143	AV2	3144	AV3	3147
AWE	3444	AX	3247	AY	3292	AZ	3660	A1E	3697	BA	4006
BAP	4098	BB	4052	BBB	3799	BBP	4144	BCOSTR	3955	BE	920
BETA	1048	BH	923	BHOLD	1064	BNBTAO	3968	BOE	3453	BRAK	3690
BRNOUT	4421	BSINTR	3954	BTANG2	3956	BTANP1	3958	BTAOA	4009	BTAOAP	4101
BTAOB	4055	BTAOBP	4147	BTAOE	928	BVX	4412	BVXX	4413	BV1	3187
BV1M	3146	BV2	3188	BV2M	3147	BX	3618	B1E	3452	B71	3181
B71M	375	B72M	376	B91	3182	B91M	377	B92M	378	CA	4007
CAA	3414	CAE	286	CAP	4099	CB	4053	CBB	3415	CBE	287
CDP	4145	CC	3416	CCC	3800	CCCE	288	CCVE	289	CDCE	290
CDVE	291	CECE	292	CEMPC	3516	CEVE	293	CFC	3519	CFIT	4417
CFO	4406	CFOL	3552	CFVL	3562	CKDUMP	2952	CLOPS	3568	CM	998

CMPTME	2197	CODEB	3528	CODET	3525	CODTI	3593	COSA	3138	COSGM1	4192
COSGM2	4190	COSTHR	4182	COSTRA	4003	COSTRB	4049	COUNT	3110	CSTAR	3594
CSTR	2510	CTRAP	4095	CTRHP	4141	DA	4004	DAP	4106	DB	4054
DBP	4146	DE	973	DEED	3571	DELC	1036	DELF	941	DELI	1051
DELIN	1038	DELIS	997	DELL	3102	DELLA	994	DELLI	3217	DELLL	1037
DELLM	995	DELLO	3103	DELLOI	3662	DELLP	3541	DELLR	3104	DELLRI	3645
DELL3	3178	DELN	1049	DELNE	1050	DELRV	3186	DELT	940	DELTA	3397
DELTSS	4423	DELTST	4433	DELTTO	4424	DELZ	2939	DEL3	3179	DEL7	3180
DEI	919	DHI	922	DIS	3538	DISB	3573	DISC	3574	DLORF	937
DLRF	936	DLTMP	3468	DN1	925	DO1A	3600	DO1B	3601	DO3	3712
DPO	4428	DPR	3679	DPRA	3681	DPRB	3683	DPS	3680	DPSA	3682
DPSB	3684	DRRF	938	DRVRF	939	DS	3842	DSI	3605	DS2	3607
DT	992	DTAU	4512	DTAUA	4513	DTAUB	4514	DTAUC	4515	DTAUD	4516
DTAUE	4517	DTAUF	4518	DTAUG	4519	DTAUH	4520	DTAUI	4521	DTAUJ	4522
DTAUK	4523	DTAUW	4524	DTAUWA	4525	DTAUWB	4526	DTAUWC	4527	DTAUWD	4528
DTAUWE	4529	DTAUWF	4530	DTAUWG	4531	DTAUWH	4532	DTAUWI	4533	DTAUWJ	4534
DTAUWK	4535	DTINT	3513	DTMAX	3590	DTMIN	3591	DTTOR	3597	DTWBR	3596
DV	3131	DVDT	4536	DWB	3605	DWDOT	3398	DWDTS	2815	DWSLTA	2804
DWSLTF	2826	EPCA	2350	EPCN	2400	EPG	3547	EPS	3548	EP1	3549
EXP1	3521	F	3546	FAVG	3554	FAVGWB	3555	FHOF	3512	FX	3563
G	3423	GAMA	932	GAMAG	2530	GAMAR	3435	GAMARO	3437	GAMAT	3445
GAMA1	3677	GAMA1A	3975	GAMA1B	4021	GAMA2	3678	GAMA2A	3976	GAMA2B	4022
GAMA2O	3654	GAM1AP	4067	GAM1BP	4113	GAM2AP	4068	GAM2BP	4114	GCR	3421
GEOM	6441	GM1	3524	GNOT	3568	GP1	3523	HCO	931	HCR	3242
HE	3132	HEFC	3121	HEI	3442	HEO	280	HER	281	HE1	278
HE2	279	HHR	301	HH2	299	HMO	320	HOLDR	3644	HRB	3425
ICHN	4397	IFLAG	4435	III	4361	IIJ	4362	IIS	4537	II2	4369
		IPLANE	4538	ISET	6361	IS1	4539	IS2	4540	KBRAK	3930
KDEG	4419	KDUMP	2960	KGAM	3929	KPLANE	4541	KRASBR	3927	KRASUB	3189
KVSTR	3971	KWIT1	3243	KWIT2	3244	KXRSBR	3928	KXRSUB	3190	LSWIT1	3245
LSWIT2	3246	MCFLAG	6360	NABRNH	4596	NABRNN	4604	NACCEL	2199	NAKRST	3052
NCSTR	4440	NEPS	4439	NI	4595	NINCPL	4414	NKGYPA	4612	NKGYPB	4620
NKGYPC	4628	NKGYPD	4636	NKGYPE	4644	NKGYPF	4652	NKGYPG	4660	NKGYPH	4668
NKGYPI	4676	NKGYPJ	4684	NKGYPK	4692	NLPPLA	4708	NLPPLB	4716	NLPPLC	4724
NLPPLD	4732	NLPPLE	4740	NLPPLF	4748	NLPPLG	4756	NLPPLH	4764	NLPPLI	4772
NLPPLJ	4780	NLPPLK	4788	NPH	4420	NPLANE	4555	NPMOIH	3796	NPMOIN	4804
NRMOIH	4812	NRMOIN	4820	NSLOT	4395	NTABE	4396	NTABH	4371	NTABN	4372
NTME	4398	NTOH	4410	NTON	4411	NZPLAN	4370	P	3396	PA	991
PCTAB	3053	PCTTAU	4375	PI	1593	PDPR	1694	PEPO	3550	PEPO1	4364
PEPO2	3551	PH	3383	PHAVWB	3558	PHI	1052	PHI1	3702	PHMAX	3530
PHOLD	3467	PHST	2620	PHX	3564	PI	4556	PIK	1039	PIO2	4557
PITER	4438	PLIT	3448	PMAX	3380	PMIN	3379	PO	3082	POA	2859
POF	2870	PON	3537	PONAWB	3559	PONX	3565	PPO1	4365	PPO2	4366
PRCRIT	6498	PRESS	2450	PRNT	4845	PRTAKR	6443	PRTFLG	4425	PSA	2837
PSAFR	6450	PSF	2848	PSFPR	6460	PSOPO	3522	PST	4432	PTMP	3469
PYPHY	1032	QLIT	3449	Q1	3656	Q2	3657	R	933	RA	3477
RAA	3972	RAAP	4064	RAB	4018	RABP	4110	RAD	3417	RAMAX	3429
RAMIN	3440	RAO	3478	RAT	3674	RAX	3428	RB	3381	RBFLAG	4434
RBHI	3404	RBRPL	2903	RBSLOT	4391	RBSLTA	2881	RBSLTF	2892	RBZ	1189
RBZTO	1391	RC	3124	RCG	3216	RCGO	1084	RETAIN	4368	RE1	274
REA	277	RF	3	RFA	24	RFB	45	RFC	66	RFD	87
RFE	108	RFF	129	RFG	150	RFH	171	RFHI	3405	RFI	192
RFJ	213	RFK	234	RFX	3339	RFY	3360	RGF	1067	RGFB	1073
RGI	1068	RGIB	1074	RGIPA	4380	RGYPB	4381	RGYPC	4382	RGYPD	4383
RGYPE	4384	RGYPF	4385	RGYPG	4386	RGYPH	4387	RGYPI	4388	RGYPJ	4389
RGYPK	4390	RHOLD	1066	RHI	295	RIG	929	RLIT	3450	RN1	314
ROE1	3845	ROPE1	3685	ROPE2	3686	ROPE3	3687	ROPE4	3688	RO11	366
RO3	350	RO5	353	RO7	356	RO9	365	RPX	3694	RPZ	367

RP1	3858	RP10	3885	RP11	3882	RP12	3879	RP13	3876	RP2	3861
RP3	3864	RP4	3867	RP5	3870	RP6	3873	RSLOTA	4392	RSLOTF	4393
RSLVR	3083	RSLVRN	3055	RSLVRX	3080	RSLVRY	3081	RSSTOR	3589	RT	3426
RV1	3219	RV2	3157	RV3	3158	RV4	3159	RV5	3160	RV7	3161
RXX	3619	R1	339	R2	5	R3	6	R4	7	R5	8
R6C	9	R7	10	R8	11	R9	340	SC	1033	SCULT	1034
SCUR	6470	SDIS	3540	SIGK	1040	SINA	3133	SINGM1	4191	SINGM2	4189
SINTHR	4181	SINTRA	4002	SINTRB	4048	SLST	3451	SLTFLG	4394	SN	1046
SNE	1045	SPHDT	3531	SPONDT	3532	SPOP	1029	STDYST	4422	STFLAG	3088
STOT	1030	STRAP	4094	STRBP	4140	SUMDV	3125	SWDOTN	6446	S1A	2690
S1B	2702	S10A	2700	S10B	2711	S11A	2701	S11B	2712	S2A	2691
S2B	2703	S3A	2692	S3B	2704	S4A	2693	S4B	2705	S5A	2695
S5B	2706	S6A	2696	S6B	2707	S7A	2697	S7B	2708	S8A	2698
S8B	2709	S9A	2699	S9B	2710	T	3395	TABHA	2790	TABHV	2820
TABNV	2910	TABNW	2850	TANGM2	4180	TANG2A	4001	TANG2B	4047	TANPH1	4183
TANP1A	4004	TANP1B	4050	TAU	3107	TAUAKR	2097	TAUBG	3499	TAUEU	284
TAUE1	285	TAUHD	1065	TAUHT	3384	TAULST	3458	TAUM	371	TAUMW	3407
TAUMX	3284	TAUNY	3329	TAUNT	3385	TAUPPL	4542	TAUSQ	3184	TAUTO	4399
TAUTOV	4403	TAUTOZ	3654	TAUW	4	TAUWA	25	TAUWB	46	TAUWC	67
TAUWD	88	TAUWDP	1492	TAUWE	109	TAUWEI	1078	TAUWF	130	TAUWG	151
TAUWH	172	TAUWI	193	TAUWJ	214	TAUWK	235	TAUWPN	4377	TAUWX	3340
TAUWY	3361	TAUZ	1088	TAUZTO	1290	TCOMB	2470	TOMAX	3599	TG2AP	4093
TG2BP	4139	THE	3424	THI	1041	THOLD	3406	THOW	6371	THR	3676
THRA	3974	THRAP	4066	THRB	4020	THRBP	4112	THRI	3850	THRO	3852
THRX	3655	THRZ	3853	THR1	3479	THSLV	3082	THSLVV	3084	THSLVX	3078
THSLVY	3079	THV	3148	TH0	4558	TH0A	4559	TH0B	4560	TH0C	4561
TH0D	4562	TH0E	4563	TH0F	4564	TH0G	4565	TH0H	4566	TH01	4567
TH0J	4569	TH0K	4569	TH0W	4570	TH1	341	TH2	372	TH3	373
TH4	374	TIMAX	3089	TIME	3388	TIMEAC	2250	TIMEPH	2550	TIMEPS	2300
TIVEW	3420	TINEWO	3595	TITL	2940	TLO	1042	TO	934	TOFLAG	4402
TPP	4418	TP1AP	4096	TP1BP	4142	TREF	1043	TSA	2914	TSF	2925
TSLOTA	4571	TSLOTF	4582	TSLVR	3083	TSLVRA	3067	TSLVRE	3068	TSLVRC	3069
TSLVRD	3070	TSLVRE	3071	TSLVRF	3072	TSLVRG	3073	TSLVRH	3074	TSLVRI	3075
TSLVRJ	3076	TSLVRK	3077	TSLVRN	3055	TSLVRV	3035	TSLVRX	3080	TSLVRY	3081
TSS	3517	TST	4431	TTMP	3470	TV2	3149	TV4	3150	TV5	3151
TV6	3152	TV7	3153	T&H	3343	TX	3566	T10M	369	T12M	359
T2M	342	T4M	343	T5M	344	T6M	357	T7M	358	T9M	370
U	3400	UA	4441	UCR	3422	UF	4452	UT	3455	UTMP	3471
V	1795	VCE	283	VCH	303	VCHINP	4408	VCN	323	VCNINP	4409
VE	3553	VEH	3659	VEX	3114	VF	3392	VFEO	282	VFH	3391
VEHEWI	3111	VEHO	302	VEHPR	3087	VFI	4427	VFINT	3534	VFN	3402
VEPP	3536	VEWFB	3536	VIS	3527	VOLCH	4373	VOLCHO	4378	VOLCN	4374
VOLCNO	4379	VP	4426	VPH	4404	VPINT	3535	VPN	4405	VPR	1896
VR	3115	VRX	3108	VSLVR	4426	VSTO	3113	VSTR	3112	WB	3533
WBE	1059	WBWEB	3557	WD	3570	WDB	3576	WDOT	3413	WDOTD	4376
WDOTI	3412	WDSLOT	4593	WE	4367	WGPORT	6444	WGTOT	6445	WI	3475
WIG	1061	WIS	3526	WISLOT	4594	WLE	1060	WP	1035	WSLOTD	4463
WSLOTI	4474	WT	3476	WTE	1063	WTH	3491	WTN	3492	WTST	1072
XBARI	3474	XBARIE	1062	XBARIH	3240	XBARIN	3241	XBARRF	1076	XBARRI	1075
XBARST	1055	XBH	3508	XBHEW	3510	XBIH	3484	XBN	3509	XCGB	1079
XCCB	1080	XMAX	3602	XO	4156	XOA	3377	XOAP	4069	XO8	4023
XOBP	4115	XO11	366	XO3	348	XO5	351	XO7	354	XO9	363
XPZ	3669	XP1	3856	XP10	3983	XP11	3820	XP12	3877	XP13	3874
XP2	3859	XP3	3852	XP4	3859	XP5	3868	XP6	3871	XR	3126
XRAY	3875	XRATA	3873	XRATAP	4060	XRATB	4019	XRATBP	4114	XRO	3427
XSAP	4050	XV7	3102	XW4	1608	X1	4162	X1A	3987	X1AP	4075
[illegible]	[illegible]	[illegible]	[illegible]	[illegible]	[illegible]	X[illegible]	[illegible]	[illegible]	[illegible]	[illegible]	[illegible]
[illegible]	[illegible]	[illegible]	[illegible]	[illegible]	[illegible]	[illegible]	[illegible]	[illegible]	[illegible]	[illegible]	[illegible]

X76	360	YA1	3703	YCG	1086	YI	3819	YMAX	3604	YN0	3854
Y0	4157	Y0A	3978	Y0AP	4070	Y0B	4024	Y0BP	4116	Y011	367
Y03	349	Y05	352	Y07	355	Y09	364	YP1	3841	YP0	3839
YP1	3857	YP10	3884	YP11	3881	YP12	3878	YP13	3875	YP2	3860
YP3	3863	YP4	3866	YP5	3869	YP6	3872	YR0	3752	YV7	1077
YI	4163	YIA	3984	YIAP	4076	YIB	4030	YIBP	4122	YIIA	3616
YI18	3617	Y2A	3981	Y2AP	4073	Y2B	4027	Y2BP	4119	Y3	4166
Y3A	3987	Y3B	4033	Y45	346	Y76	361	ZCALC	6499	ZCG	1085
ZG	3609	ZI	3847	ZMAX	3603	ZO	4158	ZOA	3979	ZOAP	4071
ZOB	4025	ZOBP	4117	ZP0	3838	ZP1	3840	ZR0	1081	Z1	4164
Z1A	3985	Z1AP	4077	Z1AT	3766	Z1B	4031	Z1BP	4123	Z2A	3982
Z2AP	4074	Z2B	4028	Z2BP	4120	Z3	4167	Z3A	3988	Z3B	4034

NUMBER OF VARIABLES = 1104

6.3.1.4 Geometry Table Storage
(Labeled CØMMØN Block "TBLK")

Plane	NGEOM_	TAUPL_	ALPPL_	AKGYP_
X	1	2	52	102
A	152	153	203	253
B	303	304	354	404
C	454	455	505	555
D	605	606	656	706
E	756	757	807	857
F	907	908	958	1008
G	1058	1059	1109	1159
H	1209	1210	1260	1310
I	1360	1361	1411	1461
J	1511	1512	1562	1612
K	1662	1663	1713	1763

End	NGEØM_	TAU_	AB_	PMØI_	RMØI_	XCG_
E	1813	1814	1864	1914	1964	2014
H	2064	2065	2115	2165	2215	2265
N	2315	2316	2366	2416	2466	2516

End Table Variable Names

NGEØEN	PMØIE
NGEØHD	PMØIHD
NGEØMN	PMØIN
TAUEND	RMØIE
TAUHD	RMØIHD
TAUN	RMØIN
ABEND	XCGE
ABHD	XCGHD
ABN	XCGN

Table Control Variables

Name	Location
NWRTAB	2566
NPUTAB	2567
GEOM	2568
IDTAB(1)	2569

6.3.1.5 Monitor System Allocation Map

OVERLAY ORIGIN CARDS AND ASSIGNED LINK NUMBERS

$ORIGIN	LOPT2	IS LINK	1, PARENT LINK IS	0
$ORIGIN	LOPT2	IS LINK	2, PARENT LINK IS	0
$ORIGIN	LOPT2	IS LINK	3, PARENT LINK IS	0
$ORIGIN	LOPT3	IS LINK	4, PARENT LINK IS	3
$ORIGIN	LOPT4	IS LINK	5, PARENT LINK IS	4
$ORIGIN	LOPT4	IS LINK	6, PARENT LINK IS	4
$ORIGIN	LOPT3	IS LINK	7, PARENT LINK IS	3
$ORIGIN	LOPT5	IS LINK	8, PARENT LINK IS	7
$ORIGIN	LOPT5	IS LINK	9, PARENT LINK IS	7
$ORIGIN	LOPT2	IS LINK	10, PARENT LINK IS	0

* MEMORY MAP *

```
SYSTEM                                  00000 THRU  01765
FILE BLOCK ORIGIN                       03766
FILES      1.    UNIT06                 (NO BUFF POOL ATTACHED)
           2.    UNIT01                 (NO BUFF POOL ATTACHED)
           3.    UNIT02                 (NO BUFF POOL ATTACHED)
           4.    UNIT05                 (NO BUFF POOL ATTACHED)
           5.    UNIT07                 (NO BUFF POOL ATTACHED)
           6.    UNIT08                 (NO BUFF POOL ATTACHED)
           7.    UNIT09                 (NO BUFF POOL ATTACHED)
           8.    UNIT10                 (NO BUFF POOL ATTACHED)
           9.    UNIT11                 (NO BUFF POOL ATTACHED)
          10.    UNIT12                 (NO BUFF POOL ATTACHED)
          11.    UNIT13                 (NO BUFF POOL ATTACHED)
          12.    UNIT14                 (NO BUFF POOL ATTACHED)
          13.    UNIT15                 (NO BUFF POOL ATTACHED)
          14.    UNIT16                 (NO BUFF POOL ATTACHED)
PRE-EXECUTION INITIALIZATION            04236
CALL ON OBJECT PROGRAM                  04245
OBJECT PROGRAM                          04252 THRU  42053
```

LINK DECK ORIGIN CONTROL SECTIONS (/NAME/=NON-0 LENGTH, (LOC)=DELETED, *=NOT REFERENCED)

```
      MAIN    04252     ///     /1630161   /TBLK  / 04254     EVEN    04253     ......  11764 *
      ACOSI   11500     EVEN    11501      ACOS     11535
      COMP    11654     EVEN    11655      COMPSC   11727
      SSOR    11743     SORT    11743
      TRANI   11777     TRAN    12017
      .LINK   12045     /.LOT  / 12045     /.LRECT/ 12060     /.LVEC / 12104
      .LXCON  12176      .LXSTO  12176      .LXSTP  12131      .LXOUT  12177 *    .LXRTN  12211      IBEXIT  12211 *
                         .LXCAL  12214      .LXERR  12216      .ORCLS  12376 *    .LEXIT  12433 *    .LXARG  12546 *
                         .LO     12571 *    .CLSE   12577 *    .LFAL   12600 *    .LUNB   12601 *    .DFCNT  12602
      .LOVRY  12623      .LOVRY (12623)     .LOT    (12045)    .LRECT (12060)     .LVEC   (12104)
      .LXSL   13400      .LXSEL  13400      LXCSEL  13401      .LXTST  13404      .LXOVL  13452      .LXRET  13465 *
                         .LXTNO  13622      .LXDIS  13630      .LXFLG  13671      .LTCN   13636
      .FPTR*  13656      .FFPT.  13656 *    .FPOUT  14013 *    .FPARG  14021 *    /.COUNT/ 14023 *   OVFLOW  14067
      .CPAS.  14076      E.1     14076      E.2     14077      E.3     14100      E.4     14101
      .XCC.   14102      CC.1    14102      CC.2    14103      CC.3    14104      CC.4    14105
      XIT     14106      EXIT    14106      .EXIT.  14106
      FXEM    14107      .FXEM.  14107      .FXOUT  14444 *    .FXARG  14452 *    /.CPTM./ 14525 *
      FCNV    14537      .FCON.  14537      .FCNV.  14562      .FKOFS  14575      .CNVSW  14577      .FDX1   14603
                         .FDX2   14604      .DBC    14606      .ARC10  14744      .DBC20  14772      .DDSW   15002
                         .DDFIX  15011      .FIXSW  15017      .DDBC   15024      EVEN    15321      .DDRSI  15340
                         .DDRS2  15342 *    .D1     15345      .D2     15347      .FERR2  15434 *    .ANPT   15470
                         .CNPT   15505      .LNTP   15570      .ACUT   15637      .DFLT   15655      .FLT    16011
                         .DEXPN  16101      .FXD    16102      .MOUT   16232      .INTG   16302      .LOUT   16420
                         .DOUT   16437      .XCF    16470      .TEST   17176      .XCUST  17201      .XIST   17204
                         .DONE   17219      .OUTBF  17267      EVEN    17261      .BUF    17312      .OSTO   17313
                         .WIDTH  17316      .GAIN   17315      .GAIN1  17316      .FROUF  17326      EVEN    17330
                         .DDOFL  17355      .DDFLG  17354      .POD    17355      .DEX    17356      .FEXP   17357
                         .DIG    17360
      FIOR    17376      .FIOR.  17376      .FFIL.  20163      .FRTN.  20213      .SWIPA  20357 *    .UNDO.  20560 *
                         EOFSW   20361 *    EOFSW   20366
```

	FIOS.	20621	..FIOS	20621	..FIOC	20679	..FSEL	20514	..FBCK	20532 *	..FTCK	20534	
			..FCHK	20655 *									
	FROD.	21062	..FROD	21062									
	FWRD.	21107	..FWRD	21107									
	FBCO.	21135	..FBCO	21135	..FBCM	21137	..FBCR	21150					
	FVIO.	21200	..FVIO	21200									
	UNIT04	21267	..UN04	21267									
	UN01	21270	.UN01.	21270									
	UN02	21271	.UN02.	21271									
	UN05	21272	.UN05.	21272									
	UN07	21273	.UN07.	21273									
	UN08	21274	.UN08.	21274									
	UN09	21275	.UN09.	21275									
	UN10	21276	.UN10.	21276									
	UN11	21277	.UN11.	21277									
	UN12	21300	.UN12.	21300									
	UN13	21301	.UN13.	21301									
	UN14	21302	.UN14.	21302									
	UN15	21303	.UN15.	21303									
	UN16	21304	.UN16.	21304									
	FLOG	21305	ALOG10	21305 *	ALOG	21306							
	FEXP	21511	EXP	21511									
	FSCN	21632	COS	21632	SIN	21633							
	FXP3	22026	.XP3.	22026									
	FSLOI	22153	.FSLI.	22171	.FSOI.	22177 *							
	FSLI	22210	.SLI.	22210	.SLII.	22214	.SOI.	22223	.SOII.	22231			
	FSLOO	22244	.FSLO.	22262	.FSOO.	22270 *							
	FSLO	22301	.SLO.	22301	.SLO2.	22307	.SOO.	22314	.SOO2.	22323			
	FTNC	22335	COTAN	22335 *	TAN	22336	CRIT	22501 *					
	FASC	22560	ARCOS	22560 *	ACOS	(116351	ARSIN	22561 *	ASIN	22561			
	FOVERF	22711	OVERFL	22711									
	TAB	22733	TAB	(227331									
	LOC	23543	ILOC	23543 *	XLOC	23544 *							
	//	23550											
1	INPT1	23550	///	/(630161	/TALK	/(042541	EVEN	23551	INP*	31531			
	IN40	31593	///	/(630161	/TALK	/(042541	INPT40	31546					
2	PCHWRT	23550	///	/(630161	/TALK	/(042541	EVEN	23551	PCHWRT	26131			
1	AFP	23550	///	/(630161	EVEN	23551	AFPSUB	30235					
	SDIOII	30247	///	/(630161	SDIOII	30760							
	FOGRE1	30776	EVEN	30777	FOGRE	32324							
	HF	32366	///	/(630161	EVEN	32367	HFSUB	32503					
	LPOAP	32515	///	/(630161	LPOAPS	33132							
	PTIAAK	33146	///	/(630161	EVEN	33147	PTIAA	33705					
	RA	33729	///	/(630161	RASUR	34734							
	RAV	34750	///	/(630161	EVEN	34751	RBVSUB	35047					
	RC	35061	///	/(630161	RCSUR	35300							
	TOGRE1	35312	EVEN	35313	TOGRE	35404							
	KR	35434	///	/(630161	EVEN	35435	KRSUB	36353					
4	AE	36367	///	/(630161	AESUB	37500							
	AFP	37512	///	/(630161	EVEN	37513	AFPSUB	37536					

	ALR	37550	EVEN	37551	ALRSUB	37630			
	ARS	37660	EVEN	37661	ARSSUB	37746			
	ASE	40000	///	/(630160)	EVEN	40001	ASESUB	40345	
	AHE	40363	///	/(630160)	AHESUB	41175			
5	MCH1	41207	///	/(630160)	/TBLK	/(042540)	MNCHN1	43053	
	ENOC	43071	///	/(630160)	ENOCSB	44167			
	PCHGI	44206	///	/(630160)	EVEN	44207	PCHGIS	44715	
	PCHPL	44731	///	/(630160)	PCHPLI	45124			
	PLNCN	45140	///	/(630160)	EVEN	45141	PLNCNS	47030	
	PLNCC	47044	///	/(630160)	EVEN	47045	PLNCCS	47651	
6	MCH2	41207	///	/(630160)	/TBLK	/(042540)	MNCHN2	43167	
7	MCH3	36367	///	/(630160)	/TBLK	/(042540)	MNCHN3	37232	
4	AIR	37746	///	/(630160)	EVEN	37747	AIRSUB	37411	
	ASUBC1	37423	///	/(630160)	ASUBC	37514			
	BRAK	37526	///	/(630160)	EVEN	37527	BRAKSB	37627	
	BSUBC1	37641	///	/(630160)	BSUBC	37732			
	DPRA	37744	///	/(630160)	EVEN	37745	DPRASB	40017	
	GAM	40031	///	/(630160)	GAMSUB	40210			
	GAMAZ	40223	///	/(630160)	EVEN	40223	GAMAZS	40534	
	HAP	40340	///	/(630160)	EVEN	40347	HAPSBC	40447	
	HA	40461	///	/(630160)	HASUBC	40561			
	HAP	40573	///	/(630160)	HAPSBC	40673			
	HA	40705	///	/(630160)	HBSUBC	41005			
	HON	41017	///	/(630160)	HONSUB	41243			
	LA	41261	///	/(630160)	LBSUB	41311			
	MSI	41329	///	/(630160)	MSISUB	41666			
	MTI	41700	///	/(630160)	EVEN	41701	MTISUB	42260	
	PO	42272	///	/(630160)	EVEN	42273	POSUB	42401	
	P1	42413	///	/(630160)	P1SUB	42671			
	P3	42703	///	/(630160)	P3SUB	43116			
	RAR	43130	///	/(630160)	EVEN	43131	RASUBB	44241	
	ROR1	44253	///	/(630160)	ROELSB	44352			
	ROP	44364	///	/(630160)	EVEN	44365	ROPSB	44442	
	SCII	44456	///	/(630160)	EVEN	44457	SCI	47314	
	SCTORA	47331	///	/(630160)	SCTOR1	50650			
	SCTORR	50662	///	/(630160)	EVEN	50663	SCTOR2	50734	
	STUPP	50750	///	/(630160)	EVEN	50751	STUPPS	51077	
	STUPR	51111	///	/(630160)	STUPRS	51230			
	S2SK1	51250	///	/(630160)	EVEN	51251	S2SK	52371	
	THETR	52405	THETAR	52445					
	VOL	52472	///	/(630160)	EVEN	52473	VOLSUB	53231	
	VSEC1	53245	///	/(630160)	VSEC	54110			
	VSTO	54124	///	/(630160)	EVEN	54125	VSTRSB	54505	
	XRR	54417	///	/(630160)	XRSUBB	55445			
	XRTHR1	55457	///	/(630160)	XRTHR	55540			
	YP	55554	EVEN	55555	YPSUB	55675			
	ZI	55737	///	/(630160)	ZISUB	56037			
*	AST	37746	///	/(630160)	EVEN	37747	ASTSUB	37401	
	RGI	37417	///	/(630160)	RGISUB	40034			

```
 10  MCH4    23550   ///    /(630016)  /TALK  /(042541)  EVEN    23551    MNCHN4  31067
     AIRSTA  31105   ///    /(630016)   AIRST   33403
     AIR     33430   ///    /(630016)   EVEN    33431    AIRSUB  34160
     CONV1   34700   ///    /(630016)   EVEN    34701    CONV    34560
     CSTR    34572   ///    /(630016)   EVEN    34573    CSTRSB  35514
     LOOK    35426   ///    /(630016)  /TALK  /(042541)  EVEN    35527    LOOKUP  36474
     LPTOSR  36525   ///    /(630016)   LPTO    40430
     MOOTNF  40444   ///    /(630016)   EVEN    40445    MOOTSB  41152
     PRTOUT  41213  /TALK   /(042541)  ///     /(630016)  OUTPUT  44344
     RBSF    44375   ///    /(630016)   RBSTSB  45115
     RBSUBA  45127   ///    /(630016)   RBSUB   46216
     SEG     46294   ///    /(630016)   EVEN    46295    SEGSUB  51753
     SETPH1  52002   ///    /(630016)   EVEN    52003    SETPH   54403
     SLOTSR  54423   ///    /(630016)   SLOT    56653
     RSPLN   56701   RSSPLN  60022
     SPLN1A  60231   SPLN1A  60256
     SPLN2A  60312   EVEN    60313    SPLN2A  60342
     SPLN3A  60364   EVEN    60367    SPLN3A  60416 *
     TISUBR  60434   ///    /(630016)   EVEN    60435    TISUB   61727
     VFPP    61755   ///    /(630016)   VFPPSB  62037

UNUSED CORE                  62054 THRU  63015
```

6.3.2 Computer System

The program is written in the FORTRAN IV computer language; however, one subroutine (SQRT) is a modified FAP version of the standard library routine which permits a negative argument. The program is designed for use on an IBM 7094 computer using an IBSYS, version 13, monitor system. In order to conserve core space the abridged output package is used by exercising the "ALTIO" system option.

6.4 Diagnostic Tools

Several intermediate, diagnostic print statements have been permanently built into the program to aid in program and data-error analysis. The complete COMMON regions are printed before program termination in the event of any convergence failure. In addition, several user-controlled dumps are available through the use of input card sets 48 and 49 as explained below.

Card Set 48 (Format (I2,1X,11E7.0))

Column	Name	Location	Definition
1-2	N		Card Set 48
4-10	CKDUMP(1)	MNCHN4	Time at which KDUMP(71) will start printing dumps 1, 2 and 3 (seconds)
11-17	CKDUMP(2)	MNCHN4	Time at which KDUMP(71) will stop printing dumps 1, 2 and 3 (seconds)
18-24	CKDUMP(3)	MNCHN4	Time at which KDUMP(72) will start printing dump 5 (seconds)
25-31	CKDUMP(4)	MNCHN4	Time at which KDUMP(72) will stop printing dump 5 (seconds)

Card Set 49 (Format (80I1))

Column	Name	Location	Definition
1	KDUMP(1)	MNCHN4	Fore-head and Aft-head calculations of TAUZ, RBZ, P, AP, ALP, WDOT and DW DOT
2	KDUMP(2)	SEGSUB	Cylindrical section reference plane calculations of TAUZ, RBZ, P, AP, ALP, W DOT and DW DOT
3	KDUMP(3)	AIBST	Start transient calculations of PD (III), DW DOT, WDOTD, AMACHD in cylindrical section

6.4 Diagnostic Tools (Continued)

Column	Name	Location	Definition
4	KDUMP(4)	SEGSUB	Anisotropic burn perimeters and burn rates.
5	KDUMP(5)	MNCHN4	COMMON and TBLK Data regions. This particular dump is turned off after printing unless it is being controlled by KDUMP(72).
6	KDUMP(6)	SEGSUB	Fuel area, port area and port perimeter for interpolation of each increment dividing plane
71	KDUMP(71)	MNCHN4 SEGSUB AIBST	This flag overrides KDUMP(1), KDUMP(2) and KDUMP(3) settings and prints these dumps according to the simulated burning times specified in CKDUMP(1) and CKDUMP(2).
72	KDUMP(72)	MNCHN4	This flag overrides KDUMP(5) and prints this dump according to the simulated burning times specified in CKDUMP(3) and CKDUMP(4).

The subroutine SPLN3A has also been included in the program to permit printing out the coefficients of the spline-fit curves used in subroutine CSTRSB. If these coefficients are desired the appropriate coding must be inserted following calls to SPLNIA which perform the curve fits.

6.5 Nomenclature

The following pages contain the nomenclature list which contains all input and output variables, all variables used in the document text and a significant number of important, internal program variables. In order to facilitate inclusion of additional variables in this third category the nomenclature lists have been punched on data cards. A copy of this nomenclature "deck" is provided with the program decks.

MATH SYMBOL	PROGRAM SYMBOL	UNIT	DESCRIPTION
A	A		GENERAL FLOW AREA OF A CROSS SECTION.
	A(I)	RADIANS	WORKING ARRAY STOREAGE LOCATION OF GRAIN DESIGN GEOMETRY ANGLES.
$\alpha_{01...05}$	AA(I) THRU AK(I)	RADIANS	REFERENCE PLANE GRAIN DESIGN GEOMETRY ANGLES.
	AAA	- - -	COEFFICIENT OF FIRST ORDER TERM IN THIRD DEGREE EQUATION IN SUBROUTINE P3SUB WHICH LOCATES THE POINT P3 ON THE OUTER ELLIPSE OF HEAD-END WITH WEB.
	AAAA	- - -	COEFFICIENT OF FIRST ORDER TERM IN THIRD DEGREE EQUATION IN SUBROUTINE STUPRS FOR THE INTERSECTING PLANES IN SUBROUTINE SCI.
	AAK(I)	- - -	STOREAGE ARRAY OF PRELIMINARY DESIGN CONSTANTS NO LONGER USED IN PROGRAM.
A_N	AAN	SQ IN	NOZZLE-AND SECTION BURN AREA.
NO	AANN	- - -	TEMPORARY VALUE OF NUMBER OF GRAIN CROSS SECTION SYMMETRICAL PARTS USED IN SUBROUTINE PT1AA.
	AAP	- - -	COEFFICIENT OF FIRST ORDER TERM IN SECOND DEGREE EQUATION X**2 +Y**2 + A*X + B*Y + D=0 USED TO APPROXIMATE ELLIPSE BETWEEN POINTS P2 AND P3 IN THE A PRIME PLANE FOR THE BLOCK 2A ANALYSIS OF THE HEAD-END WITH WEB IN SUBROUTINE SCI.

MATH SYMBOL	PROGRAM SYMBOL	UNIT	DESCRIPTION
	ABB	- - -	COEFFICIENT OF FIRST ORDER TERM IN SECOND DEGREE EQUATION X**2 + Y**2 + A*X + B*Y + D=0 USED TO APPROXIMATE ELLIPSE BETWEEN POINTS P2 AND P3 IN THE B PLANE FOR THE BLOCK 2A ANALYSIS OF THE HEAD-END WITH WEB IN SUBROUTINE SCI.
A_{Bcyl}	ABCYL	SQ IN	CYLINDRICAL SECTION TOTAL BURN AREA.
	ABHD	SQ IN	FORE-HEAD GEOMETRY TABLE BURN AREA. (DEPENDENT VARIABLE) INPUT ON SUBSET CARD NUMBER 40-5.
A_R	ABIGR	SQ IN	CROSS- SECTIONAL AREA OF WEB ZONE IN BLOCK 3 ANALYSIS OF HEAD-END WITH WEB. USED IN SUBROUTINE VOLSUB.
	ABN	SQ IN	AFT-HEAD GFOMETRY TABLE BURN AREA. (DEPENDENT VARIABLE). INPUT ON SUBSET CARD NUMBER 40-6.
	ABP		COEFFICIENT OF FIRST ORDER TERM IN SECOND DEGREE EQUATION X**2 + Y**2 + A*X + B*Y + D=0 USED TO APPROXIMATE ELLIPSE BETWEEN POINTS P1 AND P3 IN THE B PRIME PLANE FOR THE BLOCK 2A ANALYSIS OF THE HEAD-AND WITH WEB IN SUBROUTINE SCI.
A_{BSlot}	ABSLOT	SQ IN	TOTAL BURN AREA ON GRAIN SEGMENT FACES FOR SEGMENTED MOTORS.
	ABSLTA	SQ IN	BURN AREA ON SLOT AFT INTERFACE.
	ABSLTF	SQ IN	BURN AREA ON SLOT FORWARD INTERFACE.

MATH SYMBOL	PROGRAM SYMBOL	UNIT	DESCRIPTION
A_{BTot}	ABTOT	SQ IN	TOTAL MOTOR BURN AREA.
	ACC	SQ IN	INCREMENTAL AREA ON THE AFT FACE OF THE AFT END BURNING SURFACE. (FIGURE 5.20)
$\frac{a}{g_o}$	ACCEL	- G-S -	CURRENT TIME VALUE OF VEHICLE ACCELERATION OBTAINED FROM ACCELERATION-TIME CURVE IN SUBROUTINE AIBST.
	ACCELT	- G-S -	VEHICLE ACCELERATION-TIME CURVE DEPENDENT VARIABLE.
	ACGA	SQ IN	SECTOR AREA USED IN SUBROUTINE MSISUB TO OBTAIN POLAR MOMENT OF CROSS SECTION FOR HEAD-END WITH WEB.
	ACGB	SQ IN	SECTOR AREA USED IN SUBROUTINE MSISUB TO OBTAIN POLAR MOMENT OF CROSS SECTION FOR HEAD-END WITH WEB.
	ACOSTR	- - -	TEMPORARY STOREAGE LOCATION OF COSINE THETA-R FOR PLANE A IN SUBROUTINES STUPRS AND STUPPS IN THE BLOCK 1 ANALYSIS OF THE HEAD-END WITH WEB.
A_{EE}	AEE	SQ IN	AREA OF SECTOR IN SUBROUTINE AESUB FOR END SECTION ANALYSIS.
α_{ER}	AER	RADIANS	ANGLE BETWEEN MOTOR CENTER LINE AND TANGENT TO END SECTION ELLIPSE. DETERMINED IN SUBROUTINE ENDCSB.
	AFD	SQ IN	AREA OF SECTOR 3A OR 11A IN SUBROUTINE AFPSUB

MATH SYMBOL	PROGRAM SYMBOL	UNIT	DESCRIPTION
	AFF	SQ IN	CROSS SECTIONAL AREA OF INCREMENT DIVIDING PLANE IN SUBROUTINE SEGSUB.
	AFHI	SQ IN	CROSS SECTIONAL AREA OF UPSTREAM INCREMENT DIVIDING PLANE IN SUBROUTINE SEGSUB.
	AFP	SQ IN	CROSS SECTIONAL AREA OF REFERENCE PLANE IN SUBROUTINE AFPSUB.
	AFRPLA THRU AFRPLK	SQ IN	REFERENCE PLANE CROSS SECTIONAL PROPELLANT AREA IN SUBROUTINE MNCHN4. DETERMINED FROM INTEGRATION OF PERIMETER LENGTH AT EACH TIME INCREMENT.
	AFRPLX	SQ IN	REFERENCE PLANE X CROSS SECTIONAL PROPELLANT AREA IN SUBROUTINE MNCHN4.
	AFRPLY	SQ IN	REFERENCE PLANE Y CROSS SECTIONAL PROPELLANT AREA IN SUBROUTINE MNCHN4.
	AFX	SQ IN	REFERENCE PLANE X CROSS SECTIONAL PROPELLANT AREA IN SUBROUTINE SEGSUB.
	AFY	SQ IN	REFERENCE PLANE Y CROSS SECTIONAL PROPELLANT AREA IN SUBROUTINE SEGSUB.
A_H	AHH	SQ IN	HEAD-END SECTION BURN AREA.
A_{HO}	AHO	SQ IN	INITIAL AND PAST TIME VALUE OF HEAD-END SECTION BURN AREA.
I_{Bcyl}	AIBCYL	SLUG-SQ IN	CYLINDRICAL SECTION RECTANGULAR MOMENT OF INERTIA DETERMINED IN SUBROUTINE SEGSUB.

MATH SYMBOL	PROGRAM SYMBOL	UNIT	DESCRIPTION
A_{IG}	AIG	SQ IN	IGNITER OPENING SURFACE AREA DETERMINED IN SUBROUTINE AIGSUB.
	AINC	IN	TEMPORARY STOREAGE LOCATION OF CURRENT INCREMENT DIVIDING PLANE LOCATION MEASURED FROM FORWARD TANGENT PLANE.
INCA THRU INCK	AINCA THRU AINCK	IN	REFERENCE PLANE LOCATION MEASURED FROM FORWARD TANGENT PLANE. INPUT ON CARD SET NUMBER 2.
	AINCN	IN	NOZZLE SECTION REFERENCE PLANE OR AFT TANGENT PLAN LOCATION MEASURED FROM FORWARD TANGENT PLANE.
NINCPL	AINCPL	IN	INCREMENT PLANE LOCATION MEASURED FROM FORWARD TANGENT PLANE WHERE ANISOTROPIC BURN RATE COEFFICIENT IS TO BE EVALUATED DURING START TRANSIENT INTERVAL. INPUT ON CARD SET NUMBER 44.
	AINCW	IN	WORKING INCREMENT DIVIDING PLANE LOCATION IN SUBROUTINE SEGSUB.
	AINCX	IN	REFERENCE PLANE X LOCATION IN SUBROUTINE SEGSUB.
	AINCY	IN	REFERENCE PLANE Y LOCATION IN SUBROUTINE SEGSUB.
I_{Pcyl}	AIPCYL	IN**4	CYLINDRICAL SECTION POLAR MOMENT OF INERTIA OF CROSS SECTION IN SUBROUTINE SEGSUB.
ISP_{wb}	AISPWB	SEC	WEB-TIME SPECIFIC IMPULSE.
I_T	AIT	SEC	TOTAL IMPULSE

MATH SYMBOL	PROGRAM SYMBOL	UNIT	DESCRIPTION
i_{Tst}	AITST	SEC	START TRANSIENT INTERVAL TOTAL IMPULSE. WHEN THIS VALUE IS INPUT ON CARD SET NUMBER 44, THE START TRANSIENT INTERVAL WILL BE TERMINATED WHEN THE TOTAL IMPULSE, AIT, IS GREATER THAN OR EQUAL TO AITST IN SUBROUTINE MNCHN4.
J_{BB}	AJBB	SLUG-SQ IN	MOTOR PITCH AXIS MOMENT OF INERTIA ABOUT CG GRAIN.
J_{BH}	AJBH	IN**4	HEAD-END SECTION RECTANGULAR MOMENT OF INERTIA ABOUT FORWARD TANGENT PLANE FOR INCREMENTAL VOLUMES. DETERMINED IN SUBROUTINE PT1AA.
J_{BHed}	AJBHED	SLUG-SQ IN	HEAD-END SECTION TOTAL RECTANGULAR MOMENT OF INERTIA ABOUT FORWARD TANGENT PLANE.
J_{BHew}	AJBHEW	SLUG-SQ IN	RECTANGULAR MOMENT OF INERTIA OF HEAD-END WITH WEB ABOUT FORWARD TANGENT PLANE. DETERMINED IN SUBROUTINE MNCHN4
	AJBHN	SLUG-SQ IN	INTERMEDIATE VALUE OF HEAD-END WITH WEB RECTANGULAR MOMENT OF INERTIA DETERMINED IN THE BLOCK 2A ANALYSIS IN SUBROUTINE SCTOR1.
J_{BHO}	AJBHO	SLUG-SQ IN	HEAD-END SECTION INITIAL RECTANGULAR MOMENT OF INERTIA.
J_{BN}	AJBN	IN**4	NOZZLE-END SECTION RECTANGULAR MOMENT OF INERTIA ABOUT AFT TANGENT PLANE FOR INCREMENTAL VOLUMES. DETERMINED IN SUBROUTINE PT1AA.
J_{BNoz}	AJBNOZ	SLUG-SQ IN	NOZZLE-END SECTION RECTANGULAR MOMENT OF INERTIA ABOUT AFT TANGENT PLANE.

MATH SYMBOL	PROGRAM SYMBOL	UNIT	DESCRIPTION
J_{PH}	AJPH	IN**4	HEAD-END SECTION POLAR MOMENT OF INERTIA ABOUT ROLL AXIS FOR INCREMENTAL THIN SHELLS. DETERMINED IN SUBROUTINE PT1AA.
J_{PHad}	AJPHED	SLUG-SQ IN	HEAD-END SECTION TOTAL POLAR MOMENT OF INERTIA ABOUT ROLL AXIS.
J_{PHew}	AJPHEW	SLUG-SQ IN	POLAR MOMENT OF INERTIA OF HEAD-END WITH WEB ABOUT ROLL AXIS. DETERMINED IN SUBROUTINE MNCHN4.
	AJPHN	IN**4	INTERMEDIATE VALUE OF HEAD-END WITH WEB POLAR MOMENT OF INERTIA DETERMINED IN THE BLOCK 2A ANALYSIS IN SUBROUTINE SCTOR1.
J_{PHO}	AJPHO	SLUG-SQ IN	HEAD-END SECTION INITIAL POLAR MOMENT OF INERTIA.
J_{PN}	AJPN	IN**4	NOZZLE-END SECTION POLAR MOMENT OF INERTIA ABOUT ROLL AXIS FOR INCREMENTAL THIN SHELLS. DETERMINED IN SUBROUTINE PT1AA.
J_{PNoz}	AJPNOZ	SLUG-SQ IN	NOZZLE-END SECTION TOTAL POLAR MOMENT OF INERTIA ABOUT ROLL AXIS.
	AJPP	IN**4	INTERMEDIATE VALUE OF POLAR MOMENT OF INERTIA OF CROSS SECTION OF INCREMENTAL AREAS IN SUBROUTINE PT1AA.
	AJPX	SLUG-SQ IN	INTERMEDIATE VALUE OF POLAR MOMENT OF INERTIA OF CROSS SECTION OF INCREMENTAL AREAS IN SUBROUTINE PT1AA.
	AJSTB	SLUG-SQ IN	INITIAL VALUE OF HEAD-END WITH WEB RECTANGULAR MOMENT OF INERTIA. DETERMINED IN SUBROUTINE ASTSUB.

MATH SYMBOL	PROGRAM SYMBOL	UNIT	DESCRIPTION
	AJSTP	SLUG-SQ IN	INITIAL VALUE OF HEAD-END WITH WEB POLAR MOMENT OF INERTIA. DETERMINED IN SUBROUTINE ASTSUB.
K	AK	- - -	INPUT VALUE WHICH DETERMINES DISTANCE BETWEEN PLANES FOR THE HEAD-END WEB ANALYSIS AND FOR THE END SECTION ANALYSIS. INPUT ON CARD SET NUMBER 29.
KEROS	AKEROS	IN/SEC	NOZZLE THROAT EROSION RATE. INPUT ON CARD SET NUMBER 31.
KG1 THRU KG5	AKG1 THRU AKG5	- - -	CRITICAL MASS VELOCITY (G C R) PER UNIT AREA EQUATION CONSTANTS. INPUT ON CARD SET NUMBER 32.
K_{GY}	AKGY	SQ IN	RADIUS OF GYRATION OF CYLINDRICAL SECTION INCREMENTAL CROSS SECTIONS. DETERMINED IN SUBROUTINE PT1AA.
	AKGYMI	SQ IN	RADIUS OF GYRATION OF UPSTREAM CYLINDRICAL SECTION INCREMENTAL CROSS SECTIONS. INITIALIZED IN SUBROUTINE SEGSUB.
	AKGYPA THRU AKGYPK	IN**4	REFERENCE PLANE GEOMETRY TABLE RADIUS OF GYRATION OF CROSS SECTION (DEPENDENT VARIABLE). THIS VARIABLE APPEARS ON SUBSET CARD NUMBER 40-7 ONLY IF THE MOMENT OF INERTIA OPTION (KMOICG ON CARD SET NUMBER 41) HAS NOT BEEN SUPPRESSED FROM A PRIOR CASE IN WHICH THE PUNCH OPTION (PUNTAB ON CARD SET NUMBER 40) HAS BEEN SELECTED.
	AKGYX	SQ IN	RADIUS OF GYRATION OF REFERENCE PLANE X IN SUBROUTINE SEGSUB.

MATH SYMBOL	PROGRAM SYMBOL	UNIT	DESCRIPTION
	AKGYY	SQ IN	RADIUS OF GYRATION OF REFERENCE PLANE Y IN SUBROUTINE SEGSUB.
	AKINS	- - -	FRACTION OF SLIVER THAT IS INERT. INPUT ON CARD SET NUMBER 43.
KK	AKK		ADJUSTING FACTOR USED IN THE HEAD-END WEB BLOCK 2 ANALYSIS TO DETERMINE DISTANCE BETWEEN PLANES.
KR1 THRU KR39	AKR1 THRU AKR39		BURNING RATE EQUATION CONSTANTS. INPUT ON CARD SET NUMBERS 34, 35, 36 AND 37.
	AKRFB	SQ IN	INTERMEDIATE RADIUS OF GYRATION VALUE IN SUBROUTINE MNCHN4 FOR HEAD-END WITH WEB.
KRH	AKRH	- - -	HEAD-END SECTION BURN RATE COEFFICIENT. USUAL VALUE IS THE SAME AS THE CYLINDRICAL SECTION STEADY STATE BURN RATE COEFFICIENT. INPUT ON CARD SET NUMBER 44.
KRN	AKRN	- - -	NOZZLE END SECTION BURN RATE COEFFICIENT. USUAL VALUE IS THE SAME AS THE CYLINDRICAL SECTION STEADY STATE BURN RATE COEFFICIENT. INPUT ON CARD SET NUMBER 44.
	AKRTAU	- - -	START TRANSIENT BURN RATE COEFFICIENT TABLE DEPENDENT VARIABLE. INPUT FOLLOWING CARD SET NUMBER 45.
KSLOT	AKSLOT(I)	- - -	SLOT BURNING RATE EQUATION COEFFICIENT. INPUT ON CARD SET NUMBER 37.

MATH SYMBOL	PROGRAM SYMBOL	UNIT	DESCRIPTION
	AKRST	- - -	ANISOTROPIC PROPELLANT BURNING RATE EQUATION COEFFICIENT DURING THE START TRANSIENT AND TAIL-OFF INTERVALS.
KU1 THRU KU5	AKU1 THRU AKU5	- - -	CRITICAL GAS VELOCITY (U C R) EQUATION CONSTANTS. INPUT ON CARD SET NUMBER 33.
L_A	ALA	IN	INITIAL LENGTH OF SECTOR 2. DETERMINED IN SUBROUTINE PLNCNS (FIGURE 5.24).
LAA THRU LAK	ALAA THRU ALAK	IN	PERIMETER LENTH OF SECTOR LA FOR A REFERENCE PLANE. INPUT ON CARD SET NUMBER 20.
λ	ALAMDA	RADIANS	ANGLE BETWEEN MOTOR AXIS AND A LINE FROM CENTER OF TORUS GENERATING CIRCLE TO OUTSIDE ELEMENT OF SURFACE INCREMENT ON TOROIDAL END AREA IN ZONE B OF END SECTION STRAIGH THROUGH GRAIN. (FIGURE 5.23)
λ_{min}	ALAMIN	RADIANS	ANGLE BETWEEN MOTOR AXIS AND A LINE FROM CENTER OF TORUS GENERATING CIRCLE TO INSIDE ELEMENT OF SURFACE INCREMENT ON TOROIDAL END AREA IN ZONE B OF END SECTION STRAIGHT THROUGH GRAIN. (FIGURE 5.23)
L_B	ALB		INITIAL LENGTH OF SECTOR 4. DETERMINED IN SUBROUTINE PLNCNS (FIGURE 5.24)
LBA THRU LBK	ALBA THRU ALBK	IN	PERIMETER LENGTH OF SECTOR LB FOR A REFERENCE PLANE. INPUT ON CARD SET NUMBER 21.
L_C	ALC	IN	INITIAL LENGTH OF SECTOR 6. DETERMINED IN SUBROUTINE PLNCNS (FIGURE 5.24).

MATH SYMBOL	PROGRAM SYMBOL	UNIT	DESCRIPTION
L_D	ALD	IN	INITIAL LENGTH OF SECTOR 12. DETERMINED IN SUBROUTINE PLNCNS (FIGURE 5.24).
L_E	ALE	IN	INITIAL LENGTH OF SECTOR 10. DETERMINED IN SUBROUTINE PLNCNS (FIGURE 5.24).
LEA THRU LEK	ALEA THRU ALEK	IN	PERIMETER LENGTH OF SECTOR LE FOR A REFERENCE PLANE. INPUT ON CARD SET NUMBER 22.
L_P	ALP	IN	TOTAL PERIMETER LENGTH OF CURRENT INCREMENT DIVIDING PLANE CROSS SECTION FOR A SEGMENT.
	ALPHI	IN	TOTAL PERIMETER LENGTH OF UPSTREAM INCREMENT DIVIDING PLANE CROSS SECTION FOR A SEGMENT.
	ALPPLA THRU ALPPLK	IN	REFERENCE PLANE GEOMETRY TABLE PORT PERIMETER (DEPENDENT VARIABLE). INPUT ON SUBSET CARD NUMBER 40-7.
L_Q	ALQ	IN	ARC LENGTH ON PSUEDOELLIPSOID. DETERMINED IN SUBROUTINE SCTOR1 (FIGURE 5.4)
L_R	ALR	IN	LENGTH TO A POINT ON BURNING SURFACE PERIMETER IN ANY SECTOR AT THICKNESS TAU MEASURED ALONG PERIMETER FROM END OF SECTOR NEAREST MOTOR AXIS. DETERMINED IN SUBROUTINE ALRSUB. (FIGURE 5.22)
$L_{R_{max}}$	ALRMAX	IN	LENGTH OF PART OF BURNING SURFACE PERIMETER IN ANY ZONE AT THICKNESS TAU MEASURED FROM END OF SECTOR NEAREST MOTOR AXIS TO END OF SECTOR OR ZONE, WHICH EVER IS SMALLER. DETERMINED IN SUBROUTINE AESUB. (FIGURE 5.21).

MATH SYMBOL	PROGRAM SYMBOL	UNIT	DESCRIPTION
L_{RI}	ALRI	IN	LENGTH TO THE LOWEST POINT ON BURNING SURFACE PERIMETER IN ANY ZONE AT THICKNESS TAU. MEASURED ALONG PERIMETER FROM END OF SECTOR NEAREST MOTOR AXIS DETERMINED IN SUBROUTINE AESUB (FIGURE 5.21)
L_{RS}	ALRS	IN	LENGTH OF CHORD DETERMINED IN SUBROUTINE ARSSUB. (FIGURE 5.22).
L_X	ALSUBX	IN	LENGTH OF A SECTOR AT THICKNESS TAU DETERMINED IN SUBROUTINE AFPSUB (FIGURE 5.21).
L_{TA}	ALTA	IN	ARC LENGTH BETWEEN POINTS PRA AND PSA (FIGURE 5.2)
L_{TB}	ALTB	IN	ARC LENGTH BETWEEN POINTS PRB AND PSB (FIGURE 5.2)
LS1A THRU LS1K	ALS1A THRU ALS1K	IN	LENGTH FROM WEB TO INNER GRAIN POINT OF REFERENCE PLANE. INPUT ON CARD SET NUMBER 11.
LS2A THRU LS2K	ALS2A THRU ALS2K	IN	LENGTH FROM WEB TO OUTER GRAIN POINT OF REFERENCE PLANE. INPUT ON CARD SET NUMBER 12
AL_7	AL7	IN	PERIMETER LENGTH OF ANISOTROPIC PROPELLANT IN SECTOR 7 DURING TAIL-OFF.
AL_8	AL8	IN	PERIMETER LENGTH OF ANISOTROPIC PROPELLANT IN SECTOR 8 DURING TAIL-OFF.
MW	AMW	- - -	PRESENT TIME VALUE OF PROPELLANT GAS MOLECULAR WEIGHT.

MATH SYMBOL	PROGRAM SYMBOL	UNIT	DESCRIPTION
	AMWG	- - -	TABULAR INPUT VALUE OF PROPELLANT GAS MOLECULAR WEIGHT.
NITW	ANITW	- - -	NUMBER OF TIME INCREMENTS BEFORE FIRST WEB BURNOUT. INPUT ON CARD SET NUMBER 43.
NN	ANN	- - -	NUMBER OF NOZZLES. INPUT ON CARD SET NUMBER 31.
	ANGLE	RADIANS	CENTRAL ANGLE THAT DEFINES INTERSECTION OF ISOTROPIC PROPELLANT ARC LENGTH WITH CASE WALL IN SECTOR 7 DURING MOTOR TAIL-OFF.
	ANI	- - -	FLOATING POINT NUMBER OF TOTAL INCREMENT DIVIDING PLANES.
NOA THRU NOK	ANOA THRU ANOK	- - -	REFERENCE PLANE NUMBER OF GRAIN CROSS SECTION SYMMETRICAL PARTS. INPUT ON CARD SET NUMBER 3.
N2	AN2	DEGREES	NOZZLE EXPANSION CONE HALF-ANGLE. INPUT ON CARD SET NUMBER 31.
α_{01}	AOA(1) THRU AOK(1)	DEGREES	REFERENCE PLANE ANGLE OF SLOPE LAA WHICH DEFINES INITIAL GRAIN GEOMETRY. INPUT ON CARD SET NUMBER 6.
α_{02}	AOA(2) THRU AOK(2)	DEGREES	REFERENCE PLANE ANGLE OF SLOPE LBA WHICH DEFINES INITIAL GRAIN GEOMETRY. INPUT ON CARD SET NUMBER 7.
α_{03}	AOA(3) THRU AOK(3)	DEGREES	REFERENCE PLANE ANGLE OF SLOPE LCA WHICH DEFINES INITIAL GRAIN GEOMETRY. INPUT ON CARD SET NUMBER 8.

MATH SYMBOL	PROGRAM SYMBOL	UNIT	DESCRIPTION
α_{04}	AOA(4) THRU AOK(4)	DEGREES	REFERENCE PLANE ANGLE OF SLOPE LDA WHICH DEFINES INITIAL GRAIN GEOMETRY. INPUT ON CARD SET NUMBER 9.
α_{05}	AOA(5) THRU AOK(5)	DEGREES	REFERENCE PLANE ANGLE OF SLOPE LEA WHICH DEFINES INITIAL GRAIN GEOMETRY. INPUT ON CARD SET NUMBER 10.
AOE	AOE	IN	LENGTH OF SEMI-MAJOR AXIS OF INNER ELLIPSE (FIGURE 5.7)
α_{OHmax}	AOHM	DEGREES	ANGLE BETWEEN TANGENT TO FORE-HEAD ELLIPSE AND MOTOR CENTERLINE. INPUT ON CARD SET NUMBER 29.
α_{ONmax}	AONM	DEGREES	ANGLE BETWEEN TANGENT TO AFT-HEAD ELLIPSE AND MOTOR CENTERLINE. INPUT ON CARD SET NUMBER 30.
A_P	AP	SQ IN	PORT AREA OF CURRENT INCREMENT DIVIDING PLANE FOR A SEGMENT.
	APHI	SQ IN	PORT AREA OF UPSTREAM INCREMENT DIVIDING PLANE FOR A SEGMENT.
	APORTA THRU APORTK		INITIAL PORT AREA OF A REFERENCE PLANE. INPUT ON SUBSET CARD NUMBERS 40-4.
A_R	AR	SQ IN	AREA OF SECTOR BCD IN ZONE A OF THE AFT END BURNING SURFACE (FIGURE 5.22)
α_{rc0}	ARC0	RADIANS	ANGLE BETWEEN Y-AXIS AND NORMAL LINE THROUGH P0 (FIGURE 5.4). USED IN SUBROUTINE SCTOR1 FOR THE HEAD-END WITH WEB BLOCK 2A ANAL'SIS

MATH SYMBOL	PROGRAM SYMBOL	UNIT	DESCRIPTION
α_{rc1}	ARC1	RADIANS	ANGLE BETWEEN Y-AXIS AND NORMAL LINE THROUGH P1 (FIGURE 5.4). USED IN SUBROUTINE SCTOR1 FOR THE HEAD-END WITH WEB BLOCK 2A ANALYSIS
A_{RO}	ARO	SQ IN	AREA OF SECTOR AEF IN ZONE A OF THE AFT END BURNING SURFACE (FIGURE 5.22)
	ASE	SQ IN	END SECTION BURN AREA. COMPUTED IN SUBROUTINE ASESUB.
	ASI	SQ IN	BURNING SURFACE AREA OF AN INCREMENTAL STRIP DETERMINED IN THE BLOCK 2A ANALYSIS OF THE HEAD END WITH WEB IN SUBROUTINE SCI (FIGURE 5.4)
A_{Slvr}	ASLVR	SQ IN	INCREMENT DIVIDING PLANE INERT SLIVER AREA FOR ONE GRAIN CROSS SECTION SYMMETRICAL PART.
A_T	AT	SQ IN	EXHAUST NOZZLE THROAT AREA.
A_{TO}	ATO	SQ IN	AREA IN ZONE A OF THE AFT END BURNING SURFACE BETWEEN THE CHORD LRS AND THE CIRCULAR ARC LR (FIGURE 5.22)
A_{TSlot}	ATSLOT	SQ IN	TOTAL BURNING SURFACE AREA OF ALL SLOTS.
A_{TT}	ATT	SQ IN	THE POSITIVE OR NEGATIVE VALUE OF ATO DEPENDING ON RT. NEGATIVE IF RT IS NEGATIVE AND POSITIVE IF RT IS POSITIVE.
	AWE	SQ IN	TOTAL BURNING SURFACE AREA OF WEB ZONE (SECTOR 8 PLUS AFT FACE) OF THE AFT END BURNING SURFACE AT THICKNESS TAU DETERMINED IN SUBROUTINE AWESUB.

MATH SYMBOL	PROGRAM SYMBOL	UNIT	DESCRIPTION
BE	BE	IN	LENGTH OF SEMI-MINOR AXIS OF END SECTION. FORE-HEAD (H) OR AFT-HEAD (N).
β_H	BH	- - -	FORE-HEAD CASE ELLIPSE RATIO. INPUT ON CARD SET NUMBER 29.
β_N	BN	- - -	AFT-HEAD ELLIPSE RATIO. INPUT ON CARD SET NUMBER 30.
BOE	BOE	IN	LENGTH OF SEMI-MINOR AXIS OF INNER ELLIPSE OF HEAD-END WITH WEB.
	BRNOUT	- - -	PROGRAM CONTROL FLAG FOR WEB BURNOUT.
β_{OE}	BTAOE	- - -	RATIO OF HEAD END WEB ELLIPSE AXIS NORMAL TO MOTOR AXIS TO ELLIPSE AXIS PARALLEL WITH MOTOR AXIS. INPUT ON CARD SET NUMBER 29.
	BVX	RADIANS	ANGLE OF INERT SLIVER IN SECTOR 7.
	BVXX	RADIANS	ANGLE OF INERT SLIVER IN SECTOR 6.
	BV2	RADIANS	ANGLE THAT DEFINES PERIMETER LENGTH OF PROPELLANT IN SECTOR 7.
	BV2P	RADIANS	ANGLE THAT DEFINES PERIMETER LENGTH OF ISOTROPIC PROPELLANT ONLY IN SECTOR 7.
β_{71max}	B71M	RADIANS	GEOMETRY CONSTANT DETERMINED IN SUBROUTINE PLNCNS (FIGURE 5.25)
β_{72max}	B72M	RADIANS	GEOMETRY CONSTANT DETERMINED IN SUBROUTINE PLNCNS (FIGURE 5.25)

MATH SYMBOL	PROGRAM SYMBOL	UNIT	DESCRIPTION
β_{91max}	B91M	RADIANS	GEOMETRY CONSTANT DETERMINED IN SUBROUTINE PLNCNS (FIGURE 5.25)
β_{92max}	B92M	RADIANS	GEOMETRY CONSTANT DETERMINED IN SUBROUTINE PLNCNS (FIGURE 5.25)
	CAE CBE CCCE CCVE CDCE CDVE CECE CEVE	- - -	CONSTANTS USED IN CALCULATION OF COEFFICIENT FOR FOURTH-DEGREE EQUATION FOR SOLUTION OF INTERSECTION OF TOROIDAL SURFACE AND END SECTION ELLIPSE. DETERMINED IN SUBROUTINE ENDCSB.
C_{F0}	CFO	- - -	THRUST COEFFICIENT DETERMINED FROM MOMENTUM EXCHANGE ONLY WITHOUT EXPANSION FROM EXIT PRESSURE TO AMBIENT PRESSURE.
	CKDUMP(1)	SEC	LOWER TIME LIMIT FOR A DIAGNOSTIC PRINT IN SUBROUTINE MNCHN4
	CKDUMP(2)	SEC	UPPER TIME LIMIT FOR DIAGNOSTIC PRINT IN SUBROUTINE MNCHN4.
	CM	- - -	NOZZLE EFFICIENCY. INPUT ON CARD SET NUMBER 31.
	CMPTME	- - -	STORAGE ARRAY FOR INTERNAL CLOCK PRINTOUT.
	COM	- - -	BLOCK NAME IN COMMON (DIMENSIONED 6600) FOR VARIABLE STORAGE

MATH SYMBOL	PROGRAM SYMBOL	UNIT	DESCRIPTION
CRP	CRP	- - -	CONVERGENCE VALUE FOR NON-STEADY FLOW DISCHARGE PRESSURE AT EXIT OF EACH MASS ADDITION REGION. INPUT ON CARD SET NUMBER 41.
CRT	CRT	- - -	CONVERGENCE VALUE FOR NON-STEADY FLOW DISCHARGE GAS TEMPERATURE AT EXIT OF EACH MASS ADDITION REGION. INPUT ON CARD SET NUMBER 41.
CRW	CRW	- - -	CONVERGENCE VALUE FOR NON-STEADY FLOW TO COMPARE FLOW RATES AT EXIT OF GRAIN TO THAT WHICH CAN BE DISCHARGED THROUGH NOZZLE BOTH AT SAME TOTAL PRESSURE. INPUT ON CARD SET NUMBER 41.
C*	CSTAR	FT/SEC	PROPELLANT GAS CHARACTERISTICS VELOCITY. INPUT ON CARD SET NUMBER 38.

MATH SYMBOL	PROGRAM SYMBOL	UNIT	DESCRIPTION
	CSTR	FT/SEC	TABULAR INPUT VALUE OF CHARACTERISTIC VELOCITY FOR PROPELLANT GAS (DEPENDENT VARIABLE). INPUT FOLLOWING CARD SET NUMBER 31.
D_E	DE	IN	NOZZLE EXIT DIAMETER. INPUT ON CARD SET NUMBER 31.
ρ_f	DELF	LB/CU IN	PROPELLANT DENSITY. INPUT ON CARD SET NUMBER 36.
ΔL	DELL	IN	INCREMENTAL PERIMETER LENGTH USED IN APPROXIMATE INTEGRATION OF SURFACE AREAS (FIGURE 5.23)
ΔL_o	DELLO	IN	DISTANCE BETWEEN POINTS P0 AND P1 USED TO OBTAIN SURFACE AREA OF BLOCK 1 ANALYSIS OF HEAD-END WITH WEB.
ΔR	DELR	IN	DISTANCE BETWEEN POINTS P0 AND P1 USED TO OBTAIN SURFACE AREA OF BLOCK 2 B AND VOLUME IN BLOCK 3 OF HEAD-END WITH WEB.
Δt	DELT	SEC	CURRENT VALUE OF TIME INCREMENT
ρ	DELTA	LB/CU IN	PROPELLANT GAS DENSITY.
Δt_{SS}	DELTSS	SEC	FIXED TIME INCREMENT FOR STEADY STATE. INPUT ON CARD SET NUMBER 42.
Δt_{ST}	DELTST	SEC	FIXED TIME INCREMENT USED DURING START TRANSIENT. INPUT ON CARD SET NUMBER 42.
Δt_{TO}	DELTTO	SEC	FIXED TIME INCREMENT FOR TAIL-OFF OR SHUTDOWN. INPUT ON CARD SET NUMBER 42.

MATH SYMBOL	PROGRAM SYMBOL	UNIT	DESCRIPTION
ΔZ	DELZ	IN	MAXIMUM LENGTH OF MASS ADDITION REGIONS IN GRAIN SEGMENTS. INPUT ON CARD SET NUMBER ONE. AT TIME=0. AN INCREMENT DIVIDING PLANE WILL BE PLACED EVERY DELZ INCHES DOWN EACH GRAIN SEGMENT BEGINNING AT THE FORWARD TANGENT PLANE OR AT THE AFT FACE OF A SLOT AND TERMINATING AT THE AFT TANGENT PLANE OR THE FORWARD FACE OF A SLOT.
D_{E1}	DE1	IN	CASE OPENING DIAMETER (H) FORE-HEAD ORIN) AFT-HEAD. INPUT ON CARD SETS 29 AND 30.
D_{H1}	DH1	IN	FORE-HEAD CASE OPENING DIAMETER. INPUT ON CARD SET NUMBER 29.
$\frac{\Delta L}{R_f}$	DLRF	- - -	DELTA-L OVER RF, WHERE DELTA-L = INCREMENT SIZE USED FOR THE BURNING SURFACE AREA CALCULATIONS, MEASURED ALONG THE INTERNAL PERIMETER IN THE ADJACENT REFERENCE PLANE. INPUT ON CARD SET NUMBER 30.
D_{N1}	DN1	IN	AFT-HEAD CASE OPENING DIAMETER. INPUT ON CARD NUMBER 30.
	DO3	IN	DISTANCE BETWEEN POINTS P0 AND P3. DETERMINED IN SUBROUTINE SCI FOR HEAD-END WITH WEB ANALYSIS
ΔP_o	DPO	PSIA	TOTAL PRESSURE LOSS IN NOZZLE END SECTION FROM MASS ADDITION.
	DPR	IN	DISTANCE BETWEEN POINTS P0A AND P0B. DETERMINED IN SUBROUTINE SCI FOR HEAD-END WITH WEB ANALYSIS.

MATH SYMBOL	PROGRAM SYMBOL	UNIT	DESCRIPTION
	DPS	IN	DISTANCE BETWEEN POINTS POA AND POB. DETERMINED IN SUBROUTINE SCI FOR HEAD-END WITH WEB ANALYSIS
$\frac{\Delta R_V}{R_f}$	DRVRF	-	DELTA-RV OVER DELTA-RF, WHERE DELTA-RV = OUTSIDE PROPELLANT RADIUS OF ADJACENT REFERENCE PLANE. INPUT ON CARD SET NUMBER 30.
D_T	DT	IN	INITIAL NOZZLE THROAT DIAMETER. INPUT ON CARD SET NUMBER 31.
	DS	IN	DISTANCE BETWEEN POINTS P0 AND P1 WHEN P1 IS LOCATED ON THE CASE ELLIPSE (FIGURE 5.6-2) DETERMINED IN SUBROUTINE S2SK FOR HEAD-END WITH WEB ANALYSIS
$\Delta\tau$	DTAUA THRU DTAUK	IN	INCREMENTAL SIZE OF REFERENCE PLANE DISTANCE BURNED TO EVALUATE GEOMETRY TABLES. INPUT ON CARD SET NUMBER 27.
$\Delta\tau_w$	DTAUWA THRU DTAUWK		INCREMENTAL SIZE OF REFERENCE PLANE DISTANCE BURNED BEYOND WEB THICKNESS TAUW TO EVALUATE GEOMETRY TABLES. INPUT ON CARD SET NUMBER 28.
	DTTOR	- - -	RATIO OF TIME INCREMENT SIZE DURING TAIL-OFF TO NOMINAL TIME INCREMENT SIZE BEFORE FIRST WEB BURNOUT. INPUT ON CARD SET NUMBER 43.
	DTWBR	- - -	RATIO OF TIME INCREMENT SIZE DURING WEB BURNOUT TO NOMINAL TIME INCREMENT SIZE BEFORE FIRST WEB BURNOUT. INPUT ON CARD SET NUMBER 43.
ΔV	DV	CU IN	INCREMENTAL PROPELLANT VOLUME USED TO DETERMINE INITIAL PROPELLANT VOLUME IN END SECTIONS IN SUBROUTINE ASESUB.

MATH SYMBOL	PROGRAM SYMBOL	UNIT	DESCRIPTION
$\frac{dV}{dt}$	DVDT	CU IN/SEC	RATE OF CHANGE OF SLOT VOLUME WITH RESPECT TO TIME. COMPUTED IN SR SEGSUB FROM TSLOT AND RSLOT.
$d\dot{W}$	DWDOT	LB/SEC	PROPELLANT GAS GENERATED IN SEGMENT OR MASS ADDITION REGION.
$\frac{dW}{dt}$	DWDT	LB/SEC	STORED PROPELLANT GAS IN SEGMENT OR CONTROL VOLUME.
$\frac{dW_{slot}}{dt}$	DWDTS	LB/SEC	MASS OF STORED GAS IN A SLOT FOR ONE COMPUTING INTERVAL.
$d\dot{W}_s$	DWSLOT	LB/SEC	MASS FLOW GENERATED IN A SLOT.
ϵ_C	EC	LB/SQ IN	AVERAGE VALUE OF CASE MODULUS OF ELASTICITY INPUT ON CARD SET NUMBER 46.
ϵ_G	EG	LB/SQ IN	GRAIN MODULUS OF ELASTICITY. INPUT ON CARD SET NUMBER 46.
ϵ_{CA}	EPCA	- - -	MEASURED CASE STRAIN AT FORWARD TANGENT PLANE. INPUT FOLLOWING CARD SET NUMBER 46.
ϵ_{CN}	EPCN	- - -	MEASURED CASE STRAIN AT AFT TANGENT PLANE. INPUT FOLLOWING CARD SET NUMBER 46.
η_1	ETA1	RADIANS	ANGLE FROM R5 RADIUS POINT THAT DEFINES INTERSECTION OF ANISOTROPIC PROPELLANT WITH CASE WALL IN SECTOR 7 DURING MOTOR TAIL-OFF.
η_2	ETA2	RADIANS	ANGLE FROM R5 RADIUS POINT THAT DEFINES INTERSECTION OF ANISOTROPIC PROPELLANT WITH ISOTROPIC PROPELLANT IN SECTOR 7 DURING MOTOR TAIL-OFF.

MATH SYMBOL	PROGRAM SYMBOL	UNIT	DESCRIPTION
η_{11}	ETA11	RADIANS	CENTRAL ANGLE THAT DEFINES INTERSECTION OF ANISOTROPIC PROPELLANT WITH CASE WALL IN SECTOR 7 DURING MOTOR TAIL-OFF.
η_{22}	ETA22	RADIANS	CENTRAL ANGLE THAT DEFINES INTERSECTION OF ANISOTROPIC PROPELLANT WITH ISOTROPIC PROPELLANT IN SECTOR 7 DURING MOTOR TAIL-OFF.
γ	GAMA	- - -	PROPELLANT GAS SPECIFIC HEAT RATIO. INPUT ON CARD SET NUMBER 38.
γ_G	GAMAG	- - -	TABULAR INPUT VALUE OF PROPELLANT GAS SPECIFIC HEAT RATIO (DEPENDENT VARIABLE). INPUT FOLLOWING CARD SET NUMBER 39.
γ_R	GAMAR	RADIANS	ANGLE BETWEEN RADIAL VECTOR RA AND BISECTOR OF PRIMARY OR SECONDARY PROPELLANT TIP. (FIGURE 5.23)
γ_{R0}	GAMAR0	RADIANS	ANGLE BETWEEN RADIAL VECTOR RA0 AND BISECTOR OF PRIMARY OR SECONDARY PROPELLANT TIP. (FIGURE 5.22)
γ_T	GAMAT	RADIANS	ANGLE SUBTENDED AT CENTER OF RADIUS RT BY CHORD LRS (FIGURE 5.20 AND 5.21)
γ_1	GAMA1	RADIANS	ANGLE BETWEEN NORMAL LINE TO PERIMETER OF GRAIN CONFIGURATION AND NORMAL LINE TO THE LINE SEGMENT RAT (FIGURE 5.6) DETERMINED IN SUBROUTINE GAMSUB
γ_2	GAMA2	RADIANS	ANGLE BETWEEN Y-AXIS AND NORMAL LINE TO INNER ELLIPSE (FIGURE 5.7) DETERMINED IN SUBROUTINE GAMA2S.

MATH SYMBOL	PROGRAM SYMBOL	UNIT	DESCRIPTION
	GEOM	- - -	CYLINDRICAL SECTION GEOMETRY TABLE FLAG. INPUT ON CARD SET NUMBER 40. = 1.0 ONLY END SECTION(S) ARE INPUT = 2.0 ALL SECTIONS ARE INPUT
g_o	GNOT	FT/SQ SEC	GRAVITATIONAL CONSTANT
H_{CO}	HCO	IN	LENGTH OF CYLINDRICAL SECTION. INPUT ON CARD SET NUMBER 1.
h_E	HE	IN	LENGTH OF A GENERAL ELEMENT OR LENGTH OF LONGER EDGE OF ELEMENT USED IN CALCULATION OF BURNING SURFACE AREA FOR THE END SECTION ANALYSIS. DETERMINED IN SUBROUTINE HESUB.
h_{EO}	HEO	IN	GEOMETRICAL LENGTH OF END SECTION. DETERMINED IN SUBROUTINE ENDCSB. (FIGURE 5.35)
h_{ER}	HER	IN	REFERENCE LENGTH OF END SECTION. DETERMINED IN SUBROUTINE ENDCSB. (FIGURE 5.35)
h_{E1}	HE1	IN	LENGTH OF END SECTION CONIC SECTION. DETERMINED IN SUBROUTINE ENDCSB (FIGURE 5.35)
h_{E2}	HE2	IN	LENGTH OF END SECTION ELLIPTIC SECTION. DETERMINED IN SUBROUTINE ENDCSB (FIGURE 5.35)
	HOLDR	IN	PREVIOUS ITERATIVE VALUE OF PERIMETER LENGTH ALONG CURRENT SECTOR. INITIALIZED IN SUBROUTINE SCI FOR THE BLOCK 1 ANALYSIS OF THE HEAD-END WITH WEB.
	IDMOI(1) THRU IDMOI(12)	- - -	ALPHANUMERIC IDENTIFICATION OF MOMENTS OF INERTIA TABLES. INPUT ON SUBSET CARD NUMBER 40-2 FOLLOWING IDTAB.

MATH SYMBOL	PROGRAM SYMBOL	UNIT	DESCRIPTION
	IDTAB(1) THRU IDTAB(12)	- - -	ALPHANUMERIC IDENTIFICATION OF GEOMETRY TABLES. INPUT ON SUBSET CARD NUMBER 40-2
	IFLAG	- - -	CONTROL FLAG IN SUBROUTINE AIBST TO INDICATE ITERATION PASSES FOR FALSE POSITION ITERATION.
	IIS	- - -	CURRENT SLOT NUMBER. USED AS A SUBSCRIPT FOR THE SLOT VARIABLES.
	IIZ	- - -	SUBSCRIPT OF RBZ TO INDICATE DIVIDING PLANE LOCATION.
	ISET(I)	- - -	INPUT CONTROL FLAG TO SUBROUTINE INPT TO INDICATE WHICH CARD SETS ARE TO BE READ.
	IS1	- - -	NUMBER OF INCREMENT DIVIDING PLANE THAT IS LOCATED JUST DOWNSTREAM OF SLOT FORWARD INTERFACE. USED IN SR SEGSUB TO OBTAIN STATIC PRESSURE AT SLOT INLET.
	IS2	- - -	NUMBER OF INCREMENT DIVIDING PLANE THAT IS LOCATED JUST UPSTREAM OF SLOT AFT INTERFACE. USED IN SR SEGSUB TO STORE SLOT DISCHARGE STATIC PRESSURE FOR NEXT GRAIN SEGMENT.
	KMOICG	- - -	MOMENT OF INERTIA CALCULATION SUPPRESSION FLAG. A NON-ZERO VALUE WILL SUPPRESS THE MOI AND CG CALCULATION. INPUT ON CARD SET NUMBER 41.
	NACCEL	- - -	NUMBER OF TABLE INPUT VALUES OF ACCELERATION -TIME CURVE. INPUT ON CARD SET NUMBER 47.

MATH SYMBOL	PROGRAM SYMBOL	UNIT	DESCRIPTION
	NAKRST	- - -	NUMBER OF TABLE INPUT VALUES OF ANISOTROPIC PROPELLANT BURN RATE COEFFICIENT TABLE. INPUT ON CARD SET NUMBER 45.
	NCSTR	- - -	NUMBER OF TABLE INPUT VALUES OF PROPELLANT GAS PROPERTIES FOR CSTR, GAMAG, AMUG, TCOMB, AND PRESS TABLES. INPUT ON CARD SET 39.
	NEPS	- - -	NUMBER OF TABLE INPUT VALUES OF MEASURED CASE STRAIN DATA TABLE. INPUT ON CARD SET NUMBER 46.
	NGEOHD	- - -	NUMBER OF FORE-HEAD GEOMETRY TABLE VALUES. INPUT ON SUBSET CARD NUMBER 40-3.
	NGEOMA THRU NGEOMK		NUMBER OF REFERENCE PLANE GEOMETRY TABLE VALUES. INPUT ON SUBSET CARD NUMBERS 40-3.
	NGEOMN	- - -	NUMBER OF AFT-HEAD GEOMETRY TABLE VALUES. INPUT ON SUBSET CARD NUMBER 40-3.
	NI	- - -	INTEGER NUMBER OF TOTAL INCREMENT DIVIDING PLANES.
	NINCPL	- - -	DESIRED INCREMENT DIVIDING PLANE NUMBER TO DETERMINE BURN RATE COEFFICIENT TABLE INDEPENDENT VARIABLE, TAUAKR. INPUT ON CARD SET NUMBER 44.
	NPH	- - -	NUMBER OF TABLE INPUT VALUES OF HEAD END PRESSURE TABLE. INPUT ON CARD SET NUMBER 44.
	NSLOT	- - -	INTEGER NUMBER OF TOTAL SLOTS. THIS VARIABLE IS DECREMENTED IN SUBROUTINE TISUB EVERY TIME A GRAIN SEGMENT BURNS OUT LATERALLY.

MATH SYMBOL	PROGRAM SYMBOL	UNIT	DESCRIPTION
	NTABH	- - -	NUMBER OF HEAD END TABLE VALUES.
	NTABN	- - -	NUMBER OF NOZZLE END TABLE VALUES.
	NTME	- - -	NUMBER OF COMPUTED VALUES OF ANISOTROPIC PROPELLANT BURN RATE COEFFICIENT TABLE.
P_a	PA	PSIA	ATMOSPHERIC PRESSURE. INPUT ON CARD SET NUMBER 31.
	PCTAB	- - -	PERCENT CHANGE, RELATIVE TO 1.0, IN TOTAL BURN AREA REQUIRED TO CONVERGE SOLUTION TO DESIRED VALUE OF HEAD END PRESSURE AND BURN RATE COEFFICIENT. PROGRAM WILL CLOSE ON PCTAB AT EACH TIME INCREMENT FOR SET VALUE OF PH AND AKRST AS A FUNCTION OF TIME FROM INPUT TABLES.
	PCTWB	- - -	WEB TIME CONSTANT. RATIO OF INCREMENT DIVIDING PLANES BURNED OUT AT WEB TIME TO TOTAL NUMBER OF INCREMENT DIVIDING PLANES. INPUT ON CARD SET NUMBER 43.
P_D	PD	PSIA	PRESENT TIME DISCHARGE PRESSURE OF INCREMENT DIVIDING PLANE. COMPUTED IN SUBROUTINE AIBST.
P'_D	PDPR	PSIA	PREVIOUS TIME DISCHARGE PRESSURE OF INCREMENT DIVIDING PLANE. INITIALIZED IN SUBROUTINE MNCHN4
P_{HI}	PHI	PSIA	INITIAL GUESS OF FORE-HEAD PRESSURE FOR FIRST TIME INCREMENT. INPUT ON CARD SET NUMBER 41.
	PHST	PSIA	DEPENDENT VARIABLE OF HEAD-END PRESSURE CURVE FIT FOR START TRANSIENT.

MATH SYMBOL	PROGRAM SYMBOL	UNIT	DESCRIPTION
π	PI	- - -	MATHEMATICAL CONSTANT.
$\frac{\pi}{2}$	PIO2	- - -	PI DIVIDED BY TWO.
	PLANES	- - -	NUMBER OF CYLINDRICAL SECTION GEOMETRY PLANE TABLES INPUT. INPUT ON CARD SET NUMBER 40.
	PMOIHD	SLUG-SQ IN	FORE-HEAD GEOMETRY TABLE POLAR MOMENT OF INERTIA (DEPENDENT VARIABLE). INPUT ON SUBSET CARD NUMBER 40-5.
	PMOIN	SLUG-SQ IN	AFT-HEAD GEOMETRY TABLE POLAR MOMENT OF INERTIA (DEPENDENT VARIABLE). INPUT ON SUBSFT CARD NUMBER 40-6.
P_o		- - -	POINT ON A PLANE USED IN THE BLOCK 1 ANALYSIS OF THE HEAD-END WITH WEB. LOCATED ON THE INNER ELLIPSE ALONG A LINE PARALLEL WITH THE Y-AXIS AND NORMAL TO THE FORWARD TANGENT PLANE AT A POINT IN A SECTOR ALONG THE GRAIN INITIAL PERIMETER (FIGURE 5.1) OR POINT ON THE PSUEDOELLIPSOID USED IN THE BLOCK 2A, 2B, AND 3 ANALYSIS OF THE HEAD-END WITH WEB (FIGURE 5.4)
P_{ra} or P_{rb}		- - -	POINT IN PLANE A OR B DEFINING RADIAL BURNING FROM POINT PO (FIGURE 5.2) PR IS A FUNCTION OF TAU. IF TAU IS GREATER THAN OR EQUAL TO D03, THEN THE PLANE HAS BURNED OUT. IF TAU IS GREATER THAN D02, THEN PR IS LOCATED ON THE CURVE BETWEEN THE POINTS P2 AND P3. IF TAU IS LESS THAN OR EQUAL TO D02, THEN PR IS LOCATED ON THE LINE SEGMENT BETWEEN POINTS PO AND P2.

MATH SYMBOL	PROGRAM SYMBOL	UNIT	DESCRIPTION
	PRESS	PSIA	PROPELLANT GAS PROPERTY TABLE INDEPENDENT VARIABLE. INPUT FOLLOWING CARD SET NUMBER 39.
	PRNT	- - -	STORAGE ARRAY FOR EXPANDED INCREMENT DIVIDING PLANE PRINTOUT VARIABLES.
	PRNTAB	- - -	GEOMETRY TABLE PRINT FLAG. INPUT ON CARD SET NUMBER 40. = 0.0 DO NOT PRINT GEOMETRY TABLES = 1.0 PRINT GEOMETRY TABLES.
	PRTFLG	- - -	CONTROL FLAG FOR EXPANDED PRINTOUT. INPUT ON CARD SET NUMBER 41. =0.0 NO EXPANDED PRINT =1.0 EXPANDED PRINT
P_{sa} or P_{sb}		- - -	POINT IN PLANE A OR B DEFINING RADIAL BURNING FROM POINT P0 (FIGURE 5.2) PS IS A FUNCTION OF TAU. IF TAU IS GREATER THAN OR EQUAL TO D03, THEN THE PLANE HAS BURNED OUT. IF TAU IS GREATER THAN D01, THEN PS IS LOCATED ON THE LINE SEGMENT BETWEEN POINTS P1 AND P3. IF TAU IS LESS THAN OR EQUAL TO D01, THEN PS IS LOCATED ON THE LINE SEGMENT BETWEEN POINTS P0 AND P1.
P_{ST}	PST	PSIA	MAXIMUM START TRANSIENT PRESSURE. USED AS OPTION IN SUBROUTINE MNCHN4 TO TERMINATE START TRANSIENT CALCULATIONS. INPUT ON CARD SET NUMBER 41.
	PUNTAB	- - -	GEOMETRY TABLE PUNCH FLAG. INPUT ON CARD SET NUMBER 40. = 0.0 DO NOT PUNCH GEOMETRY TABLES = 1.0 PUNCH GEOMETRY TABLES

MATH SYMBOL	PROGRAM SYMROL	UNIT	DESCRIPTION
P_1		- - -	POINT ON A PLANE USED IN THE BLOCK 1 ANALYSIS OF THE HEAD-END WITH WEB. (FIGURES 5.1 AND 5.10) LOCATED IN THE Y-Z PLANE ALONG A LINE NORMAL TO THE GRAIN PERIMETER AT P0. OR POINT ON THE PSUEDOELLIPSOID USED IN THE BLOCK 2A, 2B, AND 3 ANALYSIS OF THE HEAD-END WITH WEB. LOCATED AT THE DISTANCE DELL FROM POINT P0. (FIGURE 5.4)
P_2		- - -	POINT ON A PLANE USED IN THE BLOCK 1 ANALYSIS OF THE HEAD-END WITH WEB. LOCATED ON THE OUTER ELLIPSOID ALONG A LINE NORMAL TO THE INNER ELLIPSOID AT P0. (FIGURES 5.1 AND 5.10)
P_3		- - -	POINT ON A PLANE USED IN THE BLOCK 1 ANALYSIS OF THE HEAD-END WITH WEB. LOCATED IN THE Y-Z PLANE ON THE OUTER ELLIPSOID AND IN THE PLANE FORMED BY POINTS P0,P1, AND P2 (FIGURES 5.1 AND 5.10)
	R	FT/DEG RANKIN	PROPELLANT GAS CONSTANT. INPUT ON CARD SET NUMBER 38.
R_{Amax}	RAMAX	IN	RADIAL DISTANCE FROM MOTOR AXIS TO EITHER- 1. OUTSIDE LIMIT OF A SECTOR IN A ZONE 2. OUTSIDE LIMIT OF AN INCREMENTAL AREA (SEE FIGURES 5.21 THRU 5.23)
R_{Amin}	RAMIN	IN	RADIAL DISTANCE FROM MOTOR AXIS TO EITHER- 1. INSIDE LIMIT OF A SECTOR IN A ZONE 2. INSIDE LIMIT OF AN INCREMENTAL AREA (SEE FIGURES 5.21 THRU 5.23)

MATH SYMBOL	PROGRAM SYMBOL	UNIT	DESCRIPTION
R_{A0}	RA0	IN	RADIAL DISTANCE FROM MOTOR AXIS TO A POINT ON PERIMETER OF ANY SECTOR AT THICKNESS TAU AND LENGTH L=0 (FIGURE 5.21) DETERMINED IN SUBROUTINE AESUB.
R_{aT}	RAT	IN	RADIAL VECTOR FROM MOTOR AXIS TO A POINT IN A SECTOR FOR THE BLOCK 1 ANALYSIS OF THE HEAD-END WITH WEB. (FIGURE 5.5 AND 5.6) DETERMINED IN SUBROUTINE RAD3B.
R_{AX}	RAX	IN	RADIAL DISTANCE FROM MOTOR AXIS TO A POINT ON PERIMETER OF ANY SECTOR AT THICKNESS TAU AND LENGTH L=LX FOR THE STRAIGHT THROUGH GRAIN END SECTION ANALYSIS. (FIGURE 5.21) DETERMINED IN SUBROUTINE AESUB.
R_B	RB	IN/SEC	PROPELLANT BURNING RATE OF ISOTROPIC PROPELLANT.
	RBFLAG	- - -	BURNING RATE EQUATION CONTROL FLAG FOR AKR(2) AND AKR(36). INPUT ON CARD SET NUMBER 44. IF RBFLAG = 0.0, AKR(2) AND AKR(36) ARE INPUT IF RBFLAG = 1.0, AKR(2) AND AKR(36) = AKRST AT STEADY STATE.
	RBHI	IN/SEC	ISOTROPIC PROPELLANT BURNING RATE OF UPSTREAM INCREMENT DIVIDING PLANE
R_{Bslot}	RBSLOT	IN/SEC	BURNING RATE IN A SLOT.
	RBZTO	IN/SEC	INCREMENT DIVIDING PLANE ANISOTROPIC BURN RATE FOR SECTOR. VALUE IS EQUAL TO SECTOR 8 ANISOTROPIC BURN RATE DURING MOTOR TAIL-OFF.

MATH SYMBOL	PROGRAM SYMBOL	UNIT	DESCRIPTION
R_{B7}	RB7	IN/SEC	ANISOTROPIC PROPELLANT BURNING RATE IN SECTOR 7 DURING MOTOR TAIL-OFF.
R_{B8}	RB8	IN/SEC	ANISOTROPIC PROPELLANT BURNING RATE IN SECTOR 8 DURING MOTOR TAIL-OFF.
R_{E1}	RE1	IN	END SECTION CASE OPENING RADIUS DETERMINED IN SUBROUTINE ENDCSB. (RN1) AFT-HEAD (RH1) FORE-HEAD (FIGURE 5.35)
R_{E2}	RE2	IN	RADIAL DISTANCE FROM MOTOR AXIS TO INTERSECTION OF ELLIPTIC AND CONIC SECTION DETERMINED IN SUBROUTINE ENDCSB (FIGURE 5.35)
R_f	RF	IN	OUTER RADIUS OF PROPELLANT.
	RFA THRU RFK	IN	REFERENCE PLANE OUTSIDE RADIUS OF PROPELLANT. INPUT ON CARD SET NUMBER 4.
R_{IG}	RIG	IN	IGNITER OPENING RADIUS. INPUT ON CARD SET NUMBER 29.
	RMOIHD	SLUG-SQ IN	FORE-HEAD GEOMETRY TABLE RECTANGULAR MOMENTS OF INERTIA (DEPENDENT VARIABLE). INPUT ON SUBSET CARD NUMBER 40-5.
	RMOIN	SLUG-SQ IN	AFT-HEAD GEOMETRY TABLE RECTANGULAR MOMENT OF INERTIA (DEPENDENT VARIABLE. INPUT ON SUBSET CARD NUMBER 40-6.
ρ_1	ROE1		RADIUS OF CURVATURE OF POINT P1 DETERMINED IN SUBROUTINE ROE1SB FOR THE BLOCK 2A ANALYSIS OF HEAD-END WITH WEB.

MATH SYMBOL	PROGRAM SYMBOL	UNIT	DESCRIPTION
R_{03}	R03	IN	RADIAL DISTANCE FROM MOTOR AXIS TO ORIGIN OF R3 FILLET RADIUS (FIGURE 5.26) DETERMINED IN SUBROUTINE PLNCNS.
R_{05}	R05	IN	RADIAL DISTANCE FROM MOTOR AXIS TO ORIGIN OF R5 FILLET RADIUS (FIGURE 5.26) DETERMINED IN SUBROUTINE PLNCNS
R_{07}	R07	IN	RADIAL DISTANCE FROM MOTOR AXIS TO ORIGIN OF R7 FILLET RADIUS (FIGURE 5.26) DETERMINED IN SUBROUTINE PLNCNS.
R_{09}	R09	IN	RADIAL DISTANCE FROM MOTOR AXIS TO ORIGIN OF R9 FILLET RADIUS (FIGURE 5.26) DETERMINED IN SUBROUTINE PLNCNS
R_{011}	R011	IN	RADIAL DISTANCE FROM MOTOR AXIS TO ORIGIN OF R11 FILLET RADIUS (FIGURE 5.26) DETERMINED IN SUBROUTINE PLNCNS.
R_{P1} thru R_{P13}	RP1 THRU RP13	IN	RADIAL DISTANCES DEFINING SECTOR BOUNDARIES FOR BLOCK 2B ANALYSIS OF HEAD-END WITH WEB. DETERMINED IN SUBROUTINE SCTOR1 (FIGURE 5.15)
R_{slotA}	RSLOTA	IN	RADIUS OF CASE AT SLOT AFT INTERFACE LOCATION AT PRIOR TIME INCREMENT. USED IN SR SLOT TO OBTAIN SLOT VOLUME.
R_{slotF}	RSLOTF	IN	RADIUS OF CASE AT SLOT FORWARD INTERFACE LOCATION AT PRIOR TIME INCREMENT. USED IN SUBROUTINE SLOT TO OBTAIN SLOT VOLUME.

MATH SYMBOL	PROGRAM SYMBOL	UNIT	DESCRIPTION
R_T	RT	IN	RADIUS OF CURVATURE OF PERIMETER IN ANY ZONE AT THICKNESS TAU. POSITIVE WHEN CENTER LIES INSIDE ZONE, NEGATIVE WHEN CENTER LIES OUTSIDE ZONE, AND ZERO WHEN PERIMETER HAS NO CURVATURE (FIGURES 5.20 THRU 5.22) DETERMINED IN SUBROUTINE ASESUB.
R_1	R1	IN	RADIUS OF CURVATURE FROM MOTOR AXIS TO INNER STAR POINT. (FIGURE 5.25) DETERMINED IN SUBROUTINE PLNCNS.
R_{2A} thru R_{2K}	R2A THRU R2K	IN	RADIUS OF INNER GRAIN POINT OF REFERENCE PLANE. INPUT ON CARD SET NUMBER 13.
R_{3A} thru R_{3K}	R3A THRU R3K	IN	FILLET RADIUS BETWEEN SLOPES LA AND LB FOR A REFERENCE PLANE. INPUT ON CARD SET NUMBER 14.
R_{4A} thru R_{4K}	R4A THRU R4K	IN	FILLET RADIUS BETWEEN SLOPES LB AND LC FOR A REFERENCE PLANE. INPUT ON CARD SET NUMBER 15.
R_{5A} thru R_{5K}	R5A THRU R5K	IN	FILLET RADIUS BETWEEN SLOPE LC AND THE WEB FOR A REFERENCE PLANE. INPUT ON CARD SET NUMBER 16.
R_{6A} thru R_{6K}	R6A THRU R6K	IN	FILLET RADIUS BETWEEN THE WEB AND SLOPE LD FOR A REFERENCE PLANE. INPUT ON CARD SET NUMBER 17.
R_{7A} thru R_{7K}	R7A THRU R7K	IN	FILLET RADIUS BETWEEN SLOPES LD AND LE FOR A REFERENCE PLANE. INPUT ON CARD SET NUMBER 18.

MATH SYMBOL	PROGRAM SYMBOL	UNIT	DESCRIPTION
R_{8A} thru R_{8K}	R8A THRU R8K	IN	FILLET RADIUS BETWEEN FORKS OF FORKED WAGON WHEEL FOR A REFERENCE PLANE. INPUT ON CARD SET NUMBER 19.
R_9	R9	IN	RADIUS OF CURVATURE FROM MOTOR AXIS TO OUTER STAR POINT (FIGURE 5.25) DETERMINED IN SUBROUTINE PLNCNS.
	SCUR	IN	CURRENT LOCATION OF THE SLOT INTERFACE FROM THE FORWARD TANGENT PLANE. SCUR(IIS,1) IS THE FORWARD INTERFACE AND SCUR(IIS,2) IS THE AFT INTERFACE LOCATION.
	SLTFLG	- - -	PROGRAM CONTROL FLAG TO INDICATE STATUS OF THE CURRENT SLOT WITH RESPECT TO THE CURRENT INCREMENT DIVIDING PLANE. 1 - THE CURRENT INCREMENT DIVIDING PLANE AND/OR THE Y REFERENCE PLANE ARE DOWNSTREAM OF THE CURRENT SLOT FORWARD INTERFACE. THE PROGRAM WILL SET THE WORKING INCREMENT DIVIDING PLANE TO THE SLOT FORWARD INTERFACE AND CHECK THE LOCATION OF THE Y REFERENCE PLANE. 2 - THE PROGRAM IS SEARCHING FOR THE Y REFERENCE PLANE THAT IS LOCATED DOWNSTREAM OF THE CURRENT SLOT FORWARD INTERFACE. 3,4 - THE PROGRAM IS SEARCHING FOR THE Y REFERENCE PLANE THAT IS LOCATED DOWNSTREAM OF THE CURRENT SLOT AFT INTERFACE. 5 - THE X AND Y REFERENCE PLANES HAVE BEEN UPDATED FOR THE AFT SLOT DETERMINE THE SLOT MASS BALANCE.

MATH SYMBOL	PROGRAM SYMBOL	UNIT	DESCRIPTION
	STDYST	- - -	CONTROL FLAG TO INDICATE STEADY STATE. INPUT ON CARD SET NUMBER 42.
	STFLAG	- - -	PROGRAM CONTROL FLAG FOR START TRANSIENT CALCULATIONS. IF STFLAG = 1.0, PERFORM TRANSIENT CALCULATIONS. INPUT ON CARD SFT NUMBER 41.
	S1A THRU S11A	IN	SLOT FORWARD INTERFACE LOCATION FROM FORWARD TANGENT PLANE. INPUT ON CARD SET NUMBER 24 AND STORED IN SCUR(IIS,1).
	S1B THRU S11B	IN	SLOT AFT INTERFACE LOCATION FROM FORWARD TANGENT PLANE. INPUT ON CARD SET NUMBER 25 AND STORED IN SCUR(IIS,2).
	T	DEG RANKIN	COMBUSTION GAS STATIC TEMPERATURE.
	TAUAKR	IN	ANISOTROPIC BURN RATE COEFFICIENT TABLE INDEPENDENT VARIABLE. INPUT FOLLOWING CARD SET NUMBER 45.
τ_{E0}	TAUEO	IN	MAXIMUM BURNING DISTANCE IN STRAIGHT THROUGH GRAIN END SECTION (FIGURE 5.35) DETERMINED IN SUBROUTINE ENDCSB
τ_{E1}	TAUE1	IN	MAXIMUM BURNING DISTANCE IN STRAIGHT THROUGH GRAIN END SECTION CONIC SECTION. (FIGURE 5.35) DETERMINED IN SUBROUTINE ENDCSB.
	TAUHD	IN	FORE-HEAD GEOMETRY TABLE INDEPENDENT VARIABLE (DISTANCE BURNED). INPUT ON SUBSET CARD NUMBER 40-5.

MATH SYMBOL	PROGRAM SYMBOL	UNIT	DESCRIPTION
τ_{max}	TAUM	IN	MAXIMUM BURNING DISTANCE FOR A REFERENCE PLANE. DETERMINED IN SUBROUTINE ENDCSB FROM THE GEOMETRY PLANE CONSTANTS.
	TAUN	IN	AFT-HEAD GEOMETRY TABLE INDEPENDENT VARIABLE (DISTANCE BURNED). INPUT ON SUBSET CARD NUMBER 40-6.
	TAUPLA THRU TAUPLK	IN	REFERENCE PLANE GEOMETRY TABLE DISTANCE BURNED (INDEPENDENT VARIABLE). INPUT ON SUBSET CARD NUMBER 40-7.
τ_{TO}	TAUTO	IN	ANISOTROPIC PROPELLANT THICKNESS. CALCULATED AT END OF START TRANSIENT IN SUBROUTINE SEGSUB. EQUAL TO TAUAKR (NTME).
	TAUTOV	IN	TEMPORARY VALUE FOR TAUTO IN SUBROUTINES LPDAPS AND AFPSUB
	TAUTOZ	IN	ANISOTROPIC PROPELLANT THICKNESS OVER INERT SLIVER IN SECTORS 6 AND 7.
	TAUWA THRU TAUWK	IN	REFERENCE PLANE WEB THICKNESS. INPUT ON CARD SET NUMBER 5.
	TAUWDP	IN	INCREMENT DIVIDING PLANE WEB THICKNESS.
	TAUX	IN	DISTANCE BURNED AT FORWARD REFERENCE PLANE. USED IN SR SEGSUB TO INTERPOLATE FOR INCREMENT DIVIDING PLANE DISTANCE BURNED.
	TAUXTO	IN	ANISOTROPIC PROPELLOUT DISTANCE BURNED AT FORWARD TANGENT PLANE.

MATH SYMBOL	PROGRAM SYMBOL	UNIT	DESCRIPTION
	TAUY	IN	DISTANCE BURNED AT AFT REFFRENCE PLANE.
	TAUYTO	IN	ANISOTROPIC PROPELLANT DISTANCE BURNED AT AFT TANGENT PLANE.
	TAUZTO	IN	TOTAL DISTANCE BURNED OF ANISOTROPIC PROPELLANT IN SECTORS 7 AND 8 DURING MOTOR TAIL-OFF.
	TCOMB	DEG RANKIN	TABULAR INPUT VALUE OF COMBUSTION TEMPERATURE OF PROPELLANT GAS (DEPENDENT VARIABLE). INPUT FOLLOWING CARD SET NUMBER 39.
	TDMAX	IN	MAXIMUM BURNING DISTANCE IN THE FORE-HEAD WITH A HEAD-END WEB. DETERMINED IN SUBROUTINE SCI DURING THE INITIAL INTEGRATION FOR THE BURNING SURFACE AREA IN THE BLOCK 1 ANALYSIS. EQUAL IN VALUE TO TAUMA OR D03 FOR AN INTEGRATION PLANE.
θ_o	THO	RADIANS	CENTRAL ANGLE OF SLOTTED- CONE GRAIN CONFIGURATION TO DEFINE LOCATION OF ONE-HALF OF SLOT IN ONE GRAIN CROSS SECTION SYMMETRICAL PART.
θ_{oA} thru θ_{oK}	THOA THRU THOK	DEGREES	REFERENCE PLANE SLOTTED-CONE GRAIN CONFIGURATION CENTRAL ANGLE. INPUT ON CARD SET NUMBER 23.
	THOW	RADIANS	WORKING INCREMENT DIVIDING PLANE SLOTTED-CONE GRAIN CONFIGURATION CONTRAL ANGLE.
θ_R	THR	RADIANS	ANGLE BETWEEN Z-AXIS AND A RADIAL VECTOR FROM MOTOR AXIS TO A POINT ON A SECTOR. DETERMINED IN SUBROUTINE THETAR (FIGURE 5.3)

MATH SYMBOL	PROGRAM SYMBOL	UNIT	DESCRIPTION
θ_{RI}	THRI	RADIANS	ANGLE BETWEEN Z-AXIS AND A RADIAL VECTOR FROM MOTOR AXIS TO A POINT ON A SECTOR. DETERMINED IN SUBROUTINE XRTHR (FIGURE 5.16)
θ_{RO}	THRO	IN	ANGLE BETWEEN Z-AXIS AND RADIAL VECTOR RAO.
θ_{slv}	THSLV	DEGREES	HALF ANGLE OF INERT SLIVER SECTOR OF INCREMENT DIVIDING PLANE IN SUBROUTINE SEGSUB
θ_{slvA} thru θ_{slvK}	THSLVA THRU THSLVK	DEGREES	REFERENCE FRAME INERT SLIVER SECTOR HALF ANGLE.
	THSLVV	DEGREES	INCREMENT DIVIDING PLANE INERT SLIVER SECTOR HALF ANGLE IN SUBROUTINE AFPSUB.
	THSLVX AND THSLVY	DEGREES	REFERENCE FRAME SECTOR HALF ANGLE IN SUBROUTINE SEGSUB.
θ_1	TH1	RADIANS	GEOMETRY CONSTANT DETERMINED IN SUBROUTINE PLNCNS (FIGURE 5.25)
θ_2	TH2	RADIANS	GEOMETRY CONSTANT DETERMINED IN SUBROUTINE PLNCNS. (FIGURE 5.25)
θ_3	TH3	RADIANS	GEOMETRY CONSTANT DETERMINED IN SUBROUTINE PLNCNS. (FIGURE 5.25)
θ_4	TH4	RADIANS	GEOMETRY CONSTANT DETERMINED IN SUBROUTINE PLNCNS. (FIGURE 5.25)
	TIMAX	SEC	MAXIMUM VALUE OF TIME. IF TIME IS GREATER THAN OR EQUAL TO TIMAX, PROGRAM EXECUTION WILL TERMINATE FOR THE CASE. INPUT ON CARD SET NUMBER 41.

MATH SYMBOL	PROGRAM SYMBOL	UNIT	DESCRIPTION
	TIMEAC	SEC	ACCELERATION-TIME CURVE INDEPENDENT VARIABLE. INPUT FOLLOWING CARD SET NUMBER 47.
	TIMEPH	SEC	HEAD END PRESSURE CURVE INDEPENDENT VARIABLE. INPUT FOLLOWING CARD SET NUMBER 44.
	TIMEPS	SEC	MEASURED CASE STRAIN DATA TABLE INDEPENDENT VARIABLE. INPUT FOLLOWING CARD SET NUMBER 46.
	TITL	- - -	STORAGE ARRAY FOR CASE TITLE FIELD DATA CODE. INPUT ON CARD SET NUMBER 50.
T_o	TO	DEG RANKIN	PROPELLANT GAS COMBUSTION TEMPERATURE. INPUT ON CARD SET NUMBER 38.
	TOFLAG	- - -	PROGRAM CONTROL FLAG TO SIGNAL SUBROUTINE RBSUB TO COMPUTE BURN RATE FROM ANISOTROPIC BURN RATE COEFFICIENT TABLE. SET IN SUBROUTINE SEGSUB TO COMPUTE BURN RATE OVER INERT SLIVER IN SECTORS 6 AND 7 AND SET IN SUBROUTINE MNCHN4 TO COMPUTE BURN RATE IN FORE AND AFT DOMES DURING TAIL-OFF.
	TPR	- - -	PRESSURE RATIO OF NOZZLE TOTAL PRESURE TO HEAD END TOTAL PRESSURE. USED IN SUBROUTINE RBSTSB TO DETERMINE FIRST ITERATION VALUE OF AKRST FOR EACH TIME INCREMENT. INPUT ON CARD SET NUMBER 44.
τ_{slotA}	TSLOTA	IN	ONE PAST TIME VALUE OF LATERAL DISTANCE BURNED IN A SLOT FORWARD INTERFACE. USED IN CONJUNCTION WITH SKA TO DEFINE SLOT INTERFACE LOCATION AND TO DETERMINE DV/DI OF A SLOT.
τ_{slotF}	TSLOTF	IN	ONE PAST TIME VALUE OF LATERAL DISTANCE BURNED IN A SLOT FORWARD INTERFACE.

MATH SYMBOL	PROGRAM SYMBOL	UNIT	DESCRIPTION
	TSLVR	IN	INERT SLIVER RADIUS FROM R5 FILLET TO INERT SLIVER IN SUBROUTINE SEGSUB.
	TSLVRA THRU TSLVRK	IN	DISTANCE FROM CORE INTERFACE TO INERT SLIVER FOR A REFERENCE PLANE. INPUT ON CARD SET NUMBER 26.
	TSLVRN	IN	SLIVER RADIUS OF REFERENCE PLANE ADJACENT TO NOZZLE SECTION. DETERMINED BY SUBROUTINE SEGSUB FOR USE IN SUBROUTINE TISUB TO LIMIT TAUZTO(NI) TO SLIVER RADIUS.
	TSLVRV	IN	INERT SLIVER RADIUS OF INCREMENT DIVIDING PLANE IN SUBROUTINE AFPSUB.
	TSLVRX	IN	INERT SLIVER RADIUS OF CURRENT REFERENCE PLANE IN SUBROUTINE SEGSUB.
	TSLVRY	IN	INERT SLIVER RADIUS OF NEXT REFERENCE PLANE IN SUBROUTINE SEGSUB.
	TST	SEC	START TIME. USED AS OPTION IN SUBROUTINE MNCHN4 TO TERMINATE START TRANSIENT INTERVAL. INPUT ON CARD SET NUMBER 41.
	TV6PR	IN	REFERENCE PLANE SLOTTED-CONE GRAIN CONFIGURATUON GEOMETRY CONSTANT. DISTANCE BETWEEN SIDE LC AND CASE WALL MEASURED ALONG A PERPENDICULAR LINE TO LC AT THE INTERSECTION OF LC WITH RADIUS R5.
	TV7PR	IN	REFERENCE PLANE SLOTTED-CONE GRAIN CONFIGURATION GEOMETRY CONSTANT. DISTANCE ALONG LINE TV6PR WHERE SIDE LC DISAPPEARS AS A RESULT OF PROGRESSION OF BURNING SURFACE OF SLOTTED-CONE.

MATH SYMBOL	PROGRAM SYMBOL	UNIT	DESCRIPTION
τ_{2max}	T2M	IN	MAXIMUM BURNING DISTANCE FOR A SECTOR DETERMINED IN SUBROUTINE PLNCNS (FIGURE 5.25)
.	T4M		
.	T5M		
.	T6M		
	T7M		
	T9M		
	T10M		
τ_{12max}	T12M		
	U	FT/SEC	VELOCITY OF GAS IN CONTROL VOLUME.
	V	CU IN	PRESENT TIME GAS VOLUME OF INCREMENT DIVIDING SECTION. USED IN SUBROUTINE AIBST TO COMPUTE PD.
V_{CE}	VCE	CU IN	VOLUME OF CASE IN REFERENCE END SECTION DETERMINED IN SUBROUTINE ENDCSB.
	VCHINP	CU IN	VOLUME OF FORE-HEAD CASE. INPUT ON CARD SET NUMBER 40.
	VCNINP	CU IN	VOLUME OF AFT-HEAD CASE. INPUT ON CARD SET NUMBER 40.
V_{EH}	VEH	CU IN	INITIAL VOLUME OF PROPELLANT BETWEEN TWO OBLATE SPHEROIDS. DETERMINED IN SUBROUTINE VOLSUB FOR THE BLOCK 3 ANALYSIS OF THE HEAD-END WITH WEB.
V_{fHO}	VFHO	CU IN	INITIAL PROPELLANT VOLUME IN FORE-HEAD. INPUT ON CARD SET NUMBER 40.
V'_{fH}	VFHPR	CU IN	PREVIOUS TIME VALUE OF HEAD-END FUEL VOLUME.
	VFI	CU IN	VOLUME OF FUEL IN INCREMENT DIVIDING PLANE.

MATH SYMBOL	PROGRAM SYMBOL	UNIT	DESCRIPTION
V_{FNO}	VFNO	CU IN	INITIAL PROPELLANT VOLUME IN AFT-HEAD. INPUT ON CARD SET NUMBER 40.
	VOLCH	CU IN	TOTAL HEAD END VOLUME CONSUMED.
	VOLCHO	CU IN	PREVIOUS TIME VALUE OF HEAD END VOLUME CONSUMED.
	VOLCN	CU IN	TOTAL NOZZLE END VOLUME CONSUMED.
	VOLCNO	CU IN	PREVIOUS VALUE OF NOZZLE-END TOTAL VOLUME CONSUMED.
	VPH	CU IN	FREE GAS VOLUME OF HEAD END SECTION.
	VPN	CU IN	FREE GAS VOLUME OF NOZZLE END SECTION.
V'	VPR	CU IN	PREVIOUS TIME VALUE OF INCREMENT DIVIDING SECTION GAS VOLUME.
V_{slvr}	VSLVR	CU IN	VOLUME OF INERT SLIVER.
$\dot{W}_D$	WDOTD	LB/SEC	TRANSIENT DISCHARGE WEIGHT FLOW FROM INCREMENT DIVIDING SECTION.
$\dot{W}_{Dslot}$	WDSLOT	LB/SEC	DISCHARGE MASS FLOW OF A SLOT.
$\dot{W}_{Islot}$	WISLOT	LB/SEC	INLET MASS FLOW OF A SLOT.
	XCGHD	IN	FORE-HEAD GEOMETRY TABLE CENTER OF GRAVITY LOCATION FROM FORWARD TANGENT PLANE (DEPENDENT VARIABLE). INPUT ON SUBSET CARD NUMBER 40-5.
	XCGN	IN	AFT-HEAD GEOMETRY TABLE CENTER OF GRAVITY LOCATION FROM AFT TANGENT PLANE (DEPENDENT VARIABLE). INPUT ON SUBSET CARD NUMBER 40-6.

MATH SYMBOL	PROGRAM SYMBOL	UNIT	DESCRIPTION
		IN	X-COORDINATE OF ORIGIN OF CIRCULAR ARC USED IN CALCULATION OF AFT-END SECTOR AREA IN SUBROUTINE ASESUB
X_{03}	X03	IN	X-COORNDINATE OF R3 FILLET RADIUS (FIGURE 5.26) DETERMINED IN SUBROUTINE PLNCNS.
X_{05}	X05	IN	X-COORDINATE OF R5 FILLET RADIUS (FIGURE 5.26) DETERMINED IN SUBROUTINE PLNCNS.
X_{07}	X07	IN	X-COORDINATE OF R7 FILLET RADIUS (FIGURE 5.26) DETERMINED IN SUBROUTINE PLNCNS.
X_{09}	X09	IN	X-COORDINATE OF R9 FILLET RADIUS (FIGURE 5.26) DETERMINED IN SUBROUTINE PLNCNS.
X_{011}	X011	IN	X-COORDINATE OF R11 FILLET RADIUS (FIGURE 5.26) DETERMINED IN SUBROUTINE PLNCNS.
X_R	XR	IN	X-COORDINATE OF A POINT ON THE PERIMETER OF A SECTOR. DETERMINED IN SUBROUTINE XRSUB FOR THE END SECTION STRAIGHT THROUGH GRAIN ANALYSIS
X_{ra}		IN	X-COORDINATE OF A POINT ON THE PERIMETER OF A SECTOR FOR THE BLOCK 1 ANALYSIS OF THE HEAD-END WITH WEB. (FIGURE 5.3) DETERMINED IN SUBROUTINE XRSUBB.
X_{rf}		IN	X-COORDINATE OF A POINT ON THE PERIMETER OF A SECTOR FOR THE BLOCK 2B ANALYSIS OF THE HEAD-END WITH WEB (FIGURE 5.16) DETERMINED IN SUBROUTIN XRSUBB.

MATH SYMBOL	PROGRAM SYMBOL	UNIT	DESCRIPTION
X_{Rmin}		IN	X-COORDINATE OF A POINT ON THE PERIMETER OF ANY SECTOR AT THICKNESS TAU AND RA=RAMIN(FIGURE 5.21)
X_{R0}	XR0	IN	X-COORDINATE OF THE POINT ON THE PERIMETER OF ANY SECTOR AT THICKNESS TAU AND RA=RA0. (FIGURE 5.21)
X_{RX}		IN	X-COORDINATE OF A POINT ON THE PERIMETER OF ANY SECTOR AT THICKNESS TAU AND RA=RAX. (FIGURE 5.21)
X_{45}	X45	IN	GEOMETRY CONSTANT WHICH DEFINES THE X-COORDINATE OF THE POINT LOCATED ALONG LINE 16 MAX AT THE DISTANCE R5 FROM SIDE LC (FIGURE 5.25) DETERMINED IN SUBROUTINE PLNCNS
X_{76}	X76	IN	GEOMETRY CONSTANT WHICH DEFINES THE X-COORDINATE OF THE POINT LOCATED ALONG LINE T12 MAX AT THE DISTANCE R6 FROM SIDE LD (FIGURE 5.25) DETERMINED IN SUBROUTINE PLNCNS
Y_{Amax}		IN	Y-COORDINATE CORRESPONDING TO XRMAX (FIGURE 5.21)
Y_{Amin}		IN	Y-COORDINATE CORRESPONDING TO XRMIN (FIGURE 5.21)
Y_{A0}		IN	Y-COORDINATE CORRESPONDING TO XR0 (FIGURE 5.21)
Y_{AX}		IN	Y-COORDINATE CORRESPONDING TO XRX (FIGURE 5.21)

MATH SYMBOL	PROGRAM SYMBOL	UNIT	DESCRIPTION
Y_{NO}	YNO	IN	Y-INTERCEPT OF LINE NORMAL TO INNER ELLIPSE AT RADIUS RIG WHICH IS USED TO DETERMINE ANGLE BETWEEN Y-AXIS AND NORMAL LINE IN SUBROUTINE AIGSUB (FIGURE 5.14)
Y_{0A}	YOA	IN	Y-COORDINATE OF THE P0 POINT FOR PLANE A.
Y_{0B}	YOB	IN	Y-COORDINATE OF THE P0 POINT FOR PLANE B.
		IN	Y-COORDINATE OF ORIGIN OF CIRCULAR ARC USED IN CALCULATION OF AFT-END SECTOR AREA IN SUBROUTINE ASESUB.
Y_{03}	Y03	IN	Y-COORDINATE OF R3 FILLET RADIUS (FIGURE 5.26) DETERMINED IN SUBROUTINE PLNCNS
Y_{05}	Y05	IN	Y-COORDINATE OF R5 FILLET RADIUS (FIGURE 5.26) DETERMINED IN SUBROUTINE PLNCNS
Y_{07}	Y07	IN	Y-COORDINATE OF R7 FILLET RADIUS (FIGURE 5.26) DETERMINED IN SUBROUTINE PLNCNS
Y_{09}	Y09	IN	Y-COORDINATE OF R9 FILLET RADIUS (FIGURE 5.26) DETERMINED IN SUBROUTINE PLNCNS
Y_{011}	Y011	IN	Y-COORDINATE OF R11 FILLET RADIUS (FIGURE 5.26) DETERMINED IN SUBROUTINE PLNCNS.
Y_{45}	Y45	IN	GEOMETRY CONSTANT WHICH DEFINES THE Y-COORDINATE OF THE POINT LOCATED ALONG LINE 16 MAX AT THE DISTANCE R5 FROM SIDE LC (FIGURE 5.25) DETERMINED IN SUBROUTINE PLNCNS.

MATH SYMBOL	PROGRAM SYMBOL	UNIT	DESCRIPTION
r_{76}	Y76	IN	GEOMETRY CONSTANT WHICH DEFINES THE Y-COORDINATE OF THE POINT LOCATED ALONG THE LINE T12 MAX AT THE DISTANCE R6 FROM SIDE LD (FIGURE 5.25) DETERMINED IN SUBROUTINE PLNCNS.
	ZCALC(I)	IN	STOREAGE ARRAY OF INCREMENT DIVIDING PLANE LOCATIONS.
z_{1at}	Z1AT	IN	(1) DISTANCE FROM CENTER OF ELLIPSE TO POINT ON OUTER ELLIPSE (FIGURE 5.6) (2) CODE USED IN SUBROUTINE P3SUB.
α_v		RADIANS	ANGLE BETWEEN BISECTOR OF PROPELLANT TIP AND STRAIGHT SIDE SECTOR USED IN CALCULATION OF AFT-END SECTOR AREA IN SUBROUTINE ASESUB.

7.0 RESULTS

The major modifications to the original Thiokol Chemical Corporation (TCC) program made by Boeing were done during the HIBEX program. HIBEX stands for "High G Boost Experiment." Because of its extreme flight environment and a new stapled high burning rate propellant, it was not known if the internal ballistics of the HIPEX motor would be affected, i.e., ignition transient interval, maximum chamber pressure, motor burn time, and shape of the chamber pressure-time trace. Accordingly, program modifications were made as discussed in Section 1.1.

Resulting predictions using these modifications were compared with measured results. The dimensionless fore-head pressure-time traces are shown in Figure 7.1. The prediction indicates good agreement with the results of three full scale motor firings. During the HIBEX program, various grain configurations, propellant formulations, and nozzle throat sizes were used. The three firings for which data are shown in Figure 7.1 are from identical motor configurations.

Security classification of the HIBEX program prohibits the discussion of specific numerical results in this unclassified report. Initial analysis that as conducted is reported in Reference 4, and an updated analysis using an anisotropic burning rate model developed from small scale "Forty-Pound Charge" (FPC) motor firings to predict the traces shown in Figure 7.1 is discussed in Reference 5.

Figure 7.2 shows the influence of internal gas flow along the propellant grain and the propellant burning rate model on ballistic predictions. Curve A is based on steady internal flow and isotropic burning. Curve B is based on non-steady internal flow and isotropic burning. Curve C represents use of the complete program capability except for an accelerating reference system. It is based on non-steady, interral flow and anisotropic burning during ignition and tailoff. The method of solution for these and other program options are discussed in Section 8.1.

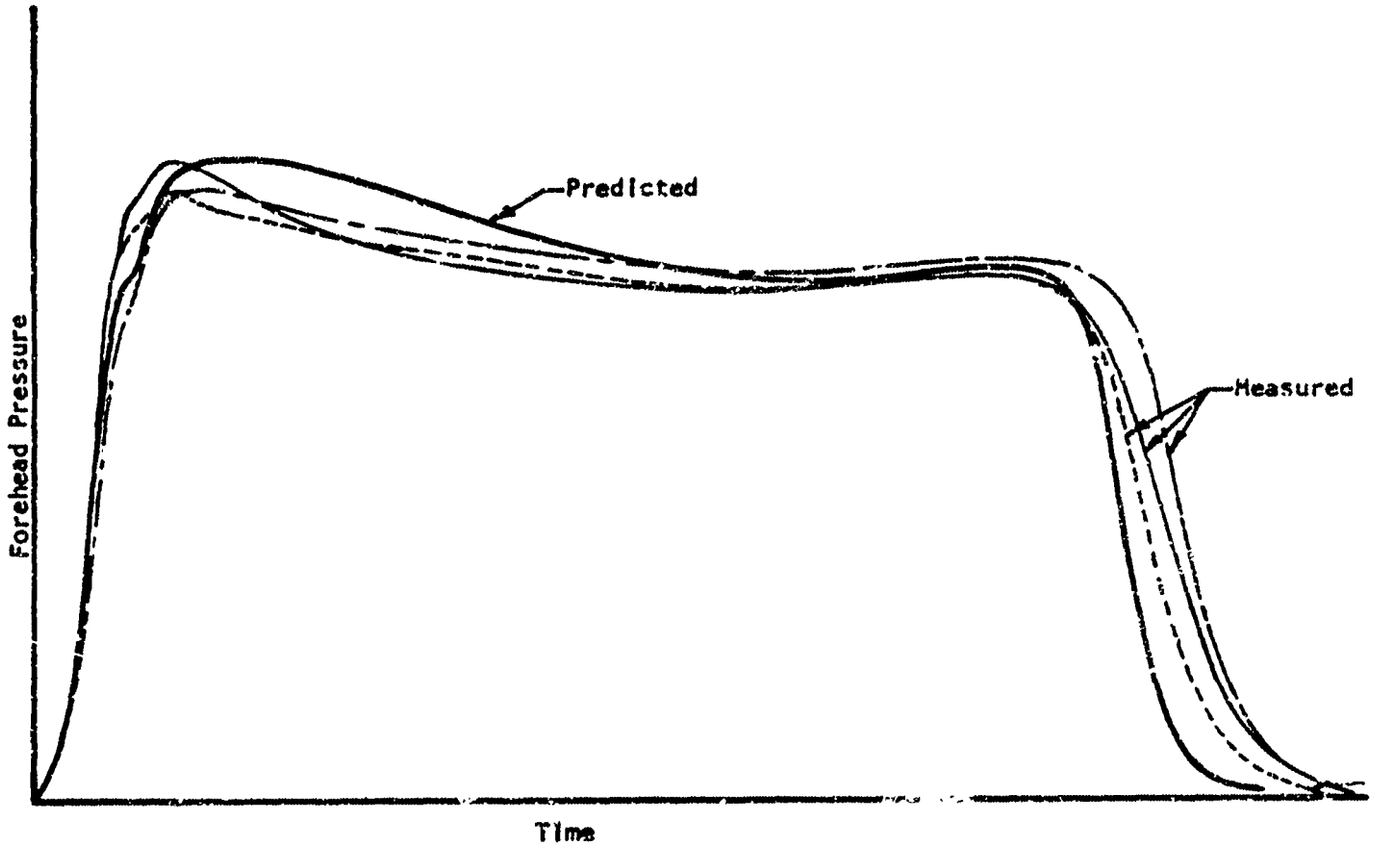


Figure 7.1. HIBEX Forehead Chamber Pressure Trace

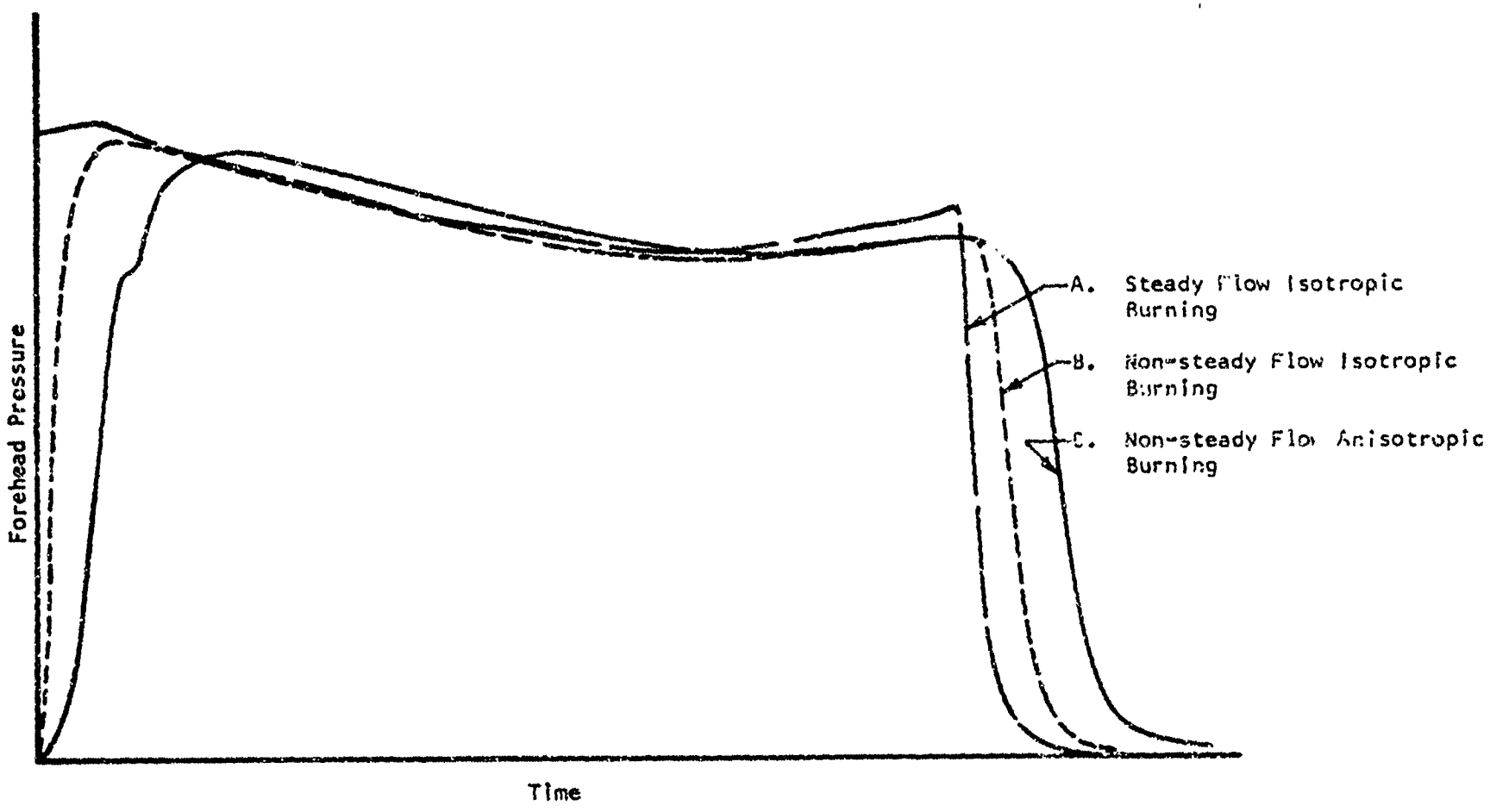


Figure 7.2. Influence of Internal Flow and Burning Rate Model